Photo induced alignment in polymer films

Varley, Helen

PHOTO INDUCED ALIGNMENT IN POLYMER FILMS

September 1997

Helen Varley

Trevelyan College

University of Durham

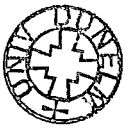

A thesis submitted to the University of Durham in partial fulfilment of the regulation

for the Degree of Doctor of Philosophy.

Declaration

The work reported in this thesis has been carried out at the Durham site of the Interdisciplinary Research Centre in Polymer Science and Technology between October 1994 and September 1997. Birefringence measurements were carried out during a series of visits to DRA, Malvern. This work has not been submitted for any other degree either in Durham or elsewhere and is the original work of the author except where acknowledged by means of an appropriate reference.

Statement of Copyright

Financial Support

I gratefully acknowledge the funding of this research from the Defence Evaluation and Research Agency (DERA), Malvern.

Photoinduced Alignment in Polymer Films

Helen Varley

Ph.D. Thesis September 1997

Abstract

Currently, alignment films for use in liquid crystal displays are produced via a mechanical rubbing process. The dust produced by mechanical rubbing along with problems due to friction and uneven roller pressure lead to defects in the display. Therefore a novel method for aligning polymers films by irradiation with polarised light has been attempted. Anisotropy introduced into the films by selective irradiation affects liquid crystal alignment.

The polymers used in this study are poly (vinyl cinnamate), poly (9-anthraceneoate ethyl methacrylate) and poly (p-azidobenzoate ethyl methacrylate). Poly (vinyl cinnamate) is a classical photoresist polymer which undergoes a [2+2] photocycloaddition in the presence of UV light. Poly (9-anthraceneoate ethyl methacrylate) and poly (p-azidobenzoate ethyl methacrylate) are both novel polymers which have the potential to undergo photo-crosslinking reactions. Poly (9-anthraceneoate ethyl methacrylate) contains an anthracene-terminated side chain which dimerises under the influence of UV light introducing anisotropy into the system. Poly (p-azidobenzoate ethyl methacrylate) contains an azido group which when irradiated with polarised light loses nitrogen to yield nitrenes which can combine to form azobenzene species.

UV spectroscopy, infrared dichroism studies, birefringence measurements and fabrication of a simple liquid crystal cell show that poly (vinyl cinnamate) and poly (9-anthraceneoate ethyl methacrylate) undergo selective photoreaction. Poly (p-azidobenzoate ethyl methacrylate) is shown to undergo reaction but not to give the desired products.

Abbreviations used in this Thesis

PVCi	Poly (vinyl cinnamate)
Polyanth	Poly (9-anthracenoate ethyl methacrylate)
Polyazide	Poly (p-azidobenzoate ethyl methacrylate)
ZnSe	Zinc Selenide
He-Ne	Helium-Neon
He-Cd	Helium-Cadmium
HOMO	Highest Occupied Molecular Orbital
LUMO	Lowest Unoccupied Molecular Orbital

Vertical/Parallel Orientation with Respect to Incoming Beam Polarisation

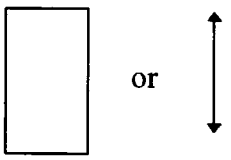

Horizontal/Perpendicular Orientation with Respect to Incoming Beam Polarisation

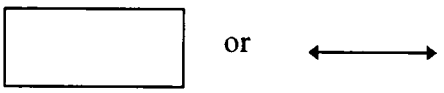

CONTENTS

ACKNOWLEDGEMENTS

I would like to express my gratitude to everyone who has helped me throughout the past three years. First and foremost, I would like to thank my supervisor, Professor Randal Richards, for his constant encouragement and support. Without him, my character would not be what it is today! Secondly, I must thank my industrial sponsors, Drs. Guy Bryan-Brown and Ian Sage at DERA, Malvern, not only for their financial support but for allowing me to invade their laboratories on numerous occasions.

Without the help of my 'partner in crime', this PhD would have been very short indeed. To Kate Foster, thank you for synthesising those two lovely polymers and making my PhD possible. I would also like to acknowledge all of the support staff here in Durham: Alan Kenwright and Julia Say for all of the NMR work, Gordon Forrest for the GPC and DSC services, Jimmy and Joe in stores for always knowing exactly which 'thingy' I was looking for, Mark for his explanations of the wonders of physics and finally to Terry for his computer genius and not laughing too much when the computer threw me out at crucial moments.

Without the friends I have made here in the IRC, the last three years would have been very quiet, so here begins a long list of thanks: To Helen, Mike, Foggy and Pecky, my long suffering physical polymer pals, to Lesley for keeping me in e-mails, to all of the truly lovely people in the IRC and to Claire for being my friend and sounding board for the past six years. I'll miss you all.

Finally, I must thank my family: my parents, my parents-in-law and Paul. I cannot express how much I love them all and how greatly I appreciate everything they have done for me.

Chapter One

Introduction

1. Introduction

1.1. Introduction to Liquid Crystal Displays (LCD)

There are two major types of display commercially available today, these are mechanical and electro-optical displays. Electro-optical displays are advantageous when compared to mechanical displays in that they allow the reading of letters, numbers and can display large quantities of information in a small space.

Liquid crystal displays are passive electro-optical displays and form a large percentage of the displays market. This is due to their extremely low power consumption, low voltage operation, readability in glaring sunlight as well as their compactness and flexibility of size. These properties make LCD's useful for consumer, industrial and military applications.

All types of LCD consist of glass plates holding the desired indium titanium oxide, ITO, electrode pattern, an alignment layer, liquid crystal, sealant, and reflectors if required, Figure 1.1.1.

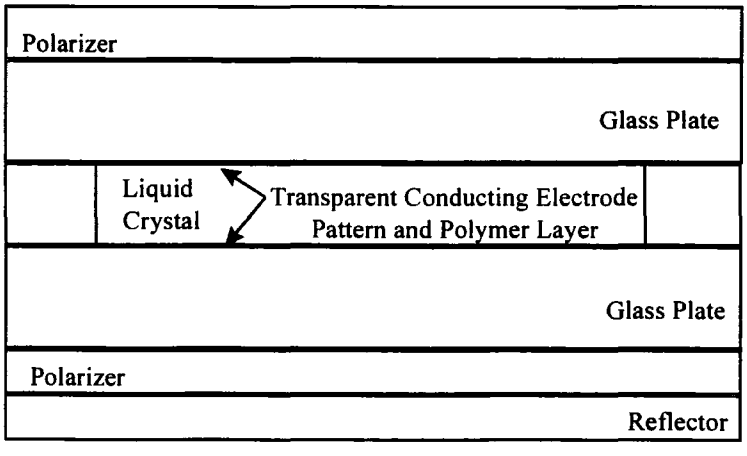

Figure 1.1.1: Schematic of a Liquid Crystal Display.[1]

Of these components, it is the liquid crystal alignment layer which is of interest in this project.

1.1.1. Liquid Crystals

What is a liquid crystal? When a crystalline solid is heated, it transforms at the melting point into an isotropic liquid. Similarly on cooling, the isotropic liquid converts to a crystalline solid. However, there are certain substances that do not pass directly from crystalline solid to isotropic liquid and vice-versa, but adopt an intermediate structure which flows as if a liquid but still possesses the anisotropic physical properties of a solid, Figure 1.1.1.1. These materials are called liquid crystals and the liquid crystal phase is known as a mesophase.

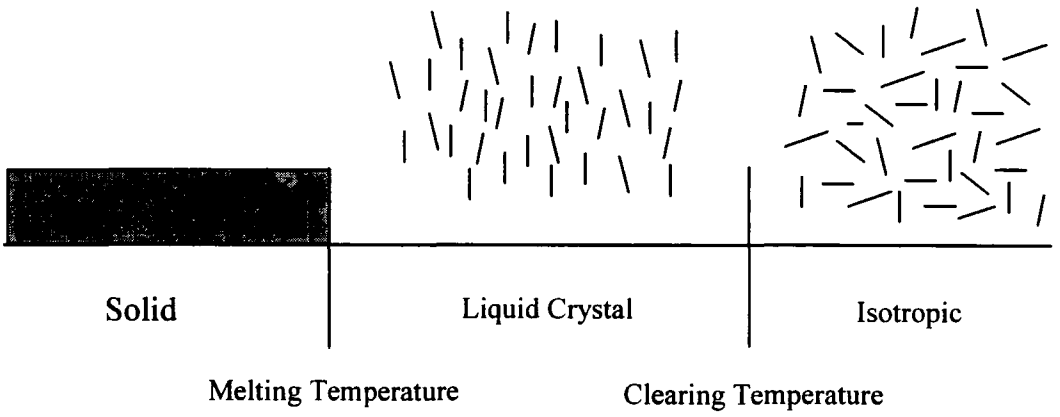

Figure 1.1.1.1: Changes of State.

An example of such a material is p-n-pentyl-p'-cyanobiphenyl (PCB),

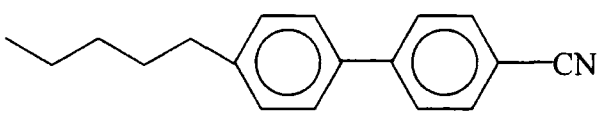

Figure 1.1.1.2: PCB.

Liquid crystal molecules are organic in nature and have a high axial ratio, giving rise to an elongated molecule. In the mesophase, these cigar shaped species lie essentially parallel to each other and their long range orientational ordering is the cause of their anisotropic physical properties. Depending on the molecular arrangement and ordering, liquid crystals can be classified as one of three types: smectic, nematic and cholesteric, Figure 1.1.1.3.

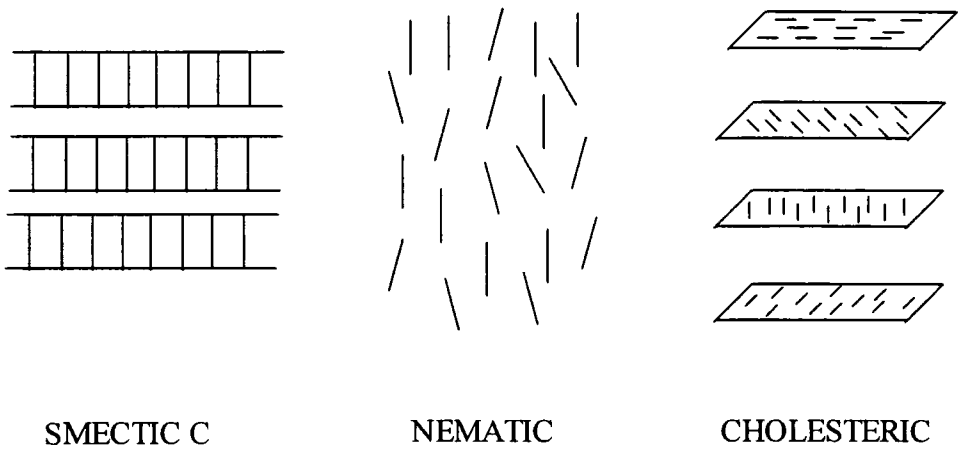

Figure 1.1.1.3: Classification of Liquid Crystals.

In the nematic state, the only restriction is that the molecules should be more or less parallel to each other. The cholesteric state can be visualised as the nematic state superimposed with a natural twist. In the smectic state, the centre of gravity of the molecules is also ordered and the molecules are arranged in layers. These layers can slide over each other and give rise to flow characteristics. Smectic liquid crystals can be further divided into subclasses depending on the molecular arrangement inside the layers. Of the three liquid crystal states, it is the nematic state that is the most technologically important class of liquid crystal and is the only type of liquid crystal used in this project.

The material properties of a liquid crystal are a result of the properties of the liquid crystal molecules and therefore, the design of liquid crystals for specific electro-optical effects is important. Figure 1.1.1.4 shows the general structure of a liquid crystal molecule.

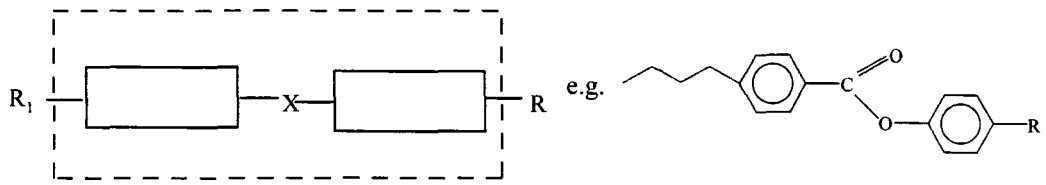

Figure 1.1.1.4: Liquid Crystal-Type Molecule.

R_1 is generally a hydrocarbon chain but R varies. If R=CN, then the liquid crystal has a strong dipole along the long molecular axis causing the liquid crystals to align parallel to an applied field, this is known as positive dielectric anisotropy. However, if R is also a hydrocarbon chain then the dipole lies across the ester group thus aligning the liquid crystal molecules perpendicular to an applied field. The liquid crystals are then said to have negative dielectric anisotropy.

The first positive dielectric anisotropic nematic liquid crystals were Schiff bases, developed for the commercialisation of LCD's in 1971[2].

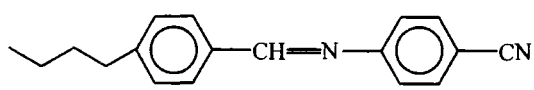

Figure 1.1.1.5: Schiff's Base.

However, the CH=N linkage in this molecule hydrolyses very easily therefore, from 1974, cyanobiphenyls, Figure 1.1.1.6, were used in most LCD's.

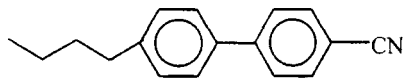

Figure 1.1.1.6: A Cyanobiphenyl.

Without the use of external forces, liquid crystal alignment is limited to microscopic domains ($\sim 1mm^3$)[3]. This is of little use in a liquid crystal cell where control of the liquid crystal is important in giving the desired images therefore, to increase control over liquid crystal alignment, an alignment layer is used.

1.1.2. Alignment Layers

In a liquid crystal cell, the initial alignment of the liquid crystal is very important. It is the alignment layer situated on the underside of the glass substrate which induces liquid crystal alignment and choice of alignment layer is crucial. Depending upon the nature of the alignment layer, the liquid crystals can lie either parallel (homogenous alignment) or perpendicular (homeotropic alignment) to the substrate surface, Figure 1.1.2.1.

Homeotropic Alignment (perpendicular)

Homogenous Alignment (parallel)

Figure 1.1.2.1: Surface Alignment of Liquid Crystals.

Surface alignment of liquid crystals was first reported in 1911 by Mauguin[4] when a glass substrate was rubbed with paper. A rubbing technique

remains the favoured industrial process for the fabrication of alignment layers for liquid crystal devices. Rubbing is carried out using a 'cloth' which can be one of a number of materials such as nylon, cellulose or polyester. It is thought[5] that localised heating arising from the rubbing process gives the alignment layer greater mobility, allowing the polymer chains to align themselves in the rubbing direction. When rubbing ceases, this re-orientation is 'frozen in'.

The material most commonly used as an alignment layer is rubbed polyimide, Figure 1.1.2.2.

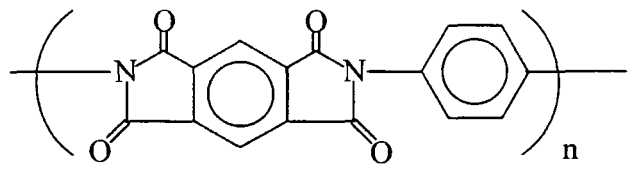

Figure 1.1.2.2: A Polyimide.

Polyimides are used in displays because of their high chemical and thermal stability. Matsunobe[6] *et al* studied the effects of rubbing pressure on polyimide films. Polarised FTIR shows that the chains orient parallel to the rubbing direction. Birefringence measurements indicate that alignment occurs very quickly, as illustrated by a sharp rise in birefringence, and then continues to rise at a much slower rate, reaching a maximum birefringence value of ~0.02. This agrees with the results of van Aerle[7] *et al* who show that orientation of the top layer occurs almost instantaneously and further rubbing leads to penetration of orientation into deeper layers of the film.

The rubbing process, although used extensively, does have its problems. Rubbing generates dust, which is undesirable when manufacturing high quality displays in a very clean environment. The rubbing cloth is attached to a large

roller, beneath which the film is passed. If the rubbing pressure is not uniform across the whole of the roller, the film will suffer surface defects due to uneven rubbing. Even a slight variation of pressure across the roller will give rise to noticeable differences in liquid crystal alignment. Finally, rubbing involves contact with the film, producing friction. Electrostatic charges may remain on the surface of the rubbed film and these will affect the workings of the display when an electric field is applied.

Due to the problems associated with the rubbing process, many researchers are attempting to devise new methods, as well as synthesise new polymers, which will produce better liquid crystal alignment layers.

In 1981, Aoyama *et al*[8] investigated the alignment of liquid crystals using stretched polymer films. Stretching films of cellulose, poly (vinyl alcohol) and polyethylene induces liquid crystal alignment in the direction of stretching. In the case of polyethylene, alignment lasts for only two days. For poly (vinyl alcohol) and cellulose, alignment is reported to last for 'a long time'. This increase in alignment lifetime indicates that polar groups present in the poly (vinyl alcohol) and cellulose alignment layers interact in some way with the cyano-species of the liquid crystal, thus stabilising the order. This polar effect, in conjunction with van der Waals interactions are proposed as being responsible for the liquid crystal alignment.

More recently, Körner *et al* [9] have devised a system in which the liquid crystal alignment is induced by an electric field. The order created by the electric field is locked into the system by annealing, giving rise to an ordered network. This cross-linked network does not interfere with the electric field alignment of

the liquid crystals, nor the formation of the mesophase. Indeed, this produces 'orientation-on-demand' films, however, this technique will be of little use in liquid crystal display technology. Orientation of liquid crystals using an electric field is the procedure used to produce the on/off contrast in a liquid crystal display. Körner's method of orienting the liquid crystals produces macroscopic alignment due to the fact that the liquid crystal molecules are now joined by cross-links. This will prevent the formation of the individually aligned domains necessary for image production in a liquid crystal display.

Current research indicates that one of the most effective ways of inducing alignment in a system is to irradiate photoactive species with UV light. This technique was first attempted by Sun[10,11] *et al.* They fabricated a simple liquid crystal cell where rubbed polyimide films, with their rubbing directions parallel, were used as alignment layers. Instead of filling the cell with an ordinary nematic liquid crystal, dye chromophores were dissolved in the liquid crystal material, creating a guest-host mixture. The molecules of this mixture aligned parallel to the rubbing direction of the polyimide films. Irradiation of the cell was then carried out using an argon ion laser polarised along the direction of rubbing. The liquid crystal molecules in the illuminated region were found to orient perpendicular to the polarisation direction of the laser and remained aligned when the radiation was switched off. Sun found that the aligning polyimide layer situated on the glass substrate upon which the laser radiation fell was permanently altered as a result of the laser-dye interaction. The change in the aligning film had subsequently induced a new aligning direction for the guest-

host liquid crystals. This work established a new technique for the formation of alignment layers for use in liquid crystal displays.

This photoalignment concept has been exploited by many other workers[12, 13, 14, 15, 16, 17]: Under the influence of UV/Vis light, azobenzene species undergo cis-trans isomerisation, Figure 1.1.2.3.

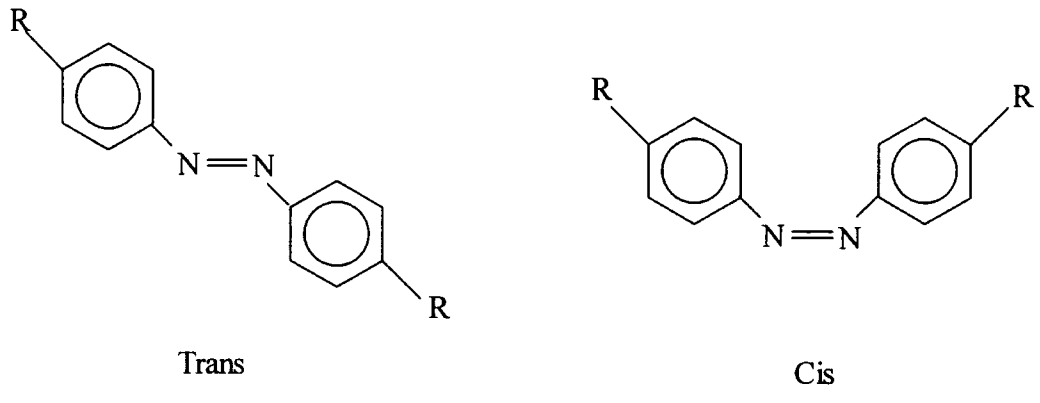

Figure 1.1.2.3: Cis-Trans Isomerisation in Azobenzenes.

This cis form of the azobenzene exists when the species is exposed to UV radiation and the trans form arises from exposure to visible radiation. In 1989, Ichimura[18] *et al* exploited this feature of azobenzene molecules and designed a 'command surface' using films of azobenzene substituted polymers. Photoresponsive nematic liquid crystal cells were formed using these command surfaces. The cell was viewed through a microscope fitted with crossed polarisers and the intensity of transmitted light was measured as the radiation was alternated between UV and visible. When the azobenzene moieties were in the trans configuration, light could not pass through the cell. When the radiation source was switched to UV, the cis configuration formed and the cell became bright. The occurrence of photoisomerisation in these azobenzene species was

effecting the way light was travelling through the display, giving rise to an on/off contrast.

Kawanishi[13] *et al* also studied the alignment of liquid crystal molecules by the photochromic isomerisation of azobenzenes. They found that the liquid crystal molecules were oriented in a homeotropic state by exposure to unpolarised visible radiation (trans isomer) whereas unpolarised UV radiation induced inhomogenous multidomain texture. However, the use of linearly polarised UV light results in the formation of uniaxial in-plane homogenous alignment of liquid crystals in a direction perpendicular to the UV polarisation direction. Consider the situation of polarised UV exposure, both cis and trans species have their π-π^* transition vector parallel to N=N. Excitation using vertically polarised UV light leads to a surface, in the direction of polarisation, rich in the cis conformation. Perpendicular to this cis rich region, is a mixture of cis and trans isomers.

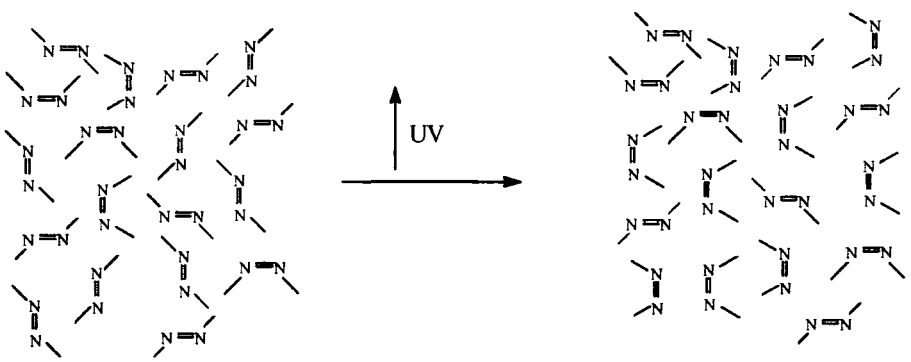

Figure 1.1.2.4: Azobenzene Induced Alignment (blue-trans, black-cis).

Earlier work has shown[19,20] that in liquid crystals containing azobenzene-moieties, the trans to cis isomerisation brings about a nematic to isotropic transition in the liquid crystal. This phase transition may be interpreted as a reduction of order in the system. However, the molecular interaction causing the

liquid crystal alignment in Kawanishi's system is clearly more complex than a simple isomerisation mechanism.

Following on from this, Ichimura[12] showed that the photoinduced orientation in azobenzene species is greatly enhanced by heating the cell above the nematic-isotropic phase transition temperature. When the liquid crystals are at room temperature, reorientation of the azobenzenes is forcing them away from their initial alignment direction. When heated, the nematic phase can form with the orientation due to the azobenzenes inherent in the liquid crystal structure.

Cinnamate species have also been studied with respect to their ability to act as alignment layers in liquid crystal displays: Schadt[21] *et al* cross-linked films of poly vinyl 4-methoxy cinnamates (PVMC), Figure 1.1.2.5, using linearly polarised UV light (λ=320nm) and then analysed the anisotropic properties introduced into the polymers.

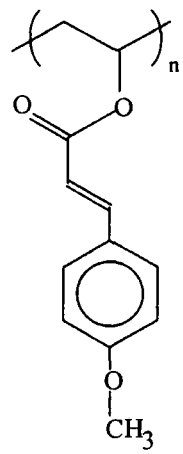

Figure 1.1.2.5: Poly (vinyl 4-methoxy cinnamate).

Before reaction commenced, the UV spectra of the films were recorded. The spectrum shows a dominant absorption peak at λ_0=300nm which disappears upon progressive irradiation of the film. Simultaneously, a second, short wavelength absorption peak appears at λ_1=195nm which rapidly becomes

dominant. This spectral shift arises from the photogenerated [2+2] cycloaddition of cinnamic acid side chains belonging to different main chains, reducing the π-electron conjugation of the system. Cis-trans isomerisation is negligible in PVMC films and the photocycloaddition reaction is assumed to be the dominant photo process.

Birefringence measurements were also carried out and can be summarised as follows: No optical anisotropy was detected in the film prior to irradiation, however, as reaction commences a weak optical anisotropy rapidly develops. The birefringence peaks with a maximum value of ~0.05 and then gradually decays. This curve can be explained by assuming a single mechanism; the preferred depletion of cinnamic acid side chains parallel to the polarisation direction of the incoming UV radiation. Prior to exposure, the cinnamic acid side chains are isotropically distributed. When irradiated, the side chains oriented parallel to the polarisation direction will cross-link. The chromophores with off-axis transition moments will barely be affected. This leads to the initial increase in birefringence. With progressive irradiation time, the chromophore depletion parallel to the polarisation direction saturates and the probability that chromophore pairs with off-axis orientation will react increases. During irradiation, the mobility of the PVMC matrix decreases and as a consequence, birefringence peaks and then begins to decrease. Reversion to zero birefringence does not occur as the decreased mobility prevents chromophores at some distance from each other from reacting.

Liquid crystal cells were formed using PVMC and the films were found to induce homogenous alignment perpendicular to the polarisation direction.

Residual 'monomeric' side chains, as well as the cyclobutane derivatives are distributed perpendicular to the polarisation direction. Due to the elongated shape of the cyclobutane species, it is thought that they may be exhibiting an orienting effect on the hydrocarbon side chains to which they are attached as shown in Figure 1.1.2.6. The residual cinnamate side chains, cyclobutane derivatives and the hydrocarbon chains all show the same uniaxiality and are assumed to be responsible for the alignment direction of the liquid crystal molecules.

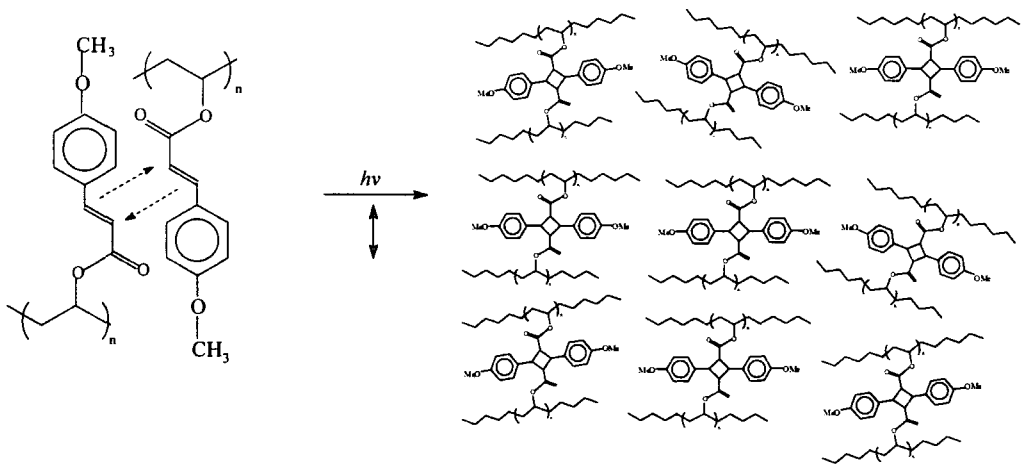

Figure 1.1.2.6: Species presented in Irradiated PVMC.

Poly (vinyl cinnamate), PVCi, reacts in a very similar fashion[17,22,23,24]. If a cell is made up using PVCi as an alignment layer, the liquid crystals are also oriented perpendicular to the UV polarisation direction[22]. If the polarisation direction is then rotated by 90°, the liquid crystal alignment can be erased. This write-erase cycle can occur approximately 10 times, with the anisotropy created becoming weaker with each successive alignment. Erasure of alignment is

thought to be due to reorientation of molecular ensembles perpendicular to the polarisation direction of the incoming UV radiation.

More recently, Schadt[17] *et al* discovered that photoreactive films of cinnamate derivatives can align liquid crystal polymer films on single substrates i.e. no need to form a twisted cell. The photoreactive films used were based on cinnamic acid derivatives containing cyano-biphenyl derivatives. The photoreactive polymer was masked before irradiation to allow varying alignment orientations to be formed. The cell was fabricated using a liquid crystalline polymer layer which was photopolymerised using unpolarised UV light, thus transferring the liquid crystal polymer photogenerated alignment pattern into the solid state. The masking and photopolymerisation of the liquid crystal polymer allow the generation of high information content photogenerated alignment patterns on single substrates.

The most promising liquid crystal alignment system to date, devised by Schadt[15] *et al*, is based on coumarin and is shown in Figure 1.1.2.7.

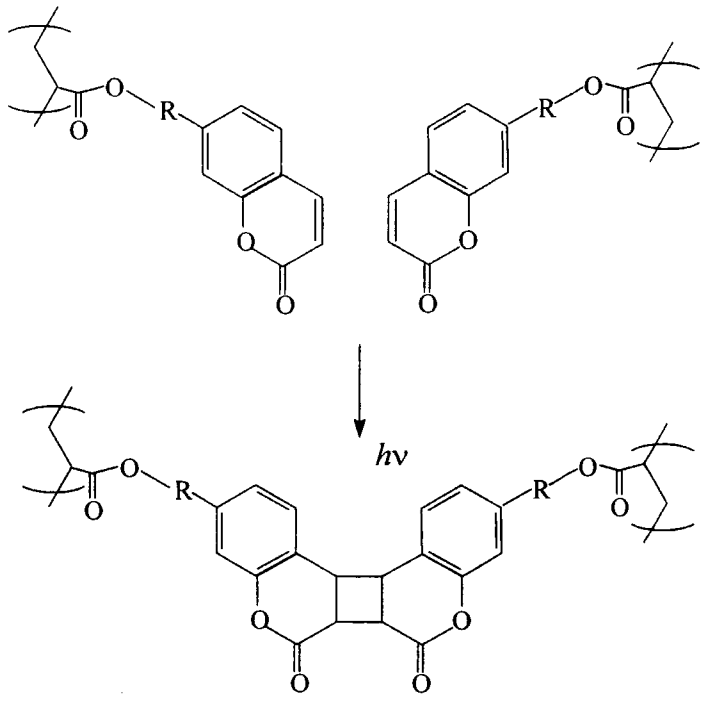

Figure 1.1.2.7: The Coumarin System for Liquid Crystal Alignment.

A photoinduced [2+2] cycloaddition reaction occurs using polarised UV light. This not only produces cross-linking giving an anisotropic film but by changing the angle of incidence of the radiation, pretilt angles ranging from 0-90° can be achieved.

The alignment and tilt of liquid crystal molecules on a treated surface is fundamental to the efficient operating of the display. However, the exact nature of the interaction between surface and liquid crystal is still unclear. A complex combination of anisotropic interactions, topological, steric, polar and Van der Waals interactions are all thought to contribute to the final liquid crystal alignment state.

A significant factor to consider when designing a liquid crystal alignment system is does the system induce 'pretilt' of the liquid crystals? This phenomenon is illustrated in Figure 1.1.2.8.

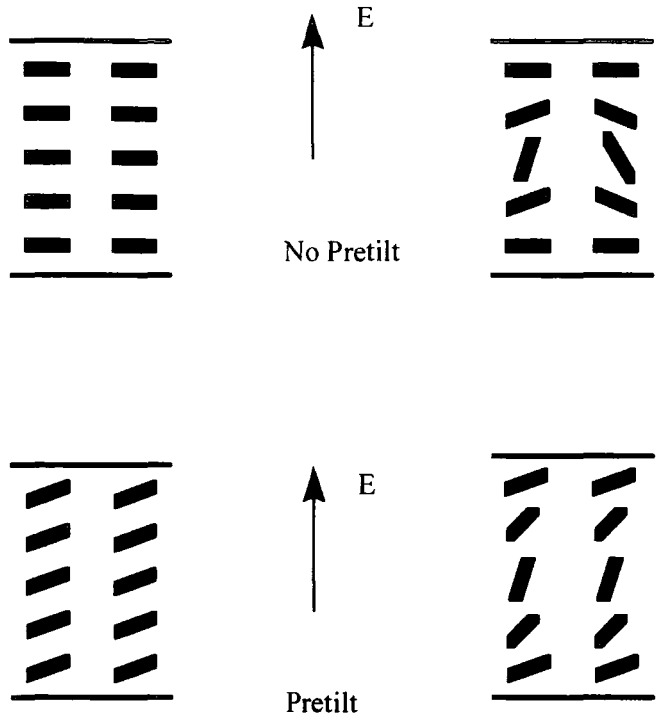

Figure 1.1.2.8: The Influence of Pretilt[25].

The uppermost diagram in Figure 1.1.2.8, shows liquid crystal alignment with no pretilt. The liquid crystals are free to move from their initial orientation in either a clockwise or anticlockwise direction when an electric field is applied. This gives rise to a patchy display with a visible transition line between the two domains.

If the polymer film tilts the liquid crystals slightly from their parallel orientation then on the application of an electric field, the liquid crystals all turn in the same direction, giving a sharp contrast between the 'on' and 'off' positions. Therefore, it is important that an alignment layer not only aligns the liquid crystals but also tilts the liquid crystals from the parallel orientation. In the rubbed polyimide systems currently used, the surface tilt angle is ~3° [15] and this slight deviation from parallel alignment prevents problems arising from reverse tilt and reverse twist.

As mentioned previously, homeotropic alignment may also be desired. This can be achieved by oblique evaporation of SiO onto the substrate surface[26,27]. However, most liquid crystal displays require homogenous alignment and it is this regime that most researchers aim to achieve.

1.1.3. Twisted Nematic Liquid Crystal Displays (TN-LCD's)

The alignment layers studied in this project are specifically for use in twisted nematic liquid crystal displays, TN-LCD. The TN-LCD, Figure 1.1.3.1, is the most common type of display and comprises >99% of the LCD market.

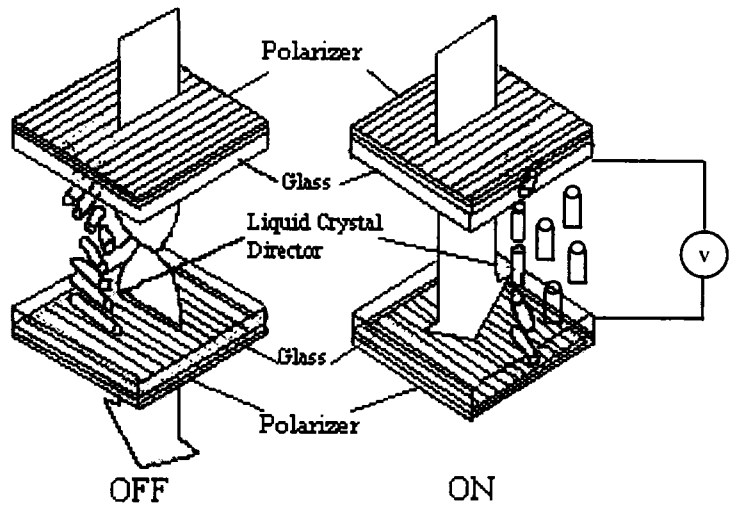

Figure 1.1.3.1: Twisted Nematic Liquid Crystal Display (TN-LCD).[2]

A thin layer of liquid crystal (~5-15μm) with a positive dielectric anisotropy is sandwiched between two glass plates containing transparent conducting electrode patterns, usually via the etching of an ITO film. These two glass plates are treated such that unidirectional homogeneous alignment of the

liquid crystal is achieved. The cell is constructed with the alignment directions of the treated plates orthogonally oriented, the cell is then sealed and filled with the appropriate liquid crystal. The liquid crystal sandwich can be thought of as consisting of liquid crystal layers. The top and bottom layers align according to the treated surfaces with which they are in contact whereas the central layers take an intermediate structure according to the distance from the treated surfaces. This produces a situation where each successive layer is skewed unidirectionally, either clockwise or anticlockwise, such that the final, bottom layer is skewed by 90° with respect to the uppermost layer. The liquid crystals are themselves birefringent, therefore each layer will act as a birefringence sheet. This twisted arrangement of birefringent piles of liquid crystals can rotate the plane of polarisation of incoming polarised light.

Consider Figure 1.1.3.1, the unpolarised beam of light, after passing through the first polariser becomes polarised along the direction of the polariser. The plane of polarisation of this light rotates as it traverses through the twisted nematic cell, giving a total rotation of 90°. If the plane of polarisation of the second polariser is 90° to that of the first, light leaving the cell passes through the second polariser and the cell appears clear. In a reflective type cell, a reflector positioned on the back of the second polariser reflects this light in a forward direction.

On application of a voltage, the liquid crystals, due to their positive dielectric anisotropy, align themselves in the direction of the electric field and hence lose the property of rotating the polarisation vector of the light. As the plane of polarisation of the light is now orthogonal to the second polariser, the

passage of light is blocked and the cell appears to be black. Thus, voltage from the circuitry is applied to the segments required to form the desired character which then appears as a black character on a colourless or neutral grey background.

1.2. Project Aims

The aim of this project was to obtain physical characterisation of potential alignment layers for liquid crystal devices using a variety of techniques. Poly (vinyl cinnamate) (PVCi), a polymer with well characterised and documented reactions was used as a model polymer for these studies.

From an initially isotropic film, irradiation with polarised UV light induces a photoreaction in the polymer system. In PVCi, this is a [2+2] photocycloaddition across the carbon-carbon double bond, giving rise to anisotropy in the film which in turn induces liquid crystal alignment. The novel polymers synthesised for this work[28] are based upon anthracene and azide molecules. For the anthracene-based polymer, the photoreaction was expected[29] to involve dimerisation across the 9,10-position of two favourably situated anthracene moieties. The azide-based polymer was thought to be a suitable candidate for a photo-elimination reaction with the azide moiety losing molecular nitrogen, forming a nitrene. Combination of two nitrenes then gives rise to an azobenzene species. As polarised light was used as the radiation source, the reactions have an orientational dependence and thus create the desired anisotropy in the polymer film.

Four techniques were used to characterise the photoinduced changes in the polymer films: UV spectroscopy, polarised FTIR spectroscopy, birefringence studies and fabrication of a simple liquid crystal cell.

UV spectroscopy was used to ensure that chromophore reaction was occurring. This technique does not give any indication as to the selectivity of the photoreaction but will show whether depletion of the chromophores initially present in the sample was taking place. The suitability of this technique for the assessment of chromophore depletion was shown by Schadt[21] *et al* on work with PVMC as well as work by Zekkat[30] *et al* on the isomerisation of azosilane molecules. Both workers followed the change in the UV absorption spectrum of the individual systems upon exposure to polarised light. The work by Schadt is especially relevant as PVMC is a derivative of the model compound used in this project, PVCi, and has an almost identical UV absorption spectrum. The only difference being that λ_{max} for PVMC is at longer wavelengths than λ_{max} for PVCi. This is due to the increased conjugation in PVMC arising from the methoxy substituted benzene ring.

Once reaction was known to take place, polarised FTIR studies are used to calculate the dichroic ratio. This is a widely employed technique and has previously been used to study orientation in stretched polymer films of poly (ethylene terephthalate)[31,32,33], poly (ether ether ketone)[34] and poly (vinyl phenol)[35], polyethylene[36,37] and polystyrene[38]. Dichroic ratios for side chain liquid crystalline polymers as a function of temperature[39,40], stretching[41] and depth into sample[42] have also been determined using polarised FTIR.

Cunningham[43] *et al* used polarised FTIR to study the changes in molecular orientation and conformation incurred by uniaxially drawing poly (ethylene terephthalate), PET.

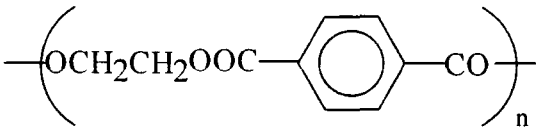

Figure 1.2.1: PET.

PET may exist in amorphous and crystalline forms, the major difference between the two being due to rotational isomerisation of the $-OCH_2CH_2O-$ group, giving rise to trans and gauche forms. In crystalline regions, the trans form is present whereas in amorphous regions both trans and gauche forms are present. Analysis of bands due to the trans and gauche conformations allow determination of the amorphous/crystalline content in the sample, as well as the orientation of each conformation. Study of the vibrations of the benzene ring allow assessment of molecular orientation of the whole polymer system to be carried out. Using polarised FTIR, Cunningham showed that at low overall molecular orientation the segments containing trans conformations, are more oriented than the gauche segments, which are almost isotropically distributed. At higher overall molecular orientation, the gauche segments become more aligned. The results infer that overall molecular orientation arises largely from molecular chains possessing trans conformation.

Polarised FTIR has also been used to study poly (ether ether ketone)[44], PEEK, drawn from an initially amorphous material. The observed IR spectrum is the sum of two overlapping spectra due to the amorphous and crystalline conformations. Polarised FTIR was used to assess the changes in molecular

conformation in the draw direction. It was found that as the film is drawn, the amorphous chains uncoil and therefore, the amorphous orientation increases. At this stage, the sample contains few crystalline regions. When the film is drawn to approximately twice its initial length, crystallinity increases greatly as many regions exist in which the molecules are very well aligned, allowing crystal formation. Further drawing increases both crystalline and amorphous orientation. If this drawn film is then annealed to 573K, the crystalline content increases to a maximum of 45%.

The above examples have shown how polarised FTIR has been used to study changes in orientation of particular groups or regions within a sample as a function of some external force. The sensitivity of this technique is further highlighted by Li & Brisson[45] in a study of stretched films of poly (vinyl phenol), PVPh.

PVPh is known to undergo self association through hydrogen bonding or to form intermolecular hydrogen bonds with guest systems containing hydrogen acceptors. Thus, PVPh can be used as a model to investigate the effects of hydrogen bonding on blend miscibility. Infrared dichroism studies can be used to determine the transition moment angle of various vibrations and compare this orientation behaviour to that of polystyrene, where hydrogen bonding does not occur. It was shown that the orientation behaviour of PVPh compared to that of polystyrene was not influenced by self association through hydrogen bonding. This is likely to be due to the dissociation of the hydrogen bonds as the draw temperature was greater then the T_g of the polymer system. The transition moment of the hydroxyl (-OH) vibration did not behave linearly with respect to

overall molecular orientation. However, when the bands were separated into free and hydrogen bonded -OH species, both behaved linearly with respect to overall orientation but behaved differently when compared to each other. This was attributed to changes in conformation of the hydroxyl group upon hydrogen bond formation.

Zhao and Lei[46] used infrared dichroism to study the effects of stretching on nematic polyacrylates.

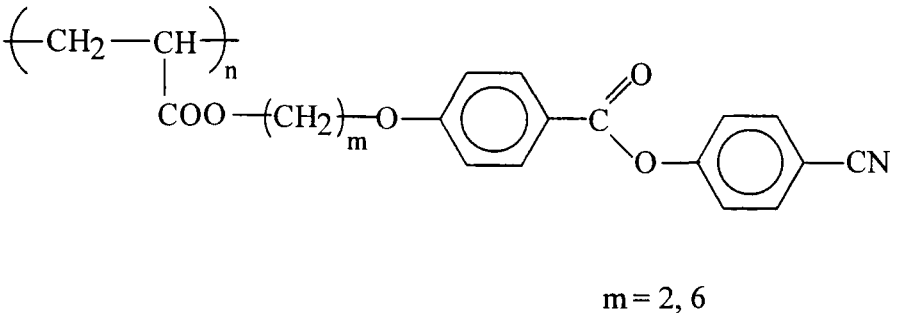

Figure 1.2.2: Nematic Polyacrylates.

Films were cast onto poly (vinyl alcohol) support films upon which they were stretched. The orientation of the mesogenic groups increased on stretching. Contrary to many polymer systems, the effect was not temperature dependent. Orientation is governed by macroscopic alignment of the nematic domains along the local director. Alignment can only occur when the molecules are in the liquid crystal state, therefore, stretching at temperatures above the clearing temperature does not align the mesogenic units, thus explaining the lack of temperature dependence.

Consider Figure 1.2.2, when m=2, alignment is increased relative to when m=6. The shorter spacer group allows strong coupling between the mesogenic group and the chain backbone. As film thickness increases, orientation of the

mesogenic group decreases. This occurs as transfer of stress from the supporting film to the polymer can only occur at the interface. Alignment of the nematic domains begins at the interface an propagates via cooperative forces throughout the film. As infrared dichroism measures average orientation, the weakening of alignment in domains far from the interface, due to the thickness of the sample, accounts for the decrease in orientation. This effect is less pronounced for m=2 relative to m=6 as the strong coupling when m=2 increases the propagation of alignment.

The results from the polarised FTIR experiments described above demonstrate the ability of the technique to describe changes occurring at a molecular level. Irradiation of the photoactive polymers used in this project will induce orientation via molecular changes and it is therefore feasible that given the effectiveness of the technique in the systems described, evidence for photogenerated molecular orientation should be achieved using infrared dichroism studies.

Birefringence measurements were also used to determine the extent of anisotropy within the sample. Cinnamate systems and their photoinduced anisotropy have been studied previously using this technique[47,48.49] as has the photoinduced isomerisation in azobenzene species[50].

If a glassy photochromic liquid crystalline polymer containing both azobenzene and mesogenic side chains is irradiated with linearly polarised UV light, repeated E↔Z isomerisation cycles of the azobenzene chains will result in rotational diffusion of the photochromic moieties to a position perpendicular to the polarisation direction of the incoming radiation[50]. In this liquid crystalline

polymer system, the optical anisotropy is influenced by two factors: the tendency of the polymer to form a liquid crystalline phase stabilises the light induced order whereas a high concentration of photochromic moieties is needed to achieve efficient photo-orientation. The higher the azobenzene content, the smaller the mesogenic content which results in a loss of liquid crystallinity. The photoinduced birefringence as a function of azobenzene concentration thus shows a maximum value at the border between the liquid crystalline and amorphous states, illustrating that there is a complex relationship between polymer structure and the extent of photoinduced anisotropy.

Birefringence studies have also been used successfully to study the effects of stretching[51,52] and spinning[53] upon orientation. As all of the samples prepared for use in this project are spin cast, the effects of spinning on optical anisotropy are especially interesting. Lin and Bidstrup[53] examined the effects of spinning speed on the optical anisotropy of spin cast polyimide films. A polyimide film based on pyromellitic dianhydride (PDMA) and 4-4'-oxydianiline (ODA) was prepared by the combination of PMDA and ODA to give a polyamic acid. Imidization was carried out thermally such that water was lost from the system to yield the PDMA/ODA film.

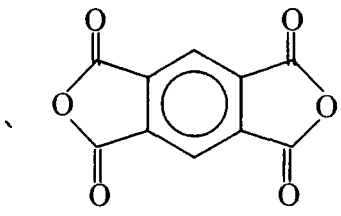

PMDA

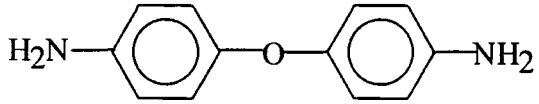

ODA

Figure 1.2.3: Monomers Used to Form Polyimide Film.

The film formed showed that as the spinning speed was increased, the birefringence of the film also increased. The film displayed uniform in-plane orientation therefore, the observed increase in birefringence was not thought to be due to orientation of the polymer molecules by mechanical stress induced by spinning. Spinning speed directly controls the film thickness: increased speed leads to a decrease in thickness. It was hypothesised that film thickness variations were causing this birefringence change. Lin and Bidstrup showed that the concentration of polyamic acid does not influence the thickness dependence of the birefringence, nor are the dynamics of solvent evaporation or thermal imidization controlling factors. The authors report that the lowering of birefringence may be a consequence of skin layer formation due to a stress gradient and the presence of air-polymer-substrate interfaces.

UV spectroscopy, polarised FTIR spectroscopy and birefringence studies probe the changes in the alignment layer upon irradiation. However, although orientation of the alignment layer is important, its occurrence does not mean that one can automatically infer that liquid crystal alignment will transpire because of this. The mechanism for liquid crystal alignment is complex and is not fully understood[21]. Therefore, only the fabrication of an actual cell[51,52] will show whether the photoinduced orientation in the alignment layer induces liquid crystal alignment.

References

1) B.Bahadur, *Mol.Cryst.Liq.Cryst,*, 1984, **109**, 3.

2) M.Schadt. *Mol.Cryst.Liq.Cryst.,* 1988, **165**, 405.

3) A.Ciferri, Liquid Crystallinity in Polymers: Principles and Fundamental Properties, VCH Publishers 1991.

4) C.Mauguin, *Bull.Soc.fr.Min*, **34**, 71 (1911).

5) J.A.Castellano, *Liquid Crystals and Ordered Fluids*, **4**, 1994, 763.

6) T.Matsunobe, N.Naga, Y.Nakagawa & H.Ishida, *J.Photopolym Sci & Tech.*, 1995, **8**(2), 263.

7) N.A.J.M.van Aerle, M.Barmentlo & R.W.J.Hollering, *J.Appl.Phys*, **74**(5), 1993, 3111.

8)H.Aoyama, Y.Yamazaki, N.Matsuura, H.Mada & S.Kobayashi, *Mol.Cryst.Liq.Cryst.*, **72**(letters), 127.

9) H.Körner, A.Shiota, T.J.Burning & C.K.Ober, *Science*, **272**, 12th April 1996.

10) W.M.Gibbons, P.J.Shannon, S-T Sun & B.J.Swetlin, *Nature*, 1991, **351**(6321), 49.

11) Shao-Tung Sun, W.M.Gibbons & P.J.Shannon, Liquid Crystals, 1992, **12**(5), 869.

12) K.Ichimura, *Mol.Cryst.Liq.Cryst.*, 1994, **246**, 331.

13) Y.Kawanishi, T.Tamaki, M.Sakuragi, T.Seki & Y.Suzuki, *Langmuir* 1992, **8**, 2601.

14) Th.Fischer, L.Läsker, J.Stumpe & S.G.Kostromin, *J.Photochem.Photobiol,A:Chem*, **80** (1994), 453.

15) M.Schadt, H.Seiberle, A.Schuster & S.M.Kelly, *Jpn.J.Appl.Phys*, **34**(1995), L764.

16) B.J.Briscoe & D.Tabor, *ASLE Transactions*, **17**, 3, 158.

17) M.Schadt, H.Sieberle & A.Schuster, *Nature*, **381**, May 1996, 212.

18) K.Ichimura, Y.Suzuki, T.Seki & y.Kawanishi, *Makromol.Chem.Rapid Comm.*, **10**, 5, 1989.

19) S.Tazuke, S.Kurihara & T.Ikeda *Chem Lett.*,1987, 911.

20) T.Ikeda, S.Horiuchi, D.B.Karanjit, S.Kurihara & S.Tazuke, *Chem Lett.*, 1988, 1679.

21) M.Schadt, K.Schmitt, V.Kozinkov & V.Chigrinov, *Jpn J.App Phys*, **31** (1992), 2155, Part 1, no 7, July 1992.

22) V.G.Chigrinov & V.M. Kozenkov, *Proc SPIE*, 1995, **2408**, 185

23) P.L.Egerton, E.Pitts & A.Reiser, *Macromolecules* 1981, **14**, 95.

24) M.Schadt, K.Schmitt, V.Kozinkov & V.Chigrinov, *Jpn J.App Phys*, **31** (1992), 2155.

25) J.van Haaren, *Nature*, 381, 1996, 190.

26) A.Mosely, *Displays*, **14**(2), 1993, 67.

27) D-S Seo, H.Matsuda, T.Oh-Ide & S.Kobayashi, *Mol.Cryst.Liq.Cryst*, 1993, **224**, 13.

28) K.E.Foster, PhD Thesis, University of Durham 1997.

29) N.J.Turro, Modern Molecular Photochemistry, The Benjamin/Cummings Publishing Co., 1978.

30) Z.Sekkat, J.Wood, Y.Geerts & W.Knoll, *Langmuir*, 1995, **11**, 2856.

31) J.B.Faisant de Champchesel, D.I.Bower, I.M.Ward, J.F.Tassin & G.Lorentz, *Polymer,* 1993, **34** (18), 3763.

32) A.Cunningham, I.M.Ward, H.A.Willis & V.Zichy, *Polymer,* 1974, **15**, 749.

33) A.Ajji, K.C.Cole, M.M.Dumoulin & J.Brisson, *Polymer*, 1995, **36**(21), 4023.

34) A.M.Voice, D.I.Bower & I.M.Ward, *Polymer,* 1993, **34** (6), 1165.

35) D.Li & J.Brisson, *Polymer* 1994, **35**(10), 2078.

36) B.E.Read & D.A.Hughes, *Polymer* 1972, **13**, 495.

37) R.A.Jones, G.A.Salmon & I.M.Ward, *J.Polym.Sci:Part B Polym Phys*, 1994, **32**, 469.

38) B.Jasse & J.L.Koenig, *Polymer*, 1981, **22**, 1040.

39) J.J.Vij, A.Kocot, G.Kruk & R.Wrzalik, *Mol.Cryst.Liq.Cryst.,* 1993, **237**, 337.

40) G.Kruk, J.K.Vij, O.Karthaus & H.Ringsdorf, *Supramolecular Science*, **2**(1995) 51.

41) Y.Zhao & H.Lei, *Polymer,* **35**(7), 1994, 1419.

42) A.Kaito, M.Kyotani & K.Nakayama, *Polymer*, 1992, **33**(13), 2672.

43) A.Cunningham, I.M.Ward, H.A.Willis & V.Zichy, *Polymer,* 1974, **15**, 749.

44) A.M.Voice, D.I.Bower & I.M.Ward, *Polymer,* 1993, **34** (6), 1165.

45) D.Li & J.Brisson, *Polymer* 1994, **35**(10), 2078.

46) Y.Zhao & H.Lei, *Polymer,* **35**(7), 1994, 1419.

47) G.P.Bryan-Brown & I.C.Sage, *Liquid Crystals*, 1996, **20**(6), 825.

48) J.Chen, B.Cull, P.L.Bos & D.L.Johnson, SID 95 DIGEST, 528.

49) M.Schadt. K.Schmitt, V.Kozinkov & V.Chigrinov, *Jpn J.App Phys*, **31** (1992), 2155. Part 1, no 7, July 1992.

50) J.Stumpe. L.Lasker, Th.Fischer, M.Rutloh, S.Kostromin & R.Ruhmann, *Thin Solid Films*, 1996, **284-285**, 252.

51) J.M.Rossignol, R.Seguela, F.Reitsch & J.Dupuis- Lallemand, *Journal of Polymer Science*: Part C :Polymer Letters, 27, 527, (1989).

52) B.E.Read, J.C.Duncan & D.E.Meyer, *Polymer Testing*, 1984, **4**, 143.

53) L.Lin & S.A.Bidstrup, *J.App.Polym.Sci.*, 1993, **49**, 1277.

Chapter Two

Experimental Techniques

2. Experimental Techniques

2.1. Polymers

Poly (vinyl cinnamate) used as a model polymer was purchased from Aldrich. Two polymers were synthesised by Miss K.Foster [1] which incorporated moieties which were susceptible to modification by photochemical means and may afford subsequent alignment. These two polymers are poly (9-anthracenoate ethyl methacrylate) and poly (p-azidobenzoate ethyl methacrylate), Figure 2.1.1. The synthesis and molecular weights of each of these polymers are reported in chapters 3, 4 & 5 where the experimental investigations are discussed in detail.

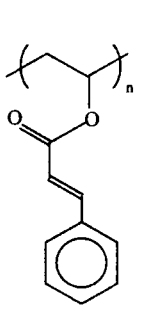

Poly (Vinyl Cinnamate)

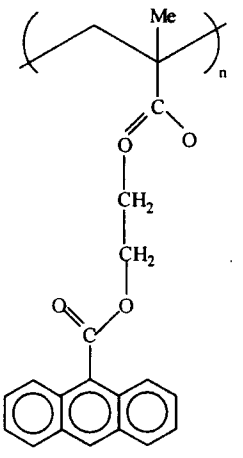

Poly (9-Anthracenoate Ethyl Methacrylate)

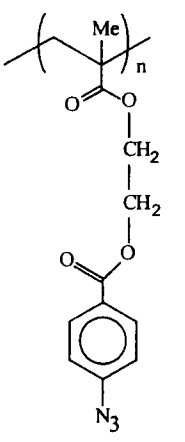

Poly (p-Azidobenzoate Ethyl Methacrylate)

Figure 2.1.1: Polymers Used in this Work.

2.2. Characterisation

NMR: Unless stated otherwise, NMR spectra were recorded using a 400 MHz spectrometer (^{1}H equivalence) at room temperature using deuterated chloroform as a solvent.

SEC: Molecular weight measurements were carried out using a Viscotek 200 differential refractometer/viscometer detector. The column set used was: Guard Column, PL Gel 5μm 100Å, PL Gel 5μm 1000Å, PL Gel 5μm 100 000Å. All samples were run at ambient temperature using filtered and degassed chloroform as the solvent.

DSC: Differential Scanning Calorimetry was carried out using a Perkin-Elmer DSC7 Differential Scanning Calorimeter.

2.3. Sample Preparation

It has been found necessary to use a range of substrates because of the variety of techniques applied. Thus for UV and birefringence studies, quartz plates (50mm x 20mm x 2mm) were used and for infrared studies, zinc selenide windows (30mm x 14mm x 4mm). Before use, the quartz slides were cleaned with acetone, dried, then immersed in chloroform in the ultrasonic bath for 30 minutes before a final drying. The ZnSe was thoroughly cleaned with hexane and dried before use. Solutions of the desired polymer (1% by weight) were prepared by dissolution in a 50:50 mixture of dichloromethane/chlorobenzene. This solution was then placed in a syringe fitted with a 2μm filter and 10 drops of the solution (7 drops when a ZnSe substrate was used) were filtered directly onto the centre of a clean substrate slide. The slide was then spun at circa 2000 rpm for 30 seconds to form a thin film with complete removal

of the solvent. Excess polymer solution on the underside of the slide was removed by wiping with methanol. Initially, slides prepared in this manner were then annealed under vacuum, above their T_g, for one hour to remove any stress or inherent orientation brought on by the spinning procedure. However, comparison of annealed and unannealed samples by both UV/Vis and birefringence studies revealed no differences. Therefore, unannealed samples were used in further studies. All samples were stored in darkness, at room temperature, until required.

After use, quartz slides were cleaned by immersion in chloroform followed by 30 minutes in the ultrasonic bath. They were then removed from the chloroform and wiped with a chloroform soaked optical tissue. When dry, the slides were wiped with an acetone soaked tissue. Before use the slides were placed under a stream of nitrogen to remove any dust particles present on the surface. If any marks were evident on the slide, spectroscopic grade methanol was used to remove them. In the case of the ZnSe substrate, the polymer film was removed using a hexane soaked cotton bud and then wiped with an optical tissue before drying with a nitrogen stream.

As the surface of the film is being analysed in all experiments and is important in bringing about liquid crystal alignment, all samples were handled by the edges whilst wearing gloves so as not to mark the polymer film. For the toxic ZnSe substrates, tweezers were used to pick up the slide.

2.4. Thickness Determination

2.4.1. X-Ray Reflectivity

Sample thickness' were determined using a Siemens D5000 X-ray Reflectometer in $\theta/2\theta$ mode.

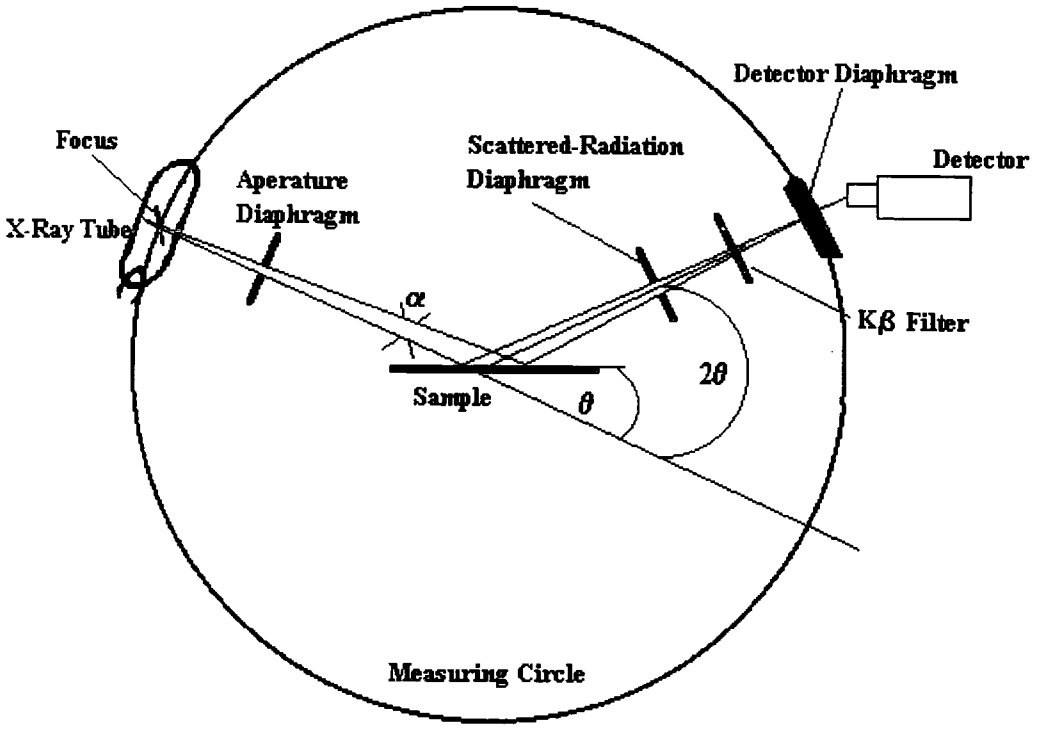

Figure 2.4.1.1: X-Ray Diffraction Stage.

For each specimen, the reflectivity profile was obtained by scanning a 2θ range from 0.2 - 4°, using a step size of 0.002°. Figure 2.4.1.2 shows a typical reflectivity profile.

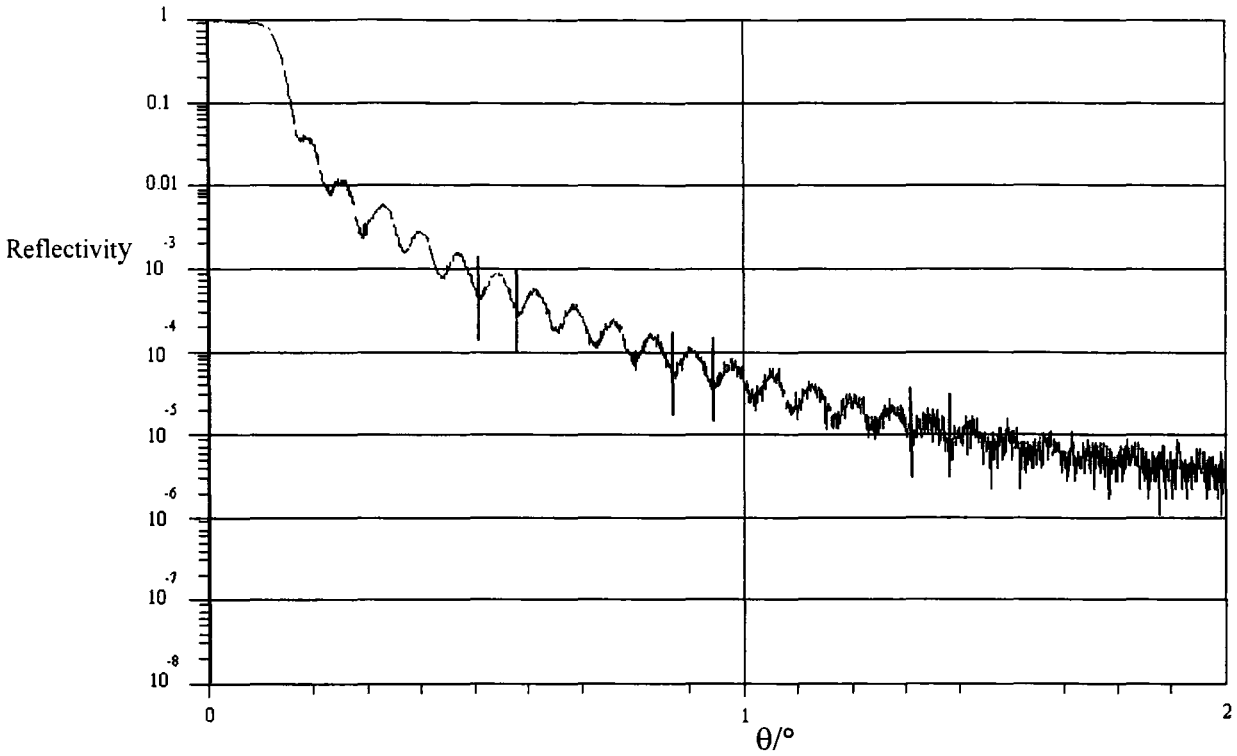

Figure 2.4.1.2: Example Reflectivity Profile of Polyanth on Quartz.

WIN-REFSIM Version 1.0 was used to perform the analysis. The sample thickness was determined in the following way [2]:

1) The fringes on the profile are observed due to the fact that at all angles of incidence greater than the critical edge, the X-ray beam is reflected and refracted. These two beams then have different path lengths, giving rise to the fringes. This can be exploited in that the difference between consecutive minima (indicated by the lines in Figure 2.4.1.2) can be used to calculate the film thickness.

2) The following equations are used to calculate film thickness:

$$d = \pi / \Delta k$$

where $\Delta k = (2 \pi / \lambda) \sin \theta$

For X-rays, λ = 1.54Å and θ is the angle between two adjacent minima. In practice, the difference between many minima are recorded and an average value

calculated. It was found that for the polymer systems studied, the film thickness remained constant, regardless of exposure time.

2.4.2. Surface Profiling.

Film thickness' were also measured using a surface profiling technique known as 'α-step'. For this technique, the surface of the polymer sample was scratched and a stylus draw across at a given pressure. Where the stylus crosses the scratch, a reduction in the line corresponding to the surface profile is observed. The depth is thus equivalent to the distance between the sample surface and the substrate below.

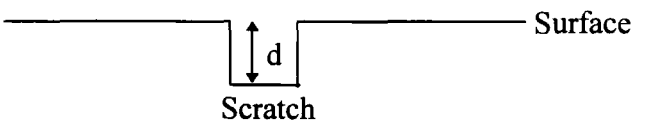

Figure 2.4.2.1: Side-on View of Sample Surface.

This technique, unlike X-ray reflectivity, is potentially destructive as a series of scratches across the sample is needed to achieve a representative sample thickness and thus can only be carried out when samples are no longer needed. Often, the sample thickness is needed before experiments are carried out as samples which are too thin (< 30 nm) are not used. Therefore, X-ray reflectivity is the preferred technique for establishing film thickness.

The sample thickness values achieved by X-ray and 'α-step' are in good agreement. To verify these results, neutron reflectivity measurements were carried out on three samples during a short visit to the Rutherford Appleton Laboratories in

Oxfordshire. This was a third method of determining sample thickness. It was found that the thickness' determined by all three methods showed good agreement (± 50 Å).

	X-Ray	Surface Profiling	Neutron
PVCi	560 Å	560 Å	610 Å
PVCi	520 Å	520 Å	560 Å
Polyanth	-	1400 Å	1450 Å

From these results, it is shown that sample thickness determined by X-ray reflectivity has an error in the region of 10%.

2.5. Sample Irradiation.

The radiation source used throughout the experiments carried out in Durham was an Ealing Deuterium Lamp (30W, 185-370 nm wavelength range). The spectral output of the lamp is shown in Figure 2.5.1.

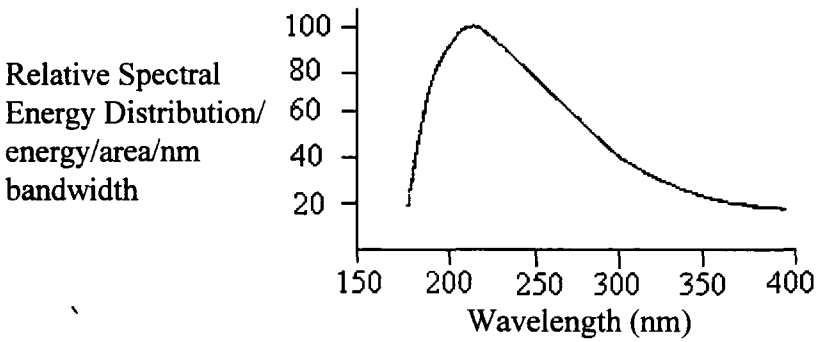

Figure 2.5.1: Spectral Range of the Deuterium Lamp.

Ideally, the light should have been monochromated by a filter to select light of wavelength λ~325 nm. This wavelength of radiation was chosen because it is removed from the absorption maximum of all polymers used. λ = 325 nm radiation is

still absorbed by the sample but at a much reduced intensity compared with λ = 280nm. Therefore, the absorbed radiation promotes reaction but does not cause considerable heating of the exposed area. A quartz lens was used to intensify the radiation incident on the sample. Comparison experiments show that the photon flux of the radiation was insufficient to promote reaction when such a filter was used. A sample of PVCi on a quartz substrate was exposed for 24 hours to unpolarised radiation, λ = 320 nm. There was no change in the UV absorption spectrum after this irradiation time. As experiments were to be carried out using polarised radiation, which further reduces the intensity of light incident on the sample, exposure times for a single measurement would have been on the scale of weeks. Consequently, all exposures were performed without using a band pass filter.

For polarised irradiation, a UV polariser was placed between the lamp and the sample, Figure 2.5.2.

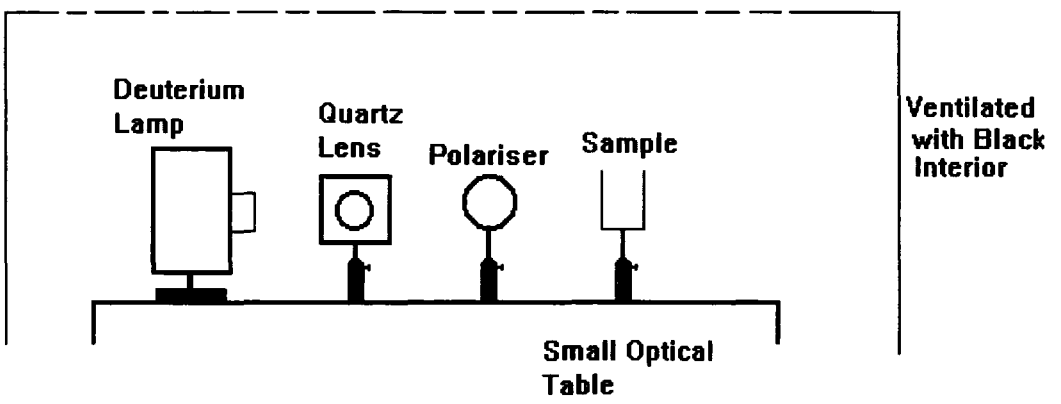

Figure 2.5.2: Exposure using the Deuterium Lamp.

The photon flux of the deuterium lamp was frequently measured using a known chemical actinometer, Aberchrome 540 [3]. As Aberchrome 540 is active only in the range 310-370nm, it is evident that the photon flux calculated from this actinometer will be lower than the actual photon flux. This is not ideal. However, a

monochromatic source is unavailable for these experiments and an actinometer covering the spectral range of the lamp could not be found. Therefore, an estimate of the photon flux must suffice and its deficiencies are duly noted.

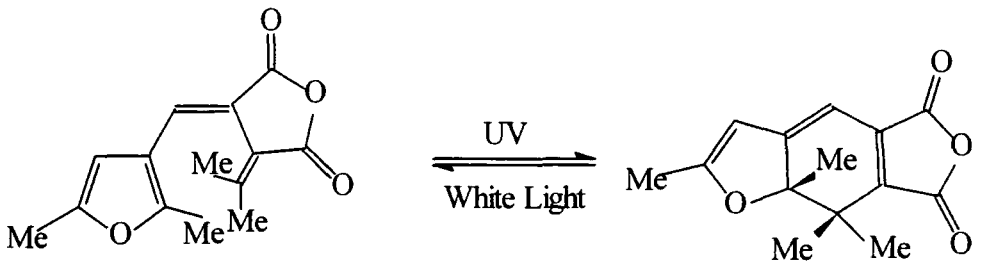

UV absorbance at 350 nm

UV absorbance at 494 nm

Figure 2.5.3: Aberchrome 540.

A known volume of Aberchrome 540 dissolved in toluene (~ 5×10^{-3} molar) was irradiated whilst being stirred for a given length of time. This promotes the formation of a molecule which absorbs at 494nm. Therefore, the reaction can be followed by monitoring the increase in absorption at this wavelength. The following equation was then used to calculate the photon flux.

$$I = \frac{A \times V \times N}{\phi_c \times \varepsilon \times t} \qquad \text{photon s}^{-1}$$

where A = the increase in absorbance at 494 nm.

V = the volume of solution irradiated (dm^{-3})

N = 6.023×10^{23} mol^{-1}

ϕ_c = 0.20 (310-370 nm)

ε = 8,200 dm^3 mol^{-1} cm^{-1} at 494 nm

t = time (s)

For irradiation experiments carried out at DRA (Malvern) a He-Cd laser (325nm, 1.01mW intensity through a 1mm aperture) was used as the source. The optical alignment varied slightly depending upon the experiment being performed. Figure 2.5.4 shows one of these alignments schematically. The optical alignment for birefringence measurements is described in section 2.8.3.

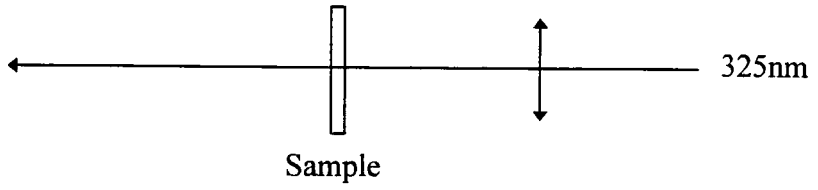

Figure 2.5.4: Irradiation using the He-Cd Laser.

2.6. UV-VIS Spectrometry [4, 5, 6, 7]

2.6.1. Theory

Photons from the UV and visible regions of the electromagnetic spectrum have sufficient energy to promote an electron of an organic molecule from the ground state to the excited state. The energy difference between these two states is quantised such that only a photon of precisely the right energy may be absorbed.

$$E = \frac{hc}{\lambda} \qquad (2.6.1.1)$$

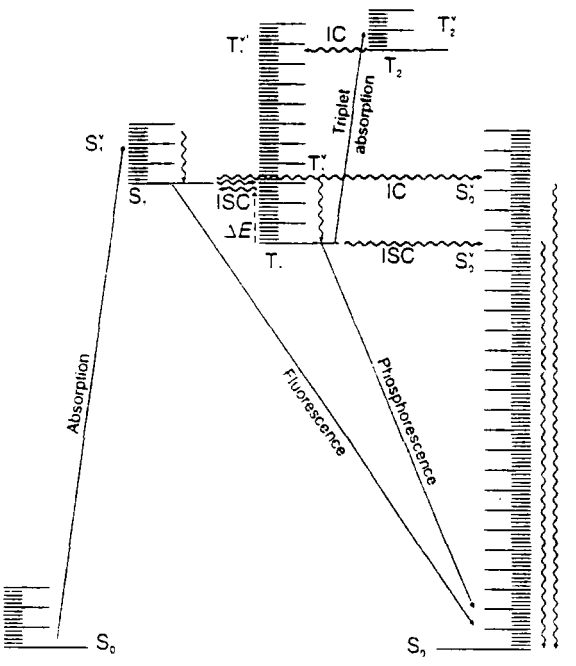

Figure 2.6.1.1 Schematic Diagram of Electronic, Vibrational and Rotational Transitions.

The Beer-Lambert Law for absorption of light states that the fraction of incident light absorbed is proportional to the number of molecules in its path i.e.

$$absorbance = \log_{10}\frac{I_o}{I_t} = \varepsilon c l \qquad (2.6.1.2)$$

where ε is the molar decadic extinction coefficient and c is the concentration of absorbing species (mol dm^{-3}).

Although an electronic transition may be energetically favourable, the associated band may not be observed or else be very weak. This is due to certain transitions being forbidden due to poor orbital overlap. However, forbidden transitions are observed as molecular vibrations distort the structure of the molecule and hence change the relative positions of the molecular orbitals.

UV absorption spectra are not observed as sharp peaks but as much broader bands. This arises from the inability to separate the bands due to rotational and vibrational transitions.

2.6.2. UV/Vis Spectroscopy Experiment

All UV spectra were recorded using either a Unicam UV2 Spectrometer or a Perkin Elmer Lambda 9 Spectrometer.

The absorption spectrum of a sample of known thickness was recorded prior to exposure. The desired wavelength range was selected and a background spectrum was run for each sample. To produce the sample spectrum, a bare substrate was placed in the reference beam and coated substrate in the sample beam. Following exposure for a given time interval, the spectrum was re-recorded. The decay of the absorption peak due to the UV active chromophore was monitored.

2.6.3. Calculation of the Quantum Yield of Cross-Linking

The definition of quantum yield is the number of molecules of reactant consumed for each photon of light absorbed [6]. In this form, the quantum yield represents the efficiency of the primary photochemical process in bringing about chemical change and also the extent of a secondary reaction. A quantum yield greater than unity suggests the occurrence of secondary reactions since the Stark-Einstein law[a] indicates that not more than one molecule can be decomposed in the primary step. Chemical change is not the only consequence of absorption of radiation; a chain reaction may be taking place in a photochemical reaction even though the quantum yield is less than one.

---

[a] ' If a species absorbs radiation, then one particle is excited for each quantum of radiation absorbed.'

The determination of overall quantum yield for a chemical change requires measurement of the numbers of molecules of reactant consumed, or of product formed, and of the number of quanta of radiation absorbed. In systems where the reacting species is UV active, consumption of the starting material can be monitored using UV spectroscopy.

Since I_o can be measured using chemical actinometry, section 2.5, the intensity (310-370nm) absorbed by the sample, I_a, can be calculated

$$I_a = \left(1 - 10^{-A_0}\right) I_o \qquad (2.6.3.1)$$

where A_0 is the absorbance before irradiation.

Using the UV absorption spectrum, the concentration of chromophores can be calculated from the Beer-Lambert law ($c = A/\varepsilon \times l$) and hence the number of chromophores remaining can be determined. Having both the intensity of the absorbed radiation and the number of molecules reacted, the quantum yield can be calculated.

It must be stated at this point that the quantum yields calculated this way in this project cannot be described as true quantum yields. This is due to the unavoidable inaccuracies incurred in the measurement of I_o as described in section 2.5. Due to this fact, I_a will be calculated to be much lower than its actual value, leading to higher values of quantum yields. It would be inappropriate to comment on differing values of quantum yield between the polymer systems as these values are known to be inaccurate. However, the trends occurring within and between samples of the same polymer remain valid and can be discussed.

2.6.4. Calculation of the Extinction Coefficient (ε)

The Beer-Lambert Law states

$$Absorbance = \varepsilon\, c\, l$$

where ε is the molar decadic extinction coefficient

c is the concentration (mol dm^{-3})

l is the pathlength

For many polymer samples, ε is already known. For new polymers, or those with ε not yet published, ε must be calculated using the Beer-Lambert equation.

For Poly (Vinyl Cinnamate), the extinction coefficient, at 278nm, for an unknown mixture of cis and trans isomers, was calculated to be **1.53×10^4 cm^{-1} mol^{-1} L**, Figure 2.6.4.1. The literature values for the individual isomers are as follows [8]: **1.2×10^4 cm^{-1} mol^{-1} L** (cis isomer) and **2.12×10^4 cm^{-1} mol^{-1} L** (trans isomer)[1]. Therefore, for a 50:50 mixture of the two isomers, a value of **1.6×10^4 cm^{-1} mol^{-1} L** would be expected. This value compares well with the experimentally determined value for the PVCi used in these experiments.

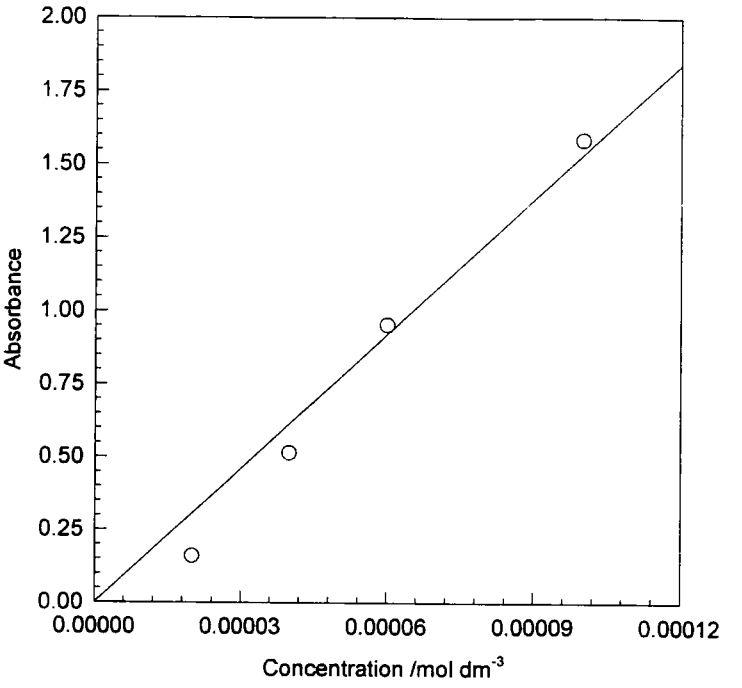

Figure 2.6.4.1: Plot to Calculate ε for PVCi.

This procedure was repeated for the Poly(9-anthracenoate ethyl methacrylate) leading to an extinction coefficient of **1.2 × 10^4 cm^{-1} mol^{-1} L** and for Poly (p-azidobenzoate ethyl methacrylate), **1.1 × 10^4 cm^{-1} mol^{-1} L** , both at λ_{max} = 278nm. As these polymers have not been previously synthesised, extinction coefficients are not available for comparison.

2.7. Infrared Spectroscopy [9-14]

2.7.1. General Infrared Theory

At ambient temperatures, the bonds of a molecule are permanently vibrating. Energy is absorbed according to quantum rules i.e. energy is not absorbed continuously but only at discrete frequencies, hence the occurrence of peaks in the absorption spectrum. When absorption occurs, the ground state rotational and vibrational energy levels are changed. The change in rotational energy is very small and therefore, the observed spectra can be considered as a measure of the vibrational modes of energy absorption of the molecule.

In a simple diatomic molecule, the only vibration that can occur is stretching along the bond.

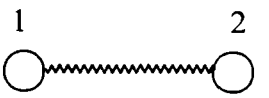

The force required to stretch the bond is given by Hooke's Law

$$F = k\,d \qquad (2.7.1.1)$$

where F is the applied force, k is the force constant and d is the distance. The vibrational frequency for this stretching is given by

$$\bar{\upsilon} = \frac{1}{2\pi c}\left(\frac{k}{\mu}\right)^{1/2} \qquad (2.7.1.2)$$

where μ is the reduced mass of the system, $\frac{m_1 m_2}{m_1 + m_2}$.

The frequency of the absorbed infrared can thus be related to the force needed to stretch the bond between atoms 1 and 2. This frequency remains constant,

irrespective of the type of molecule atoms 1 and 2 are in, allowing the production of group frequency tables which assist in the assignment of peaks in an IR spectrum.

For large molecules, there are many bonds and thus many potential IR absorbance frequencies. However, not all bond vibrations are observed in an IR spectrum as a change in dipole moment of the molecule must occur during the vibration if the mode is to be IR active. Consider CO_2

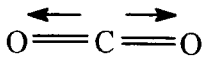

Symmetric Stretch **IR Inactive**

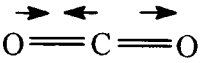

Asymmetric Stretch **IR Active**

Figure 2.7.1.1: IR Vibrations in CO_2.

IR absorption will only occur for unsymmetrical vibrations such as the asymmetric stretch shown for CO_2 or when a symmetric group is asymmetrically substituted e.g. Ph-N=N=N.

Stretching is not the only vibrational motion available to a bond, bending, wagging, twisting and rocking all contribute to the vibrational spectra. The transition moment (direction of change in the dipole moment) associated with a particular vibration lies at some angle with respect to a given direction in the molecule. This characteristic of directionality can be utilised in structure determination.

The transition moment is a vector and thus has magnitude and direction. The intensity of the IR absorption depends upon the angle the electric vector of the incident radiation makes with the transition moment. The intensity is proportional to the square of the scalar product of the transition moment and electric field vectors.

The absorption coefficient k for a particular direction of the incident electric field vector E_o may be written as Equ (2.7.1.3)

$$k = P^2 \sum_i \cos^2 \Psi_i \qquad (2.7.1.3)$$

where ψ_I is the angle between the transition moment direction of the ith absorbing centre and the direction of the electric vector; P is the magnitude of a vector and the summation extends throughout the unit volume of the specimen. Equation 2.7.1.3 forms the basis for the use of polarised IR spectroscopy in the study of oriented polymers.

2.7.2. Infrared Dichroism

When a polymer is stretched in one direction, it becomes uniaxially oriented, the principal axes of the refractive index are directed parallel and perpendicular to the stretch (orientation) direction. When the incident radiation has its electric vector parallel to the principal axis, there will be no observable change in the resulting spectrum when compared to the unpolarised spectrum. Therefore, measurements must be made with the electric vector of the incoming infrared parallel and perpendicular to the orientation axis. To interpret the optical anisotropy of the sample in terms of molecular orientation, the dichroic ratio is used. The dichroic ratio, D, of an absorption band is defined as the ratio of integrated intensities measured with light polarised parallel and perpendicular to a given direction e.g. the orientation axis.

$$D = \frac{k_\pi}{k_\sigma} \qquad (2.7.2.1)$$

where k_π and k_σ are the principle absorption coefficients for radiation vibrating parallel and perpendicular to the orientation axis respectively.

What is experimentally measured is D'

$$D' = \frac{\varepsilon_\pi}{\varepsilon_\sigma} \qquad (2.7.2.2)$$

where ε_π and ε_σ are absorbances parallel and perpendicular to the orientation axis. D' is equal to D if there are no scattering or reflection losses.

The relationship between the infrared dichroic ratio and molecular orientation was obtained by Fraser [14]. He considered a fibre where all the polymer chains were oriented parallel to the fibre axis.

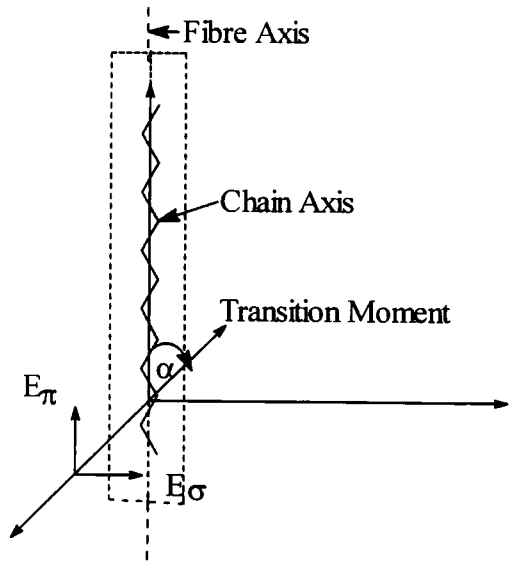

Figure 2.7.2.1: Schematic Representation of Perfect Orientation Parameters[1]

For this ideal system, ε_π is parallel to the polymer chain as well as to the fibre axis and therefore ψ will be equal to α_v.

From Equ (2.7.1.3)

$$k_\pi = NP^2 \cos^2 \alpha_v \qquad (2.7.2.3)$$

where N is the number of absorbing centres per unit volume and α_v is the transition moment angle for centres absorbing radiation of frequency ν.

For the perpendicular vector

$$k_\sigma = \frac{1}{2} NP^2 \sin^2 \alpha_\upsilon \qquad (2.7.2.4)$$

Therefore, for perfect alignment of molecules parallel to the fibre axis, the dichroic ratio is

$$D_o = \frac{k_\pi}{k_\sigma} = 2\cot^2 \alpha_v \qquad (2.7.2.5)$$

If all of the molecules are randomly oriented in a film or fibre

$$k_\pi = k_\sigma = \frac{1}{3} NP^2 \qquad (2.7.2.6)$$

and thus

$$D = \frac{k_\pi}{k_\sigma} = 1.0 \qquad (2.7.2.7)$$

In a real polymer film or fibre, the molecules are only partially oriented, therefore it is necessary to have some measure of the degree of orientation of the molecules relative to the orientation axis. Fraser proposed two solutions to this problem:

The first is to imagine the oriented sample as consisting of *f* perfectly oriented molecules and (1-*f*) randomly oriented molecules. Therefore,

$$k_\pi = NP^2\left[f\cos^2 \alpha_\upsilon + \frac{1}{3}(1-f)\right] \qquad (2.7.2.8)$$

and $$k_\sigma = NP^2\left[\frac{1}{2}f\sin^2\alpha_\upsilon + \frac{1}{3}(1-f)\right] \qquad (2.7.2.9)$$

This gives rise to a dichroic ratio, D

$$D = \frac{1+\frac{1}{3}(D_o-1)(1+2f)}{1+\frac{1}{3}(D_o-1)(1-f)} \qquad (2.7.2.10)$$

Thus

$$f = \frac{(D-1)(D_o+2)}{(D+2)(D_o-1)} \qquad (2.7.2.11)$$

However, although the fraction of oriented chains is constant, that constant is unknown. Therefore there is a problem in that there is one equation with two unknowns. To use this equation, assumptions have to be made by using molecular models or comparing transition moments in structurally similar compounds or giving f an approximate value. Using this assumed value of α_v and the measured value of D, f can be calculated. This value of f is then used in the same equation to calculate α_v from measured D values at other observed absorption frequencies. This will obviously give rise to many questionable assumptions and the value of f, and therefore α_v , obtained is an estimate.

In the second instance, the molecules can be considered to be oriented at an average angle θ relative to the orientation direction.

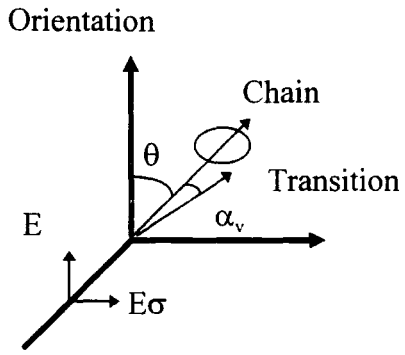

Figure 2.7.2.2: Schematic Representation of Uniaxial Orientation Parameters[1]

The dichroic ratio for this model is then given by

$$D = \frac{1+(D_o-1)\cos^2\theta}{1+\frac{1}{2}(D_o-1)\sin^2\theta} \qquad (2.7.2.12)$$

The relationship between f of the first model and θ of this model leads to

$$\frac{3\cos^2\theta-1}{2} = \frac{(D-1)(D_o+2)}{(D+2)(D_o-1)} = f \qquad (2.7.2.13)$$

Thus Fraser's fraction, f, is the same as Hermans orientation function

($f_x = \frac{3}{2}\cos^2 x$-1) when evaluated in terms of the average orientation of polymer molecules.

Hermans orientation function can be determined quantitatively by birefringence measurements. When coupled with dichroic measurements of the appropriate absorption bands, quantitative values for the transition moment angle can be calculated with no approximations or assumptions required.

2.7.3. Infrared Spectroscopy Experiment

Values of the dichroic ratio were obtained by transmission infrared spectroscopy. Samples were spin coated onto a ZnSe substrate, as described in Section 2.3 and the spectra recorded using a Perkin-Elmer 1720X Fourier Transform Infrared Spectrometer with a nitrogen cooled MCT detector. The beam was attenuated such that 6% of the total energy of the beam was incident on the sample. The experimental set-up can be seen in Figure 2.7.3.1.

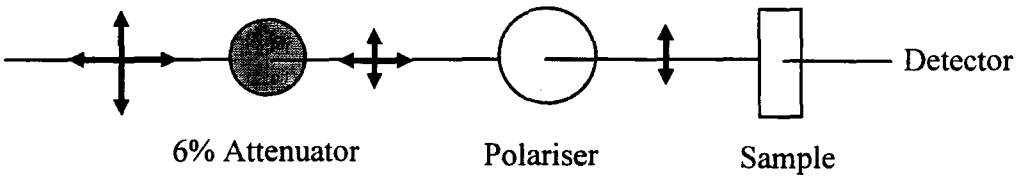

Figure 2.7.3.1: FTIR Experiment.

To obtain the sample spectra using polarised radiation, the polariser remained stationary whilst the sample was rotated. This minimised any errors incurred due to mispositioning of the polariser.

A background spectrum, using a bare ZnSe crystal, was recorded using the parameters of weak apodisation and 100 scans. The bare crystal was then replaced by the polymer coated ZnSe crystal and the spectrum recorded using the same parameters as for the background spectrum.

An example of the spectrum of an unexposed sample of PVCi on a ZnSe substrate can be seen in Figure 2.7.3.2.

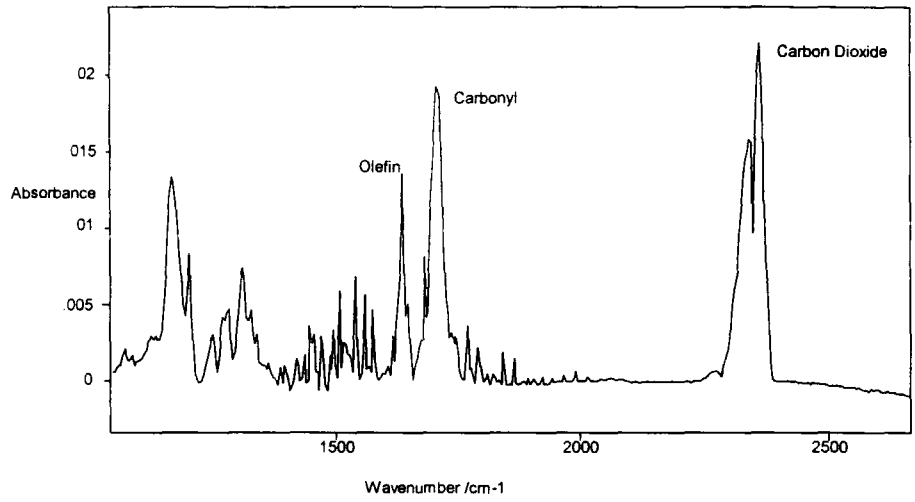

Horizontally Polarised Incident IR

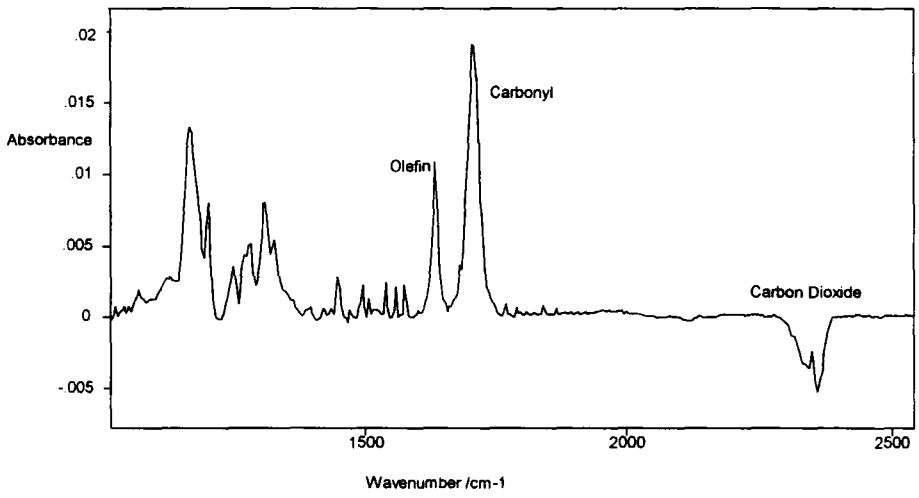

Vertically Polarised Incident IR

Figure 2.7.3.2: FTIR Spectrum of Unexposed PVCi on ZnSe.

Unexposed sample spectra were recorded using unpolarised, horizontally polarised and vertically polarised IR radiation.

Although great care was taken regarding the positioning of the sample, it was unlikely that the sample was placed in exactly the same position each time. Therefore, spectra were recorded with the ZnSe substrate in slightly varying position with respect to the incoming IR beam. This allowed the effect of sample position upon resulting spectra to be obtained. It was shown that varying the sample position gave rise to no detectable change in the absorption spectra of the film. This is reassuring from an experimental viewpoint and also shows that the film is uniform over the area analysed.

The sample was then exposed to radiation from a deuterium lamp (30W, 185-370 nm wavelength range) for a given length of time. Spectra were then re-recorded and the procedure repeated until no further change in the spectra occurred or the peaks were no longer detectable.

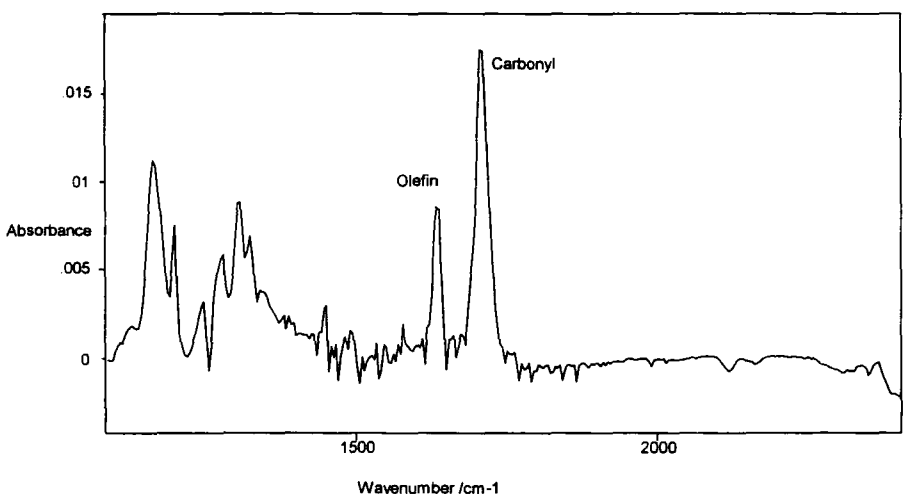

Horizontally Polarised Incident IR

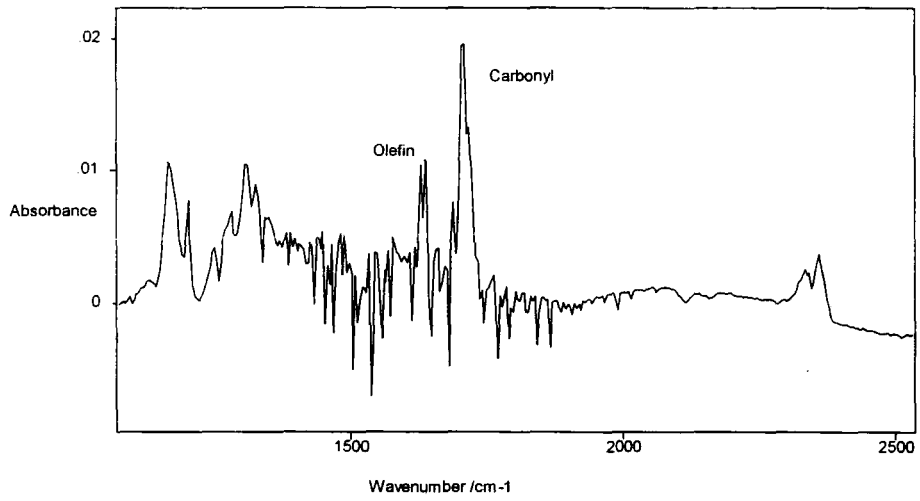

Vertically Polarised Incident IR

Figure 2.7.3.3: FTIR Spectrum of PVCi Exposed for 21 hours to Horizontally Polarised Radiation from the Deuterium Lamp.

The spectra were then analysed using a curve fitting routine within GRAMS 32c (Galactic Industries). The region containing the olefin and carbonyl peaks was selected. Suitable starting parameters were input into the program which were automatically adjusted until the simulated spectrum is consistent with the experimental spectrum. To ensure that the results were comparable, a protocol was set up such that the analysed region spanned the same wavenumber range each time including a definite zero offset for each spectrum.

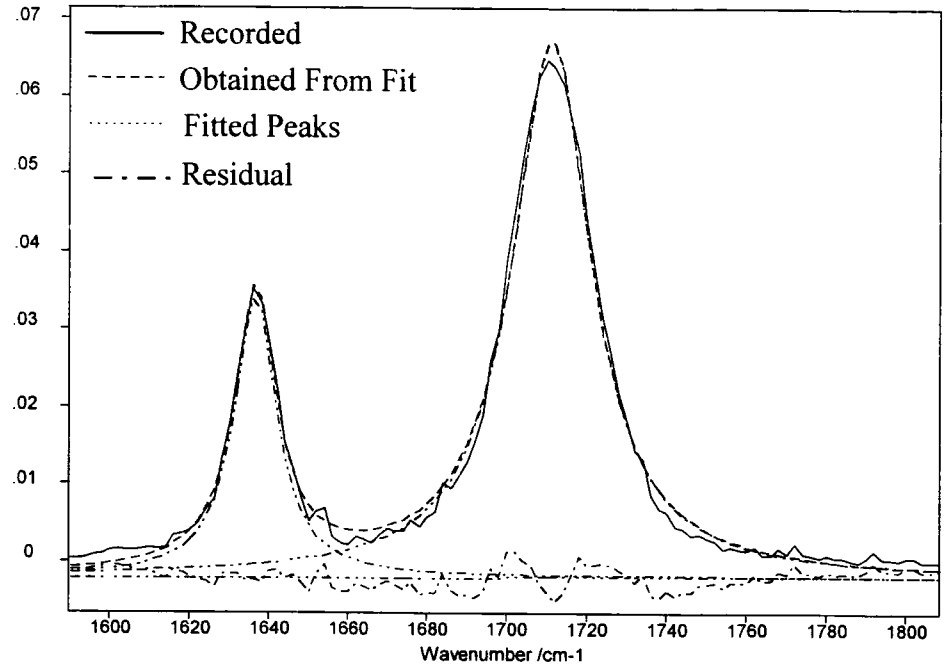

Figure 2.7.3.4: Curve-Fitted Region of PVCi Spectrum.

The areas under the peaks can then be used to calculate the dichroic ratio via

$$Dichroic\ Ratio = \frac{Abs\,(parallel)}{Abs\,(perpendicular)}$$

For the spectra shown in Figure 2.7.3.2 & Figure 2.7.3.3, the dichroic ratio before exposure, analysing the C=C area, is 0.85 and after 21 hours exposure to vertically polarised radiation from the deuterium lamp, 1.22.

2.8. Birefringence Measurements [15-18]

2.8.1. General Theory

Birefringence is a measure of the total molecular orientation of a system. For uniaxial orientation, it is the difference between the principal refractive indices parallel and perpendicular to a given direction.

$$\Delta n = n_{para} - n_{perp}$$

where Δn is the birefringence and n_{para} is the principal refractive index parallel to the orientation direction and n_{perp} is the principal refractive index perpendicular to the orientation direction.

The refractive index is defined as a measure of the velocity of light in a medium and is related to chain polarizability. Generally, the polarizability of chemical bonds is anisotropic i.e. greater along the bond than it is 90° to it. If all of the bonds are distributed randomly, this leads to an isotropic refractive index and there is no birefringence. If a film is uniaxially oriented, the chain axis of the molecules orients along a given direction e.g. the deformation axis, and the molecules have cylindrical symmetry around this axis. Since the optically anisotropic molecules now have a preferred direction, the film now manifests anisotropic optical properties. The principal refractive index for the light vibrating in the orientation direction is different from that for light having its electrical vibration in the plane perpendicular to the orientation direction. Birefringence arises from this difference in refractive indices. The magnitude of the birefringence is related to the magnitude of the difference between the two principal refractive indices and is therefore a measure of the degree of orientation in a sample. As the extent of orientation increases, the difference

between the principal refractive indices increases thus giving rise to an increase in birefringence.

2.8.2. Theory Behind the Crossed-Polarisers Experiment

This experiment consists of a polarised He-Ne laser, two crossed polarisers between which the sample is placed and a detector.

Consider a sample which is isotropic and thus is not birefringent. The laser intensity monitored at the detector is zero as the polarisers are extinct and the sample has no effect on the light travelling through it. If a birefringent sample is placed between the polarisers, the intensity of the detected light is dependent upon the angle the optical axis makes with the two polarisers. This is illustrated in figure 2.8.2.1.

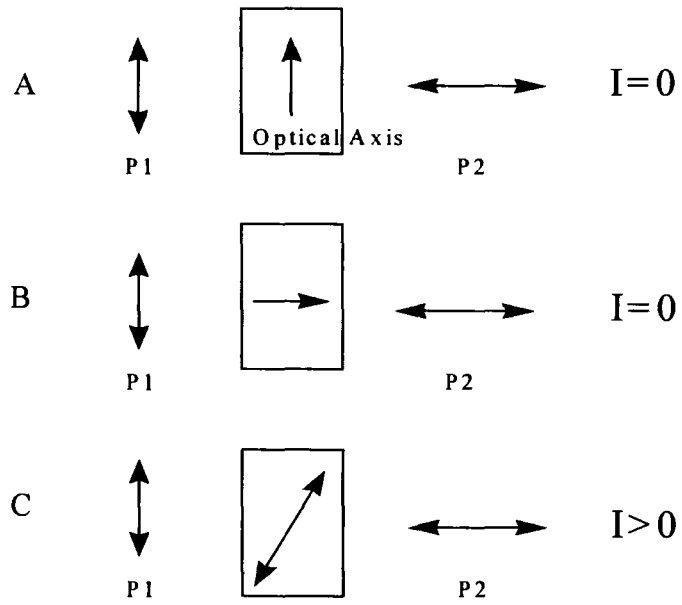

Figure 2.8.2.1: Alignment of Polarisers and Sample Optical Axis.

In A, the optical axis of the sample is parallel to the polarisation vector of the incoming radiation. This causes motion of the electrons along the optical axis and the

radiation is re-emitted as vertically polarised. This polarisation orientation cannot pass through the second polariser and therefore no light falls onto the detector.

In B, the polarisation vector of the incoming radiation and the optical axis of the sample are perpendicular. The electrons want to move along the optical axis, however, there is no component of the incident light which allows this to occur. Motion occurs perpendicular to the optical axis and once again, the light is re-emitted as vertically polarised and I=0.

In C, the optical axis lies at some angle with respect to the incoming vertically polarised light. The vector describing the polarisation of the light can be resolved into two orthogonal components.

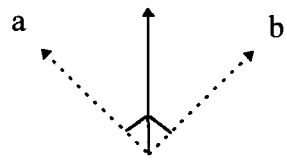

Component b gives rise to electronic motion along the optical axis of the sample. This too can be resolved into its constituent components.

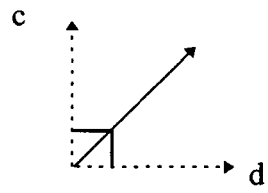

Component d is oriented such that it can pass through the output polariser and thus I>0.

When the light falls onto the sample it is linearly polarised. However, when it propagates through the sample, the polarizability of the oriented molecules effects components c and d. These waves become out of phase, one travelling faster than the

other. As the light emerges from the sample, it is no longer linearly polarised but it is elliptically polarised. The exact state of the ellipse depends upon the phase difference between the two waves as illustrated in Figure 2.8.2.2.

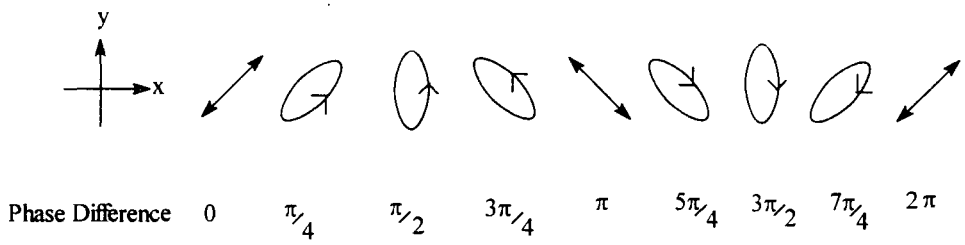

Figure 2.8.2.2: State of Polarisation Achieved with Varying Phase Differences Between Waves.

The ellipse can be resolved into two orthogonal components with varying magnitudes, one of which can pass through the second polariser. This is the basis of the crossed polarisers experiment described in section 2.8.3.

2.8.3. Birefringence Experiment [15]

All birefringence measurements were carried out at DRA Malvern. The experimental design is shown schematically in Figure 2.8.3.1.

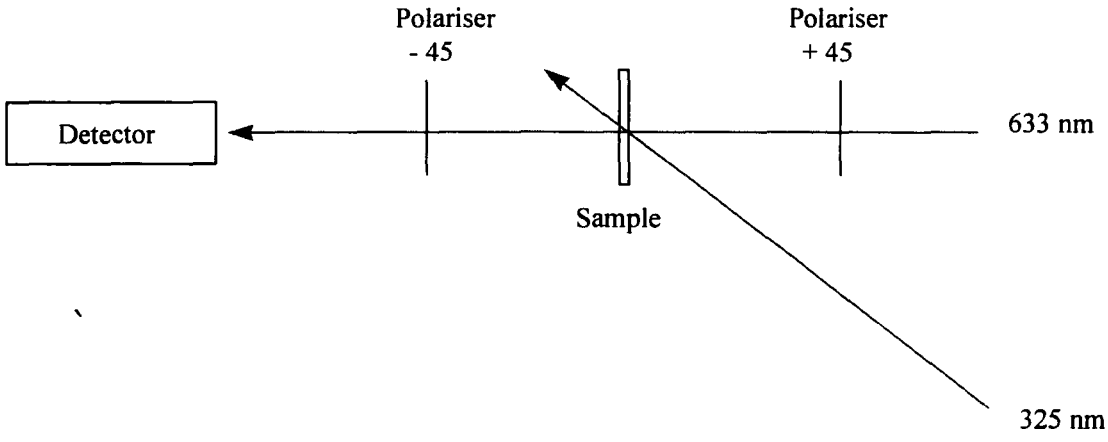

Figure 2.8.3.1: Optical Design for Birefringence Measurements.

The technique is described as 'pump-probe': He-Cd provides the exposing radiation whilst the He-Ne simultaneously probes the reaction. The polarised He-Ne radiation passes through the polariser and falls upon the sample. The He-Cd beam is aligned to fall upon the sample in exactly the same place but is set at an angle with respect to the sample, ensuring the laser radiation does not fall upon the detector. The He-Ne beam diameter is slightly greater than that of the He-Cd to ensure that the whole of the sample area has been exposed. When the He-Ne beam leaves the sample, it passes through the analyser to the detector which monitors the change in intensity. Measurement of I allows Δn to be calculated from the following equation.

$$I = I_o \sin^2\left(\frac{\pi \Delta n d}{\lambda}\right) \qquad (2.8.3.1)$$

where λ is the probing wavelength

Δn is the birefringence

d is the sample thickness

I_o is the intensity measured with parallel polarisers and an unexposed sample

The films were sampled at various positions on the slide, Figure 2.8.3.2, giving birefringence results across the whole of the sample. This will be a good indication of the uniformity of the film.

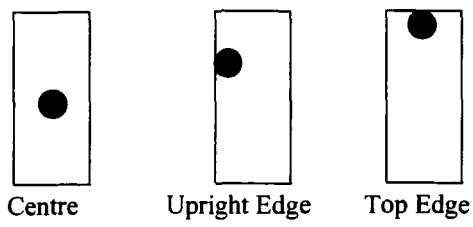

Figure 2.8.3.2: Sample Positions for Birefringence Measurements.

As the population of reactive species in a given orientation decreases, the birefringence increases. This is due to increased differences between the two principal refractive indices in the sample leading to differing polarizabilities in these two directions.

2.8.4. Compensator Method to Measure Birefringence

An experimental procedure for determining birefringence was set up in Durham, Figure 2.8.4.1. Retardation (phase difference between two orthogonal waves) induced in the sample due to photocross-linking was measured using a Soleil Babinet Compensator.

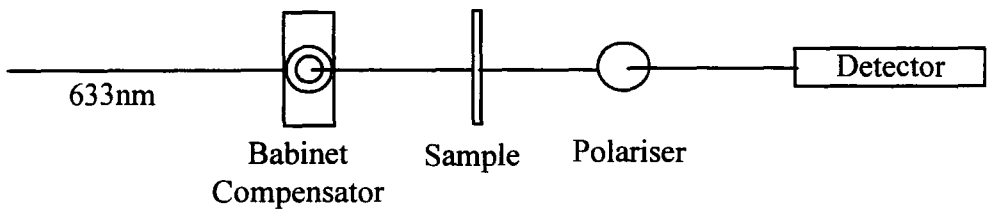

Figure 2.8.4.1: Experimental Set-up for Measuring Retardation.

Equation 2.8.4.1 is then used to determine the birefringence from the measured retardation.

$$\Delta n = \frac{\lambda R}{t} \qquad \text{Equ (2.8.4.1)}$$

where Δn is the birefringence

λ is the laser wavelength (633 nm)

R is the measured retardation

t is the sample thickness (thickness of sample and substrate in this instance)

The initial retardation of a film of PVCi on a quartz substrate was measured. This sample was then exposed to vertically polarised radiation from the deuterium lamp and the retardation was once again measured. Exposure was continued until no further change in retardation was observed.

The retardation of several bare quartz slides was measured to assess any contribution to R from the slide. A average value of R=17.51 was measured giving rise to a birefringence value of 2.2×10^{-4} due to the substrate. Consequently, this value was subtracted from all calculated birefringence values.

2.9. Laboratory Fabrication of a LCD Cell

A sample of polymer on a quartz substrate was exposed to the UV laser. Due to the small spot size of the laser, several spots on one sample can be exposed for varying times. Figure 2.9.1 shows an example of a such a slide.

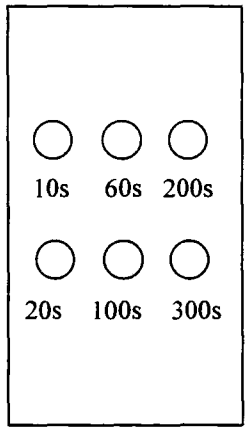

Figure 2.9.1: Sample Slide for LCD Fabrication.

The direction in which the polymer will orient the liquid crystals must be determined. For PVCi and polyanth, the cinnamate side chains and anthracene moieties parallel to the polarisation vector of the incoming UV radiation cross-link.

The residual cinnamates are thought to be responsible for the liquid crystal alignment as are the residual anthracene species. In the case of the azide system the azo-containing side chains lying parallel to the incoming polarisation vector react. However, it is the azobenzene species which is hoped to give alignment and not the residual azides. Using vertically polarised radiation and presuming all reactions occur as desired, the aligning species in PVCi and polyanth are perpendicular to the polarisation direction, whereas in polyazide, the aligning species is parallel to the polarisation direction of the incoming radiation.

A glass slide with mechanically rubbed polyimide (PI) is used in conjunction with the quartz slide to fabricate the cell. The polyimide rubbing direction is positioned perpendicular to the polymer alignment direction. This allows the formation of a twisted display, shown schematically in Figure 2.9.2. Glue containing 10 μm spacer beads is placed on the polymer sample slide such that its position coincides with the corners of the rubbed PI slide. The two slides are joined and any observed fringes are removed by pressing gently on the corners of the PI slide. Curing of the glue is achieved by placing the slide on a black surface under a Hg-lamp for 30 minutes. During this time, the irradiated portion of the sample is masked to prevent additional reaction due to radiation from the Hg-lamp. Once the glue has set, the liquid crystal can be introduced into the cell. The cell is placed on a hot plate at ~70°C and allowed to reach that temperature. When hot, the liquid crystal (E7 or 5CB) is introduced into the cell by letting a small amount flow from a pipette into the cell via one of the edges. This is possible as the liquid crystal is above its clearing temperature of 58°C. When the liquid crystal has filled the cell, the hot plate is

switched off and the cell allowed to cool to room temperature. The cell can be observed using a polarising microscope with crossed polarisers.

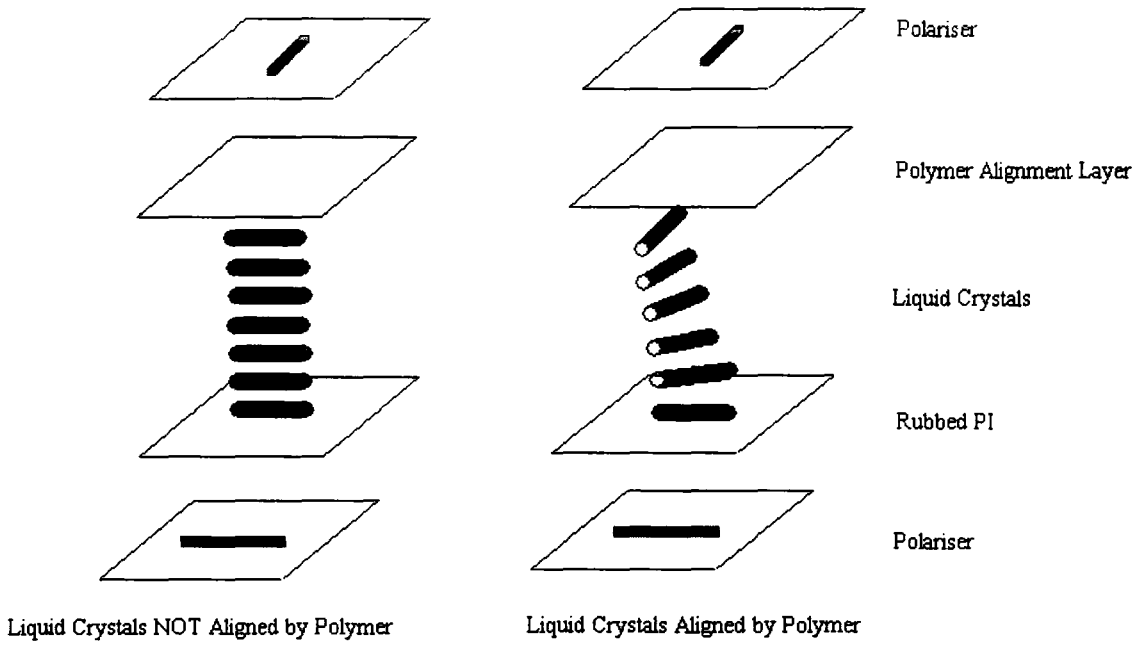

Figure 2.9.2: Twisted Liquid Crystal Display.

With the polarisers crossed and no sample cell in between, a black image is observed as no light is allowed through. The liquid crystal display cell is now placed on the stage, between the crossed polarisers. If the image is black, the passage of light passing through the first polariser and then through the sample has been blocked by the second, crossed polariser. However, if the liquid crystals are aligned by the polymer layer and the PI layer, then they form a twisted configuration. This configuration acts as a wave-guide and consequently, the polarisation vector of the light twists as it passes through the cell and a bright white spot is observed.

References

1) K.E.Foster, PhD Thesis, University of Durham 1997.

2) T.P.Russell, *Mater.Sci.Rep*, 1990, **5**, 171.

3) V.Wintgens, L.J.Johnston & J.C.Scaiano, *J.Am.Chem.Soc.*,1988, **110**, 511.

4) H.H.Jaffe & M.Orchin, Theory and Applications of Ultraviolet Spectroscopy, Wiley 1962.

5) D.W.Brown, A.J.Floyd & M.Sainsbury, Organic Spectroscopy, Wiley 1988.

6) R.P.Wayne, Principles and Applications of Photochemistry, Oxford University, Press 1988.

7) N.J.Turro, Modern Molecular Photochemistry, University Science Books 1991.

8) J.Rennert, S.Soloway, I.Waltcher & B.Leong, *J.Am.Chem.Soc*, 1972, 7242.

9) J.L.Koenig, Spectroscopy of Polymers, ACS 1991.

10) H.W.Siesler & K.Holland-Moritz, Infrared and Raman Spectroscopy of Polymers, M.Dekker, New York 1980.

11) R.Zbinden, Infrared Spectroscopy of Polymers, Academic Press 1964

12) .J.Vij, A.Kocot, G.Kruk & R.Wrzalik, *Mol.Cryst.Liq.Cryst.,* 1993, **237**, 337.

13) Y.Zhao & H.Lei, *Polymer,* **35**(7), 1994, 1419.

14) R.J.Samuels, Structured Polymer Properties, Wiley.

15) G.P.Bryan-Brown & I.C.Sage, *Liquid Crystals*, 1996, **20**(6), 825.

16) D.Campbell & J.R.White, Polymer Characterisation Physical Techniques, Chapman & Hall 1991.

17) E.Hecht & A.Zajac, Optics, Addison-Wesley 1974.

18) G.H.Meeton, Optical Properties of Polymers, Elsevier Applied Science 1986.

Chapter Three

Poly (Vinyl Cinnamate)

3. Poly (Vinyl Cinnamate)

3.1. Introduction

Dimerisation of cinnamic acid under the influence of ultraviolet light was first reported in 1895 by Berthram & Kursten[1]. Two carbon double bonds add to one another and, due to the unsymmetrical structure of cinnamic acid, two products are obtained, Figure 3.1.1.

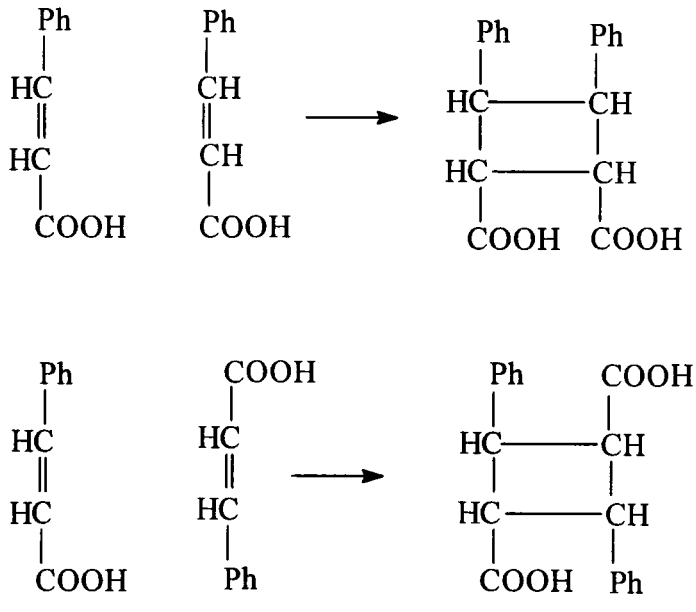

Figure 3.1.1: Cross-Link Formation in Cinnamic Acid.

The Kodak Photoresist (KPR) is based on this principle[2]. Cinnamic acid is a pendant group on a polymer chain, poly vinyl cinnamate or some derivative, and when this was coated onto a plate and dried, the coating became insoluble in the areas exposed to UV radiation. During the development procedure, the non-exposed regions of the sample were removed with solvent, leaving behind a resist pattern which was tightly adhered to the substrate below.

Poly (vinyl cinnamate), PVCi, is prepared from vinyl acetate which is first converted to poly vinyl acetate and subsequently hydrolysed to poly vinyl alcohol[3], as the vinyl alcohol monomer does not exist in the free state. This then undergoes reaction with cinnamoyl chloride to give the desired product. PVCi and its reactions under the influence of UV light have been studied extensively.

In 1979, Reiser & Egerton[3] investigated the mechanism of cross-link formation in solid PVCi.

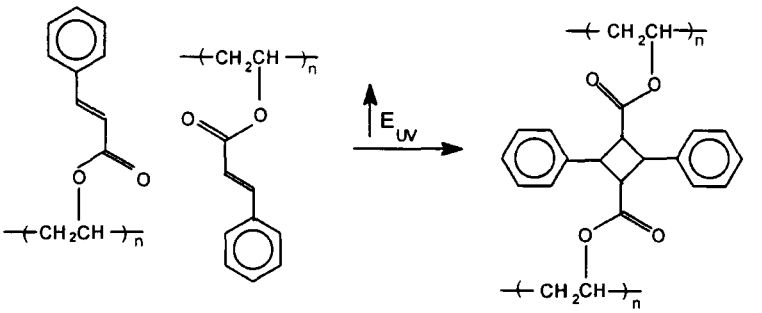

Figure 3.1.2: Cross-Link Formation in PVCi.

Formation of cross-links occurs via a [2+2] cycloaddition reaction across the carbon-carbon double bonds in two favourably oriented cinnamate side-chains. [2+2] cycloaddition reactions are stereospecific and may proceed via one of two possible pathways[4]:

1) Concerted addition of the excited S_1 (π, π^*) state to a molecule in the ground state.

2) Formation of a singlet exciplex by interaction of S_1 (π, π^*) and the ground state species followed by direct collapse to the cycloadduct or by collapse to a singlet 1, 4-diradical which collapses to the cycloadduct faster than it loses the memory of its initial stereochemistry.

In the case of PVCi, cycloaddition has been shown to originate from the singlet excited state chromophore[3], although which of the mechanisms overleaf is responsible is unknown. In the presence of a triplet sensitiser, cycloaddition from the triplet excited state is observed. Cycloaddition from the singlet state is virtually activation-free while the triplet pathway has an activation energy of 1.1 kJ mol^{-1}.

The ability of PVCi to align liquid crystals has only recently been investigated[5,6]. In 1993, Marusii & Reznikov[6] studied liquid crystal alignment on films of PVCi irradiated with UV light using polarising microscopy. They found that PVCi aligns liquid crystals in a direction perpendicular to the polarisation vector of the incoming UV radiation. When irradiated for a time such that maximum conversion had occurred, the degree of twist introduced into the cell was measured to be 90°.

More recently, Ichimura *et al*[5] studied derivatives of PVCi and concluded that photoalignment is induced not by photodimerisation as suggested by Egerton *et al*[7] but by polarised isomerisation. The extent of competing reaction between dimerisation and isomerisation has been investigated in this project using the method described by Egerton *et al*[7] to establish whether dimer formation or isomerisation induces photoalignment of liquid crystals.

3.2. Characterisation

PVCi used in this work was purchased from Aldrich and had a molecular weight of 46,000 mass units and a polydispersity of 1.8 was recorded using SEC methods. Calibration of the instrument is carried out using linear polystyrene of known molecular weight. DSC measurements were recorded and it was found that the

PVCi has a glass transition temperature, T_g, of 90°C (363K). The transition is not sharp but ranges from 358-366K. This is indicative of the polydispersity of the polymer and also the presence of impurities such as residual monomer, oligomers, or unreacted functional groups. TGA was used to assess the thermal stability of PVCi. Figure 3.2.1 shows that the polymer is stable to a temperature of 300°C (573K) above which, rapid decomposition of the sample occurs. PVCi is reported to be amorphous[3], the DSC trace, see appendix for chapter three, showed no evidence for a crystallisation or a melting transition and thus inferring that if the material contains any crystalline regions, they constitute such a small percentage of the sample that they are undetectable by this method.

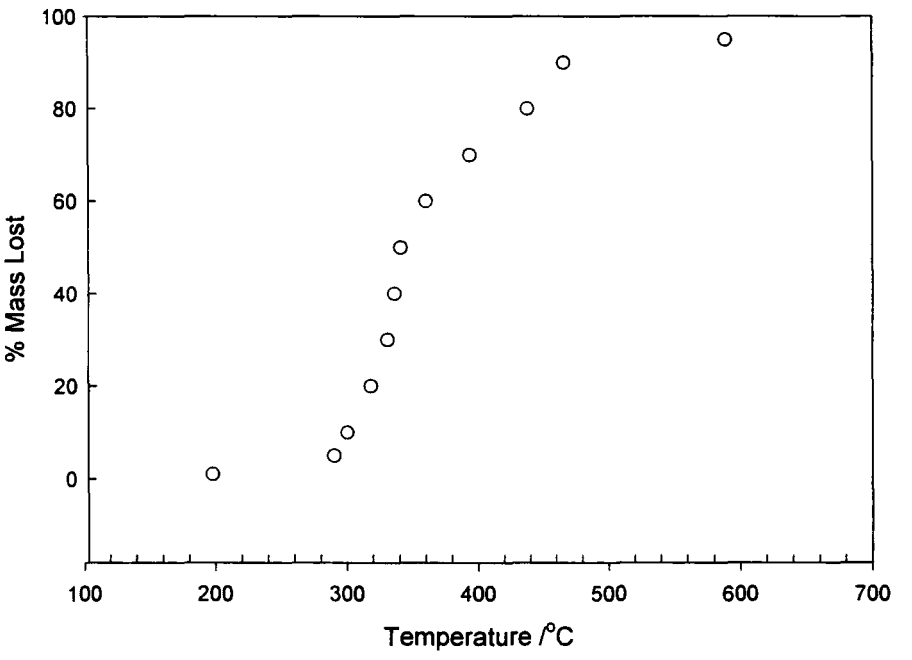

Figure 3.2.1: Percentage Mass Loss as a Function of Temperature for PVCi.

^1H and ^{13}C NMR spectra are shown in Figures 3.2.2 & 3.2.3, and the peaks have been assigned as follows:

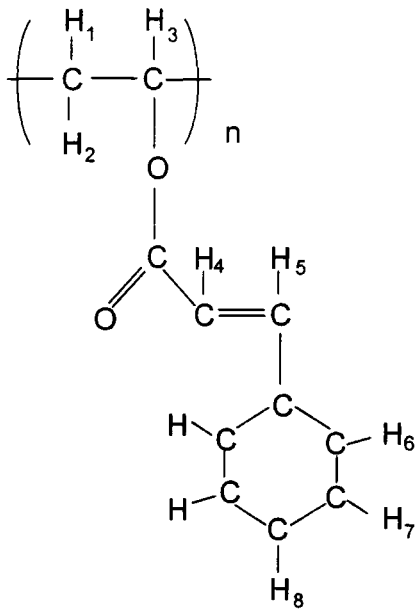

ppm	Assignment
1.5-4	1, 2
~2	3
5.2, 6.3	4, 5
~7.2	6, 7
7.6	8

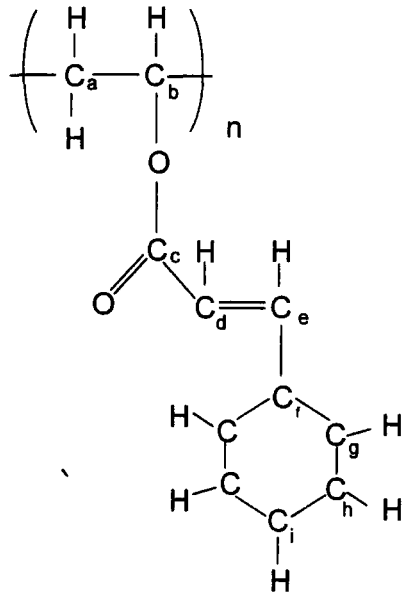

SHIFT (ppm)	ASSIGNMENT
39	a
67	b
118, 145	d, e
128, 129	h, g
130	i
134	f
166	c

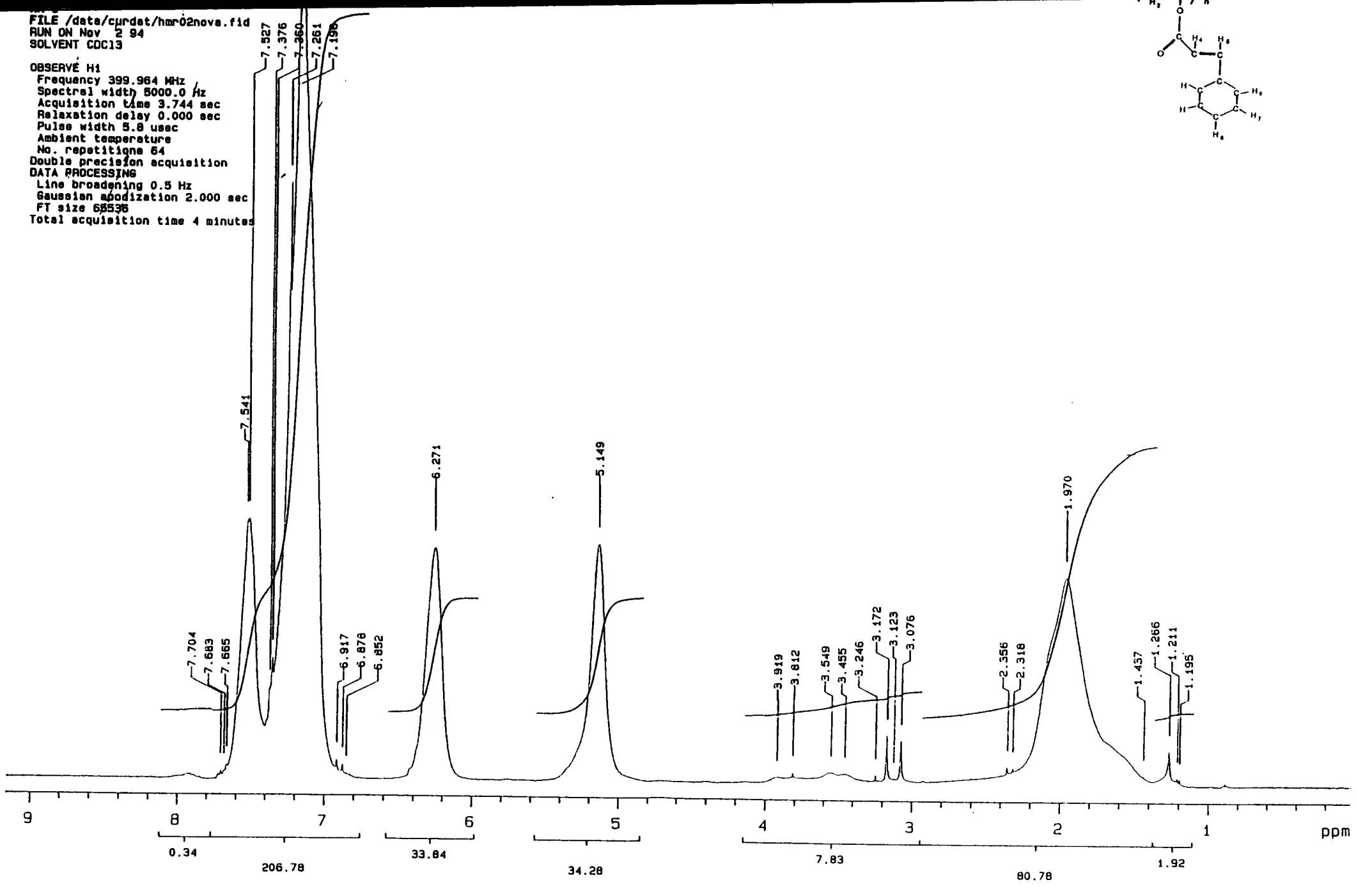

Figure 3.2.2: ^{1}H NMR Spectrum of PVCi in $CDCl_3$.

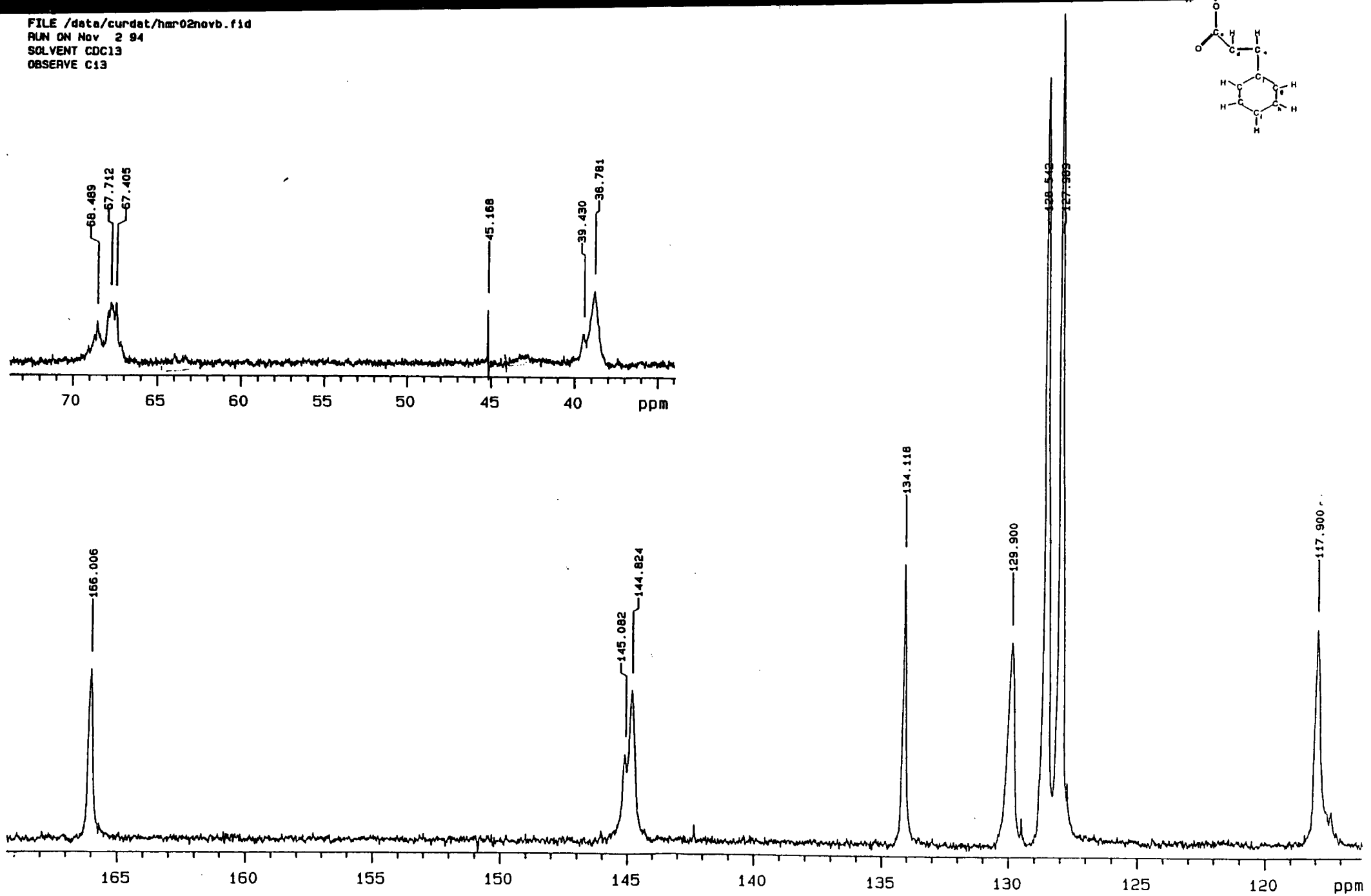

Figure 3.2.3: ^{13}C NMR Spectrum of PVCi in $CDCl_3$.

In the ^{13}C spectrum, C_d and C_e are the carbons present in the double bond of the cinnamate side chain. Isomerisation can occur about the double bond and if a mixture of isomers was present in the sample, it would be reflected in the spectrum; splitting of the peaks would be observed. The peak corresponding to C_d has a shoulder on the left hand side, however, the peak corresponding to C_e is not split. The proton spectrum shows no splitting of H_4 and H_5, the double bond protons, indicating that only one isomeric form is present in the sample. This result contradicts those of the calculation of the extinction coefficient ε in chapter two which indicate that a 50:50 mixture of cis/trans isomer is present in the sample. However, NMR is likely to have the smaller error when compared to the technique for calculating ε. Samples of both pure cis and trans polymer would be needed to confirm which form is present, however, these are not available. The trans form is thought to be the most likely of the two isomers as it is the least sterically hindered and therefore the trans structure was assessed using molecular modelling. A molecular mechanics calculation was carried out in which equations of motion are solved for a given molecular conformation in order to optimise the initial geometry of the PVCi molecule which has been constructed from a series of molecular fragments. The forcefield used in this minimisation calculation is the Consistent Valence Forcefield (CVFF) and the algorithm used is the Steepest Descent algorithm of the Biosym molecular modelling package with ten thousand iterations being carried out. For a given conformation, the algorithm is evaluated and the conformation is subsequently adjusted in order to reduce the value of the potential energy surface expression of the molecule as a function of it atoms coordinates i.e. bond lengths and angles. Caution must be adopted when using this type of minimisation as the energy minimum achieved may

only be a local minimum. Minima found are related to the starting conformation and do not explore higher energy conformations, hence the 'minimised' structure is not necessarily the global minimum. However, if a suitable building package is used, the final conformation should provide a reasonable description of the conformation of the system under investigation. The minimised structure of PVCi containing six monomer units is shown in Figure 3.2.4.

The synthetic route to PVCi has been described in Section 3.1. NMR spectra show trace impurities but accurate assessment regarding peak intensity is difficult due to the poor signal to noise ratio in the ^{13}C spectrum and broad peaks in the ^{1}H spectrum giving rise to uncertainties in the number of peaks located beneath them. The sharp peaks at ~ 3.1ppm in the proton spectrum are thought to be non-polymeric material. Samples of such material would be needed to confirm this.

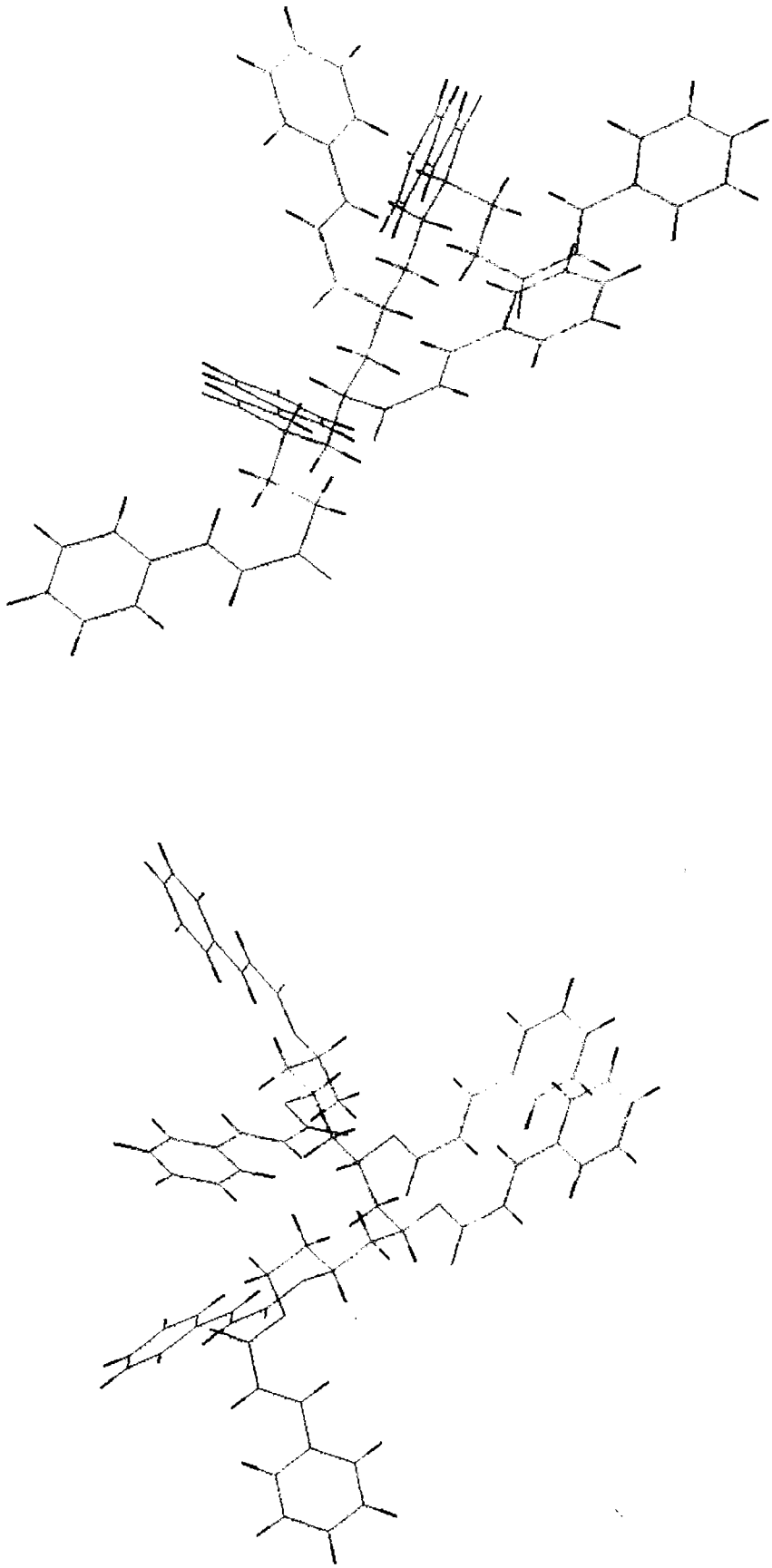

Figure 3.2.4: Minimised Structure of PVCi (6 Monomer Units).

3.3. Results and Discussion

3.3.1. UV Spectroscopy

Thin films of PVCi on quartz plates were exposed to unpolarised radiation from the deuterium lamp. The UV absorption spectrum was monitored to ensure that irradiation of the film was promoting reaction, Figure 3.3.1.1.

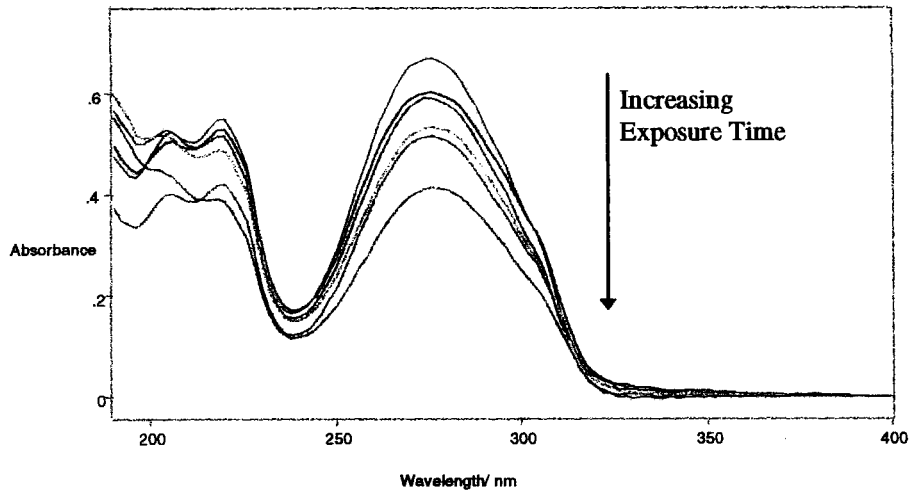

Figure 3.3.1.1: UV Absorption Spectra of PVCi Exposed to Unpolarised Radiation.

The shape of the spectral curve arises from π-π^* transitions occurring throughout the conjugated side chain. Upon irradiation, the intensity of the dominant absorption peak at λ=280nm was reduced and a second short wavelength absorbance peak appears at λ=195nm. This spectral shift is due to the reduction in π-electron conjugation of the system[9]. From Figure 3.3.1.1., the change in chromophore concentration with increasing exposure time can be calculated, Figure 3.3.1.2, and following this, the quantum yield for chromophore depletion, Figure 3.3.1.3.

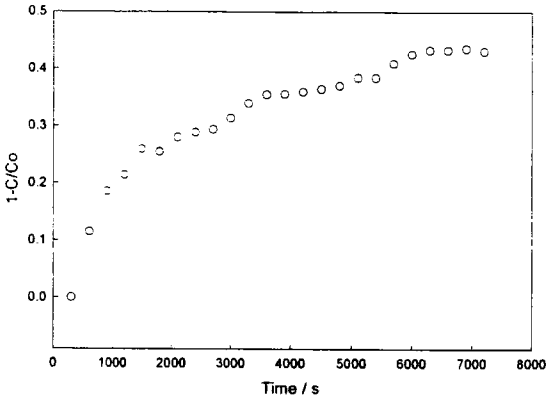

Figure 3.3.1.2: Fraction of Chromophores Converted Using Unpolarised Radiation.

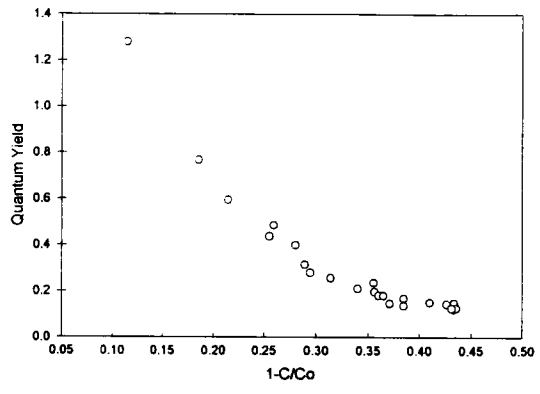

Figure 3.3.1.3: Quantum Yield for Chromophore Decay Using Unpolarised Radiation.

The general shape of the quantum yield decay shown in Figure 3.3.1.3 is analogous to that reported by Egerton *et al*[7]. The absolute values of quantum yield differ due to the uncertainties in the measured I_o, as described in chapter 2.6.3.

Using the absorption spectra, it is possible to monitor the isomerisation and cyclisation reactions simultaneously. This allows assessment of the extent that isomerisation is interfering with the bimolecular process. The method used is that of Egerton[7].

In a dilute solution of ethyl cinnamate, isomerisation is the only reaction pathway and the spectral curves obtained on progressive irradiation intersect at an isobestic point at 250nm. When a different reaction competes with isomerisation, this isobestic point is lost and the changing absorbance at 250nm can be used to measure the extent of competing reaction. Spectroscopy at two wavelengths, the isobestic point and absorption maximum, make it possible to monitor dimerisation and isomerisation concurrently via the following equations.

$$\frac{n_a}{n_0} = \frac{\varepsilon_a}{\varepsilon_a - \varepsilon_b}\left[\frac{D_2}{D_2^0} - \frac{\varepsilon_b}{\varepsilon_a}\frac{D_1}{D_1^0}\right] \qquad \text{Equation 3.3.1.1}$$

$$\frac{n_b}{n_0} = \frac{\varepsilon_a}{\varepsilon_a - \varepsilon_b}\left[\frac{D_1}{D_1^0} - \frac{D_2}{D_2^a}\right] \qquad \text{Equation 3.3.1.2}$$

$$\frac{n_c}{n_0} = 1 - \frac{D_1}{D_1^0} \qquad \text{Equation 3.3.1.3}$$

where subscript a denotes the trans isomer, b the cis isomer and c the cyclic species; n is the number of moles of component at time t with n_o being the total number of moles of chromophore; D_1 is the absorbance at 250nm, D_2 is the absorbance at 275nm; ε_a & ε_b are the molar extinction coefficients of the cis and trans forms at 275nm[8].

From the spectra obtained on exposure of PVCi to the complete spectrum of light emitted by the deuterium lamp, the absorption parameters required for equations 3.3.1.1, 3.3.1.2 and 3.3.1.3 were obtained. The values of ε_a and ε_b used were those reported by Rennert *et al*[8].

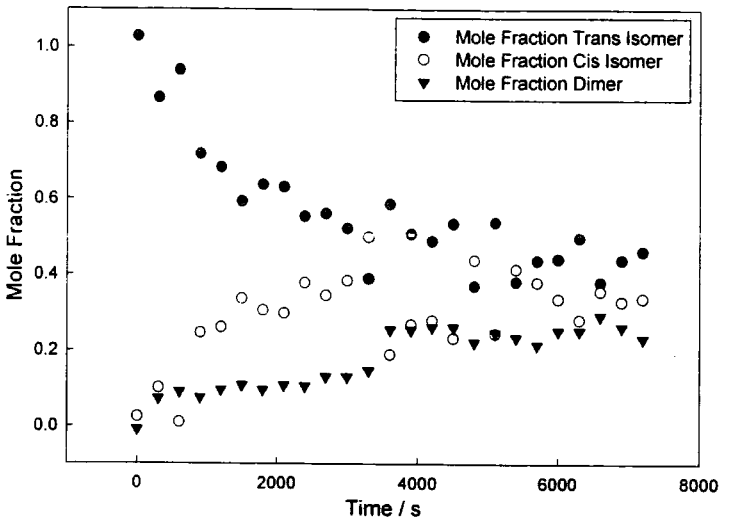

Figure 3.3.1.4: Extent of Competing Reaction in PVCi Exposed to Unpolarised Radiation.

Figure 3.3.1.4 indicates that the start of the reaction, the PVCi has the majority of its double bonds in the trans conformation, with little cis isomer and no cyclic species present in the sample. As the reaction proceeds, the mole fraction of the trans isomer decreases while the mole fraction of both the cis isomer and the dimer increase. This indicates that when using unpolarised radiation, isomerisation competes effectively with cyclisation. Although contradictory to the results of Egerton, this data supports the theory that the reaction sites are set when the sample is spun. If there is no ground state cinnamate species nearby for the excited state cinnamate to react with, isomerisation may occur.

When PVCi was irradiated using vertically polarised UV radiation, the following UV absorption decay was observed, Figure 3.3.1.5.

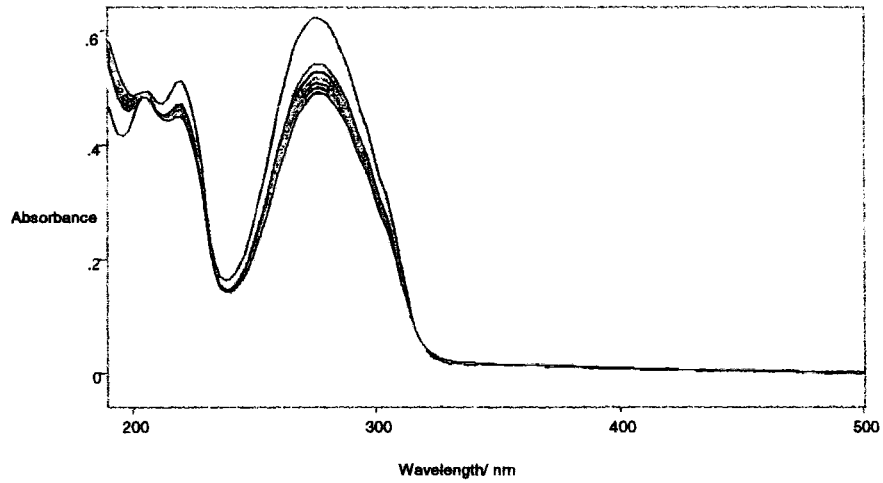

Figure 3.3.1.5: UV Absorption Decay of PVCl Exposed to Vertically Polarised Radiation.

There is an initial, sharp decrease in the major peak centred at λ=275nm. However, during the remaining eight hours exposure, the peak height changes only slightly. Converting this to the fraction of chromophores reacted, Figure 3.3.1.6.

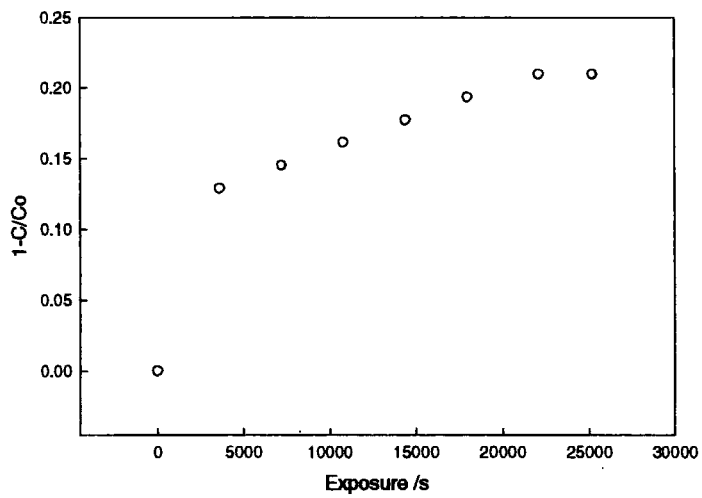

Figure 3.3.1.6: Fraction of Chromophores Converted Upon Exposure to Vertically Polarised UV.

Figure 3.3.1.6. shows that after eight hours exposure, only 20% of the chromophores initially present in the sample have reacted. Figure 3.3.1.7 shows the corresponding quantum yield change.

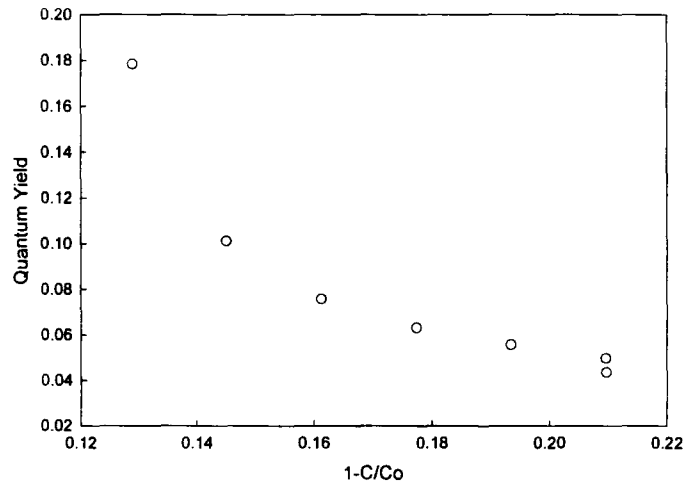

Figure 3.3.1.7: Quantum Yield Change for Exposure of PVCi to Vertically Polarised Radiation.

The experiment was repeated and the combined results are shown in Figure 3.3.1.8.

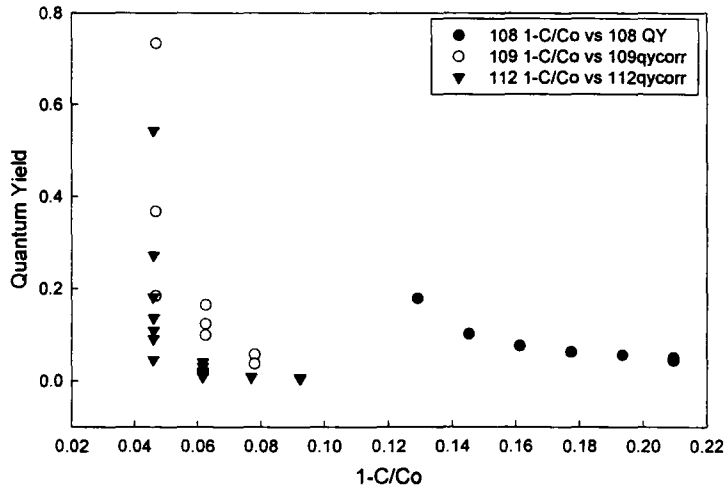

Figure 3.3.1.8: Overlay of Quantum Yield Results for Vertically Polarised Radiation.

These results show significant inaccuracies in the quantum yield value at a given chromophore conversion due to the uncertainty in I_o associated with these calculations. Once again, the extent of competition between isomerisation and dimerisation can be determined, Figure 3.3.1.9.

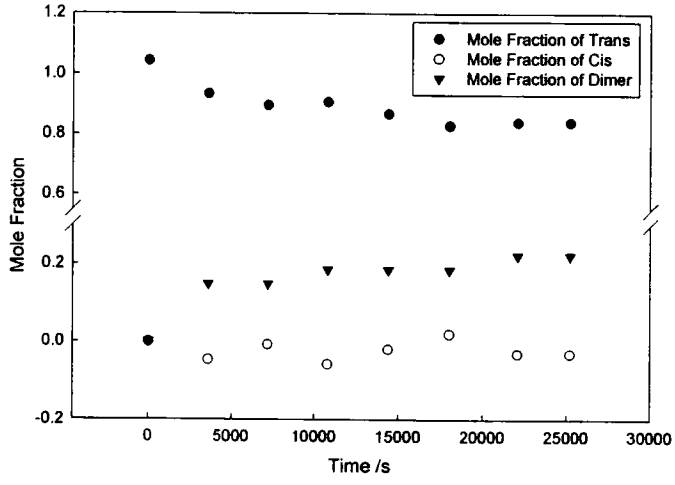

Figure 3.3.1.9: Extent of Competing Reactions in PVCi Exposed to Vertically Polarised Radiation.

Although the total extent of reaction is small, it can be seen that dimerisation is favoured and isomerisation plays only a minor role.

The polarisation vector of the incident light was rotated by 90° and the experiments were repeated using horizontally polarised incident radiation.

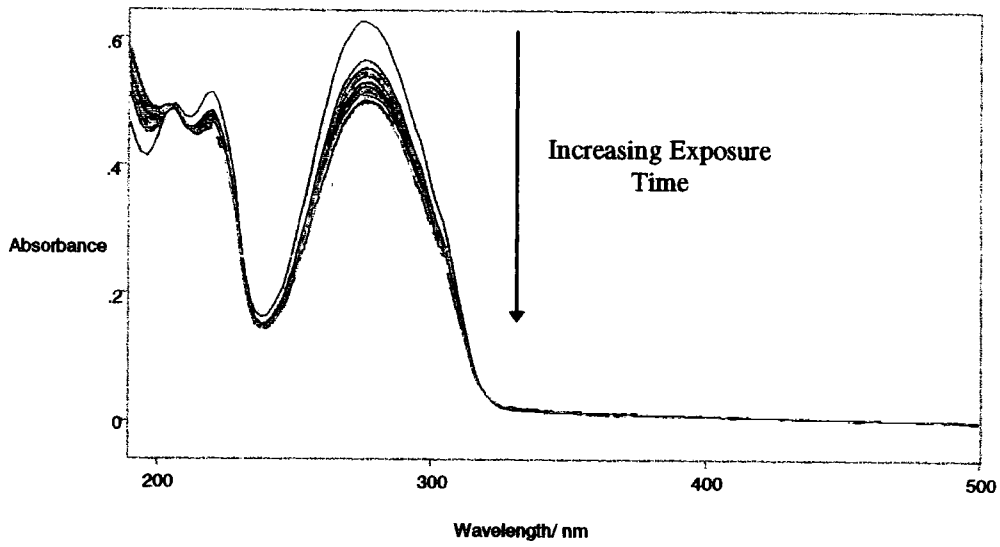

Figure 3.3.1.10: UV Absorption decay for PVCi Exposed to Horizontally Polarised Radiation.

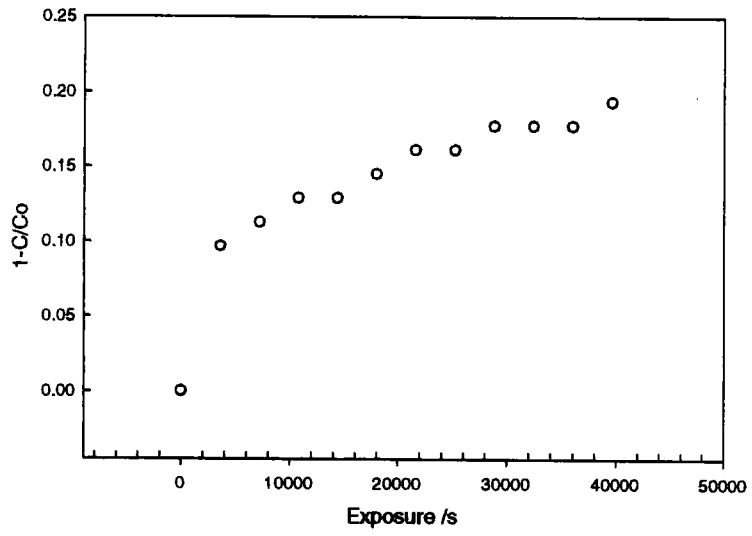

Figure 3.3.1.11: Fraction of Chromophores Converted Upon Exposure to Horizontally Polarised Radiation.

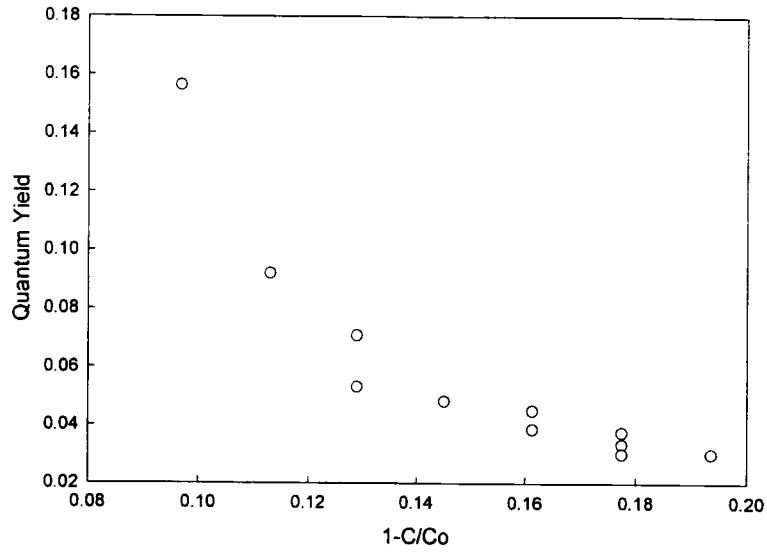

Figure 3.3.1.12: Quantum Yield for PVCi Exposed to Horizontally Polarised Radiation.

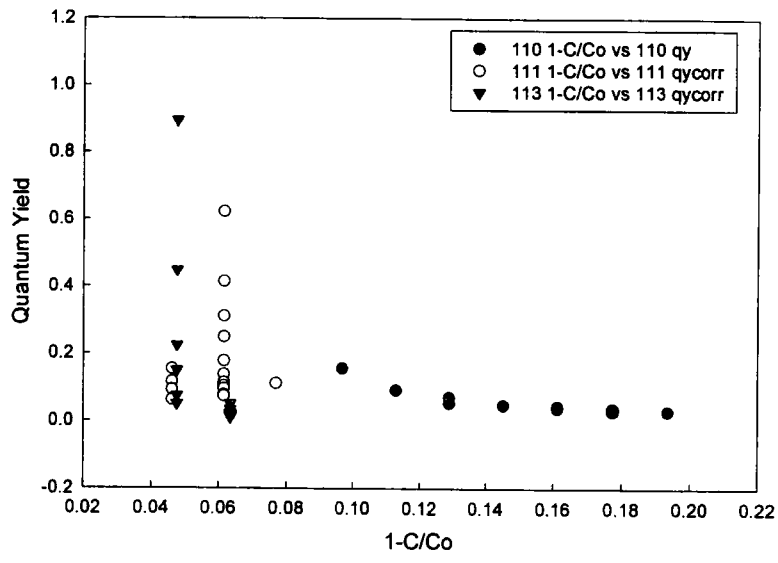

Figure 3.3.1.13: Combined Quantum Yield for PVCi Exposed to Horizontally Polarised Radiation

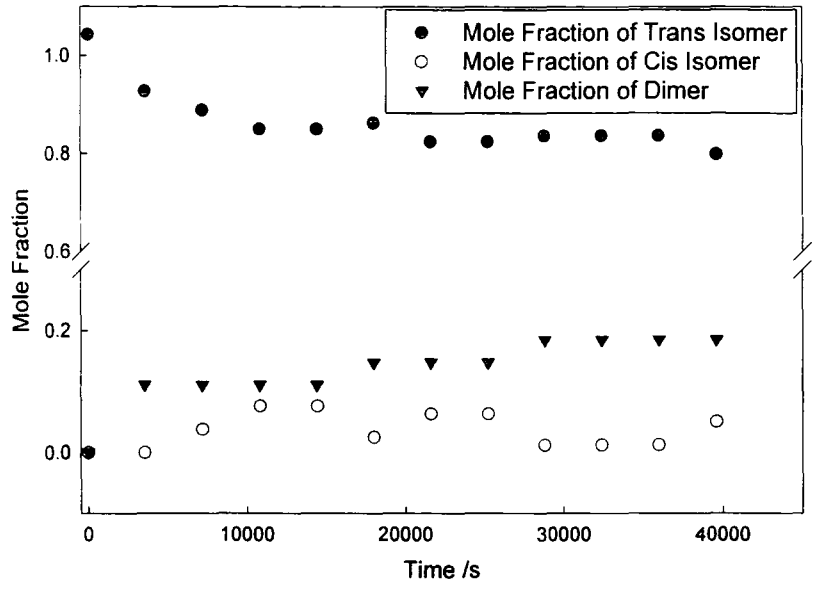

Figure 3.3.1.14: Extent of Competing Reaction Upon Irradiation of PVCi with Horizontally Polarised UV.

The results in Figure 3.3.1.11, Figure 3.3.1.12, Figure 3.3.1.13 and Figure 3.3.1.14 compare well with those obtained for vertically polarised radiation. In both cases, approximately 20% of the initial chromophores react and dimerisation is the favoured reaction pathway. The numbers of double bonds reacting fall short of the value of approximately 50% achieved by Egerton[7]. This is thought to be caused by the broad wavelength of the radiation emitted by the 30W deuterium lamp. Insufficient radiation of the correct wavelength for promotion of an electron into a π^* orbital results in few chromophores reacting. In contrast, Egerton used a 500W medium pressure mercury lamp and irradiated through pyrex, eliminating radiation below 320nm.

To determine whether a lack of photons of the correct wavelength is the underlying experimental problem, irradiation of PVCi was also carried out using a

vertically polarised laser (λ_0=325nm). The spectral curves obtained upon successive irradiation are shown in Figure 3.3.1.15.

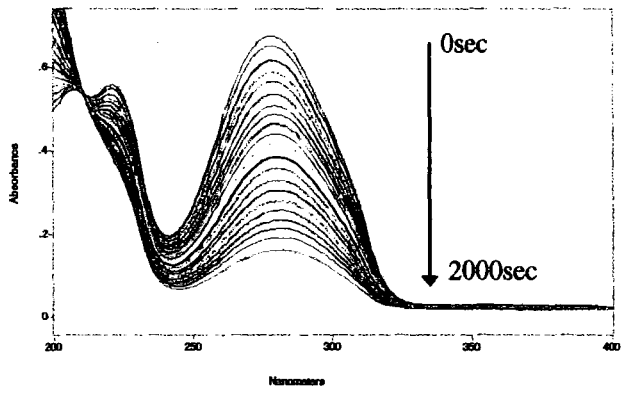

Figure 3.3.1.15: Spectral Curves for Progressive Irradiation of PVCl with 325nm Laser.

The spectra were recorded with up to 30 minutes polarised laser exposure and approximately 80% of the chromophores were depleted in this time, Figure 3.3.1.16. Figure 3.3.1.16 shows a clear isobestic point at λ~225nm. This arises from the loss of conjugation in the cinnamate side chain and is due to the π-π^* transitions of the isolated benzene ring.

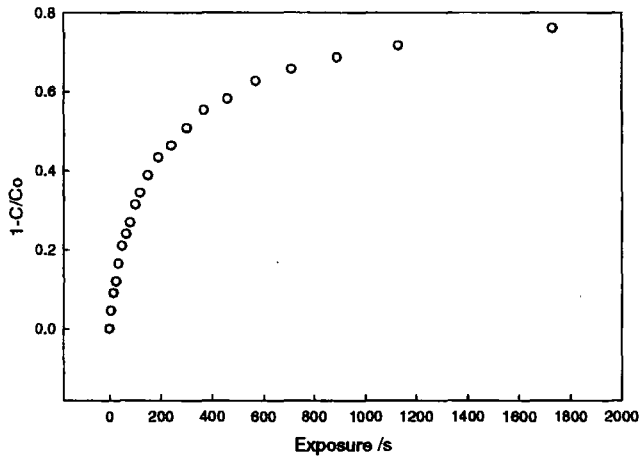

Figure 3.3.1.16: Chromophore Conversion in PVCl Using Polarised Laser Radiation.

The quantum yield was measured more accurately as monochromatic radiation of know intensity was used as the radiation source, Figure 3.3.1.17.

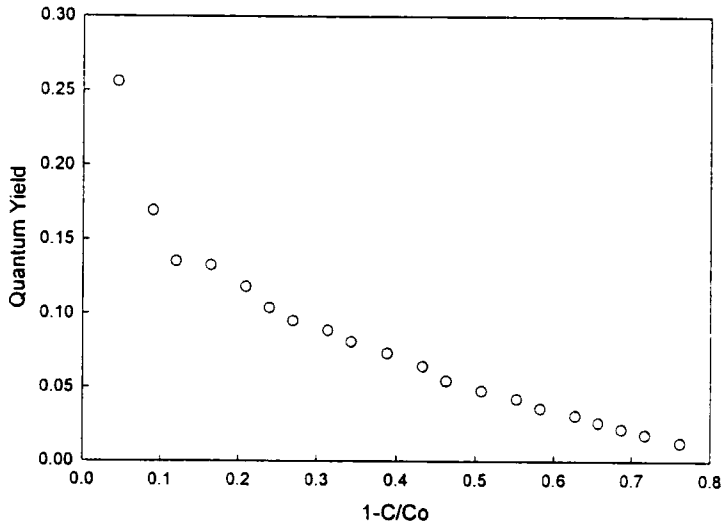

Figure 3.3.1.17: Quantum Yield Using Polarised Laser Radiation.

Quantum yield values for the first 30% of chromophores reacted are very similar to those obtained by Egerton *et al*[7], beginning at a quantum yield value of ~0.25 and steadily falling to ~0.07.

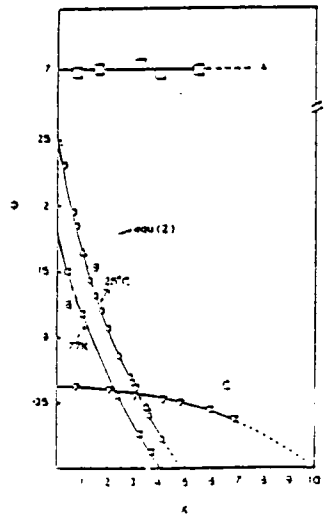

Quantum yield of cycloaddition between cinnamoyl groups as a function of reactant conversion, in three states of segregation: (A) crystalline cinnamic acid, α form; (B) solid film of poly(vinyl cinnamate); (C) solution of poly(vinyl cinnamate) in dichloroethane.

Figure 3.3.1.18: Results Achieved by Egerton *et al*[7].

After this point, deviations of the results from those obtained by Egerton occur. The mercury lamp used by Egerton induces reaction in ~50% of the chromophores. In contrast, ~80% of the chromophores react using the laser. The relatively high energy of the monochromatic laser is inducing larger numbers of molecules to react than the broad wavelength range, lower power lamp.

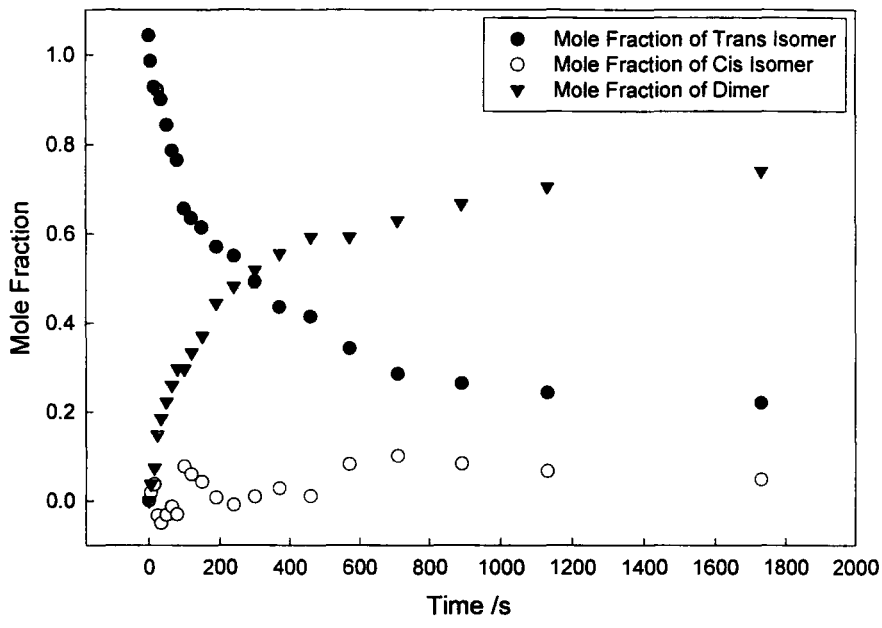

Figure 3.3.1.19: Extent of Competing Reactions in PVCi Upon Laser Irradiation.

Figure 3.3.1.19 shows dimerisation to be the major reaction pathway, isomerisation accounts for only ~10% of the reacted chromophores. These results confirm the observations of Egerton[7] and contradict those of Ichimura *et al*[5]. However, the polymers used by Ichimura are polymethacrylates bearing regioisomeric cinnamate side chains, an example of which is shown in Figure 3.3.1.20.

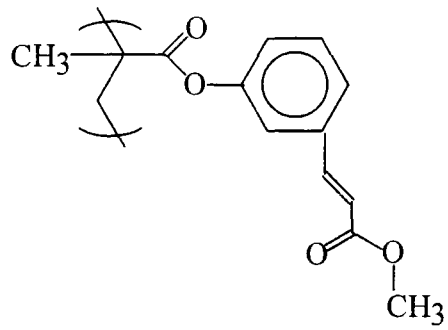

Figure 3.3.1.20: Meta-Derivative used by Ichimura[5].

These derivatives, because of their stereochemistry, may not react in an identical manner to PVCi and the validity of the results obtained by Ichimura cannot be challenged as experiments on derivatives of PVCi with this stereochemistry have not been carried out in the project.

3.3.2. Infrared Spectroscopy.

PVCi was spin-coated onto ZnSe as described in chapter 2.3. The films were then analysed using polarised FTIR incorporating the Grams 32c software, chapter 2.7. A typical example of the IR spectra obtained using this technique is shown in Figure 3.3.2.1 & Figure 3.3.2.2. The two absorbances obtained will be defined as 'absorbance parallel' and 'absorbance perpendicular' referring to the IR radiation remaining vertically polarised and the sample slide positioned upright and horizontally respectively.

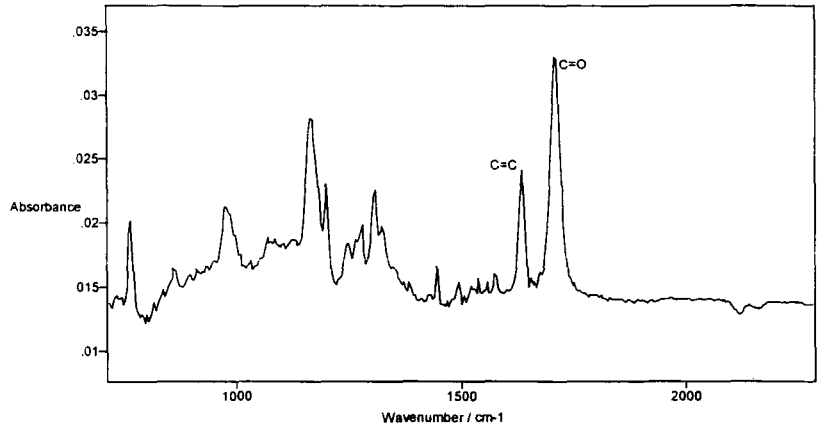

Figure 3.3.2.1: IR Spectrum Obtained using Vertically Polarised Incident IR (parallel).

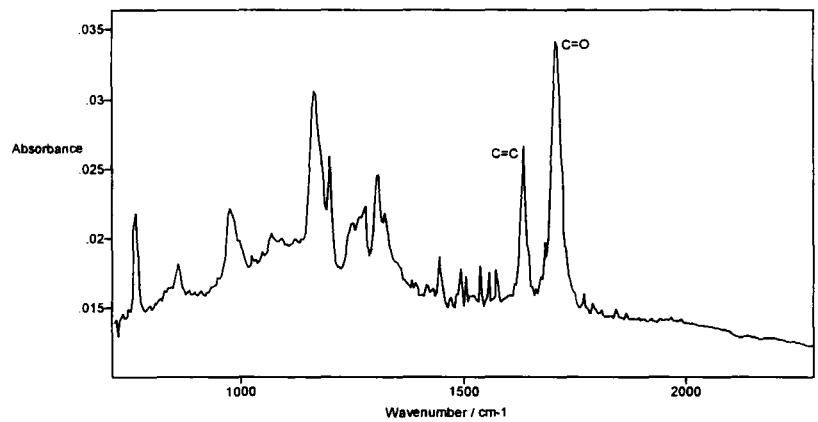

Figure 3.3.2.2: IR Spectrum Obtained using Horizontally Polarised Incident IR (perpendicular).

As Figure 3.3.2.1 and Figure 3.3.2.2 show, the spectra of the unexposed sample recorded in both parallel and perpendicular orientations are very similar. The carbon double bond peak for horizontally polarised incident IR is slightly larger in height, 0.011 compared to 0.009 for vertically polarised light. However, the integrated absorption area is smaller for the horizontally polarised light, 0.21, than for the vertically polarised light, 0.24. This shows that before irradiation, the sample displays little preferential orientation of the double bonds.

The film is progressively irradiated using vertically polarised radiation from the deuterium lamp (I_o= 2.42 × 10^{12} photon s^{-1}). From the change in double bond absorbance at 1640cm^{-1}, the dichroic ratio can be calculated.

As irradiation increased, side chains oriented parallel to the polarisation direction of the incoming light should be depleted. This would lead to a reduction in absorbance parallel and retain a constant value for absorbance perpendicular. It was found that both absorptions fluctuate randomly, thus giving rise to a random change in dichroic ratio, Figure 3.3.2.3.

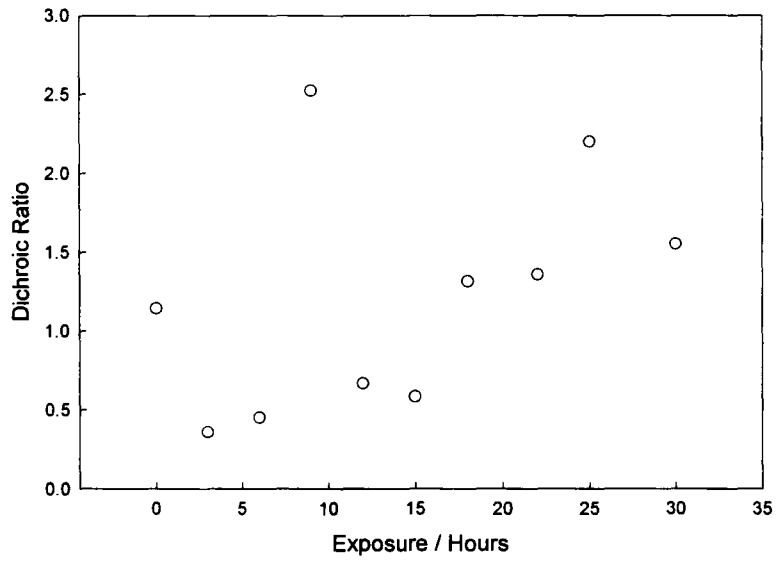

Figure 3.3.2.3: Dichroic Ratio for PVCi Exposed to Vertically Polarised Radiation.

Consider the PVCi film on a ZnSe substrate. Those side chains parallel to the incoming polarisation vector are able to react.

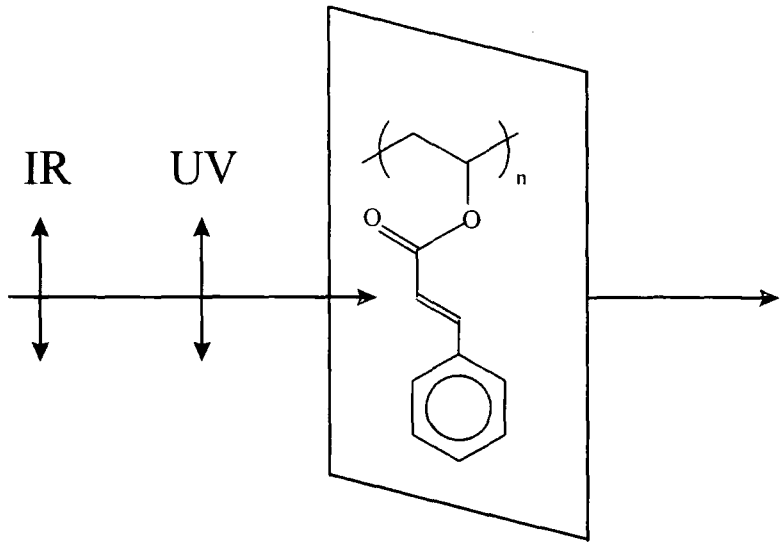

Figure 3.3.2.4: PVCi on ZnSe.

The film is then analysed using polarised IR. Figure 3.3.2.4, shows that the transition moment vector of the carbon double bond vibration and the polarisation vector of the incoming infrared are not in the correct orientation to interact. Using the minimised structure for PVCi shown in Figure 3.2.2, the angle that the double bond makes with the side chain axis and therefore the incoming IR polarisation direction was found to be 120°. Thus, in the experimental design, the polarisation vector must be rotated clockwise by 120°. However, the double bonds of the side chains parallel to the IR polarisation vector will not all be oriented at +120° from the side chain axis. Double bonds can also lie at -120°, Figure 3.3.2.5.

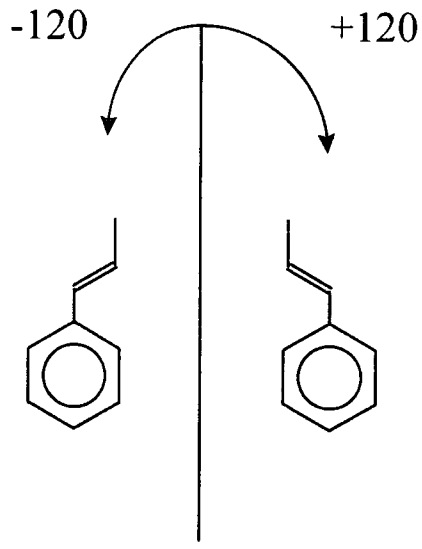

Figure 3.3.2.5: Side Chain Orientation.

The overall picture of the film is much more complex than this simplistic view. In theory, the double bonds can lie at any angle around the 360° about which the side chain can rotate. However, as Figure 3.3.2.6 shows, although the cinnamate side chain can potentially be situated at any point in the x-z plane, the incoming polarisation can only be selected in the x-y plane. Therefore, the dichroic ratios were calculated only for cinnamate groups lying at ±120° from the side chain axis.

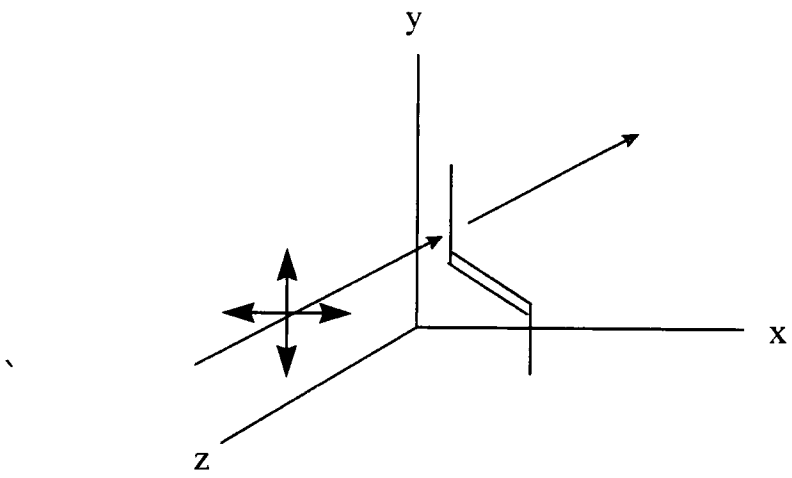

Figure 3.3.2.6: Orientation of Side Chains in PVCi With Respect to IR Polarisation.

Recording of the polarised IR spectra was not as facile as for species with transition moments and polarisation vectors parallel. It was important that the polariser remained stationary as movement leads to large uncertainties in polariser position for each sample and thus significant errors. Therefore, following technique schematically represented by Figure 3.3.2.7 was employed.

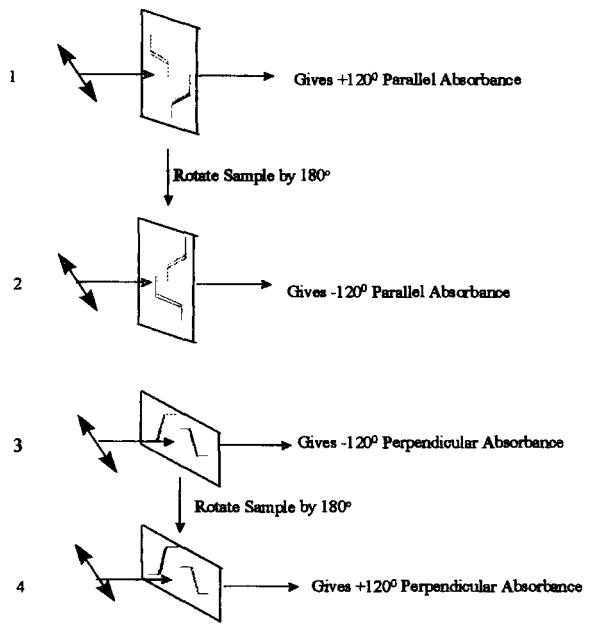

Figure 3.3.2.7: Sample Orientation for PVCi Dichroism Measurements.

The dichroic ratio equations are now represented as follows.

$$D_{+120} = \frac{Orientation\,1}{Orientation\,4}$$

$$D_{-120} = \frac{Orientation\,2}{Orientation\,3}$$

The experiment was carried out by recording spectra at before exposure to the vertically polarised radiation from the deuterium lamp and then again at 10 minutes exposure. In this period of time, the peaks due to the double bond vibration had been reduced to such an extent that they were not distinguishable from the baseline noise, Figure 3.3.2.8.

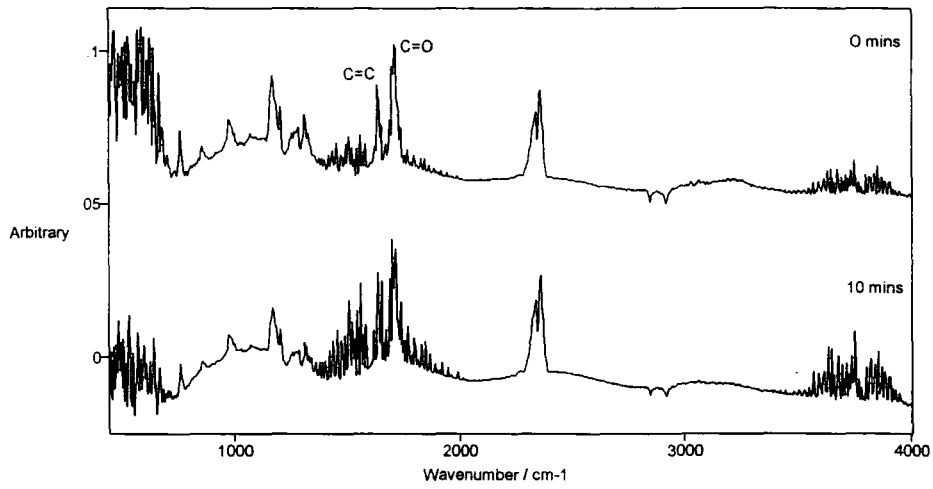

Figure 3.3.2.8: PVCi Spectrum After 10 Minutes Vertically Polarised Exposure.

The experiment was repeated using exposure intervals of 2 minutes and the results are collated in the appendix for chapter three. Figure 3.3.2.9 shows the change in dichroic ratio with increasing exposure time.

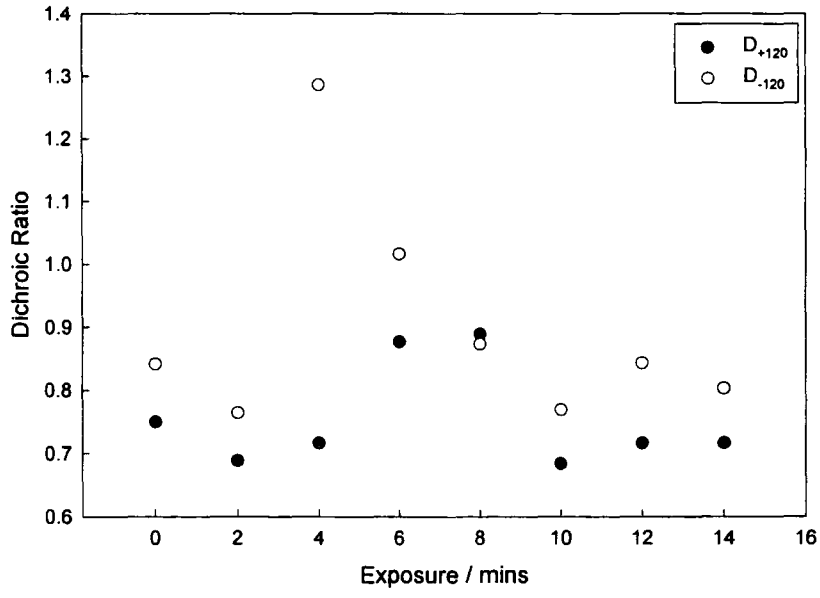

Figure 3.3.2.9: Dichroic Ratios for PVCi.

The experiment was repeated and the results are summarised in Figure 3.3.2.10.

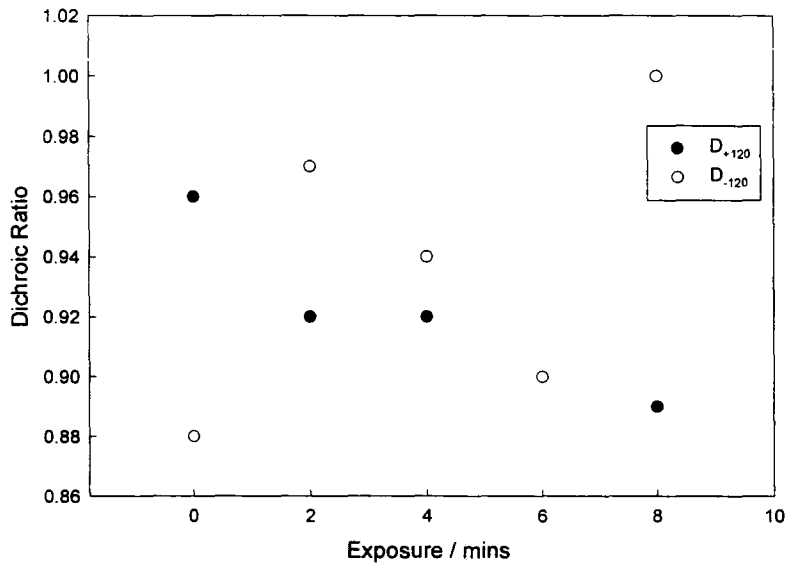

Figure 3.3.2.10: Repeated PVCi Dichroism Experiment.

The experiments described in this section have been unsuccessful in establishing a trend for the change in dichroic ratio achieved when PVCi is irradiated with vertically polarised light from the deuterium lamp. As shown by polarised UV spectroscopy, section 3.3.1, a maximum of 20% of the double bonds present in the sample react. Although the same procedure for selecting and analysing the peaks was adopted each time, repetition of the analysis showed an error of ±10% in the value for the absorption area, giving an error of the same order of magnitude in the dichroic ratio. Ichimura *et al*[5] obtained dichroic ratios of ≤0.05 for the prolonged polarised UV exposure of polymethacrylates with regioisomeric cinnamate side chains. Such a small change in dichroic ratio could not be detected by the polarised IR experiments described here for PVCi.

The films used for the IR studies are ~1000Å thick and give double bond absorption maxima of ~0.1. At long exposure times, 20% of the double bonds react, giving a new absorption maximum of ~0.08. The error in the analysis, ~10%, would place this new absorption in the region 0.072-0.088, a change which is barely detectable.

The results obtained by the IR dichroism studies of PVCi are inconclusive. Such small changes are occurring that it is not possible to distinguish them from the experimental error.

3.3.3. Birefringence Studies

Birefringence measurements were first attempted in Durham using the Babinet compensator method as described in chapter 2.8.4. The retardation measured by the compensator is converted to birefringence using the equation below.

$$\Delta n = \frac{\lambda R}{t}$$

where λ is the laser wavelength (633nm) and t is the sample thickness.

To begin, the retardation inherent in the bare quartz plate was measured. This gave a birefringence value of 2.2×10^{-4}. Samples of PVCi on quartz were irradiated and the retardation measured. The corrected birefringence values were determined from the actual sample birefringence minus the birefringence value for quartz. Figure 3.3.3.1 shows the corrected birefringence values for PVCi exposed to vertically polarised radiation from the deuterium lamp.

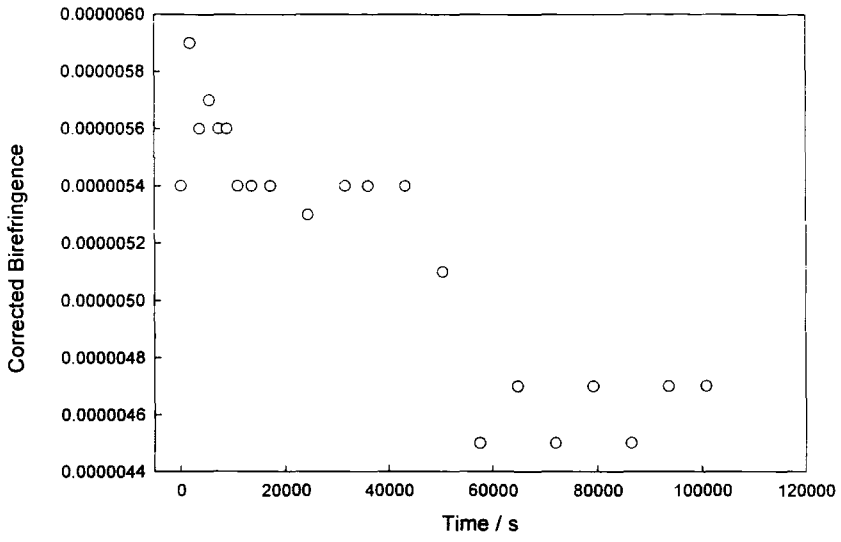

Figure 3.3.3.1: Corrected Birefringence for PVCi (Compensator Method).

The birefringence change in Figure 3.3.3.1 does initially appear to follow a decreasing trend. However, the actual value of the birefringence is so small ($\sim 10^{-6}$ with changes of $\sim 1.5 \times 10^{-6}$) that these results are most likely to be due to experimental variations. The experimental design, calibration and calculation were all thoroughly checked and no errors became evident. The apparent lack of birefringence in PVCi cannot be accounted for and it was therefore decided to employ the crossed-polariser method to establish birefringence.

PVCi was again exposed to vertically polarised radiation from the deuterium lamp. In this instance, birefringence changes were monitored using the crossed-polariser method described in chapter 2.8.3 and Figure 3.3.3.2 shows the results.

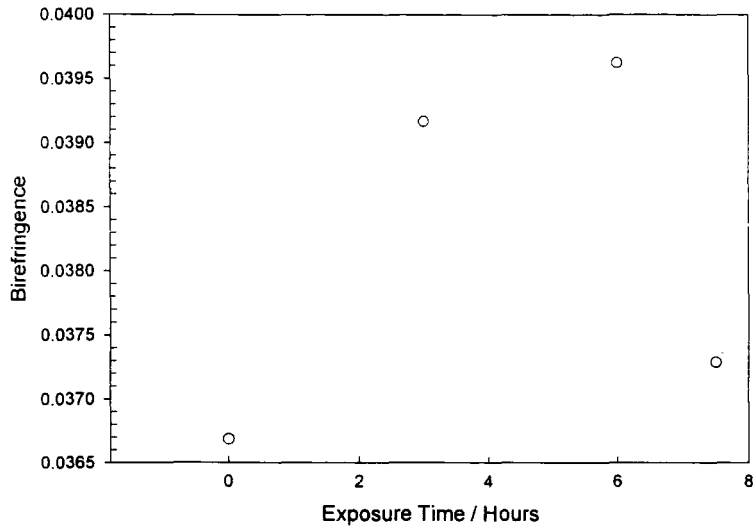

Figure 3.3.3.2: Birefringence Changes in PVCi using the Crossed-Polariser Technique.

The birefringence of a bare quartz slide was measured using this technique and was found to be 9.3×10^{-7}. However, due to the magnitude of this value relative to the measured birefringence value, the absolute value of the sample birefringence remained unchanged when the bare quartz value was subtracted. As Figure 3.3.3.2 shows, the experiment was initially carried out with birefringence measured at three hourly intervals with the birefringence slowly increasing then appearing to fall off. Therefore, the experiment was repeated using a 0-3 hour timescale and the results are summarised in Figure 3.3.3.3.

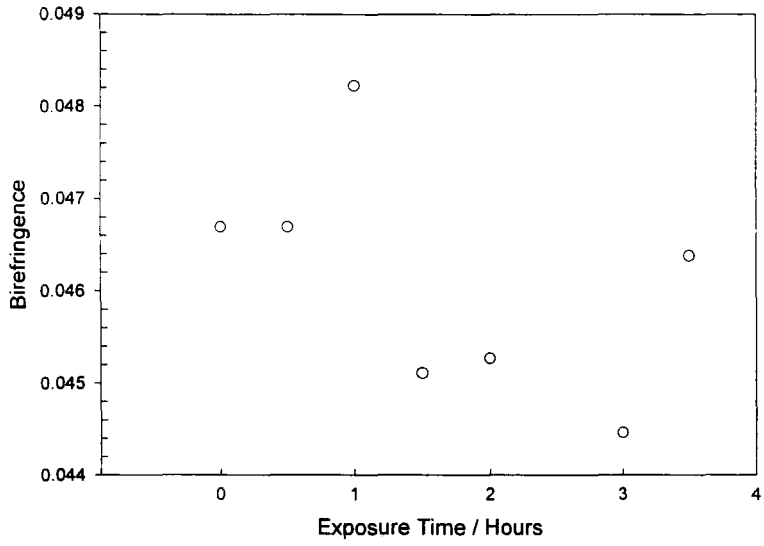

Figure 3.3.3.3: Birefringence Changes in PVCi using the Crossed-Polariser Technique.

This data set is quite erratic with no trend evident. In both Figure 3.3.3.2 & Figure 3.3.3.3, birefringence is measured at three hours exposure and similar values would be expected for both measurements. The values differ by ~12% which is within experimental error. A more accurate comparison is to look at the overall change in birefringence between 0-3 hours exposure. In the case of the sample where birefringence was measured every three hours, the value for the birefringence has increased. For values recorded every 30 minutes, the birefringence decreases. This implies that taking readings at varying time intervals is having differing effects on the sample.

Exposure to vertically polarised radiation from the deuterium lamp does not give rise to any obvious trend in birefringence. One possible explanation for this is that the lamp does not produce enough energy of the correct wavelength to affect cross-linking. However, this explanation is contrary to the evidence provided by

polarised UV studies, section 3.3.1. These results show a clear decrease in chromophore concentration upon exposure to the deuterium lamp.

An alternative explanation is that the polariser through which the lamp radiation passes is 'leaky' and although material is being depleted, it is not specific to any one direction. This would explain why a change is observed in the UV spectrum: the results obtained are not orientationally dependant due to unpolarised UV being used to obtain the absorption spectrum. Nevertheless, if the polariser was 'leaky' it would not be reasonable to assume that it was 'leaky' to such an extent that it caused the polarised radiation to have the same effect as unpolarised radiation. Hence, some birefringence should be detectable.

It should be noted that the birefringence values for bare quartz are considerably different depending on the method used to measure it. This shows that one or both techniques are inaccurate. It is most likely that the compensator method is for some reason invalid as birefringence values measured using crossed-polarisers are of similar orders of magnitude to those obtained using an identical analytical technique at DERA Malvern.

Due to obvious inadequacies somewhere in the experimental design, all future birefringence measurements were carried out during visits to DERA Malvern using the simultaneous irradiate/monitor technique described in chapter 2.8.3. An example for a typical birefringence curve produced by this method is shown in Figure 3.3.3.4.

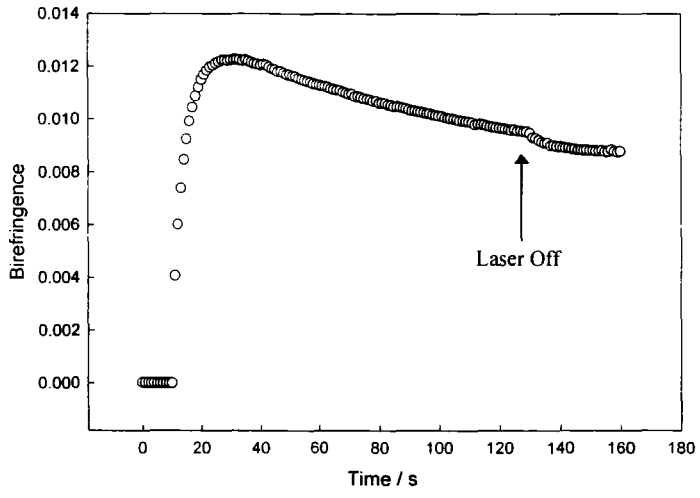

Figure 3.3.3.4: Birefringence Curve for PVCi Obtained using Laser Irradiation.

As can be seen in Figure 3.3.3.4, the birefringence remains at a constant value for the first few seconds of the experiment. This is due to intensity measurements being recorded before the He-Cd laser is switched on. The birefringence then rises quite sharply as the cinnamate side chains located parallel to the polarisation vector of the incoming radiation react quickly[5]. Once all of the double bonds in this orientation have been consumed, effects due to the reaction of side chains not parallel to the polarisation vector become more important. Once these bonds begin to react, the refractive index difference between parallel and perpendicular directions lessens and the birefringence falls[9].

The birefringence curve shown in Figure 3.3.3.4, although representative of many of the curves obtained for PVCi, is not exclusive. Figure 3.3.3.5 shows another typical plot.

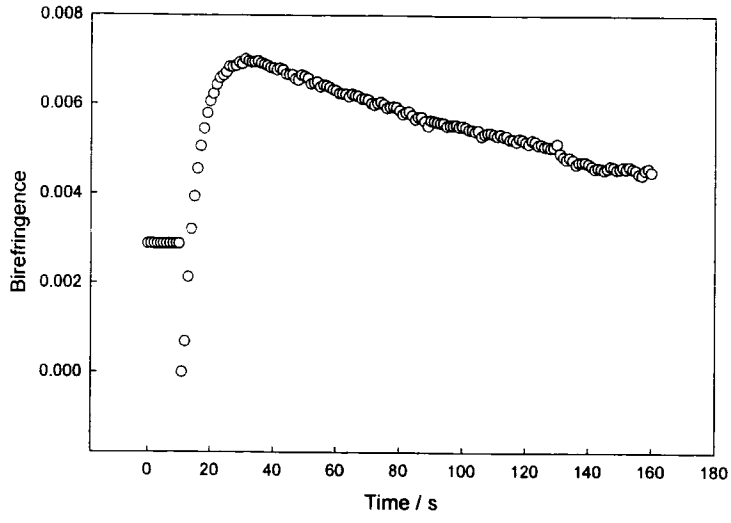

Figure 3.3.3.5: Alternative Birefringence Curve for PVCi.

In Figure 3.3.3.5, there is a sudden drop in birefringence before a steady rise commences. Decreasing birefringence is indicative of destruction of order. This therefore implies that there is some inherent order in the sample perpendicular to the direction in which order was to be created.

Remember that $\Delta n = n_{para} - n_{perp}$ and it has been assumed that the sample is initially isotropic, Figure 3.3.3.6.

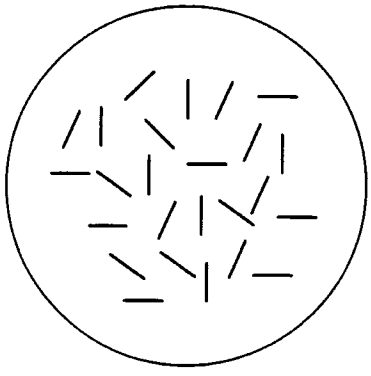

Figure 3.3.3.6: Random Orientation in PVCi.

If this is true, then the sample will display no inherent birefringence, i.e. $n_{para} = n_{perp}$. Once irradiation with vertically polarised light from the He-Cd laser begins, the birefringence will increase as the difference between n_{para} & n_{perp} increases, Figure 3.3.3.7.

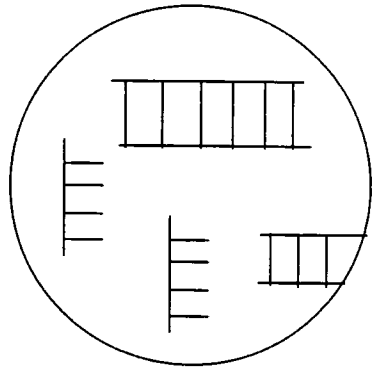

Figure 3.3.3.7: $n_{para} > n_{perp}$

Consider the situation where there is some inherent order within the sample, the initial birefringence will be non-zero.

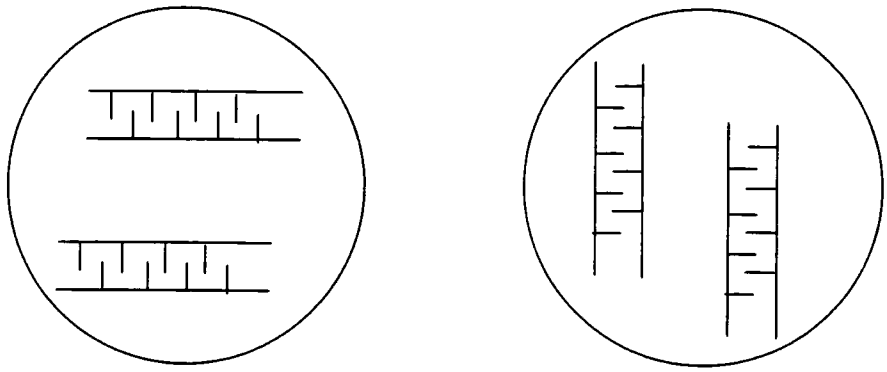

Figure 3.3.3.8: Inherent Order in PVCi.

In Figure 3.3.3.8, the situation where order is parallel resembles that of Figure 3.3.3.7 and birefringence will increase with increasing exposure time until a maximum is reached where it will begin to fall. For the situation where order is perpendicular , the initial birefringence will be negative, giving rise to Figure 3.3.3.9.

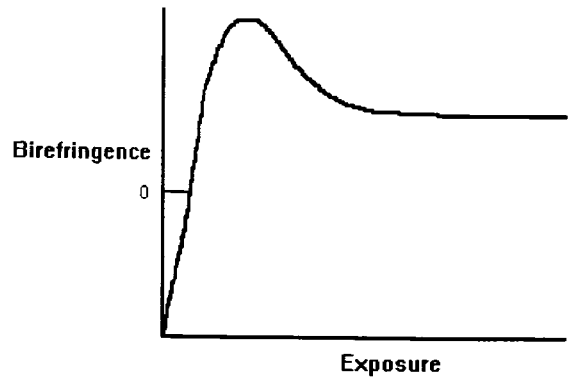

Figure 3.3.3.9: Birefringence Curve Showing Negative Values.

However, as $|\Delta n|$ is being considered, Figure 3.3.3.9 becomes Figure 3.3.3.10.

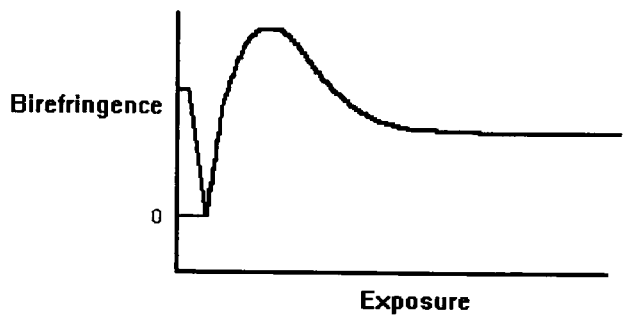

Figure 3.3.3.10: $|\Delta n|$.

Zero birefringence is achieved when $n_{para} = n_{perp}$.

As birefringence had been observed before laser irradiation had occurred, samples were annealed in an attempt to remove any inherent orientation brought about by the spin casting process. PVCi has a T_g of 362K, therefore one sample was heated to 365K and a second to 430K. Results for these samples are shown in Figure 3.3.1.11.

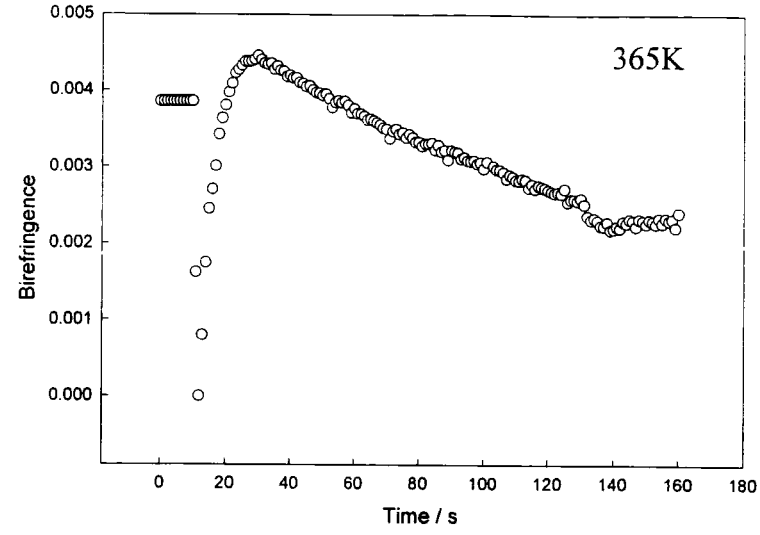

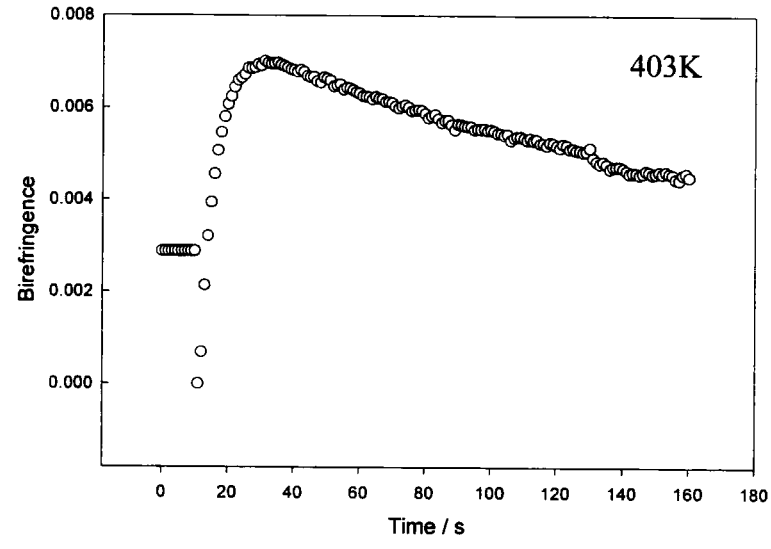

Figure 3.3.3.11: Birefringence of PVCi After Annealing at 365K & 403K.

Figure 3.3.3.11 shows that annealing of the sample does not remove any inherent birefringence. Chain orientation was set when the sample was spin cast and was not altered by the annealing process.

As stated previously, irradiation of PVCi with vertically polarised UV light induces a cross-linking reaction of the cinnamate side chains lying parallel to the UV polarisation vector. Any side chains lying at some angle from this orientation will also react, but as they are not in such a favourable position, i.e. their dipoles are not aligned with the polarisation vector in the incoming radiation, reaction is much slower. If the birefringence were influenced solely by the reaction of the parallel side chains, then a curve such as that shown in Figure 3.3.1.12 would be expected.

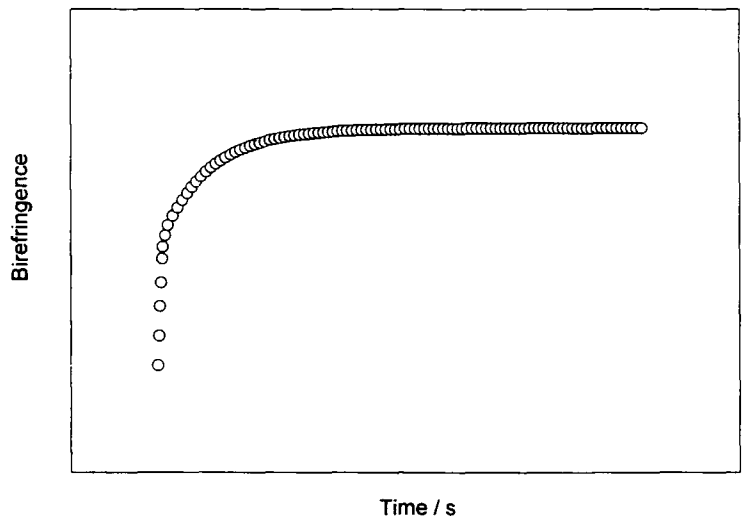

Figure 3.3.3.12: Fast Decay of Side Chains Parallel to Polarisation Vector.

An initial fast rise in birefringence is observed as all of the favourably aligned double bonds react. This is followed by a plateau caused by the lack of further bonds in this orientation and therefore no further reaction is possible and hence the birefringence remains constant.

If the reaction of side chains at an angle to the polarisation vector of the incoming radiation controlled the shape of the observed birefringence curve, a plot as shown in Figure 3.3.3.13 would result.

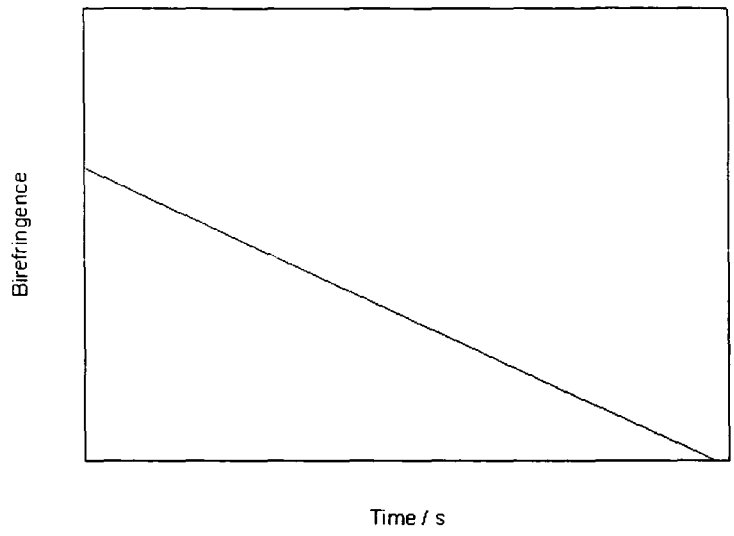

Figure 3.3.3.13: Slow Decay of Side Chains At An Angle to Polarisation Vector.

A much slower, gradual decrease in birefringence is observed as bonds in much less favourable orientations react as irradiation time increases.

In PVCi, both reactions occur, giving rise to birefringence curves as shown in Figure 3.3.3.14. The birefringence increases rapidly as the side chains lying parallel to the polarisation vector of the incoming light react. This increases the anisotropy in the sample and hence increases the birefringence. The birefringence then begins to decrease as the side chains at an angle to the UV polarisation vector react. This reaction begins to remove the anisotropy in the sample and therefore leads to a decrease in birefringence.

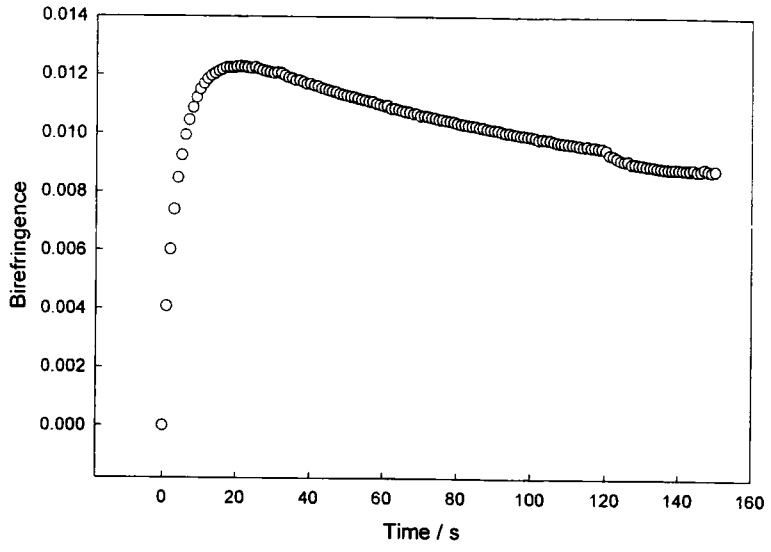

Figure 3.3.3.14: Birefringence Curve for PVCi.

This composite curve can be described mathematically by the following equation

$$\Delta n(calc) = A\left(\exp^{-k_1 t} - \exp^{-k_2 t}\right)$$

which is a combination of an exponential rise and an exponential decay. The experimental birefringence curves can be fitted using this equation to obtain values for A, k_1 and k_2. Some example fits to the data are shown in Figure 3.3.3.15 and the values obtained for all fits are summarised in Table 3.3.3.1.

Laser Position	A	k_1	k_2
Centre	6.56×10^{-3}	9.17×10^{-3}	0.19
Centre	4.92×10^{-3}	5.66×10^{-3}	0.22
Centre	7.60×10^{-3}	3.65×10^{-3}	0.19
Top Edge	8.07×10^{-3}	4.42×10^{-3}	0.25
Horizontal Edge	7.70×10^{-3}	6.09×10^{-3}	0.13
Horizontal Edge	0.01	1.72×10^{-3}	0.25
Upright Edge	6.23×10^{-3}	3.52×10^{-3}	0.24
Upright Edge	7.46×10^{-3}	3.47×10^{-3}	0.28
Upright Edge	8.10×10^{-3}	3.98×10^{-3}	0.23
Upright Edge	7.66×10^{-3}	3.54×10^{-3}	0.21
Upright Edge	1.53×10^{-2}	2.21×10^{-3}	0.31
Upright Edge	1.13×10^{-2}	3.05×10^{-3}	0.24
Upright Edge	1.29×10^{-2}	2.72×10^{-3}	0.27

Table 3.3.3.1: Fits Values for PVCi.

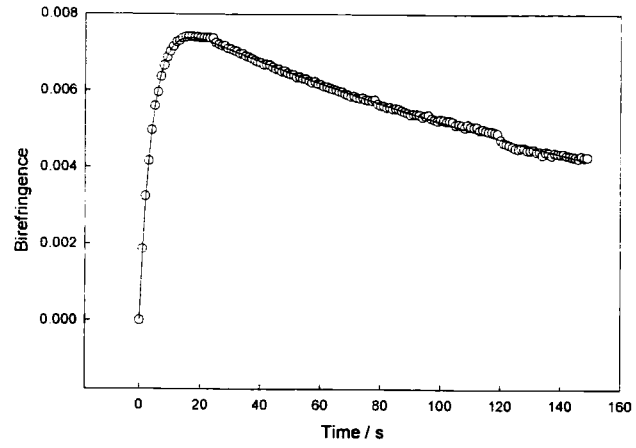

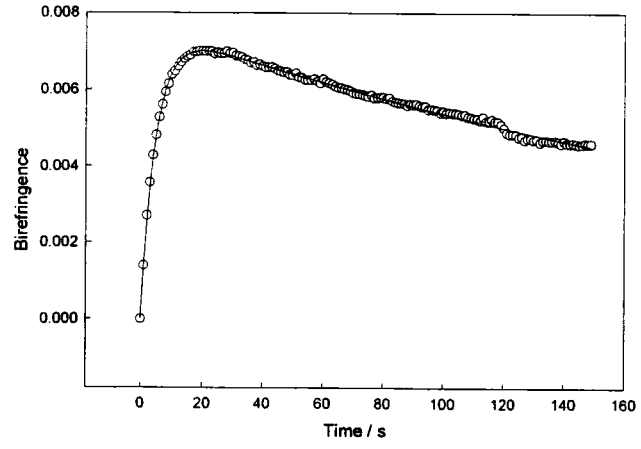

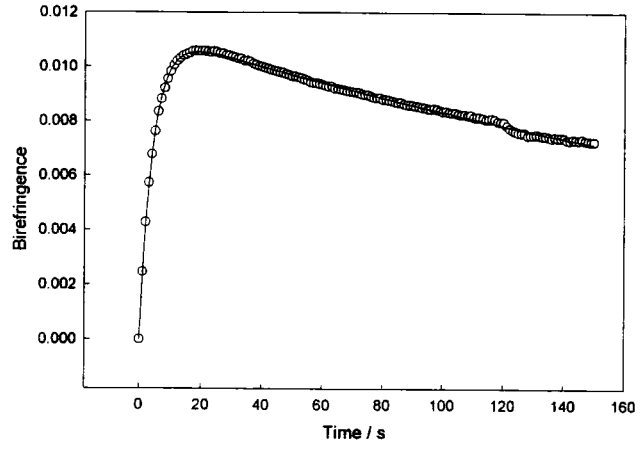

Figure 3.3.3.15: Fits to PVCi Birefringence Data.

Figure 3.3.3.15 shows a small drop in the birefringence at ~ 120s exposure. This is the point at which the irradiating He-Cd laser was switched off and the small drop is due to relaxation of the side chains. The birefringence data was fitted both with and without the data after the drop present and the values of all parameters showed insignificant variations (0>variation<10%). From the magnitude of the reaction rates, it is postulated that the value of k_1 is the rate constant for the reaction of side chains at an angle to the polarisation vector while k_2 is the rate constant for reaction parallel to the polarisation vector of the incoming radiation. In all cases, the value of k_2 is much larger than that of k_1, indicating as expected, that the reaction of chains parallel to the polarisation direction is much faster than the reaction of chains at some angle to it.

As noted in chapter 2.8.3, measurements were recorded at various positions within the sample. For data recorded at the upright edge of the sample, the values of k_1 and k_2 are reasonably constant:

$$k_1 = 3.21 \times 10^{-3} \pm 1 \times 10^{-3}\ s^{-1}$$

$$k_2 = 0.25 \pm 0.06\ s^{-1}$$

At the centre of the sample, the values for k_2 are similar 0.2 ± 0.02 but there is much variation in k_1. Although there may be slight trends within data measured in the same region of the sample, there is no correlation between position and orientation. The side chains do not react faster or slower at any one position in the sample.

The values obtained for the rate of reaction, k_1 and k_2, of the cinnamate side chains are of the order of 10^{-3} and 0.1 s^{-1} respectively. This indicates very slow reaction, even with the high power density obtained from the irradiating source. Rate constants for other photoreactions in the solid state are not available for comparison.

However, rate constants for solution and gaseous reactions are available: the gas phase photolysis of 2,4-dimethylpenta-1,3-diene with 254nm radiation forms a cyclobutene species with a rate constant of 2×10^9 s^{-1} [10]. In solution, decay of the exciplex formed between anthracene and N,N-dimethylaniline occurs at a rate of ~10^6 s^{-1} [11] and the formation of an anthracene dimer from a singlet state exciplex occurs at 6.4×10^7 s^{-1} [11].

Reactions occurring in solution generally occur much faster than those in the solid state due to the greater mobility of the reacting species. Despite this fact, the photodimerisation occurring when a film of PVCi is irradiated with monochromatic light is a very slow process. It is therefore unsurprising that only a small extent of reaction was achieved when using the deuterium lamp as the irradiating source.

Similar birefringence curves for PVCi were fitted using equations proposed by Bryan-Brown & Sage[12].

$$\Delta n \approx K(3Q - P) \qquad \text{Equation 3.3.3.1}$$

where

$$P = \int_{\theta=0}^{\pi} \int_{\phi=0}^{2\pi} \sin\theta \exp^{-\cos^2\theta} d\theta d\phi = 2\pi \left(\frac{\pi^{1/2} Erf\left(t^{1/2}\right)}{t^{1/2}} \right) \qquad \text{Equation 3.3.3.2}$$

$$Q = \int_{\theta=0}^{\pi} \int_{\phi=0}^{2\pi} \sin\theta \cos^2\theta \exp^{-t\cos^2\theta} d\theta d\phi = 2\pi \left(\frac{\pi^{1/2} Erf\left(t^{1/2}\right)}{2t^{3/2}} - \frac{1}{t \exp^{-t}} \right) \qquad \text{Equation 3.3.3.3}$$

and K̀ is an arbitrary value.

What is obtained from these equations is a 'universal' birefringence curve which is manipulated 'manually' by varying K. Figure 3.3.1.16 shows the non-linear

least squares fit to the PVCi birefringence data obtained using the equations of Bryan-Brown & Sage[12] within Jandel Sigmaplot 3.0.

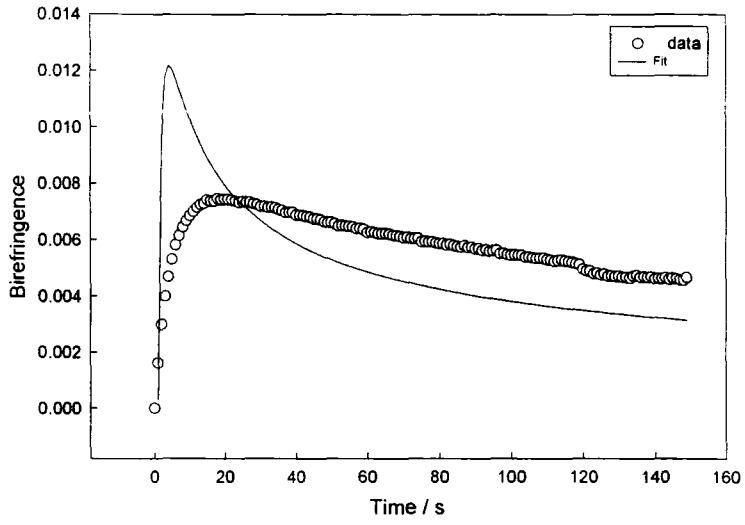

Figure 3.3.3.16: Fit to PVCi Data Using Equations of Bryan-Brown & Sage[12].

Figure 3.3.3.16 shows that the birefringence data for PVCi cannot be fitted using standard non-linear least squares fitting procedures. A fit can be obtained if the universal curve is scaled 'by eye' with respect to time and birefringence. The universal birefringence curve was obtained using equation 3.3.3.1 with K=1. The universal curve obtained is identical in shape to the curve for the fit in Figure 3.3.3.16. The maximum birefringence point is multiplied by a factor which is given by equation 3.3.3.4.

$$Factor\,1(\Delta n) = universal\,\Delta n\,\max imum\left(\frac{actual\,measured\,\Delta n}{universal\,\Delta n\,\max imum}\right) \quad \text{Equation 3.3.3.4}$$

This scales the birefringence maxima so that they coincide. The universal curve is then scaled along the time axis using equation 3.3.3.5.

$$Factor\,2(time) = universal\,time\left(\frac{actual\,time}{universal\,time}\right) \qquad \text{Equation 3.3.3.5}$$

This then gives the 'manual' fit to the birefringence data, Figure 3.3.3.17.

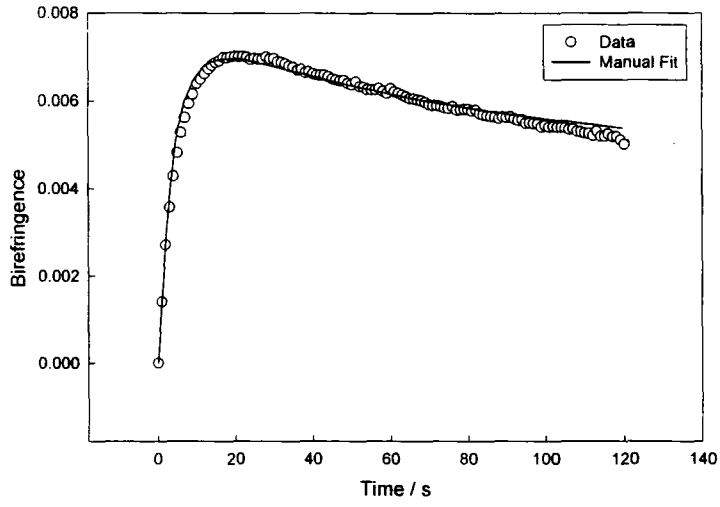

Figure 3.3.3.17: Fit 'By Eye' to PVCi Birefringence Data.

However, equations fitted 'manually' have no physical scientific meaning. Indeed, an infinite number of equations could be used in such a manner to produce a 'fit' to the data and as such, do not produce valid scientific parameters.

3.3.4. Fabrication of a Simple Liquid Crystal Cell.

A film of PVCi on quartz was exposed to a vertically polarised laser (λ=325nm). This will induce the depletion of the chromophores with their side chains parallel to the laser polarisation direction. Construction of a cell as shown in Figure 3.3.4.1 was expected to give rise to a twisted display. The sample was irradiated for 0.1, 2, 5, 10, 20, 80, 200, & 600 seconds with a beam intensity of 1.6mW through a 400μm aperture. Irradiation for one tenth of a second does not induce any change in

the film. The irradiated area corresponding to two seconds exposure, although visible, does not show enough contrast to produce a good quality photograph.

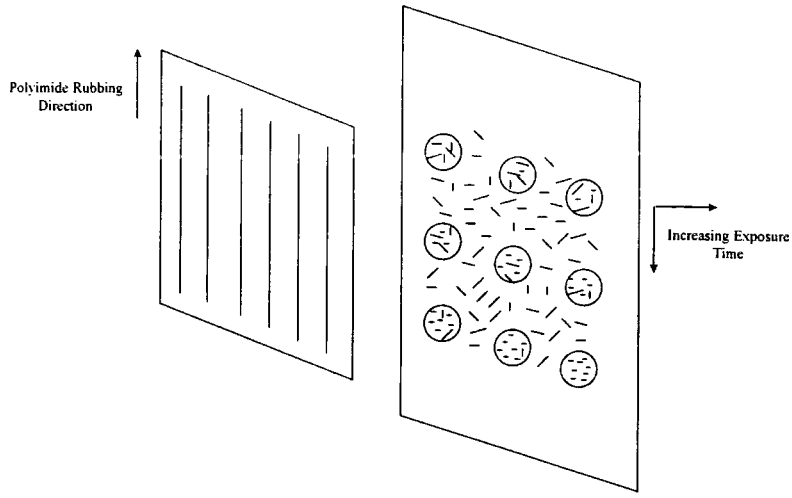

Figure 3.3.4.1: Formation of a Liquid Crystal Cell Using PVCi.

The cell was filled with the liquid crystal E7 which is mixture of liquid crystals, the main component being 5CB, and then viewed through a microscope with crossed polarisers.

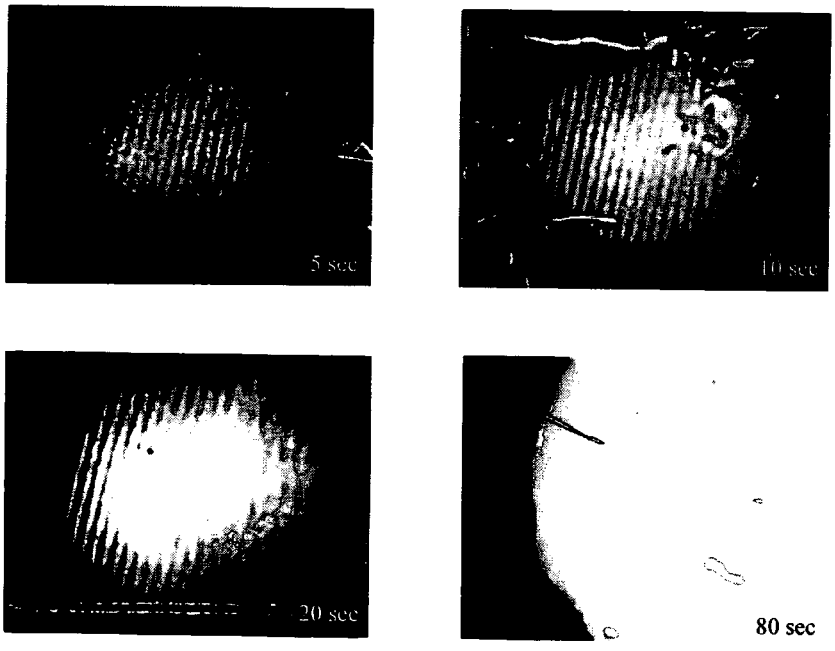

Figure 3.3.4.2: Images from PVCi Cell (. ——— ~ 2mm)

A small white spot was observed where the laser had been positioned on the sample. Figure 3.3.4.2 shows the images obtained for 5, 10, 20 & 80 seconds exposure. The size of the spot increases with increasing irradiation time. The lines that appear across the spot are caused by back reflection through the sample and cannot be avoided. This sample was also irradiated for 200 & 600 seconds. After this time, the spots sizes increase dramatically and the spot appears brighter. The photographic capabilities of the camera were insufficient to capture the whole of the spot and therefore these images are not shown. Spot diameter increases with increasing exposure as the laser beam intensity can be represented by a gaussian distribution. Thus, the longer the laser resides on a given region, the greater the effect the edges of the beam have on that region and hence the spot diameter increases.

In an ideal situation, a cell would be formed with a 90° twist. The twist angle of the cell can be measured by setting the rubbing direction of the polyimide layer parallel to the input polariser. This was achieved by obtaining extinction of the unexposed regions. The analyser was then rotated until white light extinction is achieved within the exposed region for each individual spot. The results of twist angle measurements on irradiated PVCi are summarised in Table 3.3.4.1.

Exposure / s	Twist Angle (°)
0.1	-
2	2
5	10
10	31
20	45
80	63
200	67
600	69

Table 3.3.4.1: Twist Angles for PVCi.

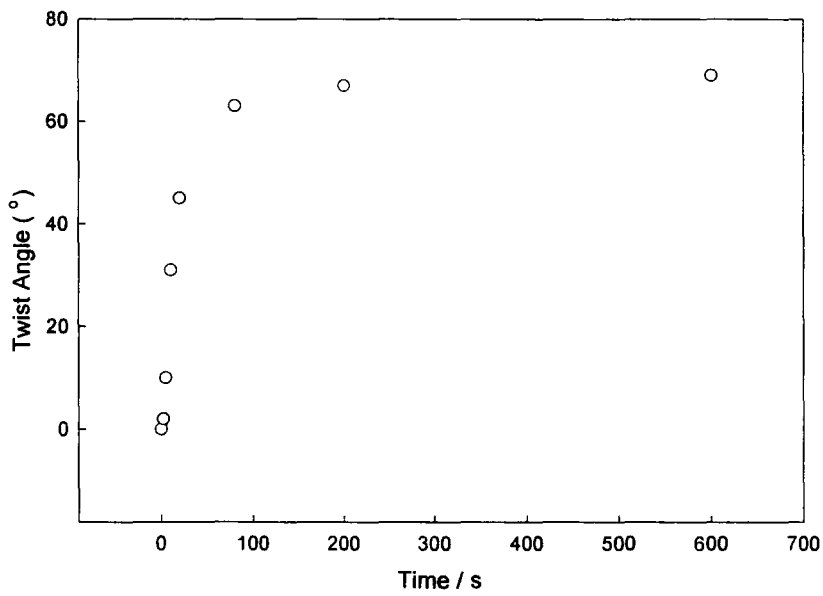

Figure 3.3.4.3: Variation of Twist Angle with Irradiation Time in PVCi.

As Figure 3.3.4.3 shows, the twist angle increases rapidly for short exposure times. As irradiation increases, the twist angle begins to level off, indicating that prolonged exposure would not produce further improvement to the twist angle value

of 69°. Approximately 100 seconds exposure gives rise to a maximum twist angle and it is interesting to note that this does not correspond to the irradiation time of ~20 seconds at which maximum birefringence is induced. The birefringence is measured using the bulk of the sample whereas the twist angle is a feature of the sample surface. These data indicate that either reaction and hence alignment at the surface takes much longer to induce or that alignment of layers deeper into the sample has an effect on liquid crystal orientation. These results highlight the complexity of the alignment mechanism and imply that liquid crystal alignment does not rely solely upon the anisotropy created in the alignment layer.

3.4. Conclusions

PVCi is an ideal model compound for studies using polarised UV exposure. Its reactions under the influence of UV radiation are well documented. This allowed exposure experiments similar to those cited in the literature to be undertaken using a deuterium lamp as the radiation source.

When attempting quantum yield calculations, the main problem was found to be accurate determination of the photon density absorbed by the sample. The deuterium lamp produces a broad wavelength radiation range for which no suitable chemical actinometer could be found. However, quantum yield calculations were still carried out but caution has to be adopted when assessing the absolute value of the quantum yield. The UV spectroscopy does not give results with any orientational dependence as the spectrometer uses an unpolarised beam. Nevertheless, any reaction

induced by the exposing radiation which gives rise to chromophore depletion can be monitored.

Upon exposure to unpolarised radiation, the quantum yield decay curve was shown to be similar to those obtained by Egerton *et al*[7] for exposure to a medium pressure mercury lamp. However, results disagree with respect to the extent isomerisation competes with dimerisation. In this work, isomerisation and dimerisation were shown to compete effectively in some instances.

When irradiating with polarised light, fewer chromophores react due to the considerable decrease in photon density falling on the sample when the polariser was used. PVCi reacted similarly with both vertically and horizontally polarised radiation.

Using a laser (λ=325nm) as the radiation source, ~80% of the chromophores present in the sample react and dimerisation was the preferred reaction pathway. These results indicate that the deuterium lamp may not be the most efficient source to induce the cross-linking reaction due to a low photon flux at the desired wavelength.

Infrared dichroism indicated that there was no preferred reaction of cinnamate groups on exposure to polarised radiation from the deuterium lamp. However, due to the complexity of the experimental design, absolute dichroism of the magnitude reported by Ichimura[5] , ~0.05, would not be detected by this method.

Birefringence studies show that large variations in side chain orientation exist both within and between samples. This reinforces the fact that control of initial chain orientation has not been possible, even with annealing. One explanation for this is that the side chains are entangled and very long annealing times are required to remove the entanglements. This obviously causes problems as each sample may give very different results with no distinct links between them, such as area of the sample

analysed. Birefringence was not detected when the deuterium lamp was used as the radiation source. This is to be expected when the rates of reaction achieved with laser irradiation are considered. With the laser as the UV source, the rate of the cross-linking reaction is extremely slow, even when the double bonds are most favourably aligned for reaction.

PVCi has been shown to align liquid crystals in a simple cell with increased cell twist achieved by increased UV exposure. Once again, the deuterium lamp fails to induce sufficient reaction to effect alignment.

The most important results to be carried forward from the work on PVCi is that the sample variations appear to be uncontrollable and therefore lead to variations in some results, additionally, although the deuterium lamp promotes reaction, the rate is very slow.

References

1) J.Berthram & R.Kursten, *J.Prakt.Chem*, **2**, 51, 325 (1895).

2) J.Kosar, Light-Sensitive Systems, Wiley, 1965.

3) A.Reiser & P.L.Egerton, *Photogr.Sci.& Eng*, **23**(3), 114 (1979).

4) N.J.Turro, Modern Molecular Photochemistry, Univ.Sci.Books 1991.

5) K.Ichimura, Y.Akita, H.Akiyama, Y.Hayahsi & K.Kudo, *Jpn.J.Appl.Phys.*, **35**(1996), L992.

6) T.Y.Marushi & Y.A.Reznikov, *Mol.Mat.,* 1993, **3**, 161.

7) P.L.Egerton, E.Pitts & A.Reiser, *Macromolecules* 1981, **14**, 95.

8) J.Rennert, S.Soloway, I.Waltcher & B.Leong, *J.Am.Chem.Soc*, 1972, 7242.

9) M.Schadt, K.Schmitt, V.Kozinkov & V.Chigrinov, *Jpn.J.Appl.Phys*, **31**(1992), 2155.

10) D.Bryce-Smith, Photochemistry Volume 3: A Review of the Literature Published Between July 1970 and June 1971, The Chemical Society.

11) A.Gilbert & J.Baggot, Essentials of Molecular Photochemistry, Blackwell Sci.Pub.1991.

12) G.P.Bryan-Brown & I.C.Sage, *Liq.Cryst.*,**20**(6), 825.

Chapter Four

Poly (9-Anthracenoate Ethyl Methacrylate)

4. Poly(9-Anthracenoate Ethyl Methacrylate)

4.1. Introduction

Dimerisation of anthracene was among one of the first examples of photodimerisation of an aromatic compound[1]. The reaction proceeds under the influence of light with a wavelength λ_0>290nm and gives rise to the 9,10-9,10-dimer of anthracene, Figure 4.1.1.

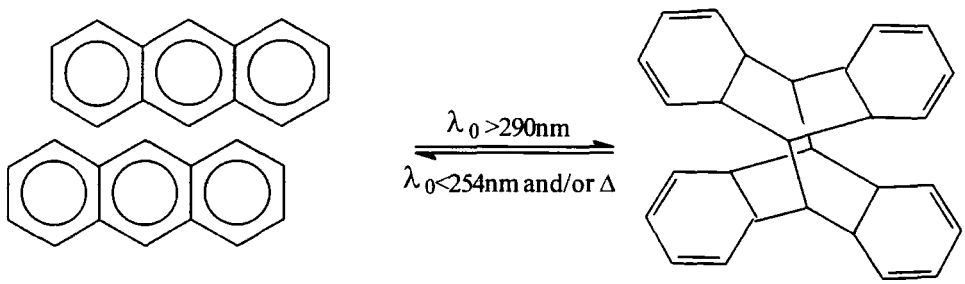

Figure 4.1.1: Dimerisation of Anthracene.

The central rings of the anthracene molecule lose their aromaticity while the outer rings are bent outward from their original molecular planes by electrostatic repulsions. This reaction may be reversed thermally and/or by irradiation with radiation of a shorter wavelength (λ_0<254nm). The photodimerisation reaction may be quenched by oxygen or by conjugated dienes.

Photodimerisation of anthracene has been studied for crystal and solution states as well as for substituted anthracenes[1,2,3]. For the crystalline form, the structure of the product is governed by the relative orientation of the monomeric species in the lattice and this is known as topochemical control. The ideal topochemical orientation is a 'sandwich', Figure 4.1.2.

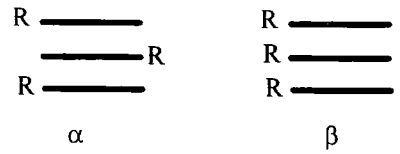

Figure 4.1.2: Monomer Orientations in Crystalline Anthracene.

Dimerisation of crystal structure α will produce centric dimer whereas dimerisation of β will give mirror-image dimers. In practice, centric dimers are most commonly observed[1, 2]. This can be explained by considering the orientation of the β structure. Both electrostatic repulsions and steric hindrance will impede the formation of mirror-image dimers.

In anthracene photodimerisation, the reactive state is the S_1 arene. An excimer is formed by the reaction of this S_1 arene with a ground state anthracene molecule and subsequent reactions are summarised in Figure 4.1.3.

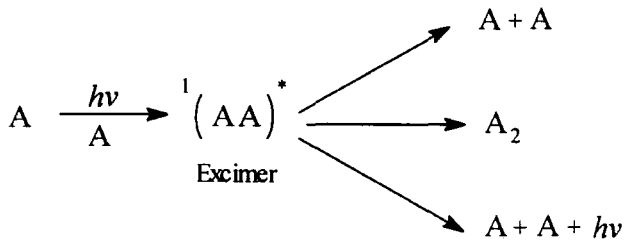

Figure 4.1.3: Photoreactions of Anthracene.

Substitution in the 9 and/or 10 positions modifies the dimerisation due to steric hindrance. This is summarised in Table 4.1.1 which indicates the extent of hindrance of various groups[4].

	Hindrance	Substituent Group
I	Negligible Hindrance	1-methyl & 2-methyl derivatives
II	Photodimerisation occurs, but less efficient than **I** due to increased hindrance.	9-methyl, 9-ethyl, 9-n-propyl, 9-methoxy, 9-acetoxy, 9-anthracene carboxylic acid & 9-methyl 10-methoxyanthracene
III	Hindrance such that photodimerisation does not occur.	9,10-dimethyl, 9-methyl 10-ethyl, 9,10-n-propyl, 9-phenyl & 9-benzyloneanthracene.

Table 4.1.1: To show the effect of Substituents on Photodimerisation[4].

When irradiating anthracene, it is important to be aware of the possibility of energy migration or energy 'hopping'[1,5,6,7,8,9]. Complete localisation of excitation on one particle in a sample of identical particles is improbable. Identical particles with electronic states of equal energy perturb each other and this causes the excitation to 'hop' from one particle to another. The energy can hop until it is quenched by some uni- or bimolecular process.

Molecular diffusion is one process by which energy can be transferred from an excited state molecule (A^*) to a ground state molecule (B). In the solid state this process unlikely due to the separation between the molecules.

Long range interactions between A^* and B can occur via radiative and non-radiative processes. For the radiative pathway, energy emitted by A^* can be reabsorbed by B. This process requires the emission spectrum of A^* to overlap with the absorption spectrum of B.

In the case of non-radiative energy transfer, there are two distinct pathways. In Coulombic energy transfer, the A^* dipole, i.e. the excited electron, interacts with the B dipole, the unexcited electron in the HOMO of B. This dipole-dipole interaction causes the electron in the HOMO of B to oscillate more violently and the electron becomes more energetic. This may lead to the excitation of this electron into the LUMO of B, providing the LUMO of B is equal or lower in energy to the HOMO of A, with a corresponding de-excitation of the excited electron on A^*.

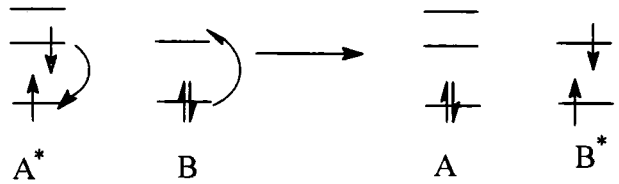

Energy has been transferred from A^* to B despite the fact that the two species have not come into close contact and no electrons have been passed between them.

In contrast, electron exchange energy transfer requires much closer contact between A and B. The excited electron on A^* transfers to the LUMO of B with simultaneous transfer of a electron from the HOMO of B into the corresponding A orbital. This transfer requires the overlap of A and B electronic orbitals.

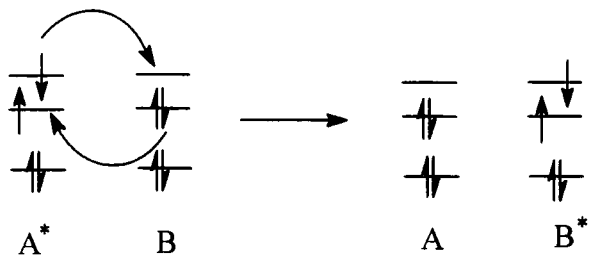

Non-radiative energy transfer may occur over large (20-100Å) or small (6-20Å) separations depending on the mechanism involved. Excitons in anthracene crystals have been shown to permeate up to ~460Å (singlet state) and ~10μm (triplet state) [9].

4.2. Synthesis and Characterisation

Poly (9-anthracenoate ethyl methacrylate) was synthesised by free radical polymerisation of the corresponding monomer in 2-butanone using AIBN as an initiator. This synthesis was performed by Kate Foster[10] as part of a PhD synthesising potential alignment layers for liquid crystal displays and a polymer of molecular weight (Mn) 14,000 and a polydispersity of 2.0 was obtained.

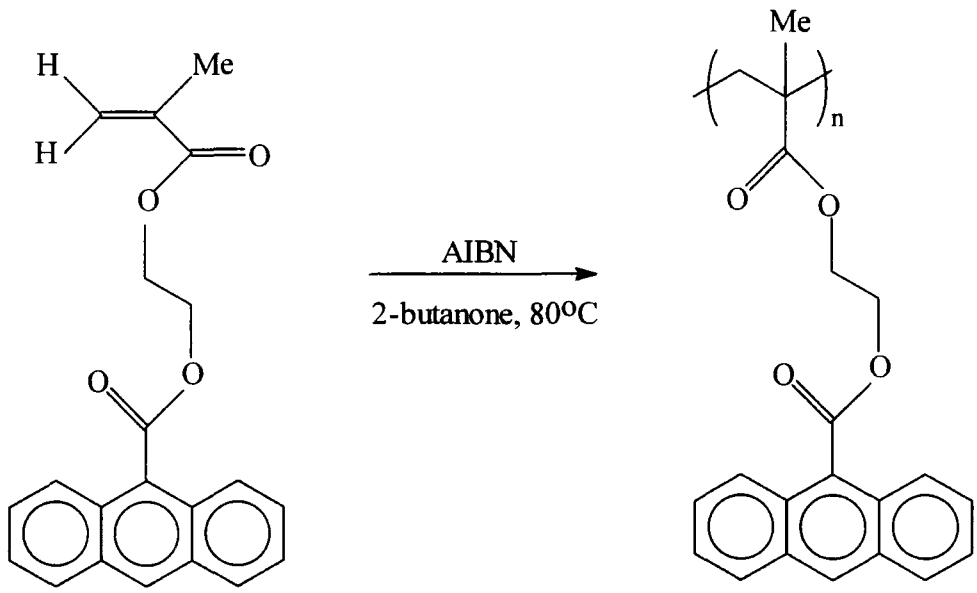

Figure 4.2.1: Synthesis of Poly (9-anthracenoate ethyl methacrylate).

The thermal stability of the polymer was assessed using TGA. Figure 4.2.2 shows a plot of percentage mass loss of polyanth as a function of temperature. Polyanth was found to be stable to a temperature of ~593K, after which mass is lost at a steady rate.

DSC was used to determine the crystallinity of polyanth. The trace obtained showed no evidence of melting or crystallisation transitions but did show a glass transition temperature, T_g, of 374K (range 363-381K), see appendix for chapter four.

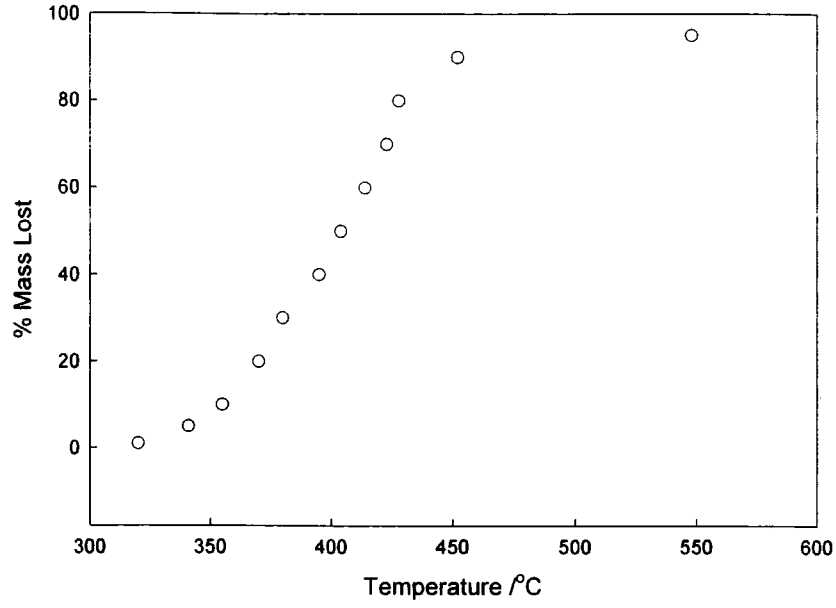

Figure 4.2.2: Mass Lost on Heating For Poly (9-anthracenoate ethyl methacrylate).

From the ^{13}C nmr spectrum, the tacticity of the polymer can be calculated. The peaks due to the carbonyl species attached to the backbone are located at 155-177ppm. The relative orientation of the carbonyl groups and hence the side chains themselves can be determined solely in terms of orientation with respect to the neighbouring groups, Figure 4.2.5.

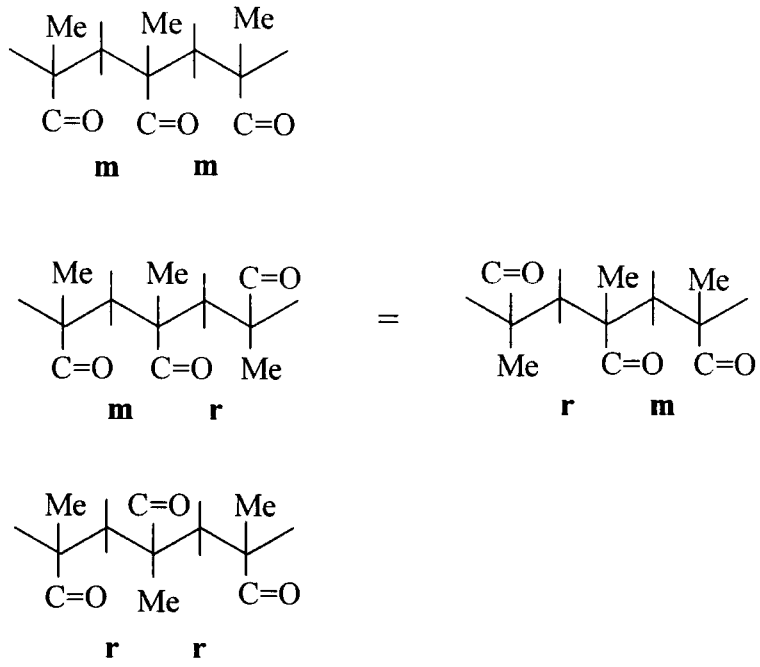

Figure 4.2.5: Polyanth Tacticities.

Figure 4.2.5 shows that if the polymer was completely randomly oriented, then a ratio of 1:2:1 would be expected for the carbonyl peaks. As the ^{13}C nmr shows, little of the mm dyad, 9%, found at ~175ppm exists. The polymer consists of ~40% of the mr/rm dyad at 175.7ppm and 51% of the rr dyad at 176.4ppm. This indicates that the stereochemistry of the polymer is tending towards syndiotactic and the dyads can be represented as in Figure 4.2.6.

r r r r r m r r r r r m r r r r r r r m r r r r r r r r m r r r r r m

Figure 4.2.6: Dyads in Syndiotactic Polyanth.

NMR

^{1}H and ^{13}C NMR spectra are shown in Figures 4.2.3 & 4.2.4.

The following tables summarise the NMR peak assignments.

^{1}H

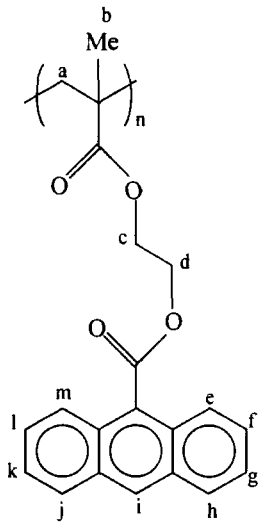

ppm	Assignment
0.70	b
1.59	impurities (sharp peak)
1.59	a
4.02	c
4.30	d
7.20	e, h, j, m
7.80	f, g, k, l
8.16	i

^{13}C

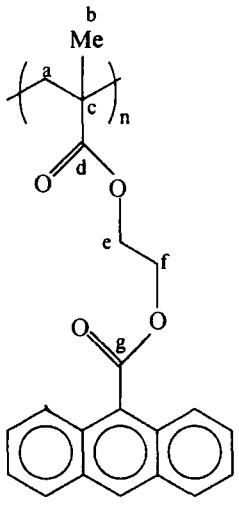

ppm	Assignment
18	b
44	a, c
62	e, f
77	chloroform
125-130	Ring Carbons
168	g
175-177	d

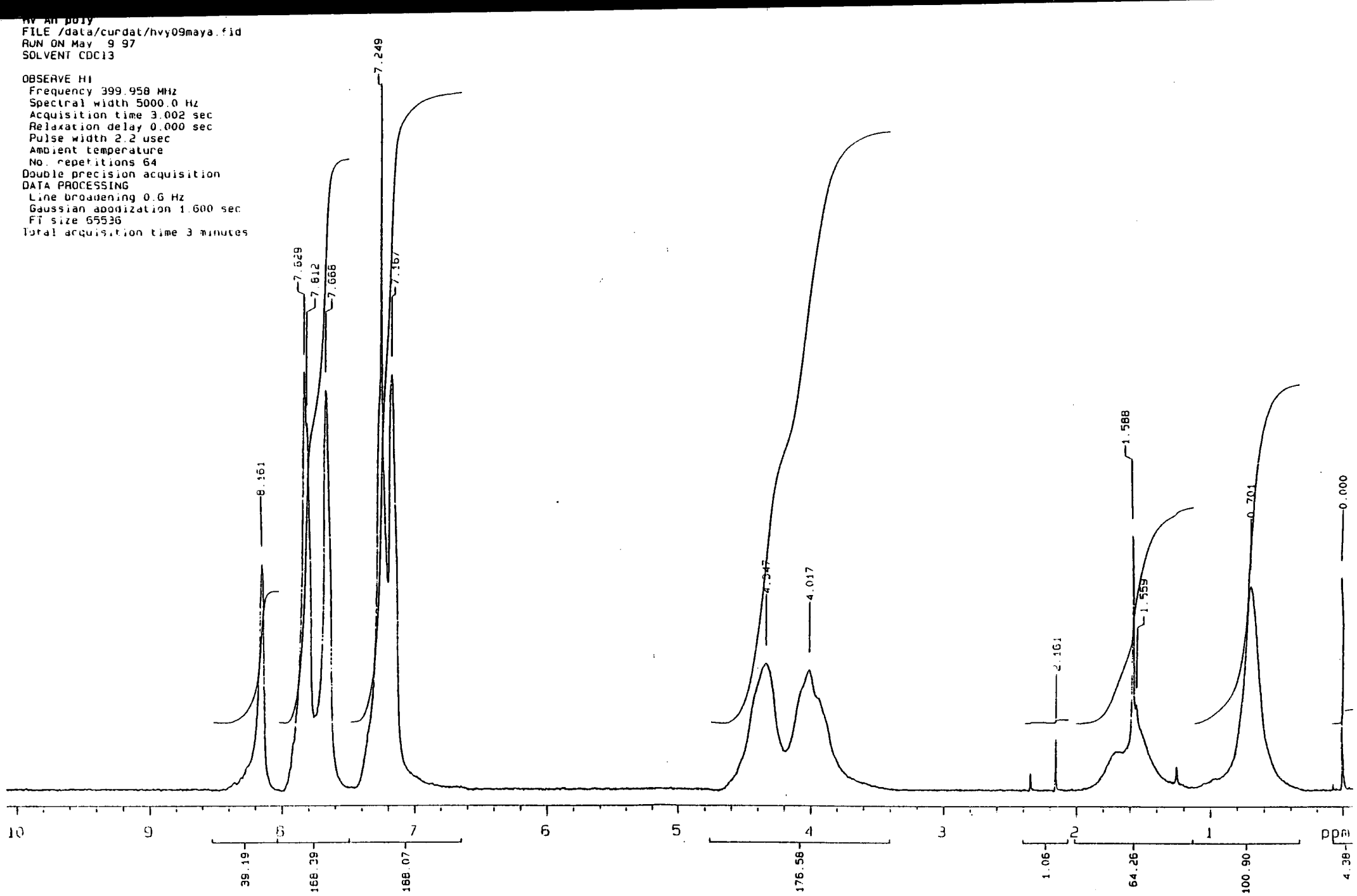

Figure 4.2.3: ^{1}H NMR Spectrum of Polyanth in $CDCl_3$.

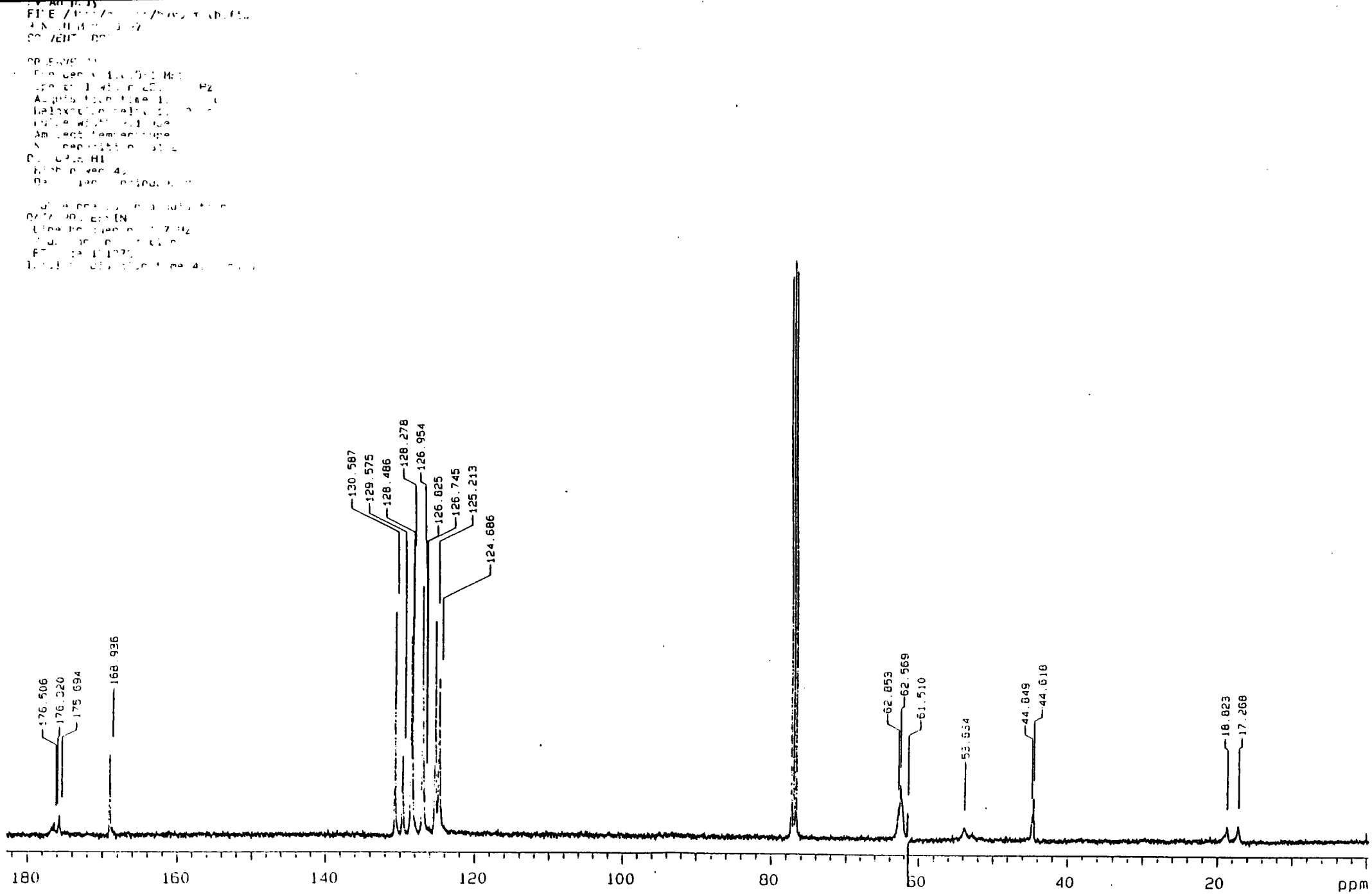

Figure 4.2.4: ^{13}C NMR Spectrum of Polyanth in $CDCl_3$.

Molecular mechanics calculations were performed on a section of polyanth six monomer units long (syndiotactic orientation of monomer units). The minimised structure for the polyanth was calculated using the Steepest Descent algorithm in the Biosym molecular modelling package. The forcefield used was CVFF and 10,000 iterations were performed. Figures 4.2.7 and 4.2.8 show the minimised structures obtained using this method. These structures clearly show that the schematic representation of polyanth, such as that shown in Figure 4.2.1 is rather misleading. Figure 4.2.1 indicates that the anthracene moiety lies perpendicular to the side chain to which it is attached. Polyanth structures achieved by molecular modelling techniques show this to be the case for some units, however, a considerable number of anthracene molecules are oriented parallel to the side chains to which they are attached. This has obvious consequences when irradiating the sample with polarised light. The strongest dipole in the anthracene molecule lies along the direction of the long axis.

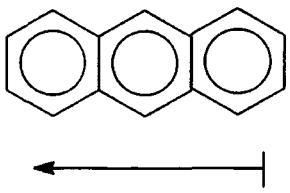

Therefore, when the polarisation vector of the exposing radiation and the anthracene dipole are coincident, excitation can occur. Consequently, it is very important to know in which direction the anthracene species are lying. The anthracene molecules lying parallel to the polarisation vector of the incoming radiation react preferentially.

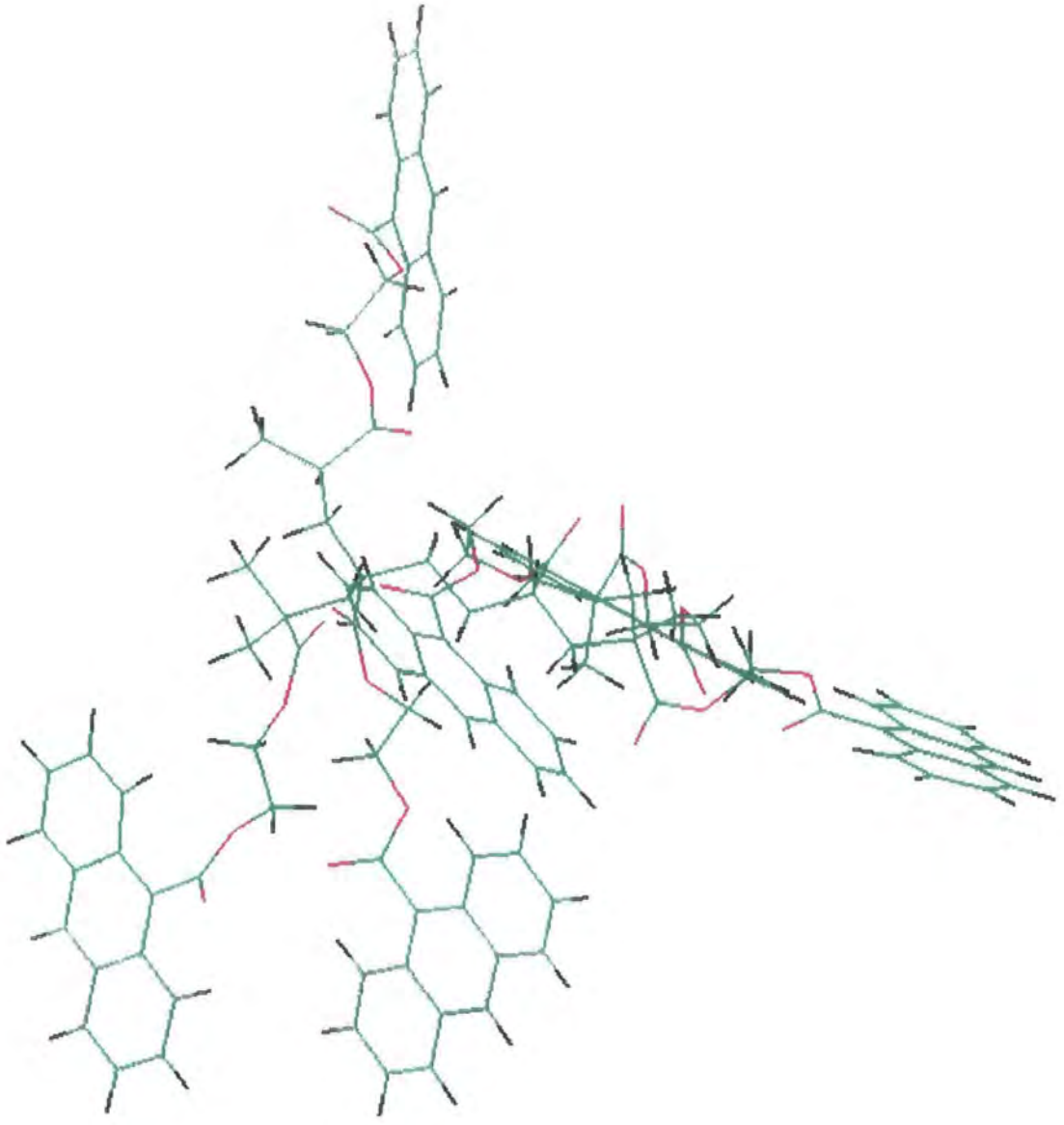

Figure 4.2.7: Minimised Structure of Polyanth (6 Monomer Units).

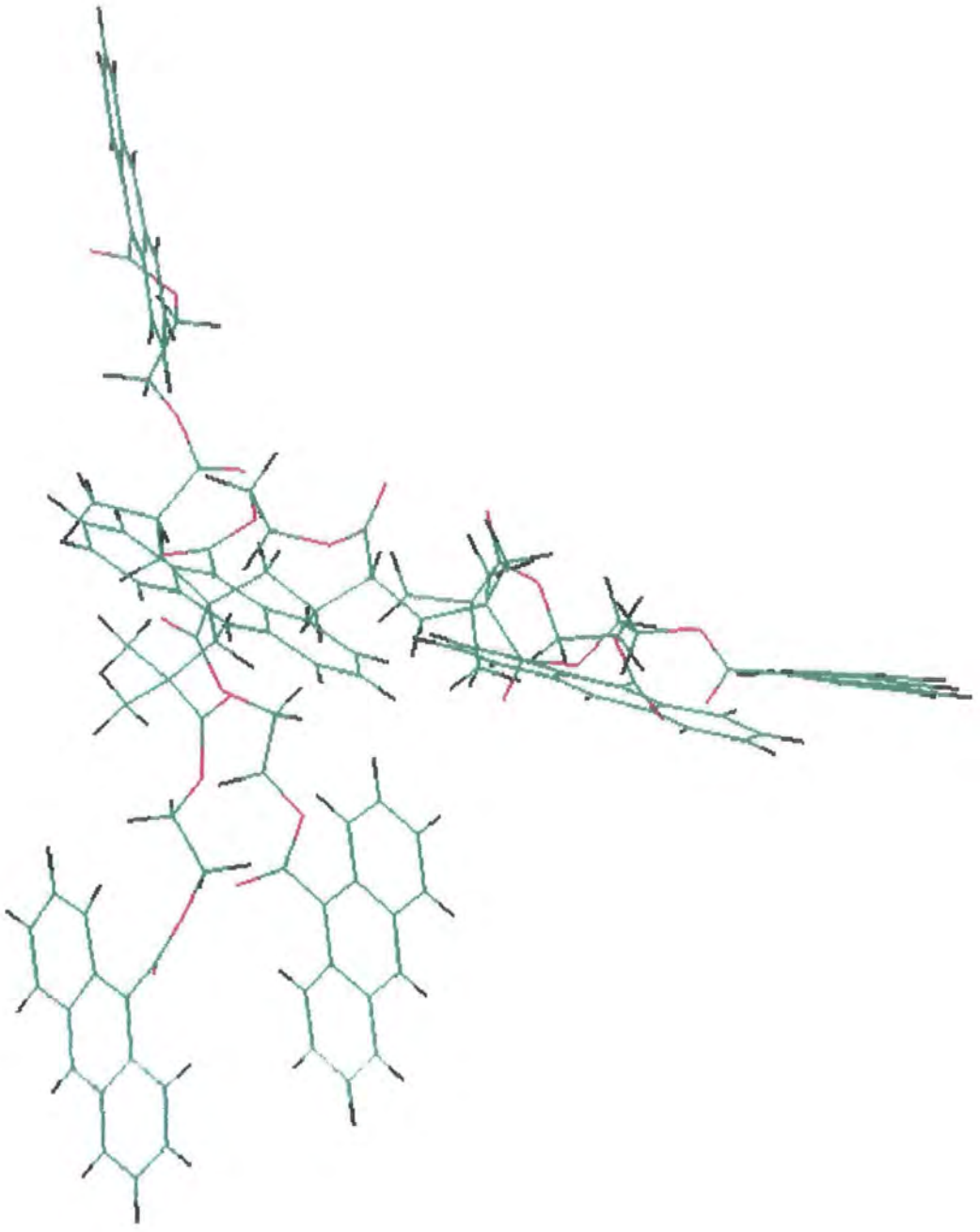

Figure 4.2.8: Minimised Structure of Polyanth (6 Monomer Units).

Desired Reactions

It is well known[1,4,8] that anthracene molecules cross-link via the 9,10-position to give anthracene dimers when irradiated with radiation of wavelength λ_o>290nm. If the anthracene moiety is incorporated into a polymer, it is expected that the cross-linking reaction will also occur. When irradiating with polarised light , this reaction is anticipated to have orientational dependence, with vertically polarised light reacting anthracene molecules lying parallel to the polarisation direction.

When the reaction is followed by UV spectroscopy, a decrease in the absorbance due to the anthracene chromophore is expected as the dimerisation reaction removes the conjugation across the molecule. For infrared dichroism studies, the C-H in-plane bend of the central benzene ring will change due to the loss of aromaticity. The magnitude of this change will be small, however, with an anthracene moiety situated on every second side chain, the overall change should be significant and can be monitored to yield the dichroic ratio. Irradiation with vertically polarised light, will induce reaction in anthracenes parallel to the polarisation direction. The C-H in-plane bend is parallel to the long axis of the anthracene and as these species react, the absorbance measured using vertically polarised radiation (A_{para}) will decrease. As $D = A_{para}/A_{perp}$, the dichroic ratio is expected to decrease. As bonds are selectively depleted in a given orientation, anisotropy is created within the film. This chemical modification leads to refractive index differences within the film and hence birefringence should be observed. Finally, if reaction of the anthracenes parallel to the polarisation direction of the radiation occurs, liquid crystals are expected be aligned along the direction of the residual groups. Therefore twist will arise in a simple cell constructed as described in chapter 2.9 .

4.3. Results and Discussion

4.3.1. UV Spectroscopy

Quartz plates coated with thin films of polyanth were exposed to unpolarised radiation from the deuterium lamp and the UV absorption spectrum was monitored to follow the extent of reaction, Figure 4.3.1.1

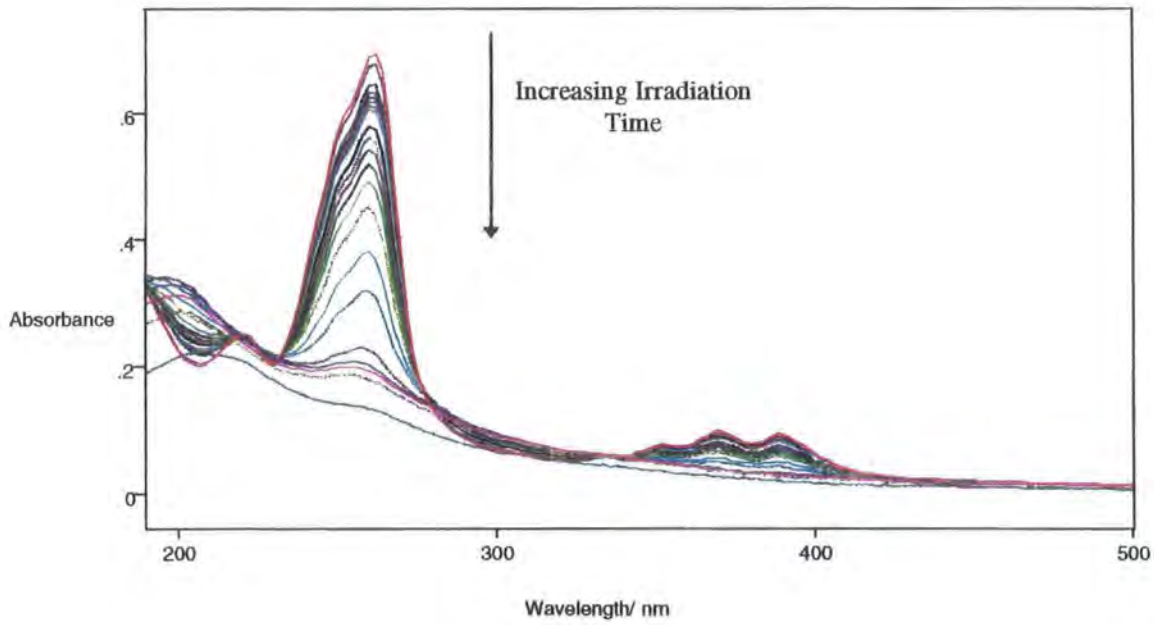

Figure 4.3.1.1: UV Absorption Spectrum for Polyanth Exposed to Unpolarised Radiation from the Deuterium Lamp.

This compares well with the spectrum of anthracene in cyclohexane, Figure 4.3.1.2, indicating that the anthracene present in the polymer is in a chemical environment similar to that of pure anthracene. It would appear as if the ester moiety attached to the anthracene species and the anthracene itself are not conjugated.

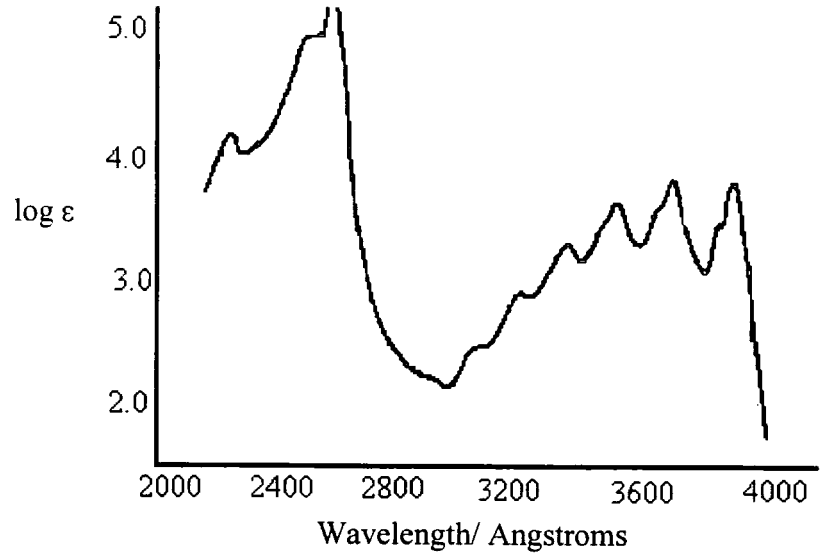

Figure 4.3.1.2: Anthracene in Cyclohexane[11].

Figure 4.3.1.1 shows the spectrum of polyanth which contains two distinct features. In the region 300-400nm are the characteristic fingers of the S_0-S_1 transitions in anthracene[8], shown in Figure 4.3.1.3. This is the weakest intensity band and is transversely polarised. Figure 4.3.1.4 show excited state resonance structures which represent this state of polarisation.

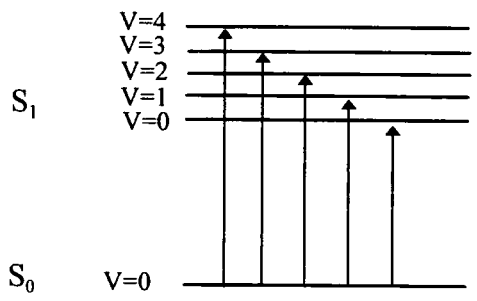

Figure 4.3.1.3: S_0-S_1 Transitions in Anthracene.

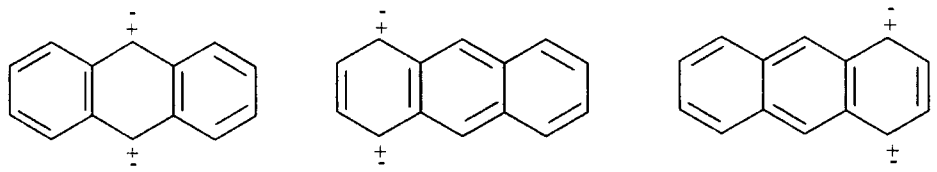

Figure 4.3.1.4: Transverse Polarisation in Anthracene.

There is a second major band at λ~280nm, which is the band in the spectrum of greatest intensity. This arises from the $^1B_b \leftarrow ^1A$ transition (S_0-S_n) and the polarisation in this state is longitudinal, Figure 4.3.1.5.

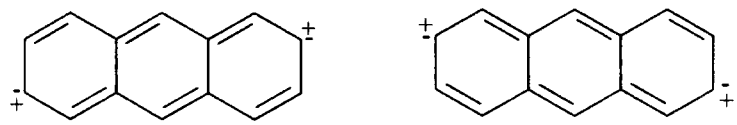

Figure 4.3.1.5: Longitudinal Polarisation in Anthracene.

This transition is the most probable in this system due to its large extinction coefficient. When an electron is promoted into the higher excited states, it will lose energy by vibrational motions until it reaches the S_1 state from which reaction occurs[1] It must be noted that the weaker S_0-S_1 transition may also occur when irradiating with the broad wavelength range deuterium lamp. This will induce reaction in those anthracene species lying with their long axis perpendicular to the polarisation vector of the incoming radiation. However, the probability of this transition occurring, as shown in Figure 4.3.1.1, is significantly lower than the probability of longitudinal absorption. The anisotropy created by the reaction of anthracenes with their long axis parallel to the polarisation vector will therefore be reduced slightly due to the reaction of anthracenes lying perpendicular to the polarisation direction. There is a second chromophore present in the polyanth system, the carbonyl group. The n-π^* transition of this species occurs at 280nm, however, this is a forbidden transition and the

absorption intensity will therefore be weak. This will create a low intensity band which is likely to be hidden beneath the lower wavelength transition of the anthracene moiety.

The π-system was initially thought to be delocalised across the anthracene and carbonyl species. However, work by R.S-L Shon *et al*[12] on the photodimerisation of 9-anthroate esters in solution, Figure 4.3.1.6, suggests that steric interactions of the ring hydrogens and the carbonyl group keep the 9-substituent almost 90° out of the plane of the anthracene group, thus impeding delocalisation.

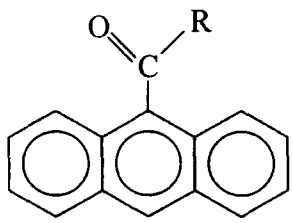

Figure 4.3.1.6: 9-Anthroate Ester.

The extent of delocalisation in polyanth can be determined by considering the UV absorption spectrum, Figure 4.3.1.1. It is possible that the loss of planarity in solutions of 9-antroate esters also occurs in the polyanth film. Yet it is also possible that the spinning down of the polymer film is achieved so quickly that the molecules are set in the configuration in which they fall onto the substrate and this may give rise to a more planar conformation. The most likely of these two suggestions is that little conjugation is occurring in the polyanth system. Jones[13] carried out a survey on the factors influencing the UV absorption spectra of polynuclear aromatic compounds. His work showed that the appearance of fine structure within the UV spectrum was indicative of poor conjugation, as conjugation gives rise to much broader bands. As

Figure 4.3.1.1 shows, fine structure is observed in the UV spectrum of polyanth, indicating that ineffectual conjugation occurs through this system.

On successive irradiation of polyanth, the intensity of the bands in the UV spectrum decrease. This arises as irradiation of the polymer with UV light causes excitation of an electron into the π^* orbitals of anthracene, giving an excited state species. Reaction of an anthracene moiety in the ground state with an excited state species gives rise to a dimer, providing the two molecules are favourably aligned. The aromaticity of the central ring is lost, as is the delocalisation across the anthracene moiety and thus the intensity of the peaks in the absorption spectrum decreases. This intensity decrease acts as a probe into the changing chromophore concentration, Figure 4.3.1.7. From this, an estimation of the quantum yield for chromophore depletion can be determined, Figure 4.3.1.8.

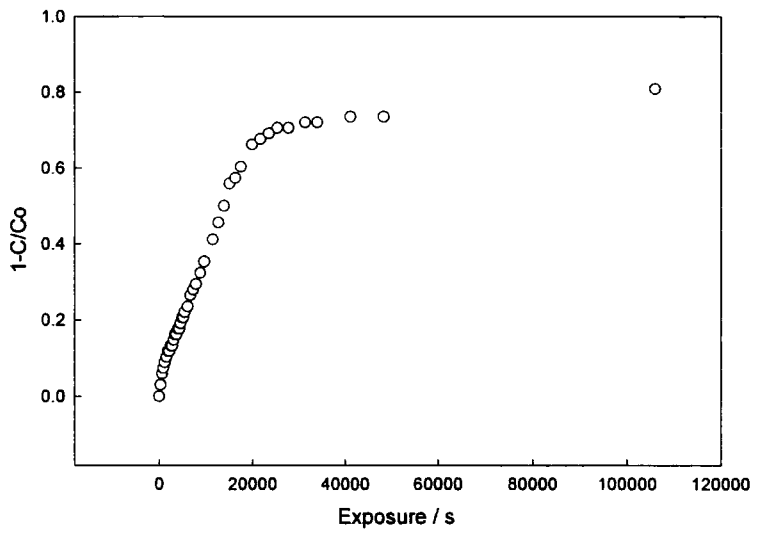

Figure 4.3.1.7: Change in Chromophore Concentration for Polyanth Exposed to Unpolarised Radiation from the Deuterium Lamp.

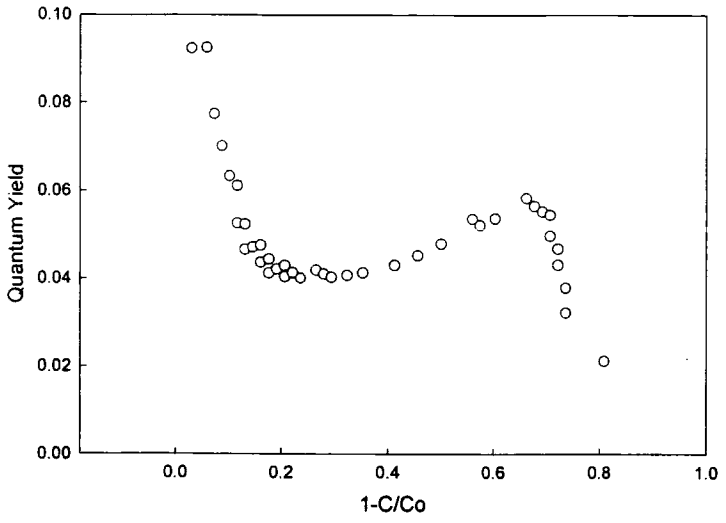

Figure 4.3.1.8: Quantum Yield Decay for Polyanth Exposed to Unpolarised Radiation from the Deuterium Lamp.

The change in concentration of the anthracene species occurs quite steadily until ~75% of the species initially present have reacted. After this, reaction takes place much more slowly and the plot begins to level off, indicating no further reaction.

As Figure 4.3.1.8 shows, the quantum yield decay for polyanth is somewhat different to those achieved for PVCi, chapter three, and shall be discussed later. However, it is important to note that ~80% of the chromophores have reacted.

Upon irradiation with vertically polarised light from the deuterium lamp, the UV absorption decay in Figure 4.3.1.9 was observed. In contrast to the extent of reaction using unpolarised radiation, Figure 4.3.1.1, the absorption intensities change only slightly, indicating only a small number of anthracene moieties have undergone chemical change. Only ~8% of the chromophores present in the sample react as is shown by Figure 4.3.1.10.

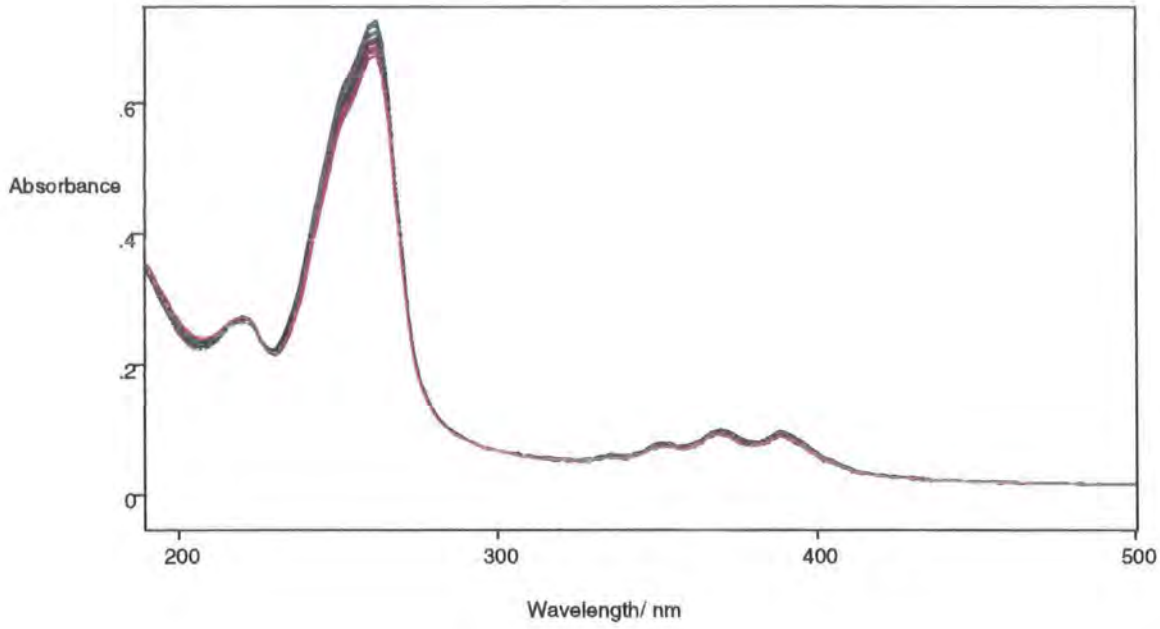

Figure 4.3.1.9: UV Absorption Spectrum for Polyanth Exposed to Vertically Polarised Radiation from the Deuterium Lamp.

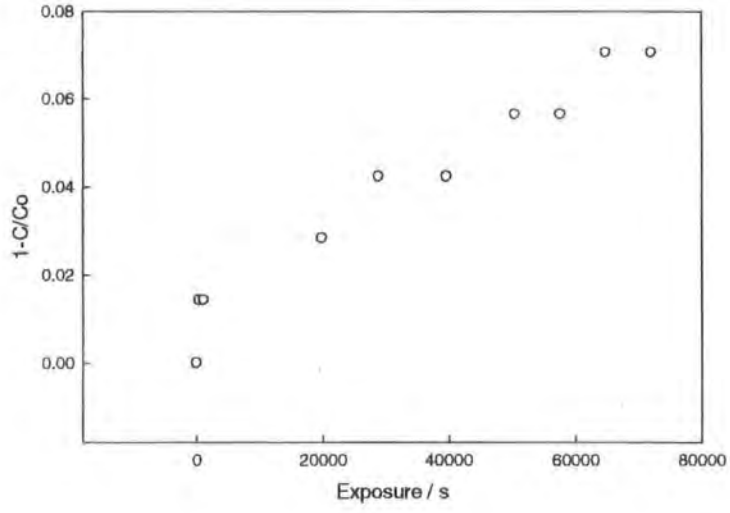

Figure 4.3.1.10: Change in Chromophore Concentration for Polyanth Exposed to Vertically Polarised Radiation from the Deuterium Lamp.

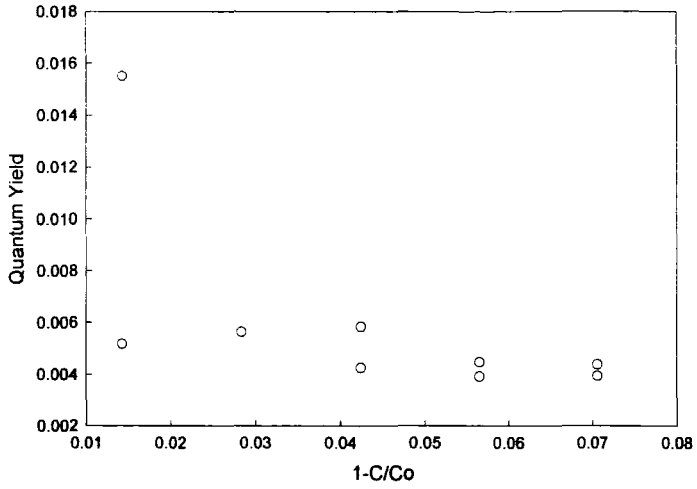

Figure 4.3.1.11: : Quantum Yield Decay for Polyanth Exposed to Vertically Polarised Radiation from the Deuterium Lamp.

This decay does not follow the same trend as for exposure to unpolarised radiation and to ensure that this was a representative decay, the reaction was repeated. The combined plots are shown in Figure 4.3.1.12 and proves that the decay shown in Figure 4.3.1.11 is a true reflection of the quantum yield decay when polyanth is exposed to vertically polarised radiation from the deuterium lamp.

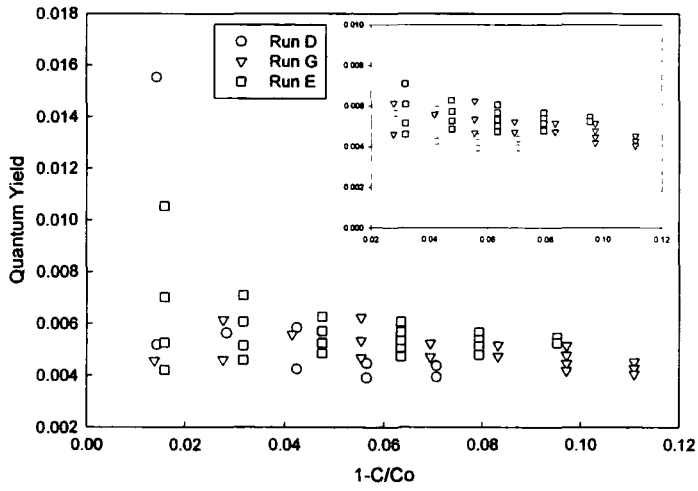

Figure 4.3.1.12: Combined Quantum Yield Decay for Polyanth Exposed to Vertically Polarised Radiation from the Deuterium Lamp.

The experiment was repeated using horizontally polarised radiation and the results collated in Figure 4.3.1.13, Figure 4.3.1.14 and Figure 4.3.1.15. From Figure 4.3.1.13, it can be seen that horizontally polarised radiation induces a much greater extent of reaction than when using vertically polarised radiation.

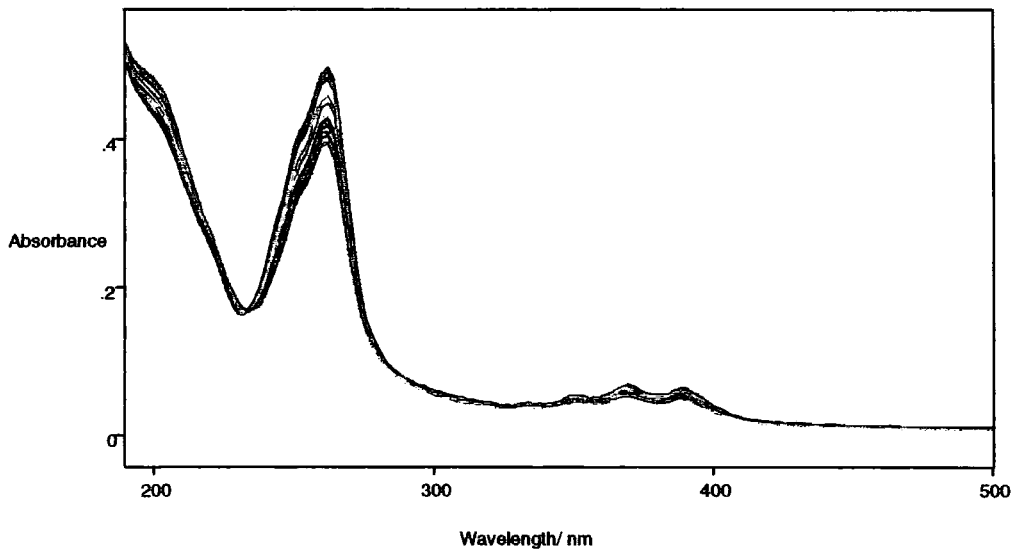

Figure 4.3.1.13: UV Absorption Spectrum for Polyanth Exposed to Horizontally Polarised Radiation from the Deuterium Lamp.

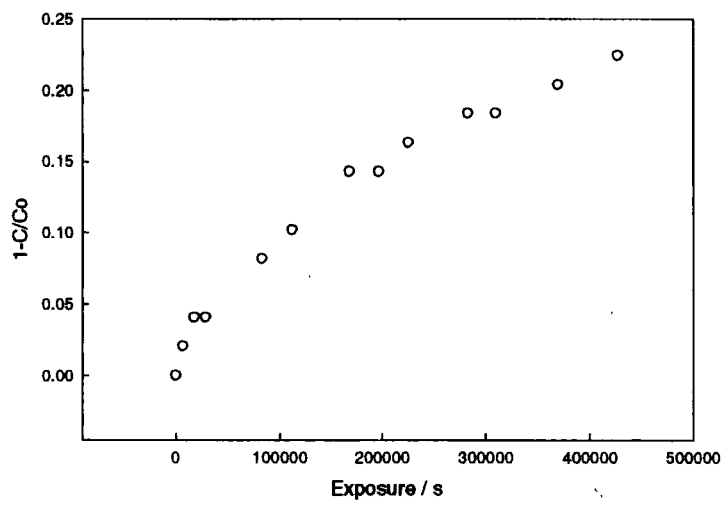

Figure 4.3.1.14: Change in Chromophore Concentration for Polyanth Exposed to Horizontally Polarised Radiation from the Deuterium Lamp.

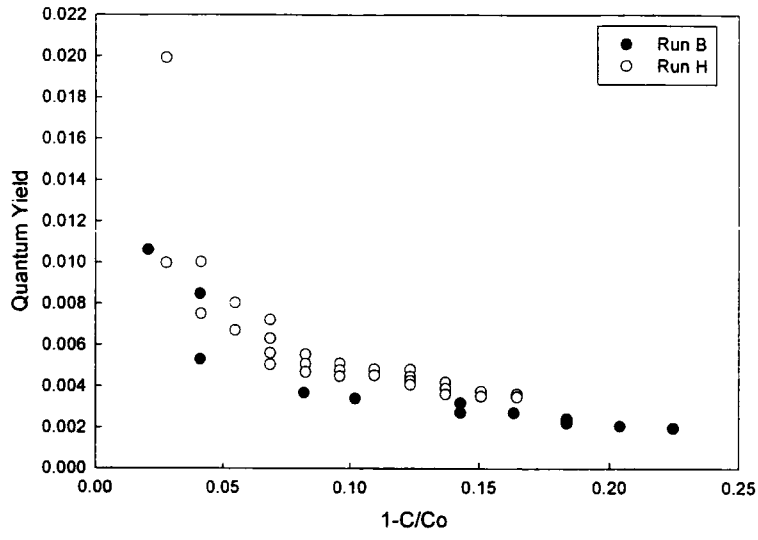

Figure 4.3.1.15: Combined Quantum Yield Decay for Polyanth Exposed to Horizontally Polarised Radiation from the Deuterium Lamp.

When using horizontally polarised radiation, ~24% of the chromophores react, three times as many as when using vertically polarised radiation. This suggests that a large number of anthracene molecules are lying in the orientation shown in Figure 4.3.1.16.

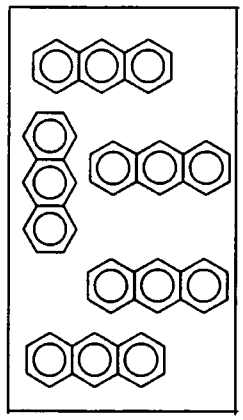

Figure 4.3.1.16: Suggested Orientation of Anthracene Molecules.

When irradiated with vertically polarised radiation from the deuterium lamp Figure 4.3.1.16 shows that there are very few anthracene moieties lying in the correct

orientation to interact with the radiation and thus the change in the UV absorption spectrum is small.

The experiments were once again carried out, however, in this instance a vertically polarised UV laser (λ=325nm) was used as the radiation source. This yields a change in UV absorption as shown in Figure 4.3.1.17. Using a monochromatic laser as the radiation source induces a similar extent of reaction to that achieved using unpolarised radiation from the deuterium lamp.

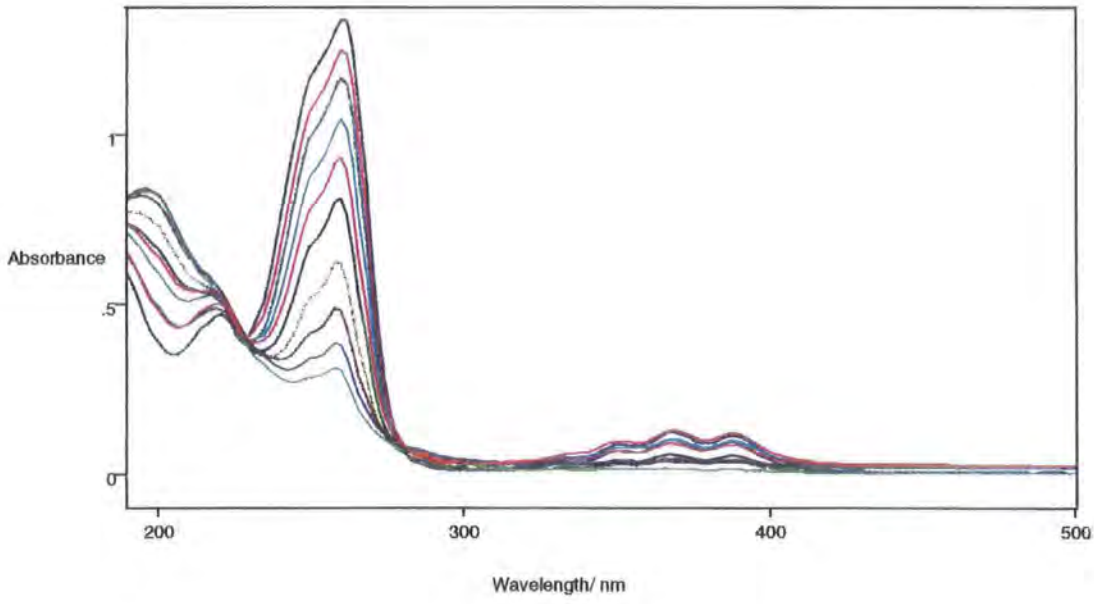

Figure 4.3.1.17: UV Absorption Spectrum for Polyanth Exposed to Vertically Polarised UV Laser (λ=325nm).

This gives rise to the chromophore conversion and quantum yield changes in Figure 4.1.3.18 and Figure 4.1.3.19.

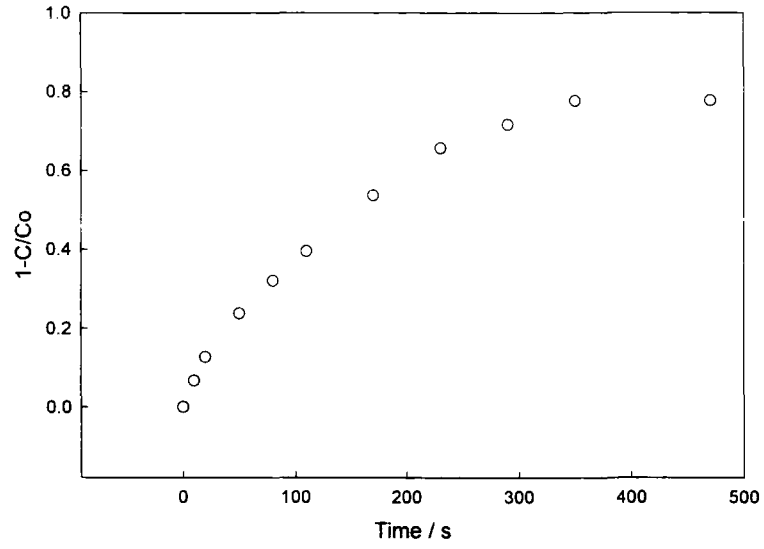

Figure 4.3.1.18: Change in Chromophore Concentration for Polyanth Exposed to Vertically Polarised UV Laser (λ=325nm).

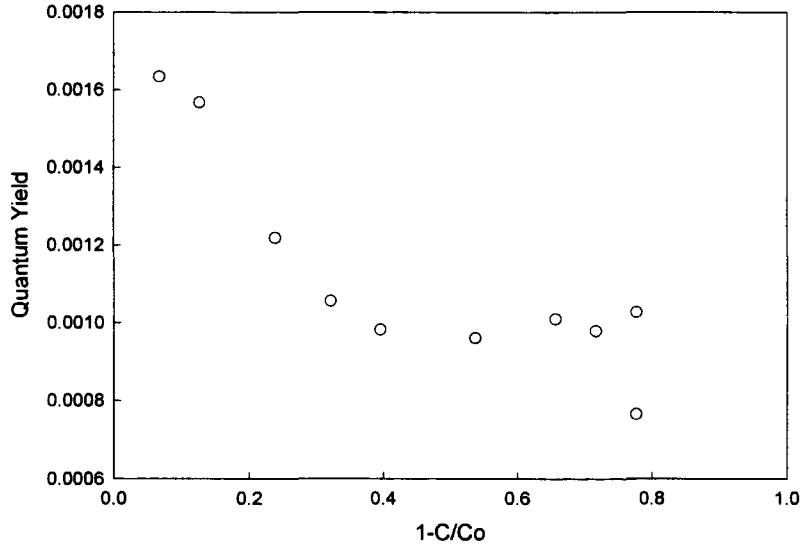

Figure 4.3.1.19: Quantum Yield Decay for Polyanth Exposed to Vertically Polarised UV Laser (λ=325nm).

It is interesting to note that the effects of unpolarised radiation from the deuterium lamp and vertically polarised laser radiation are very similar: ~80% of the chromophores react and the quantum yield decays follow the pattern of decreasing quantum yield followed by a plateau, then a slight increase in quantum yield before

the quantum yield decreases once more. It is unfortunate that the accuracy of the quantum yield values for exposure to the deuterium lamp radiation is questionable as it would be interesting to compare the quantum yield values for both experiments.

Anthracene is known to cleave upon exposure to radiation of lower wavelengths, $\lambda<260nm$[1]. It was initially thought that as the deuterium lamp provided radiation capable of both dimerising and cleaving the anthracene molecule, it was probable that both reactions were occurring in the system, giving rise to the unusual quantum yield decay curve. However, if this were true, then such plots would only be evident in samples irradiated using the broad wavelength range deuterium lamp and not in those irradiated with the monochromatic laser. The unusual decay/rise/decay in the quantum yield plot is visible in samples exposed to both the unpolarised radiation from the deuterium lamp and polarised laser radiation. Therefore, an alternative explanation must be sought.

Energy migration between anthracene moieties will be occurring continuously. The mechanism by which it occurs is unknown, however, from chapter 4.1, it is known that energy transfer may be radiative or non-radiative and can occur over a range of distances. The radiative process is the least likely due to the relatively poor overlap between the emission and absorption spectrum of the anthracene molecule. At the start of the experiment, energy migration will be able to proceed via both long-range and short-range transfer processes. As the anthracenes begin to dimerise, 'holes' will appear in the polymer chains making short-range transfer less likely and long-range processes will dominate. The extent of energy migration can be described pictorially by Figure 4.3.1.20.

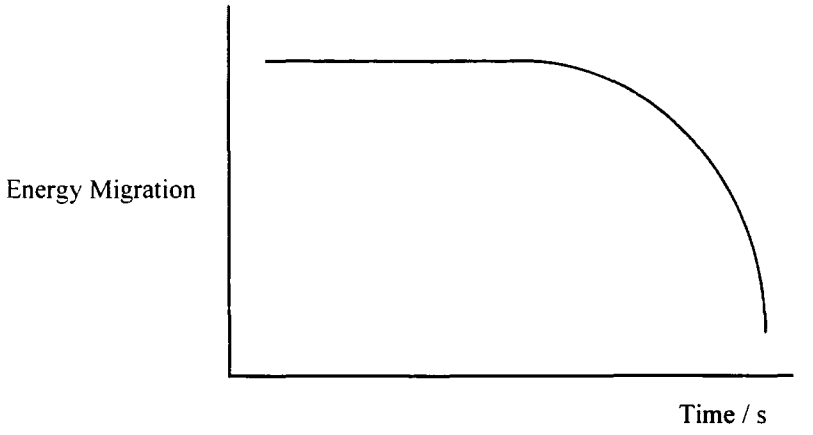

Figure 4.3.1.20: Extent of Energy Migration in Polyanth.

In the early stages of the exposure, energy migration will be occurring at its maximum efficiency, as indicated by the plateau in Figure 4.3.1.20. As the anthracene species dimerise, energy migration becomes more difficult and its efficiency gradually begins to fall.

Decay of the quantum yield commences upon exposure to UV light. The quantum yield is defined as the number of molecules of reactant consumed for each photon of light absorbed. As the population of anthracene species is depleted, fewer anthracene moieties are available for reaction to give dimers, although those remaining can still absorb photons. Therefore, the quantum yield decreases, Figure 4.3.1.21.

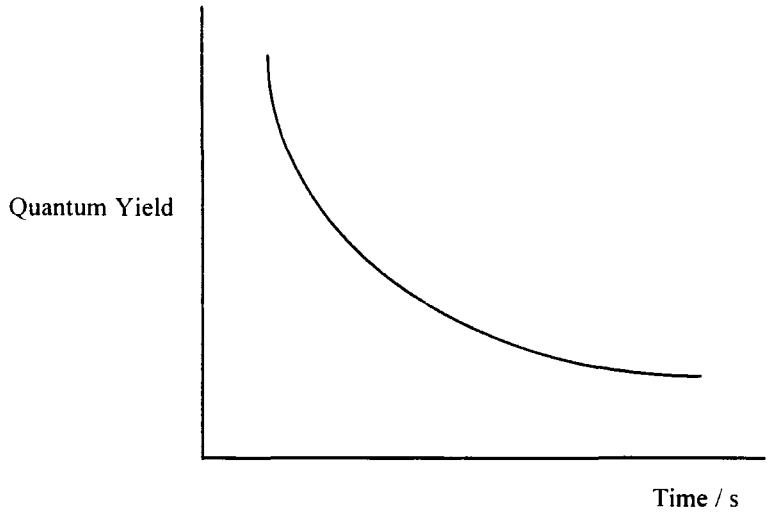

Figure 4.3.1.21: Expected Quantum Yield Decay.

In the polyanth system studied, both energy migration and dimerisation can occur. Combination of both of these plots gives rise to Figure 4.3.1.22.

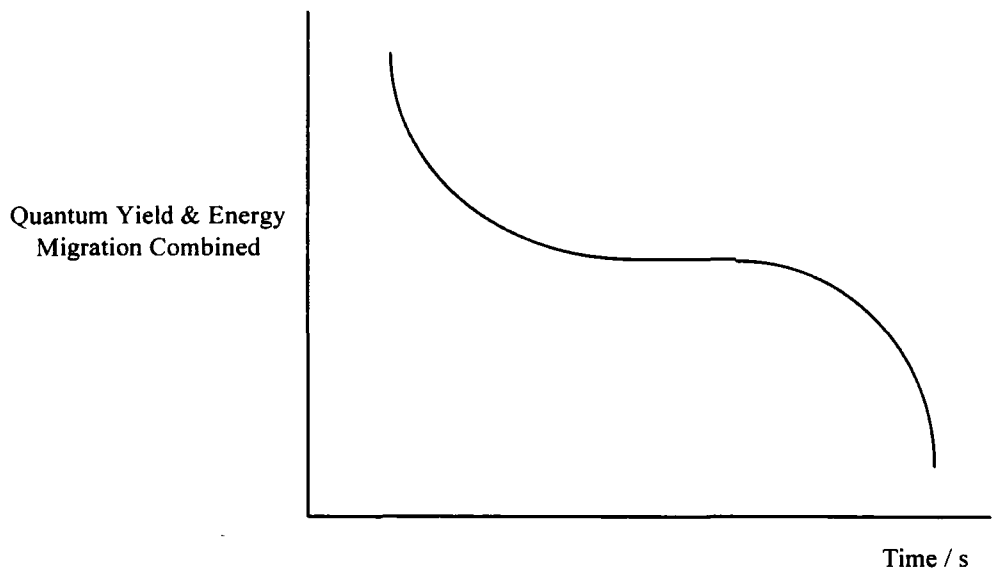

Figure 4.3.1.22: Quantum Yield and Energy Migration Combined.

` It must be stated at this point that Figure 4.3.1.20, Figure 4.3.1.21 and Figure 4.3.1.22 have no physical, scientific basis. They are merely employed as an aid to assist in describing the shape of the experimentally determined quantum yield decays. The first part of the curve shown in Figure 4.3.1.22 appears to be controlled by the quantum yield decay. This will be true if the rate of dimerisation is faster than the rate

of energy migration and therefore those anthracene units favourably aligned with respect to dimer formation react before an energy transfer event can occur. Once these species are reduced in number, a photon can be absorbed by an anthracene which does not have a neighbour in a configuration which affects the dimerisation reaction in the appropriate timescale and therefore the energy can 'hop' onto a nearby anthracene molecule[1,8]. This can occur by the processes described earlier in this chapter until the energy hopping is quenched e.g. by formation of a dimer[8] or by fluorescence. The side chains of the polymer are quite rigidly held in the solid state although slight motion of the side chains will occur due to the elevated temperature of the exposed region. Thermal relaxation of a polymer film occurs ~10^{13} times slower than vibrational relaxation of the photochemically excited state[14], therefore, anthracene pair orientations do not change appreciably before a transfer event occurs.

The rise in quantum yield is much more prominent in the samples exposed to the unpolarised deuterium lamp, Figure 4.3.1.8. This is thought to be due to experimental error. When the sample was exposed to the UV laser, Figure 4.3.1.19, the plot greatly resembles the shape of the curve in Figure 4.3.1.22. At the point where no further change in the absorption spectra was achieved upon exposure, it is reasonable to assume that the residual anthracene units are randomly scattered throughout the area sampled and are too far away from their neighbours to take part in energy transfer. This hypothesis is supported by the work of M^{c}Inally *et al*[15] who looked at poly (vinyl toluene) capped with terminal anthracene species. They found that no intramolecular energy transfer occurred between the anthracene groups on the chain ends as their low concentration placed them too far apart.

Extensive studies have been carried out on anthracene-containing systems. In 1966. Chandross *et al* [3] studied on the photodimerisation of anthracene, in its crystalline form. dispersed in a KBr matrix. The dimerisation reaction was followed by monitoring the decrease in the long wavelength absorption band. The dimers were found to form in a columnar-type structure and could be cleaved by light of lower wavelength.

When the anthracene moiety reaches its excited state, a number of pathways are available to the radiation: vibrational relaxation to the first singlet excited state, dimerisation of this state via reaction with a ground state anthracene, fluorescence, energy migration, internal conversion of S_1 to S_0 and intersystem crossing to the triplet excited state.

Triplet migration in molecular anthracene held in a polystyrene matrix has also been studied by Burkhart *et al*[16]. Here, the separation between molecules is larger than in the crystal, yet energy migration occurs more quickly, i.e. energy transfer is more 'liquid-like'. This suggests that the relative spatial orientations or the donor and acceptor pairs is critical in the rate of energy transfer and if such orientations are not realisable in the crystal structure, less efficient transfer will occur. In polymer matrices, there is thought to be a high probability that of those neighbouring molecules close enough for transfer to occur, one of those molecules will have to proper orientation for efficient energy transfer. This system is comparable to polyanth where the anthracene moieties lie on every second backbone carbon, giving rise to a high concentration of anthracene molecules in a small area and will thus allow efficient energy transfer to occur.

4.3.2. Infrared Spectroscopy

Figure 4.3.2.2 and Figure 4.3.2.3 show the infrared absorption spectrum of polyanth on a ZnSe substrate before exposure to vertically polarised radiation from the deuterium lamp. The orientation definitions are shown schematically in Figure 4.3.2.1.

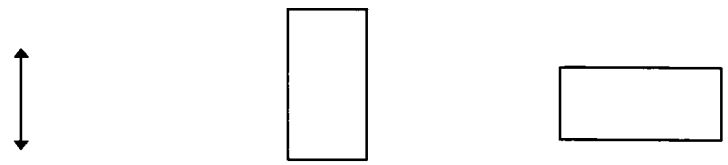

IR Polarisation Vector Parallel Orientation Perpendicular Orientation

Figure 4.3.2.1: Orientation Definitions for IR Measurements on Polyanth.

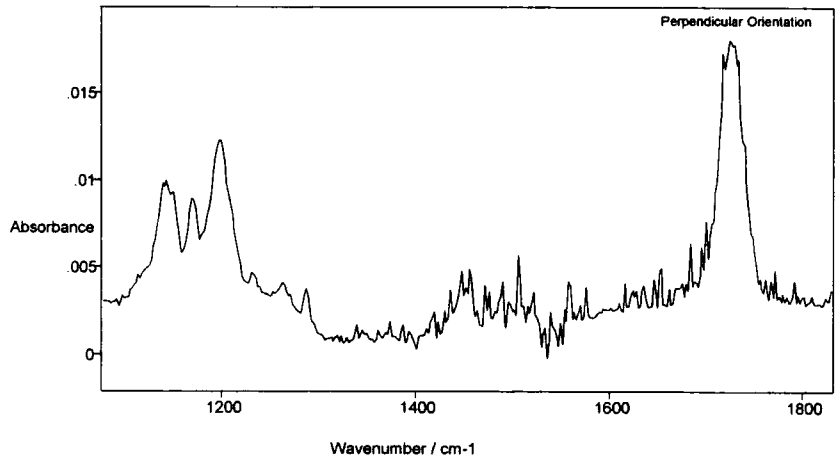

Figure 4.3.2.2: IR Spectrum of Polyanth (Perpendicular Orientation).

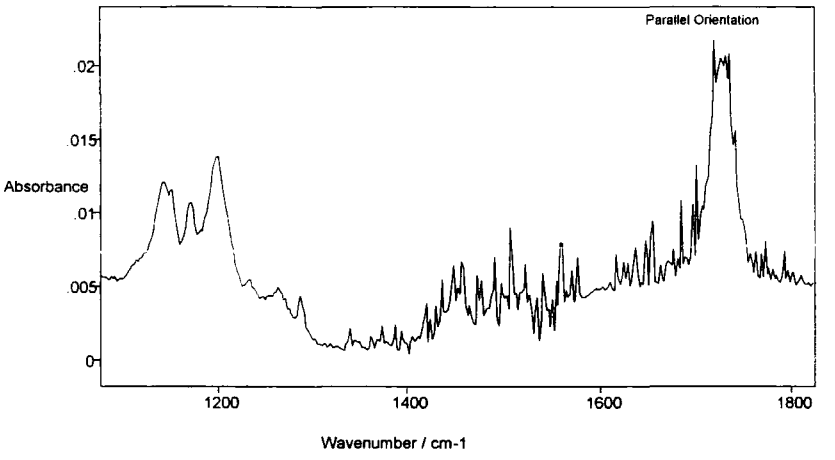

Figure 4.3.2.3: IR Spectrum of Polyanth (Parallel Orientation).

The sample of polyanth was irradiated using vertically polarised radiation from the deuterium lamp and the spectra were recorded. As Figure 4.3.2.2 and Figure 4.3.2.3 show, the IR spectrum of polyanth contains relatively few distinct peaks. The dimer is formed by cross-linking across the 9,10-position in the molecule. This reaction will change the chemical environment of the hydrogens located at the 10-position in the anthracene moiety. This will give rise to a change in the peaks in the IR spectrum arising from the aromatic C-H vibrations. In arenes, the Ar-H in-plane bend lie in the region 950-1250cm^{-1} [17]. As the spectra for polyanth show, there are peaks lying in this region and therefore, it is these peaks that were analysed and their dichroic ratios calculated. The spectra show three peaks in this region, however, the central peak situated at 1170cm^{-1} is not always present to the same extent. When this peak is strong in a given sample, its intensity does not change significantly upon exposure. Tentative suggestions for the origins of this peak may be due to the C-O stretch of the ester group or alternatively, C-H in-plane bends which have not been affected by the loss of aromaticity. One further consideration when irradiating the

polyanth is that the reaction was carried out in the presence of oxygen. H.Bouas-Laurent *et al*[18] reported quantities of endoperoxide, Figure 4.3.2.4, as well as dimer when irradiating an aerated solution of anthracene with UV light. When the experiment was repeated with degassed solution, only the dimer was formed. It is therefore feasible that when the anthracene solution was prepared and stored, some endoperoxide formation may have occurred.

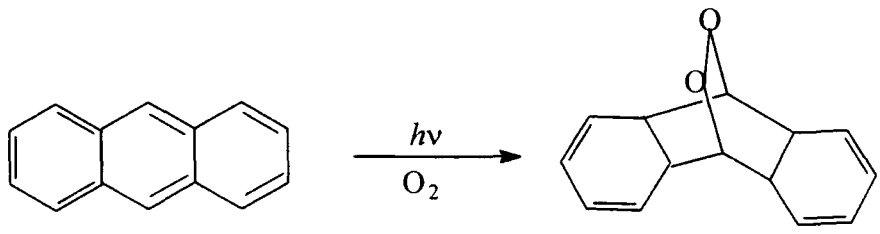

Figure 4.3.2.4: Endoperoxide Formation.

The C-C-O absorption in aryl peroxides occurs in the region[19] 1176-1198cm^{-1} and the central peak could possibly originate from this absorption. Therefore, only the peaks centred at 1142cm^{-1} and 1197cm^{-1} were analysed.

The dichroic ratio is defined as

$$D = \frac{absorbance(parallel)}{absorbance(perpendicular)}$$

and the results obtained for polyanth during three separate experiments are shown in Figure 4.3.2.5.

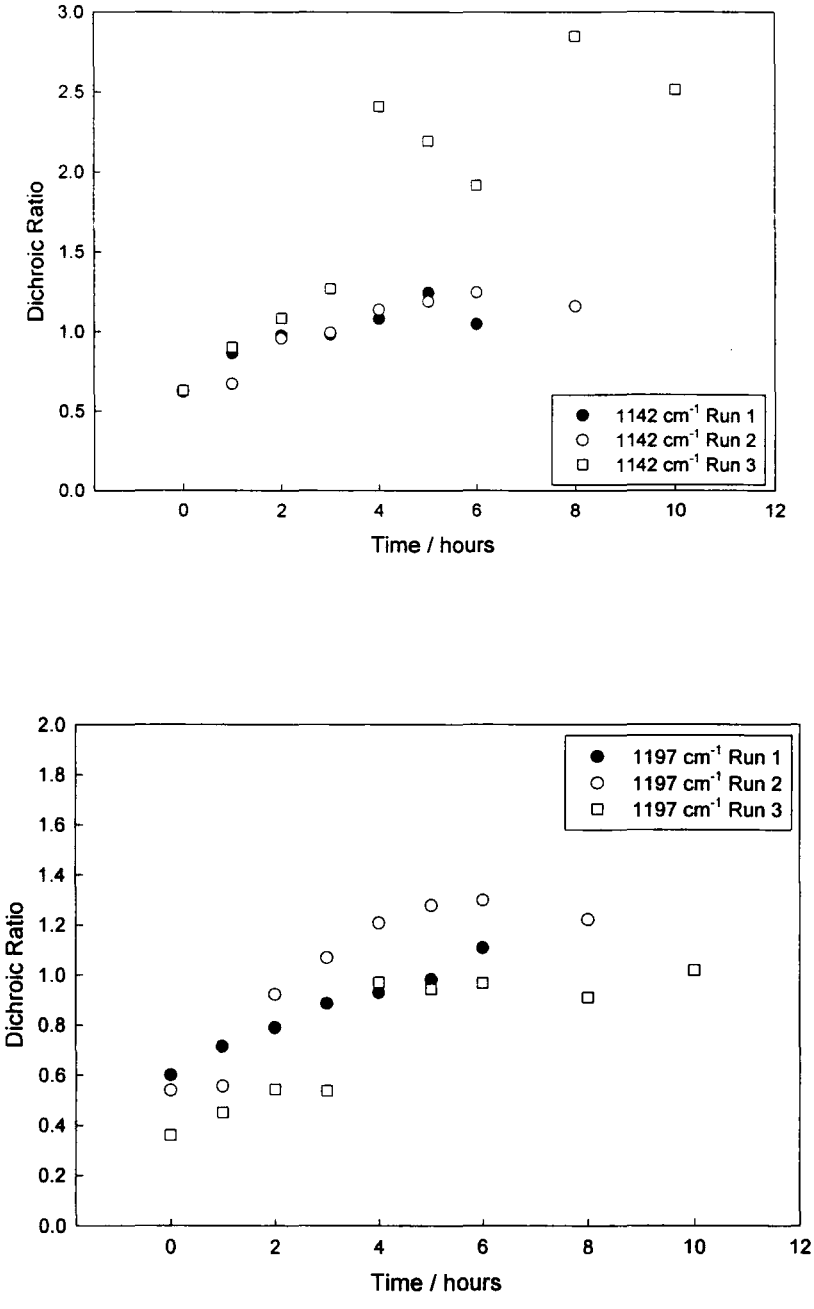

Figure 4.3.2.5: Dichroic Ratio for Polyanth Obtained by Analysis of the Peaks Centred at 1142cm^{-1} and 1197 cm^{-1}.

Considering the peaks centred at 1142cm^{-1}, the results obtained during run 1 and run 2 compare well, giving an increase in dichroic ratio from initial to final value of 40% and 46% respectively. The third run gives a dichroic ratio increase from initial to final value of ~75%.

The dichroic ratio data for 1197cm^{-1} show good agreement in all three runs, giving rise to a dichroic ratio increase in the region of 45-65%. The data for both peaks shows that the dichroic ratio of polyanth increases on exposure to vertically polarised radiation from the deuterium lamp.

As stated in the previously, the dichroic ratio was expected to decrease when polyanth was irradiated with vertically polarised light from the deuterium lamp. As $D = A_{para}/A_{perp}$, it is essential to consider the orientation of the anthracene moieties with respect to the incoming IR polarisation vector, Figure 4.3.2.6.

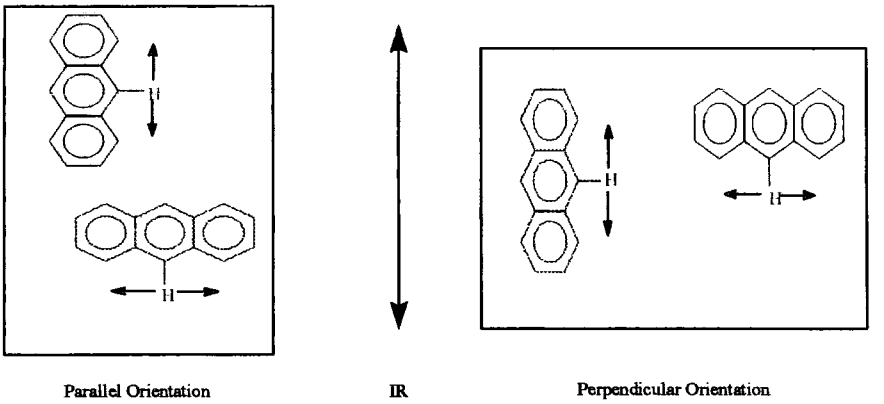

Figure 4.3.2.6: Orientation of Anthracene Moieties.

It was found that the absorbances measured in the parallel orientation remain constant whereas the absorbances measured in the perpendicular orientation decrease. This is a somewhat surprising result. Only those anthracenes oriented with their dipole parallel to the UV polarisation direction can absorb radiation and become excited. Therefore, it is reasonable to assume that it is these molecules which will react. However, if the dichroic ratios are examined, it can be seen that the initial value for the dichroic ratio is ~0.5. This indicates that there is some inherent

orientation in the sample and the anthracene molecules are arranged as previously shown in Figure 4.3.1.16.

From the peak absorbances[20], it is estimated that almost three times as many anthracene molecules are lying horizontally as vertically. Upon irradiation, it is the absorbance due to the horizontally aligned anthracenes which decreased, while the absorbance due to the vertically aligned anthracenes remained constant. The anthracene molecules lying vertically are the only molecules able to absorb the vertically polarised radiation. However, there are relatively few anthracene molecules lying in the vertical orientation relative to those lying in the horizontal orientation and even if ~10% of these dimerise, a change of this magnitude on a reading of 0.22 will not be significant enough to separate it from experimental error and the absorbance value will appear to remain constant. When the vertically aligned anthracenes able to dimerise have reacted, those remaining are unlikely to be clustered together such that they too dimerise. The most conceivable explanation for why the horizontally aligned anthracenes react is that energy hops between the vertically aligned anthracene units which have absorbed the radiation and those aligned horizontally. Presumably, with such a large concentration of anthracene molecules in the horizontal orientation, the probability of finding two aligned favourably for dimerisation is quite high. Once the vertically aligned anthracene has 'passed on' its excitation, it can absorb another photon and hence the hopping and dimerisation process can continue. Depletion of the horizontally aligned anthracene molecules whilst the vertically aligned remain monomeric accounts for the increase in dichroic ratio.

When the dichroic ratio is unity, the concentrations of the anthracene moieties in both orientations are equal. However, although identical in number, the preferred

alignment in the horizontal direction is not lost and thus the dichroic ratio may climb above one.

4.3.3. Birefringence Studies

Thin films of polyanth on a quartz substrate were simultaneously irradiated with a vertically polarised He-Cd laser (λ=325nm) whilst monitoring the intensity of the He-Ne laser (λ=633nm) passing through the sample. This technique is described in chapter 2.8.3.

The sample holder allows the substrate to be moved up/down and left/right with respect to the incoming laser radiation. On carrying this out, it was noticed that there were large variations in the initial intensity for any one sample, 0-136nW.

Figure 4.3.3.1 shows representative birefringence curves obtained from regions in the sample exhibiting low and high initial birefringence.

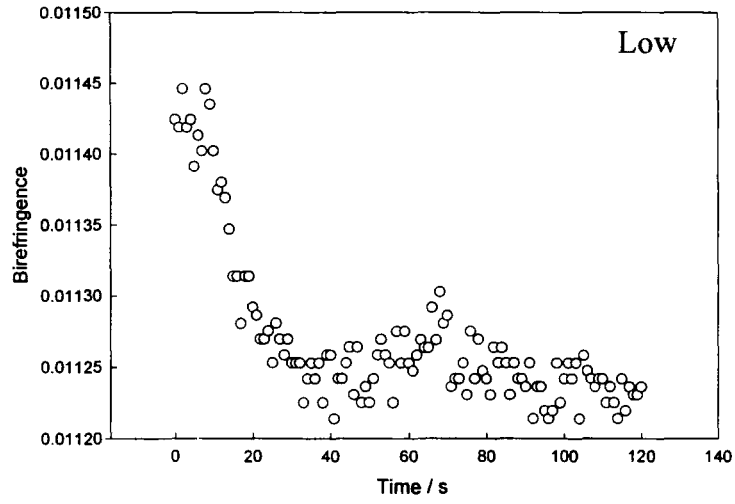

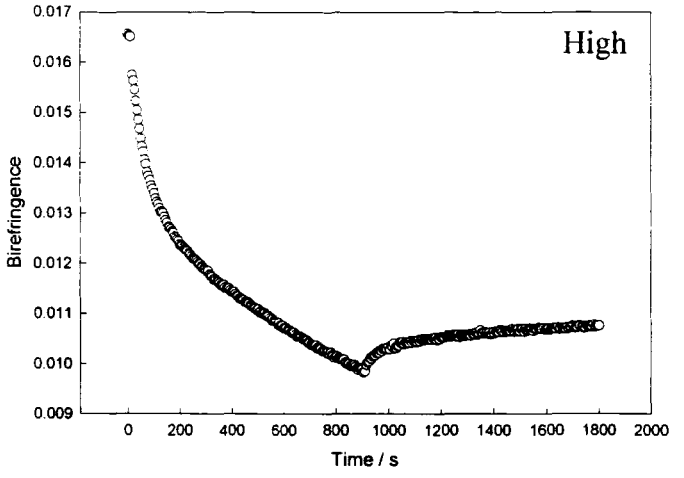

Figure 4.3.3.1: Birefringence Curves for Polyanth.

The first plot in Figure 4.3.3.1 shows the results obtained from a region in the sample where the initial value of the birefringence was low. The general shape of the curve appears to be a decay. However, if the actual values of the measured birefringence are considered, they show a change in initial to final values of 0.00025 i.e. 2%. A variation of this magnitude cannot be accurately measured by the experimental design employed in recording these data and therefore the apparent change is merely experimental error. Further birefringence has not been introduced into the sample by irradiation with vertically polarised laser radiation. This indicates that the sample is absorbing the light isotropically. If dimerisation is occurring, it is doing so uniformly thus giving rise to no preferential orientation and no birefringence. If a region has no initial birefringence then the region can be deemed isotropic. Anthracene requires a very definite initial alignment for excimer formation and thus dimerisation to occur. If this alignment is not available to an excited species, then the energy can hop until it finds a site where a dimer can form. Indeed, energy migration occurs constantly. However, it has been presumed that when an anthracene in its

excited state is aligned with a ground state species such that dimerisation occurs. energy migration is not favoured i.e. the rate of dimerisation is faster than the rate of energy migration. As there is no initial birefringence, there is little preferred orientation and favourably aligned anthracenes will be situated throughout the sample. Energy migration will occur until it reaches such a pair and induces dimerisation. This would lead to a random distribution of dimer and hence no birefringence is observed.

The second plot in Figure 4.3.3.1 shows the results obtained when the initial birefringence of the sampled region was high. The birefringence decreases rapidly in the first 200 seconds exposure after which, the decrease becomes more gradual. At the point where the exposing laser was switched off, there is a sharp change in birefringence which then begins to rise. This increase is small and can be attributed to a combination of relaxation of the sample to its equilibrium state and the changing temperature of the analysed area when the laser is switched off. The overall change in birefringence is a decrease of ~40%. If a region has initial birefringence then there exists some inherent order within the area sampled. As birefringence is shown to decrease, order is being created in the direction perpendicular to that in which in initially exists. As birefringence is a measure of the difference in refractive index in two mutually perpendicular directions, definition of the direction in which order exists is not possible using this technique.

The plots shown in Figure 4.3.3.1 were recorded with the sample slide in a vertical orientation. The experiment was repeated with the slide rotated by 90° such that it lay in a horizontal orientation, Figure 4.3.3.2.

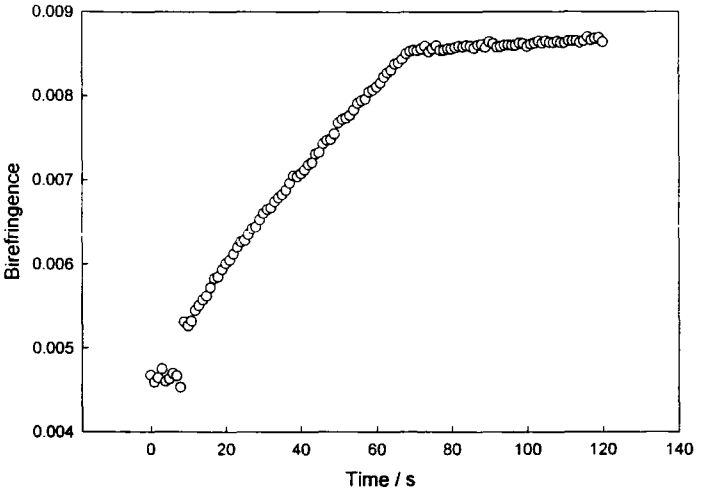

Figure 4.3.3.2: Birefringence results for Slide in a Horizontal Orientation.

Figure 4.3.3.2 shows that when the slide was placed in a horizontal orientation and birefringence measurements recorded, the birefringence increases. This is indicative of creation of order in the direction in which it already exists.

It is apparent that there is orientation inherent in films of polyanth prepared by spin casting. Annealing of the samples (403K, 30 minutes) was carried out in an attempt to remove the inherent order. However, birefringence measurements indicated that the annealing process had no observable effect on the film. It is likely that the bulky disposition of the anthracene moiety makes significant motion difficult. The side chains themselves are rather long which may give rise to entanglements between the chains. Annealing for a much greater time at elevated temperature may remove the inherent order, however, time constraints did not allow this hypothesis to be tested.

Polymers similar in structure to polyanth have been analysed in terms of their photophysics. Hargreaves & Webber[5] looked at systems of poly (9-anthrylmethyl methacrylate) and poly (9-anthrylmethyl ethyenyl ether), Figure 4.3.3.3.

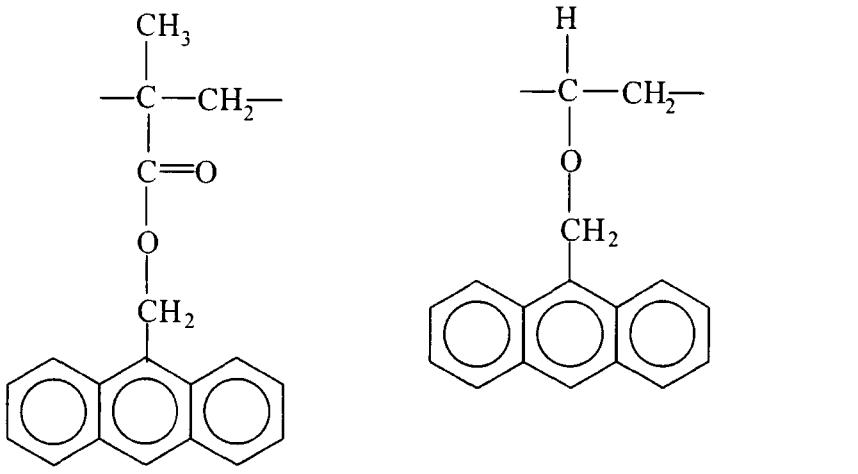

poly (9-anthrylmethyl methacrylate) poly (9-anthrylmethyl ethyenyl ether)

Figure 4.3.3.3: Polymer Systems Studied by Hargreaves and Webber.

For the methacrylate system, fluorescence studies at room temperature and 77K were found to be almost identical and provided evidence of a high density of preformed excimer sites due to partially eclipsed chromophores. The change in temperature was not found to significantly change the molecular orientation of the system. This is consistent with the results obtained for polyanth where annealing the sample did not give rise to increased side chain mobility. In contrast, in the ether system there is sufficient local mobility to allow the configuration whereby the chromophores are fully eclipsed to be achieved. This increased mobility with respect to the methacrylate systems may be due to a combination of side chain length and structure effects. By retarding the formation of partially eclipsed dimers via the introduction of a phenyl group in the 10-position, singlet energy migration was enhanced. Good overlap between chromophores is needed if dimerisation is to occur. If this overlap is not achieved, the extent of energy migration increases.

Films used in these birefringence measurements were viewed through a microscope equipped with crossed polarisers. If no initial order were present in the

sample, a black image would be observed for any sample orientation. In practice, it was found that when the sample is oriented at 45° with respect to the first polariser, a brighter image is observed. This confirms that there is inherent orientation over the whole sample area and the birefringence measurements carried out simply highlight greater and weaker sources of this order.

From the results of the UV spectroscopy and IR dichroism, it would appear as if the anthracene units are lying in a horizontal orientation, giving rise to ordering. When the birefringence decreases, this order is being destroyed as the anthracences parallel to the UV polarisation vector absorb radiation. Reaction of only a small number of these species is sufficient to create a birefringence change parallel to the UV polarisation vector and order is decreased. The timescale of the birefringence experiment is ~60 seconds in most cases, one tenth of that for UV spectroscopy using the laser and therefore, energy hopping is much less prominent.

An increase in birefringence occurs when those molecules already aligned react to form dimers. These species are chemically changed as well as being much more restricted in their motions. The loss of aromaticity of the central ring in the anthracene unit changes the way the light travels through the sample in comparison to how it travels through ordered monomeric units and thus birefringence increases.

Polyanth is a homopolymer. Copolymers of the polyanth monomer with methyl methacrylate were prepared. However, UV and birefringence studies did not indicate the occurrence of dimer formation, even for the copolymer containing one anthracene side chain for every methacrylate side chain. Ng And Guillet[21] have studied the effects of increasing the proportion of anthracene in a copolymer of (9-phenanthryl) methyl methacrylate and (9-anthryl) methyl methacrylate, Figure 4.3.3.4.

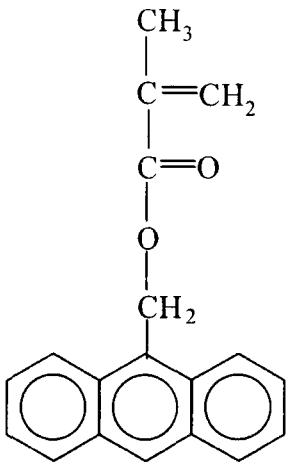

(9-anthryl) methyl methacrylate

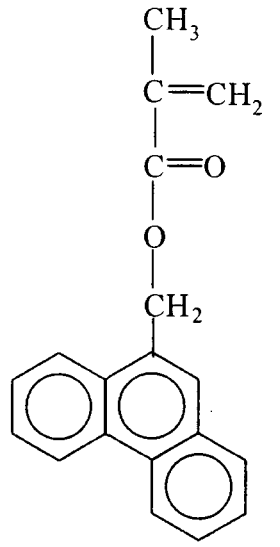

(9-phenanthryl) methyl methacrylate

Figure 4.3.3.4: Copolymer Constituents.

They measured efficiency of intrachain singlet electronic energy transfer in fluid solution from phenanthrene to anthracene. As the mole fraction of anthracene in the copolymer increased, the efficiency of the intrachain energy transfer as determined by fluorescence studies also increased. Although the mole fraction of anthracene was high, the average number of anthracene units on the chain was relatively low. Thus, the high efficiency of the transfer is attributed to the extended sequence of 9-phenanthrene donors in the copolymer, highlighting the importance of the relative spatial locations of the donor and acceptor species.

In polyanth, the dimerisation process can, in theory, occur both inter- and intramolecularly. De Schryver *et al*[22] carried out work into the photochemistry of bichromorphic compounds i.e. molecules with more than one chromophore, such as a polymer chain. They studied the photopolymerisation of alkylene bis-9-anthroates, Figure 4.3.3.5.

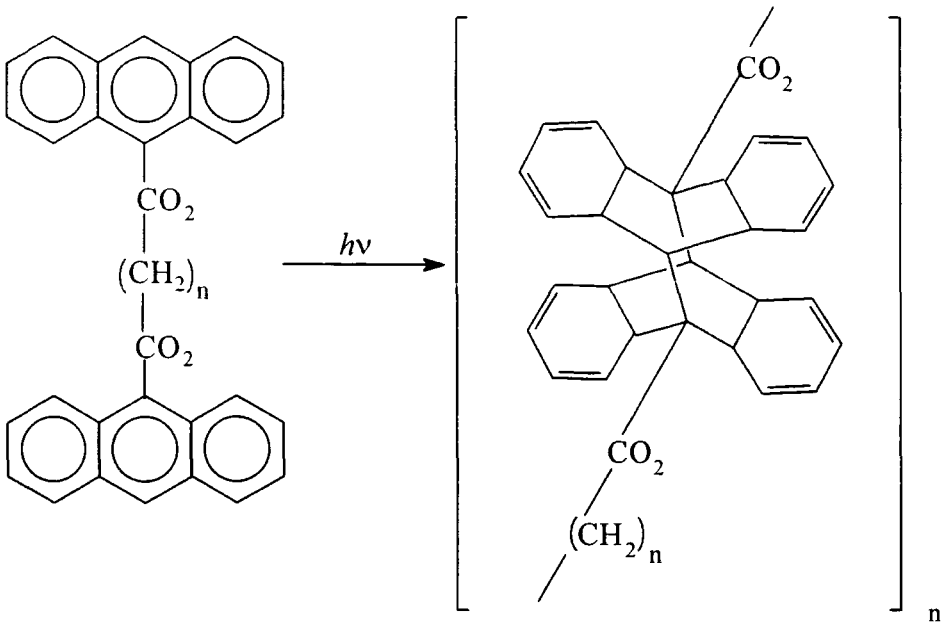

Figure 4.3.3.5: Photopolymerisation of Alkylene Bis-9-Anthroates.

The process was found to occur intermolecularly via a singlet excited state having a lifetime of 10ns. At high conversion, i.e. low chromophore concentration, the intramolecular process was found to compete more strongly. However, this reaction was carried out in solution, giving the chains greater mobility when compared to a solid film. The intra- vs. intermolecular addition may not be as important in polyanth as the process occurring will depend largely upon the nature of the neighbouring anthracene as dictated by the spinning process. It is likely that intermolecular reactions will be occurring as the polymer chains will be stretched out by the centrifugal forces used in preparing the films. Even at low anthracene concentrations, the chains in the film will not have sufficient flexibility to undergo intramolecular addition.

4.3.4. Fabrication of a Simple Liquid Crystal Cell.

From the techniques discussed earlier in this chapter, it can be assumed that a large proportion of the anthracene molecules lie in a horizontal orientation. As the birefringence studies show, when the slide is in a vertical orientation and is irradiated with vertically polarised light, the anthracenes lying parallel to the polarisation direction of the light react. If a liquid crystal cell is constructed as shown in Figure 4.3.4.1, after 10 seconds exposure to vertically polarised (λ=325nm) laser radiation, Figure 4.3.4.2 results

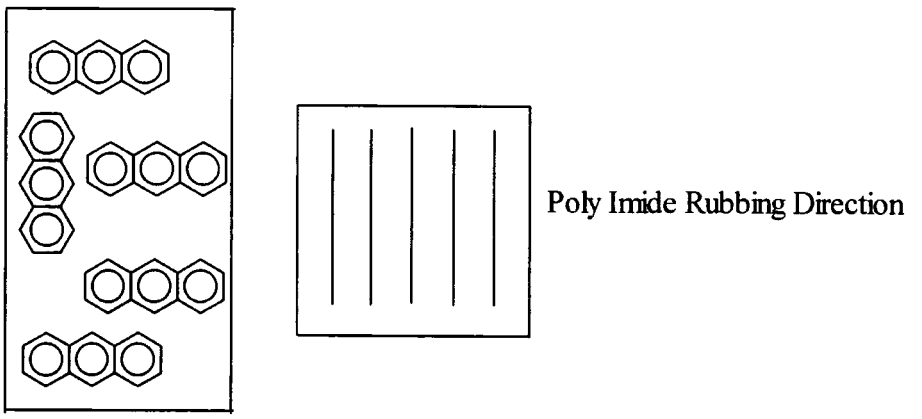

Figure 4.3.4.1: Construction of a Polyanth Liquid Crystal Cell.

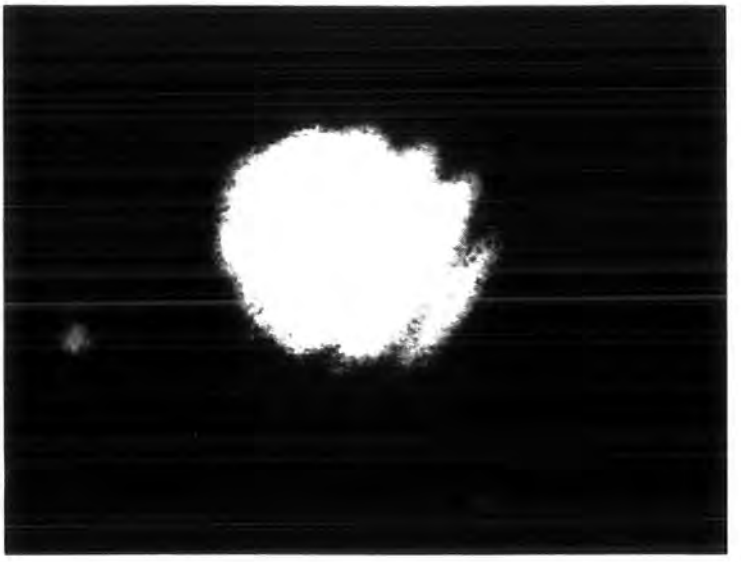

Figure 4.3.4.2: 10 Seconds Exposure.

This image in Figure 4.3.4.2 arises due to the interactions of the horizontally aligned anthracene molecules with the liquid crystals, giving rise to a twisted display.

Upon prolonged exposure, energy hopping becomes more prominent, cross-linking the horizontally aligned anthracene units and thus causing loss of liquid crystal alignment. This is indicated by the dark exposure region shown in Figure 4.3.4.3.

Figure 4.3.4.3: 300 Seconds Exposure.

The region surrounding the dark image is much paler as some light is being transmitted through the sample due to the inherent orientation in the unexposed regions of the polymer film.

4.4. Conclusions

Studies on poly (9-anthracenoate ethyl methacrylate) have indicated that this polymer has potential for use as an alignment layer in liquid crystal displays.

Results from all experiments show that the anthracene moieties attached to the end of the side chains have an initial preferred alignment direction which is not removed by annealing. The side chains are relatively short and are terminated by the bulky anthracene substituents. If these chains are entangled when spin-cast onto the slide, then it will be very difficult for the side chains to achieve sufficient mobility to remove any inherent orientation. An elevated temperature and/or increased annealing time further to that documented in this report may allow a more isotropic film to form.

The existence of initial orientation is somewhat more difficult to account for. Numerous samples prepared for four different techniques show this to be a real phenomenon and not an anomaly. Quartz and ZnSe are the two substrates used and both show preferential horizontal orientation of the anthracene groups. The only suggestion as to where to begin to look for the cause of this alignment would be to look at the only constant factor in all experiments, the spinning process. Literature investigation of anthracene provided no further insight as to why the molecules spin down in a preferred orientation. Unfortunately, time does not allow further analysis into the spinning procedures to be carried out.

From literature surveys, it would appear that energy migration is a viable process in the polyanth system. To fully assess the extent and the mechanism of this migration, extensive studies into the photophysics of the system need to be carried out.

References

1) A.Gilbert & J.Baggot, Essentials of Molecular Photochemistry, Oxford: Blackwell 1991.

2) D.Bryce-Smith, Photochemistry Volume 3: A review of the literature published between July 1970 and June 1971, The Chemical Society.

3) E.A.Chandross & J.Ferguson, *J.Chem.Phys.*, 1966, **45**(10), 3564.

4) J.B.Birks, Photophysics of Aromatic Molecules, Wiley 1970.

5) J.S.Hargreaves & S.E.Webber, *Macromolecules,* 1984, **17**, 235.

6) D.A.Holden & J.E.Guillet, *Macromolecules,* 1980, **13**, 289.

7) J.S.Hargreaves & S.E.Webber, *Macromolecules,* 1984, **17**, 1741.

8) N.J.Turro, Modern Molecular Photochemistry, 1978.

9) I.B.Berlman, Energy Transfer Parameters of Aromatic Compounds, Academic Press 1973.

10) K.E.Foster, PhD Thesis, University of Durham 1997.

11) H.H.Jaffe & M.Orchin, Theory and Applications of Ultraviolet Spectroscopy, Wiley 1962.

12) R. S-L Shon, D.O.Cowan and W.W.Schmiegel, *J.Chem.Phys,* **79**(20), 2087, 1975.

13) R.N.Jones, *J.Am.Chem Soc.*, 1945, **67**, 2127.

14) A.D.Jenkins, *Prog.Polym.Sci.*, **5**, 61, 1977.

15) I.M^{c}Inally, R.F.Reid, M.Rutherford & I.Soutar, *Eur.Polym,Jour.*, **15**, 273, 1979.

16) R.D.Burkhart & E.R.Lonson, *Chem.Phys.Lett.*, 1978, **54**(1), 85.

17) D.W.Brown, A.J.Floyd & M.Sainsbury, Organic Spectroscopy, Wiley 1988.

18) H.Durr & H.Bouas-Laurent, Photochroism: Molecules and Systems, Elsevier 1990.

19) R.M.Silverstein, G.C.Bassler & T.C.Morrill, Spectrometric Identification of Organic Compounds, Fifth Edition, Wiley 1991

20) Appendix for Chapter Four.

21) D.Ng & J.E.Guillet, *Macromolecules*, 1982, **15**(3), 724.

22) F.C.De Schryver, N.Boens, J.Huybrechts, J.Daemen & M.De Brackeleire, *Pure & Appl Chem*, 1977, **49**, 237.

Chapter Five

Poly (p-Azidobenzoate Ethyl Methacrylate)

5. Poly (p-Azidobenzoate Ethyl Methacrylate)

5.1. Introduction to Azides [1, 2, 3]

5.1.1. Molecular Structure and Bonding

Azides are molecules of the general formula RN_3 where R = H, alkyl, vinyl or aromatic. The general shape of the azide molecule, along with its two canonical forms is schematically shown below.

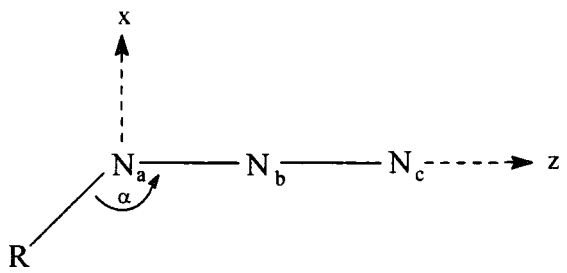

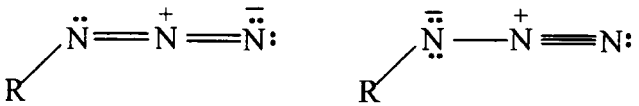

There are sixteen valence shell electrons, five donated from each nitrogen and one from the R group. Six of the electrons are located in three σ-bonds, four electrons are found as two lone pairs, two electrons are in localised π-bonds and the remaining four electrons are located in two delocalised π-bonds.

The molecular shape of the azide is determined by the spatial distribution of the σ-bonds which in turn depend on the states of hybridisation of the atoms. Table 5.1.1.1 shows the valence states of the nitrogen atoms in the general azide structure $RN_aN_bN_c$.

Nitrogen	Lone Pair	σ-electrons	π-electrons
N_a	$(s\delta p)^2$	$p\delta s'$ $p\delta s''$	p_y
N_b		sp sp	$(p_y)^2$ p_x
N_c	$(s)^2$	p_z	p_y p_x

Table 5.1.1.1: Valence States of Nitrogen Atoms in RN_3.

σ-Bonds

The sp hybridisation of N_b is responsible for the linear shape of the azido group. The σ-orbitals of N_a consist of three non-equivalent hybrids made up from s, p_z and p_x. One of the hybrids has more pronounced s character, termed sδp, and is occupied by one pair of electrons. The remaining two hybrids, pδs′ and pδs″ are involved in bonding N_a to R and N_b respectively. N_c uses its p_z orbital for σ-bonding and its s-orbital contains a lone pair of electrons. The bond formed between R-N_a consists of a σ-bond from R and a pδs′ from N_a, the bond between N_a and N_b consists of a pδs″ and an sp-orbital and the bond between N_b and N_c is made up of an sp- and a p-orbital.

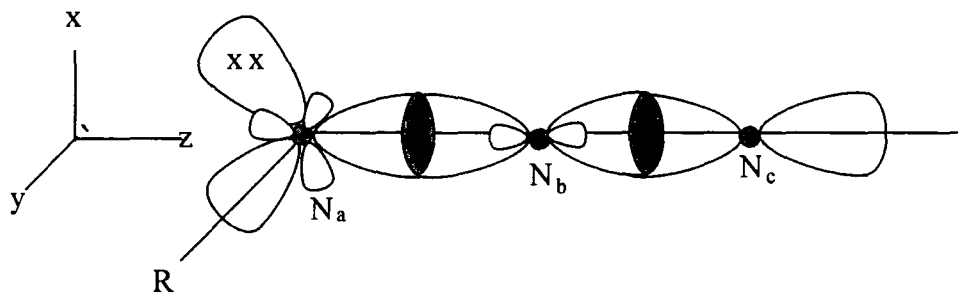

Figure 5.1.1.1: σ-Bonding in RN_3

π-Bonding

The π-bonding in RN_3 is shown schematically in Figure 5.1.1.2

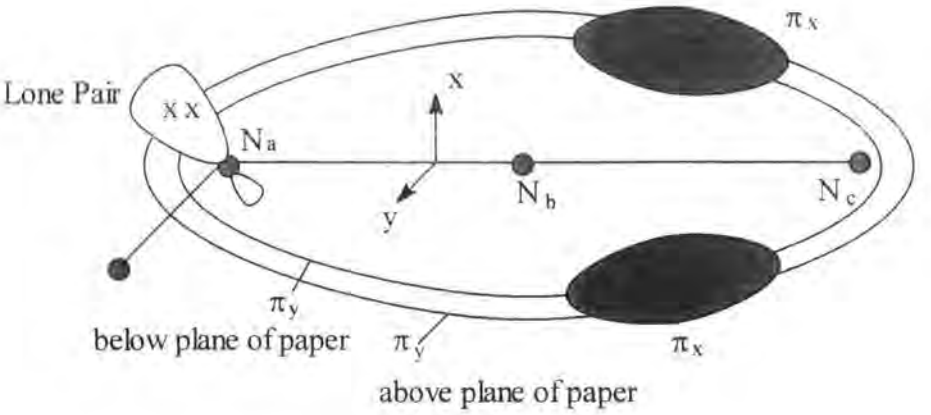

Figure 5.1.1.2: π-Orbitals in RN_3

The p_x orbitals of N_b and N_c form a localised orbital π_x which accommodates two electrons and a corresponding, vacant antibonding orbital. The p_y orbitals of the three nitrogens form three delocalised π-orbitals, two accommodating four electrons (π_y) and a third vacant antibonding orbital (π_y^*).

Lone Pairs of Electrons

There are two lone pairs of electrons in the valence shell of the azido group: one pair in the 2s orbital of N_c and one pair in the sδp orbital of N_a.

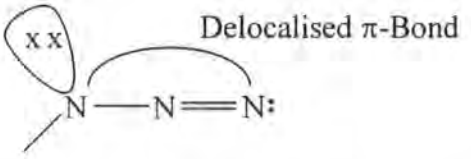

The central nitrogen is bonded to its neighbours by two σ-bonds, one localised π-bond (π_L) and one delocalised π-bond (π_D).

5.1.2. Photochemistry of the Azide Group:

When organic azides are irradiated, molecular nitrogen is readily lost.

$$RN_3 + h\upsilon \longrightarrow RN: + N_2$$

The primary product of the reaction, RN, is termed a nitrene. Although nitrenes have been postulated as intermediates for some time[2], the final products of azide reactions could easily be accounted for by other mechanisms such as a general reaction where the elimination of nitrogen is concerted with formation of a new bond.

Physical proof for the existence of organic nitrenes came in 1962 when an e.s.r. experiment carried out by Wasserman *et al* [4] identified two strongly interacting unpaired spins localised on a single atom. This was assigned to the triplet ground state of an aromatic azide.

Spectra of organic azides identify the excited states which arise in the act of light absorption. The spectrum of the simplest azide HN_3 has two UV absorption bands: a weak band at 260nm ($\varepsilon \sim 40$) and a stronger band at ~ 200nm ($\varepsilon \sim 500$).

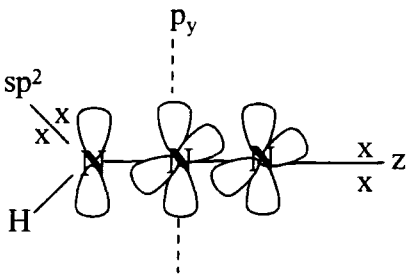

Nitrogen bonded to hydrogen is sp^2 hybridised whilst the two remaining nitrogens are sp hybridised. The five p-orbitals of nitrogen give rise to five delocalised molecular orbitals, π_y, π_y^n, π_y^*, π_x and π_x^* which in the ground state of HN_3 are occupied in order of increasing energy $(\sigma_{23})^2\ (2s)^2\ (\sigma_{12})^2\ (\pi_y)^2\ (\pi_x)^2\ (sp_2)^2\ (\pi_y^n)^2$.

The absorption band at 260nm is attributed to the promotion of an electron from the highest occupied π_y^n orbital to the lowest unoccupied π_x^* orbital, giving rise to an electronic configuration $(\sigma_{23})^2\ (2s)^2\ (\sigma_{12})^2\ (\pi_y)^2\ (\pi_x)^2\ (sp_2)^2\ (\pi_y^n)^1\ (\pi_x^*)^1$. An absorption band at 200nm is assigned to the transition sp_2-π_y^* and brings about a new electronic configuration $(\sigma_{23})^2\ (2s)^2\ (\sigma_{12})^2\ (\pi_y)^2\ (\pi_x)^2\ (sp_2)^1\ (\pi_y^n)^2\ (\pi_x^*)^1$. Both of these transitions are symmetry forbidden, hence the low extinction coefficients. Occupation of an antibonding π_x^* orbital forces the HN_2-N bond out of its trigonal planar configuration in order to reduce repulsive overlap of the orbitals. This change in equilibrium geometry between ground state and excited state plays an important role in dissociation of the molecule.

While the absorption spectrum of alkyl azides resembles that of the isolated azide, the spectrum of aromatic azides is essentially that of the parent hydrocarbon with a weak additional band due to the azido group, appearing as a shoulder on the long wavelength side of the hydrocarbon spectrum. Coupling the azido group with the aromatic system corresponds to a charge flow from nitrogen to the ring. This lowers the energy of the non-bonding π_y^n orbital below the level of sp^2. The azido band is assigned to the transition sp^2-π_y^* where π_y^* now extends over the whole aromatic system.

The mechanism for the elimination of nitrogen has been studied for hydrazoic acid [2]. Photodecomposition of HN_3(g) has a quantum yield equal to unity for the primary photolytic step. Therefore, it is assumed that the excited states of HN_3 are spontaneously dissociative. Elimination of nitrogen occurs as follows:

Absorption of a photon promotes the molecule to the singlet excited state HN_3^* ($^1A''$), which in the first instance appears in the linear configuration of the ground

state. Since the equilibrium configuration of HN_3^* ($^1A''$) is angular, light absorption also leads to some vibrational excitation. The vibrational energy released is not sufficient to break the HN-N_2 band but promotes interaction (mixing) of $^1A''$ state with other energetically accessible states. At least one of these is repulsive in the critical bond co-ordinate and brings about dissociation of the molecule.

In aromatic azides, the mechanism of the primary step is slightly different from that of the isolated azide group. The upper excited states are those of the parent hydrocarbon and upon irradiation, energy is absorbed by the aromatic system as a whole. Decomposition is therefore preceded by transfer of excitation energy from the hydrocarbon to the azido group.

On absorption of a photon in aromatic azides, promotion to an upper excited state occurs. Excess vibrational energy is transmitted until the lowest vibrational level of the lowest lying excited state is reached. Here, the molecule enters the excited $n\pi^*$ azide state (excitation transfer) and will either decompose by the HN_3 mechanism or cross over to the triplet state and dissociate in a similar manner. In aromatic azides, both alternatives apply[5] and it can therefore be said that the rate of intersystem crossing from singlet to triplet state is comparable to the rate of dissociation of the singlet excited state.

As transfer of excitation energy from hydrocarbon to azido group occurs at some stage in the reaction, the structure of the aromatic moiety has some effect on the quantum yield for photolysis. It has been found that polynuclear aromatic azides have higher quantum yields of photolysis than their phenyl counterparts[2].

5.2. Nitrenes (RN)

5.2.1. Structure and Bonding

On loss of molecular nitrogen from an azide group, a nitrene is formed. The nitrogen in the nitrene species is bonded to a single carbon centre and is, therefore, sp-hybridised. Of the five valence electrons, one takes part in a σ-bond to carbon, one pair occupy a non-bonding sp-orbital and the two remaining electrons are located in unhybridised p_x and p_y orbitals.

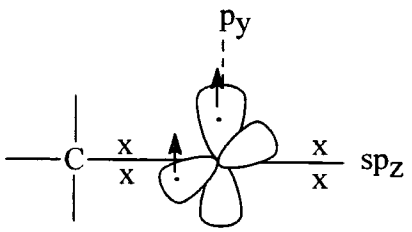

The two p-orbitals have equivalent energies and each carry one electron. As both electrons have the same spin, ground state nitrenes are expected to be triplet species. In aromatic nitrenes, one of the unpaired electrons is delocalised into the aromatic system.

Phenyl nitrenes have seven π electrons in their aromatic shell. Lower triplet excited states originate from the transition of an electron from the highest occupied molecular orbital to the lowest unoccupied molecular orbital.

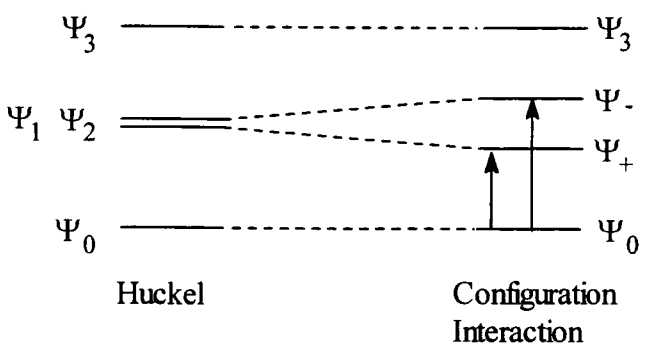

In the Huckel approximation, the two excited states ψ_1 and ψ_2 are nearly degenerate and will be split by configuration interaction into upper ψ_- and lower ψ_+ states. The transition ψ_0-ψ_- is observed as a strong band at 314nm and the weaker band at 402nm is attributed to the ψ_0-ψ_+ transition. Such a band pair is typical of an open aromatic shell (an odd number of electrons) and is observed generally in aromatic π radicals.

5.2.2. General Reactions of Nitrenes

Recombination

$$2RN: \rightarrow R\text{-}N{=}N\text{-}R$$

This reaction is allowed for nitrenes in both the singlet and triplet states. It is rarely seen in the continuous photolysis of azides due to the low concentrations of nitrene present at any one time. However, this is the preferred reaction if flash photolysis is used due to the high, localised concentration of nitrenes. It is also the only reaction to occur at low temperatures due to the low activation energies required.

Insertion into C-H Bonds

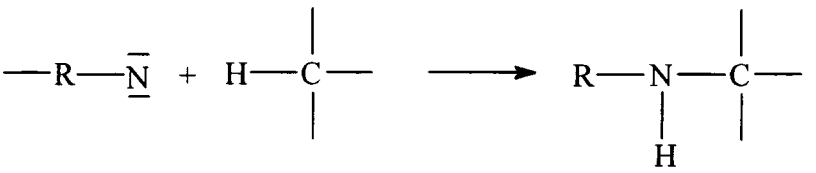

This reaction occurs with singlet nitrenes only.

Hydrogen Abstraction

This is the most general reaction of triplet nitrenes. Two separate abstractions are required to saturate the electron deficiency of the triplet species.

The first hydrogen abstraction leaves behind a carbon radical. Both of the radicals formed in this first step have unpaired spins and they cannot couple unless spin is reversed. The time required for spin inversion is usually sufficient to allow the radicals to diffuse away.

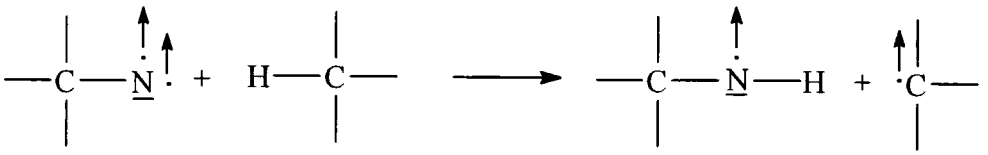

In the second step, the amino radical abstracts a second proton to form a primary amine.

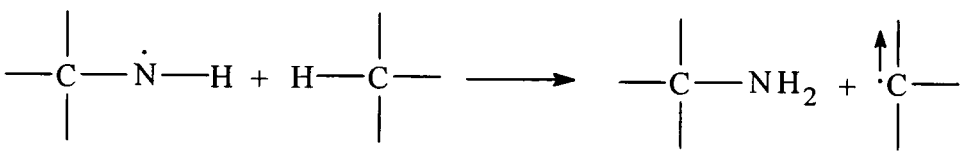

Other reactions are also possible

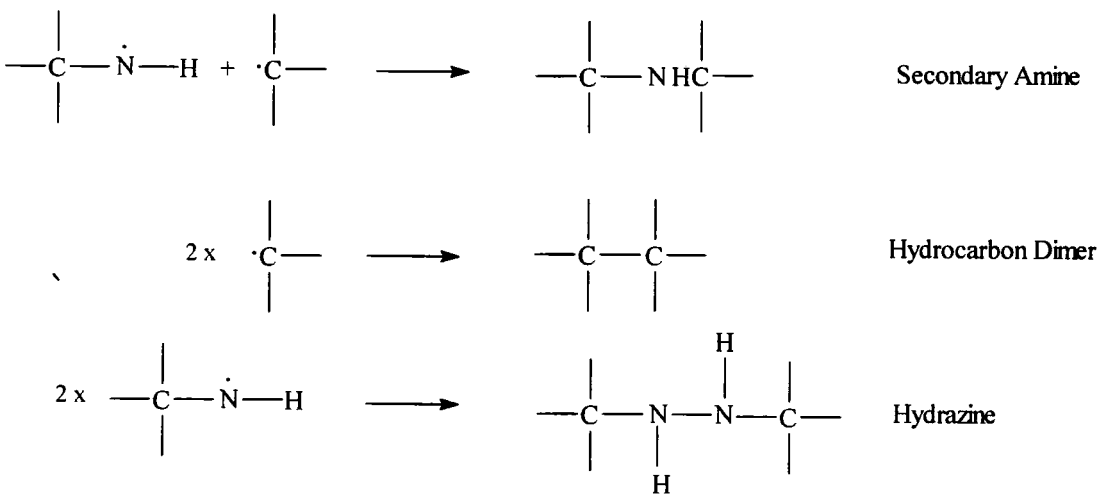

5.3. Synthesis and Characterisation of Poly (p-azidobenzoate ethyl methacrylate)

Poly (p-azidobenzoate ethyl methacrylate), polyazide, was synthesised by free radical polymerisation of the corresponding monomer in 2-butanone at 50-65°C with AIBN (azobisisobutyronitrile) as an initiator. The synthesis was carried out by Kate Foster [6] and a polymer of molecular weight 27,000 with a polydispersity of 3.0 was obtained using this method of polymerisation.

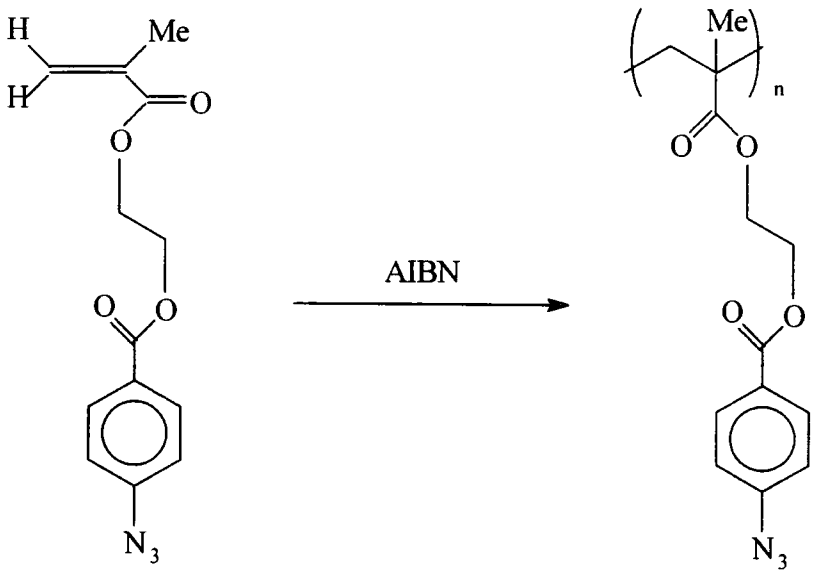

Figure 5.3.1: Synthesis of Poly (p-azidobenzoate ethyl methacrylate).

Generally speaking azides are known to be unstable, therefore a TGA was carried out to assess the polymer's thermal stability. Figure 5.3.2 shows a plot of the percentage mass loss of the polyazide as a function of temperature.

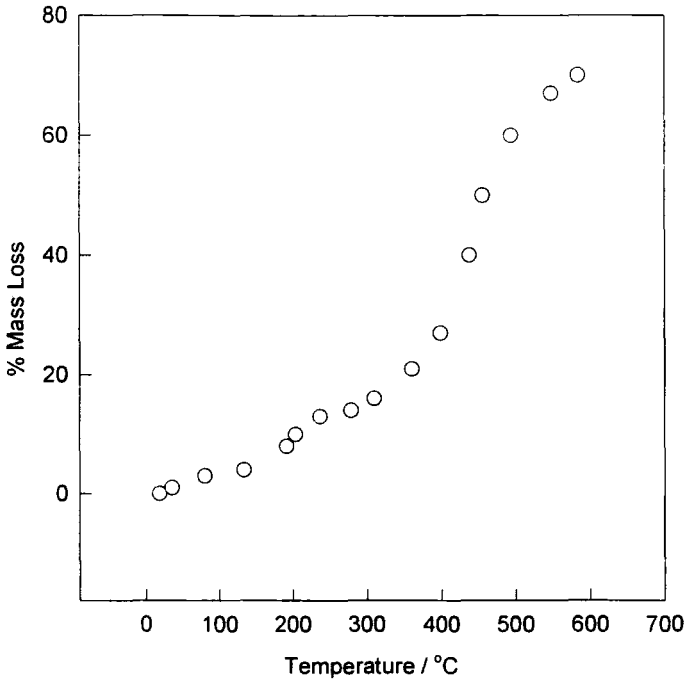

Figure 5.3.2: Percentage Mass Loss as a Function of Temperature for Polyazide.

At 100°C, there is a 5% change in the mass of the polymer. At this rate of decomposition, a DSC measurement is inappropriate due to the potential damage to the machine by the decomposition products. Powder X-ray diffraction is a second potential technique for the study of sample crystallinity. However, the polyazide cannot be left out at room temperature as it undergoes reaction and hence the reflectivity profile of the polymer will be changing over the duration of the reaction. Information regarding sample crystallinity is therefore unavailable. Due to this thermal instability, all solid samples of the polyazide are stored at 253K (freezer) and solutions at 277K (refrigerator).

NMR

^{1}H and ^{13}C NMR spectra are shown in Figure 5.3.3 & Figure 5.3.4.

The following tables show the NMR peak assignments [7].

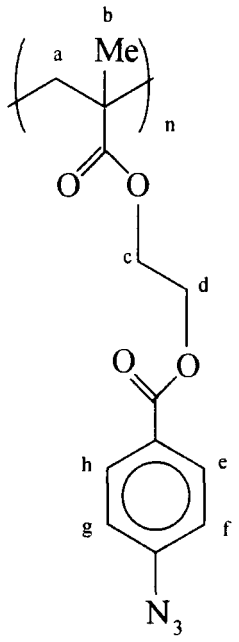

Proton	Assignment (ppm)
a	1-2
b	1-2
c	4.2
d	4.4
e & h	7.0
f & g	7.9
Chloroform	7.3

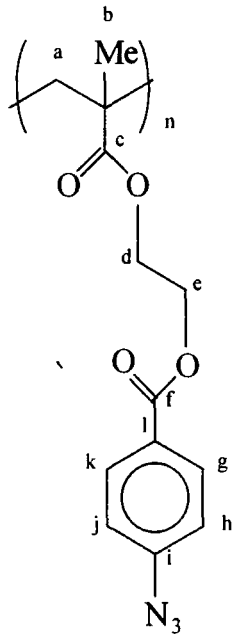

Carbon	Assignment (ppm)
a	44-46
b	18.0
c	165
d	62-63
e	62-63
f	165
g, h, i, j, k, L,	118-146
Chloroform	77

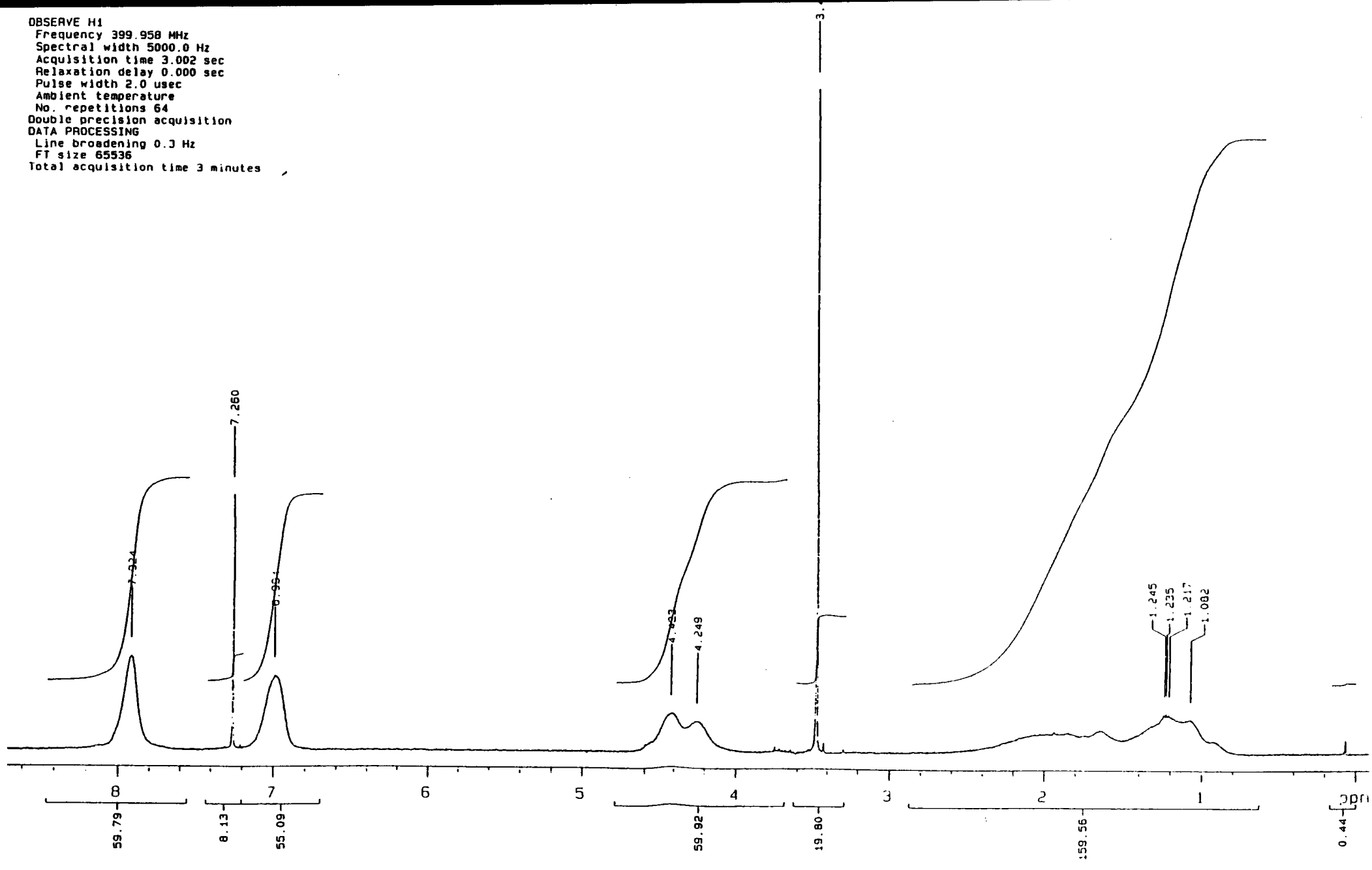

Figure 5.3.3: ^{1}H NMR Spectrum of Polyazide in $CDCl_3$.

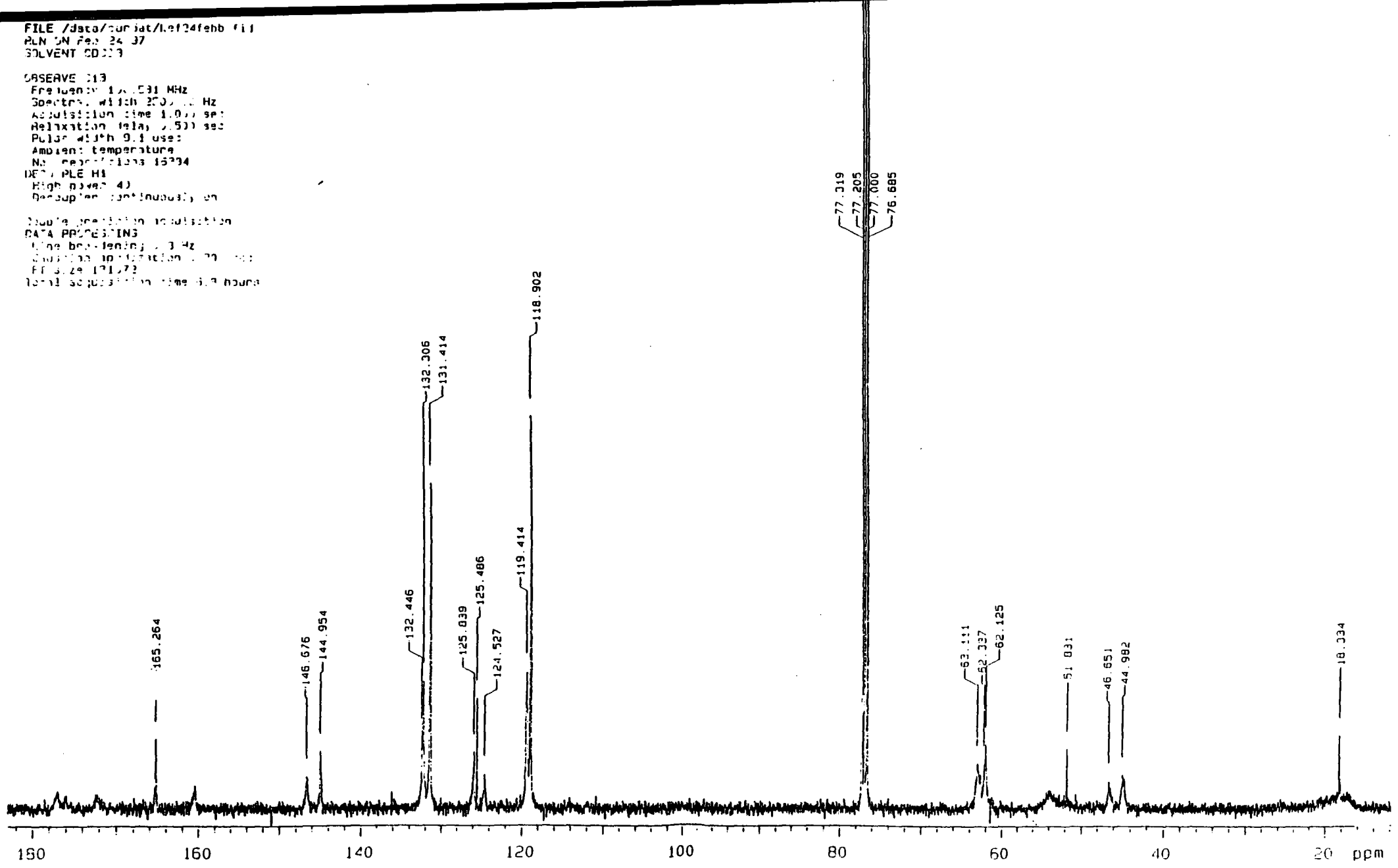

Figure 5.3.4: ^{13}C NMR Spectrum of Polyazide in $CDCl_3$.

The broad nature of the peaks indicate that the sample is polymeric. The lack of C=C peaks (5-6 ppm) in the ^{1}H spectrum show that there is no residual monomer contained in the sample. The poor quality of the ^{13}C spectrum is due to the poor solubility of the polyazide in $CDCl_3$.

5.4. Desired reactions

Upon irradiation with UV light, it was hoped that the polyazide side chains would dimerise, via nitrene radicals, with the loss of nitrogen to form either inter- or intramolecular azobenzene moieties, Figure 5.4.1.

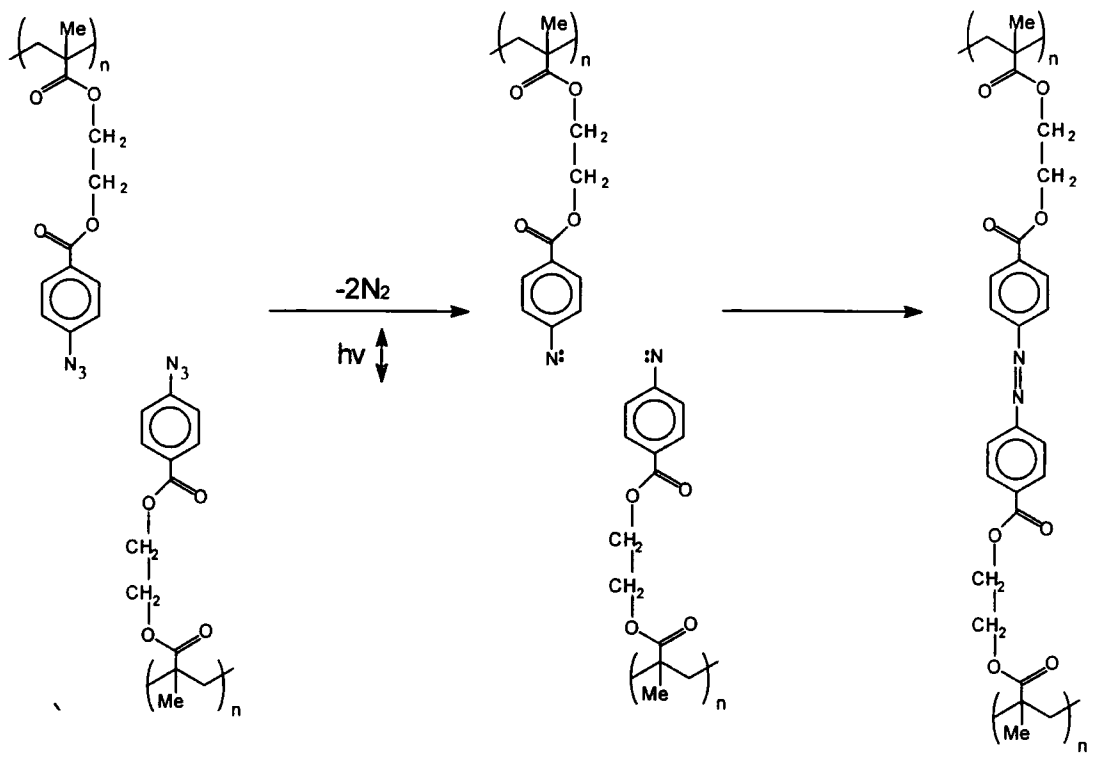

Figure 5.4.1: The Desired Reaction of Polyazide Initiated by Exposure to Polarised UV Radiation.

Following the reaction by UV spectroscopy, would produce a decrease in the absorbance peak due to the azide (278nm) and form a new absorbance peak due to the azobenzene (300-350nm & 400-500nm).

Figure 5.4.2 shows that azobenzenes have large absorbances in the region 300-350nm and a smaller absorbance at 400-500nm. In the polyazide system, the absorbance bands may move to longer wavelength due to the conjugation through the carbonyl group which is not present in the azobenzene molecule.

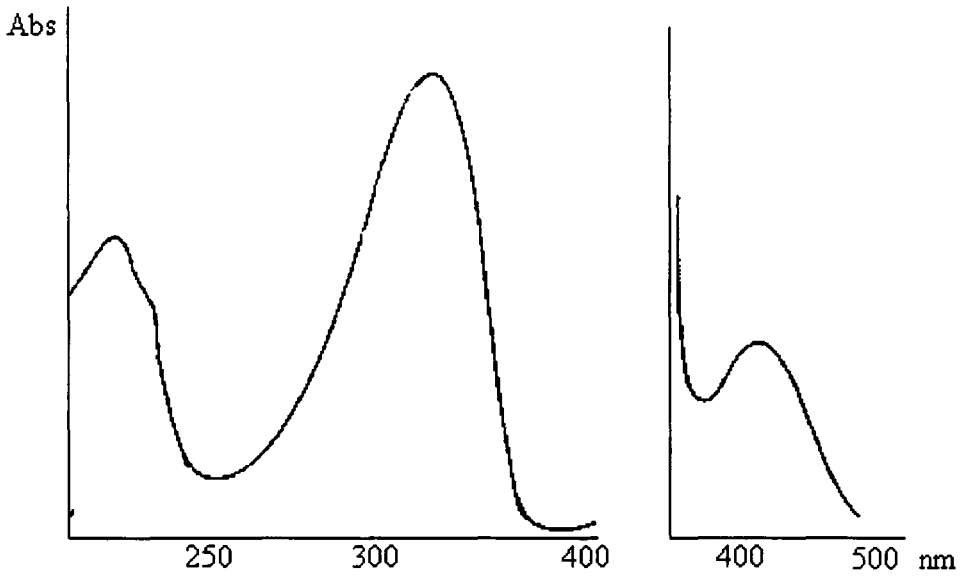

Figure 5.4.2: Absorption Spectrum of Azobenzene[8].

A decrease should also be observed in the azide peaks in the IR spectrum (~1279 cm^{-1} & ~2127 cm^{-1}). By using polarised radiation, the loss should have an orientation dependence and IR dichroism should be observed. As irradiation uses light with its polarisation vector parallel to the long edge of the sample, reaction of the azide groups should also occur parallel to this direction and the residual groups

remain in a perpendicular orientation. If the dichroic ratio is defined as $D = A_{para}/A_{perp}$, D is expected to decrease as A_{perp} remains at a constant value and A_{para} decreases.

As with PVCi and Polyanth, birefringence is expect to increase as selectively depleting one orientation of chromophores creates anisotropy in the refractive index.

The azobenzene species created by the reaction have much greater conjugation than the azide starting material and it therefore has a larger polarizability associated with it. It is expected that the liquid crystals will align along the direction of the azobenzene and not along the direction of the residual azides. This is in contrast to the results expected for PVCi and Polyanth, therefore a cell formed with the UV polarisation direction perpendicular to the rubbing direction of the polyimide should give rise to a twisted liquid crystal cell.

5.5. Results and Discussion

5.5.1. UV Spectroscopy

Figure 5.5.1.1 shows the UV absorbance spectrum of an unexposed 48nm thick film of Polyazide.

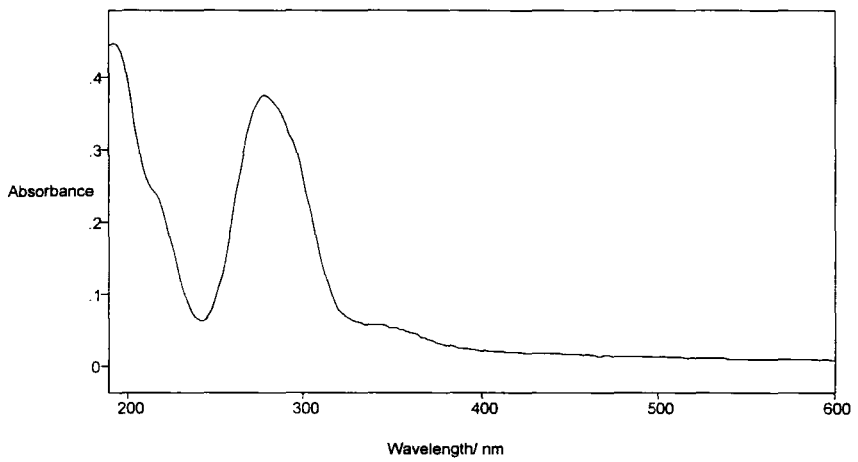

Figure 5.5.1.1: UV Absorbance Spectrum of 'as-spun' Polyazide.

The main peak is shown at 278nm. This spectrum is essentially the spectrum of the parent hydrocarbon molecule with a low-lying shoulder on the long wavelength side of the main peak. The shoulder is due to the n-π^* transition in the azide.

Irradiation with unpolarised radiation from the deuterium lamp was carried out to ensure that exposure induced reaction in the sample. The change in absorbance with increasing exposure time is shown in Figure 5.5.1.2.

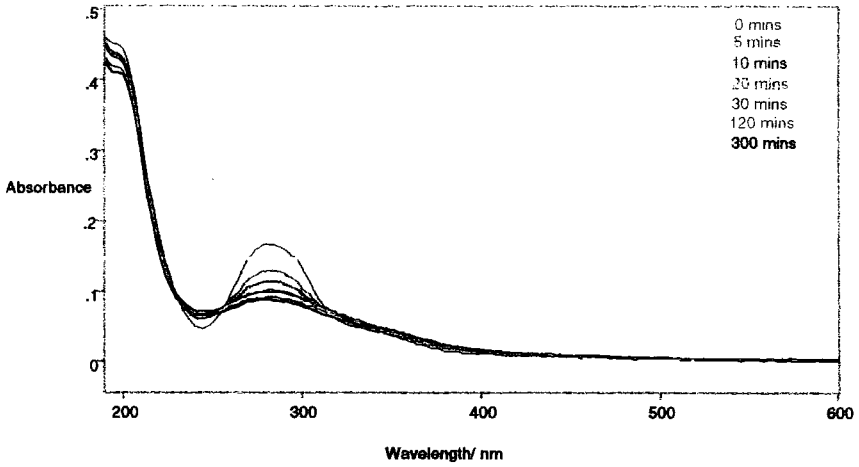

Figure 5.5.1.2: Decreasing UV Absorbance as a Function of Exposure to Unpolarised Radiation from the Deuterium Lamp.

Figure 5.5.1.2 shows no evidence of azobenzene formation upon UV irradiation, although almost 50% of the chromophores have reacted. The change in chromophore concentration as irradiation proceeds is shown in Figure 5.5.1.3.

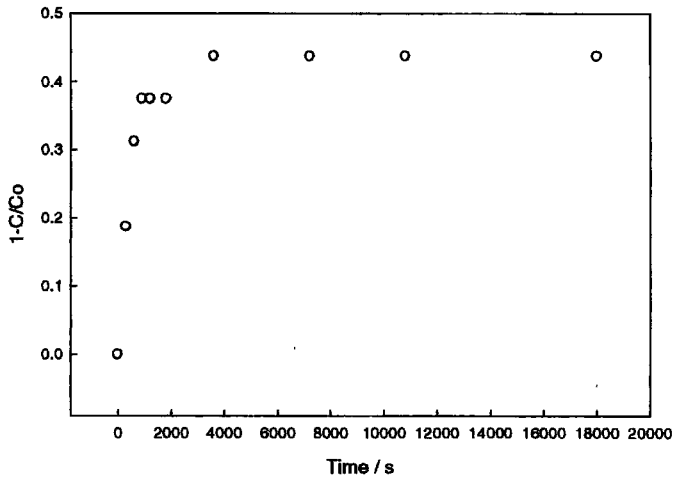

Figure 5.5.1.3: Change in Concentration of Starting Material with Exposure Time.

From the absorbance spectra, the quantum yield for the reaction of the starting material can be calculated, Figure 5.5.1.14 and the resulting data are shown in Table 5.5.1.1.

Exposure Time (s)	$1-C/C_0$	Quantum Yield
0	0	-
300	0.19	1.22
600	0.31	1.18
900	0.37	1.02
1200	0.37	0.77
1800	0.37	0.51
3600	0.44	0.33
7200	0.44	0.16
10800	0.44	0.11
18000	0.44	0.07

Table 5.5.1.1: Data for Exposure to Unpolarised Radiation from the Deuterium Lamp.

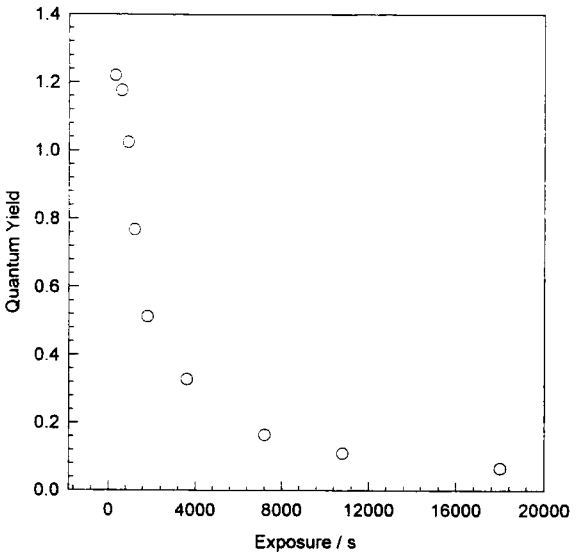

Figure 5.5.1.4: Quantum Yield for Unpolarised Exposure of Polyazide.

Figure 5.5.1.4 shows the value of the quantum yield to be greater than one. This is a result of the ambiguity in calculating I_o, described in Chapter 2. If quantum yield is plotted as a function of concentration, a different shaped curve is obtained, Figure 5.5.1.5. The reasoning behind this is discussed in the following pages.

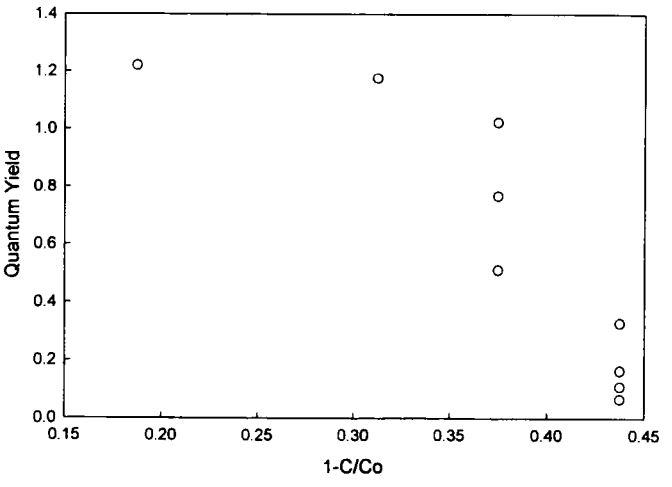

Figure 5.5.1.5: Quantum Yield as a Function of Concentration for Polyazide.

Figure 5.5.1.2 shows that the chromophores present in the polymer are being depleted upon irradiation with the deuterium lamp. As reaction was shown to occur, polarised radiation was used to induce orientation within the sample.

Upon irradiation with polarised radiation from the deuterium lamp, the peak at λ=278nm decreases, Figure 5.5.1.6. This is the only spectral change upon irradiation. The change in the peak intensity is small when the 25 hour irradiation time is considered. Only 9% of the chromophores present in the sample have reacted.

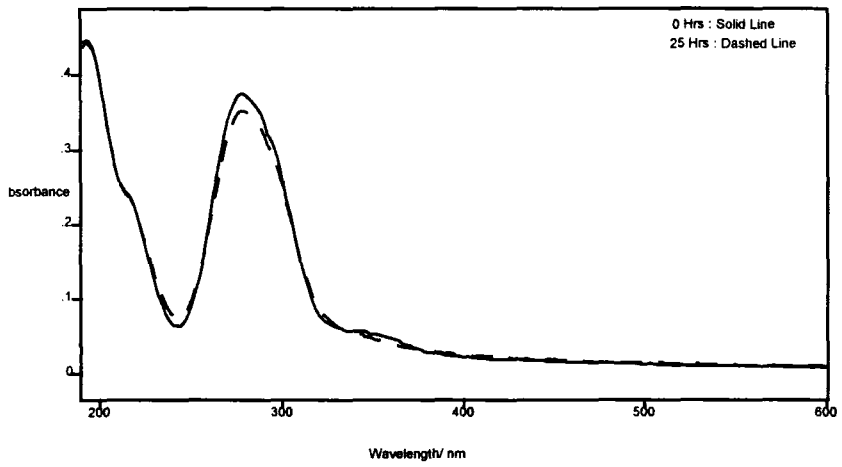

Figure 5.5.1.6: UV Spectrum of Polyazide Before & After 25 Hours Polarised Exposure.

No new peaks are evident in the spectrum following irradiation. If azobenzene species had been formed, their presence in the sample would be indicated by an absorbance peak at λ = 300-350nm & 400-500nm. From this data, it can be concluded that although some of the starting azide species have been consumed, the desired azobenzene moiety has not been formed.

The quantum yield for the depletion of the azide species can be calculated, the resulting plot is shown in Figure 5.5.1.7 and data in Table 5.5.1.2.

Exposure Time (s)	$1-C/C_o$	Quantum Yield
0	0	0
300	0	0
600	0	0
900	0	0
1800	0	0
2700	0	0
3600	0.054	0.12
4500	0.054	0.094
5400	0.054	0.079
7200	0.054	0.059
10800	0.054	0.039
14400	0.054	0.030
21600	0.054	0.020
32400	0.054	0.013
37800	0.054	0.011
91800	0.081	0.006

Table 5.5.1.2: Data for Exposure to Polarised Radiation from the Deuterium Lamp.

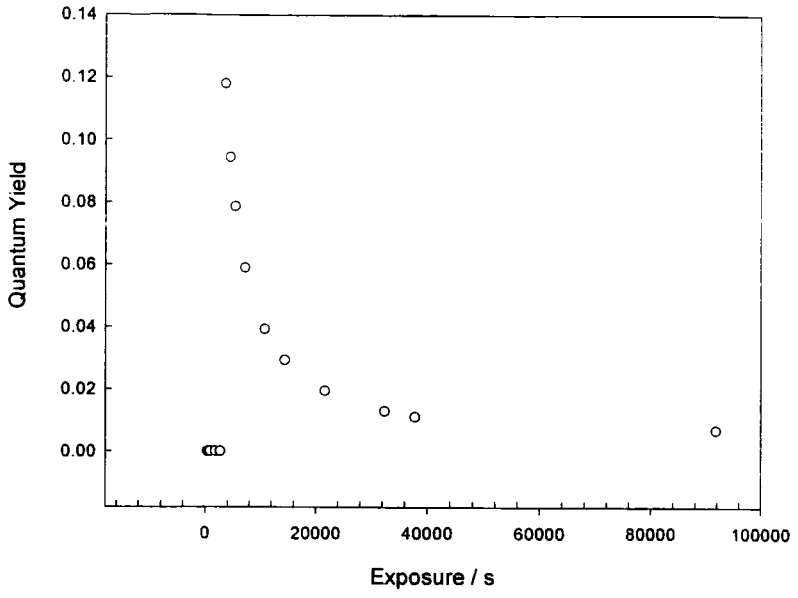

Figure 5.5.1.7: Quantum Yield for the Decay of Polyazide.

Consider the quantum yield, it is the change in concentration of reacting species per photon absorbed. It is therefore necessary to look at how the concentration of the azide group changes with irradiation time, Figure 5.5.1.8.

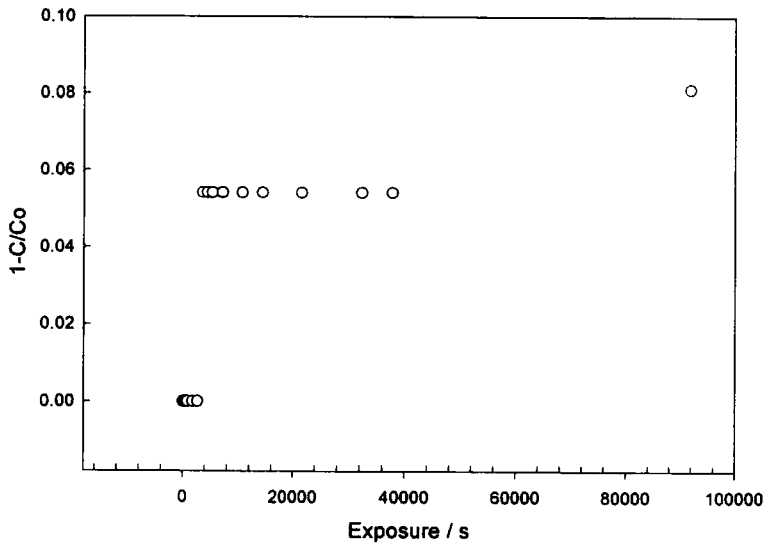

Figure 5.5.1.8: Change in Concentration of Azide with Exposure Time.

Figure 5.5.1.8 shows that for the first 45 minutes of irradiation, no reaction occurs. After 60 minutes, some of the azide has reacted, approximately 5%. Further reaction does not occur until nine hours later. With a concentration change such as this, it does not seem possible to produce a decay curve such as that shown in Figure 5.5.1.7.

A plot of quantum yield vs fraction of chromophores reacted is shown in Figure 5.5.1.9.

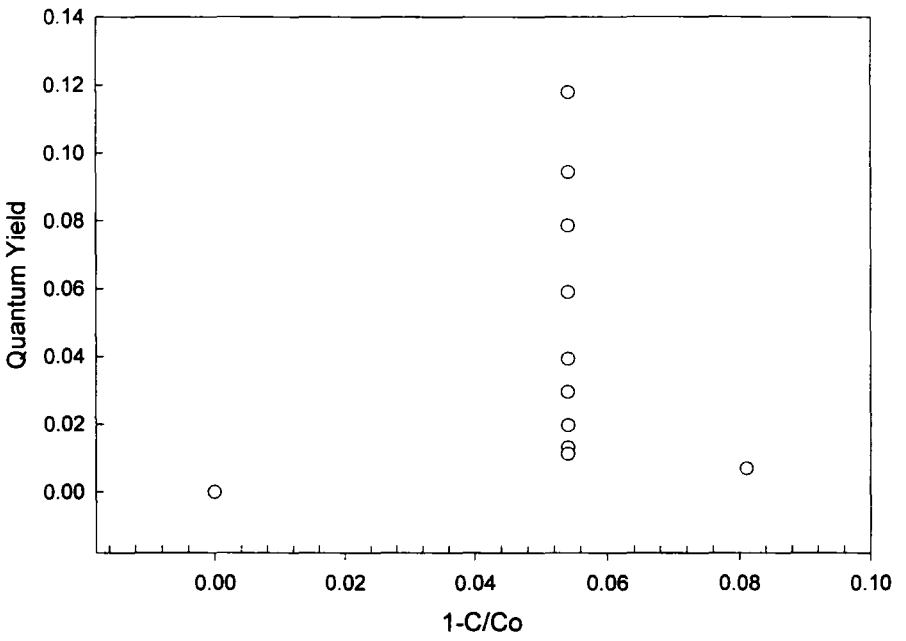

Figure 5.5.1.9: Quantum Yield vs Chromophore Conversion for Polyazide.

In Figure 5.5.1.9 it appears as if one concentration can yield a range of quantum yields. Quantum yield is calculated via

$$Quantum\,Yield = \frac{[Azide]}{I_a \times t}$$

If the chromophore concentration is constant, then I_a must also be constant, the only variable being exposure time. Therefore, the quantum yield curve shown in

Figure 5.5.1.7. materialises due to varying the irradiation time. To illustrate this time effect, a plot of 'x vs 1/t' is simulated, Figure 5.5.1.10.

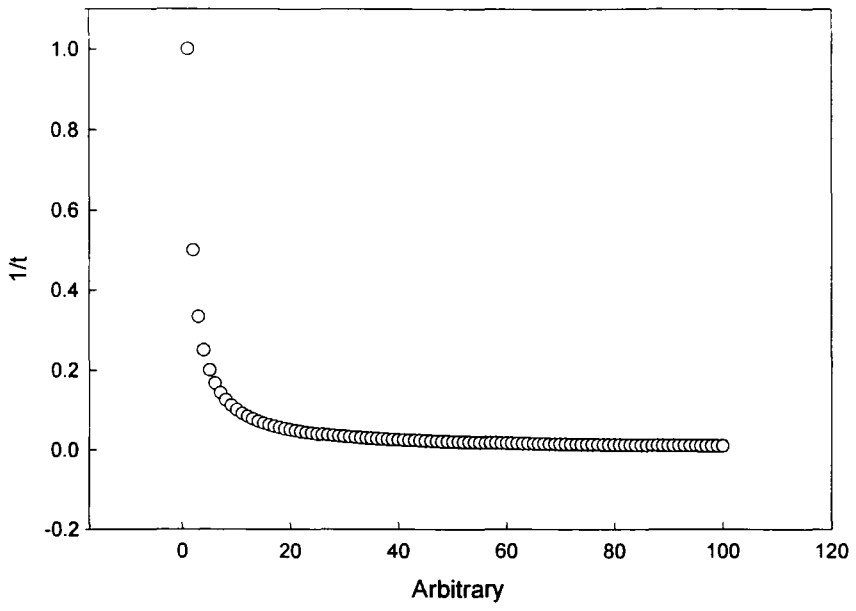

Figure 5.5.1.10: Simulation of 'x vs 1/t'.

Figure 5.5.1.10 follows the same decay curve as the quantum yield function. These results show that the decay curve obtained for Polyazide is a manifestation of 1/t in the quantum yield equation. All future quantum yields will therefore be concerned with quantum yield as a function of concentration.

There appears to be very little reaction occurring in the polyazide film when it is irradiated using the deuterium lamp. The lamp provides 30W of a broad wavelength range of radiation, λ= 185-370nm. When compared to alternative radiation sources such as a mercury lamp fitted with a filter or a UV laser, this is a relatively lower power source. The wavelength range is very broad and a large proportion of the incoming radiation can be absorbed by other chromophores in the polymer, for example, the benzene ring (π-π^* transition, λ~260nm) and the carbonyl

group (n-π^* transition, λ~280nm). The largest proportion of the lamps output radiation is in the region 200-275nm, ideal for electron promotion in these chromphores. As reported earlier, the azide n-π^* transition lies to the long wavelength side of the main peak i.e. ~300nm. Relatively small amounts of radiation of this wavelength are emitted by the lamp and hence only a small amount of reaction of the azide group is observed.

The rigidity of the matrix formed by spin casting the film may also be preventing increased reaction. As the T_g of the polymer is unknown, the ability of the molecules to move at room temperature is uncertain. Therefore, to test the likelihood of azobenzene formation in this particular polymer system, a solution of the polymer (10^{-5}M) in stabiliser-free chloroform was irradiated for two hours with unpolarised radiation from the deuterium lamp. Figure 5.5.1.11 shows the resulting spectra.

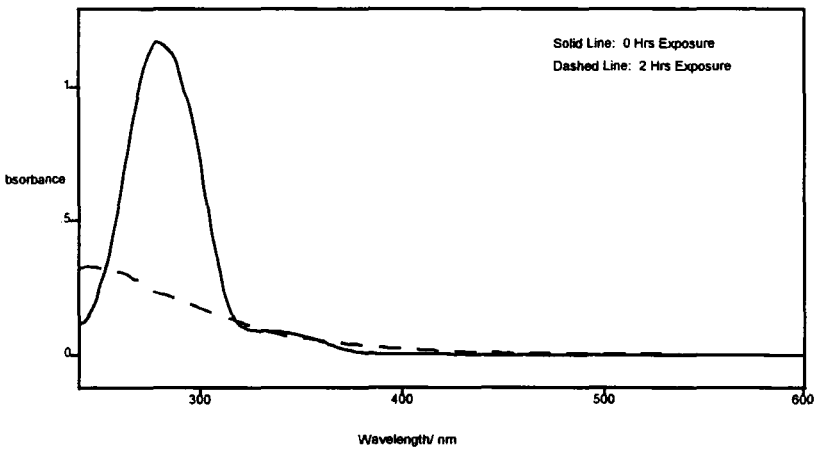

Figure 5.5.1.11: UV Spectra of Polyazide in Chloroform Before and After 2 Hours Unpolarised Exposure to the Deuterium Lamp.

After 2 hours exposure, the main peak at 278nm has been greatly reduced, 80% of the azide chromophores have reacted. However, the region 300-400nm has not changed. From these results, it can be inferred that in solution, a large proportion of the azide groups have reacted but their reaction products are not azobenzene.

Irradiation using the deuterium lamp provides relatively low intensity, continuous exposure. As a consequence of this, only a very low concentration of nitrene radicals will be present in the sample at any one time. The probability of finding two nitrenes in the correct orientation and proximity to react to form an azobenzene is small. However, exposure to the laser is a short, sharp burst of high intensity radiation. This will produce a high concentration of nitrene radicals in a very small area. These reaction conditions are, therefore, the most likely to induce azobenzene formation.

To test this hypothesis, a 39nm thick film of Polyazide was exposed to a depolarised laser with λ_o=325nm (intensity = 0.9mW through a 400μm aperture). Depolarisation of the laser beam allows maximum probability for azobenzene formation. An unexposed sample was irradiated in two separate regions: one area exposed for 5s and the second for 120s. These spectra are shown in Figure 5.5.1.12.

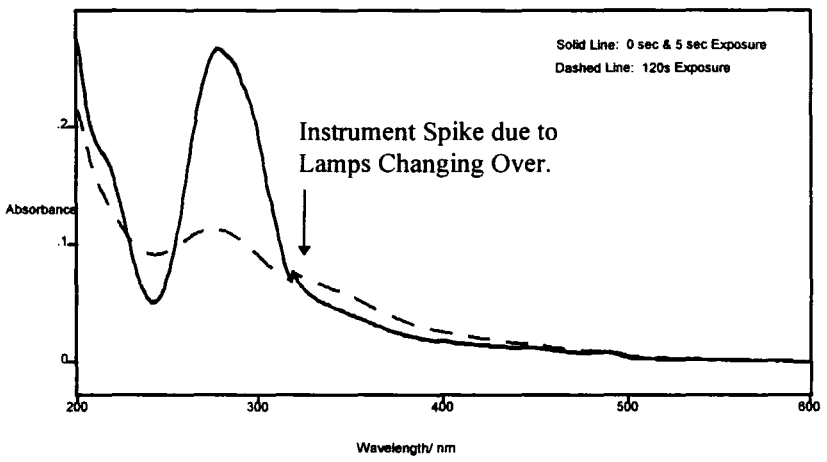

Figure 5.5.1.12: UV Spectra of Polyazide Exposed to Depolarised 325nm Laser.

After 5s exposure, there is no change in the spectrum. When the sample is irradiated for 120s, 60% of the chromophores react and the main peak decreases. There is a slight increase in absorbance in the region 300-450nm. However, this cannot be attributed to azobenzene formation due to the uncertainty in intensity when

the lamps change over. Therefore, the experiment was repeated using a wider range of exposure times and the spectra were recorded using an HP 8453 UV-Vis spectrometer. The resulting spectra are shown in Figure 5.5.1.13 and data in Table 5.5.1.3.

Exposure Time (s)	1-C/C$_o$	Quantum Yield
0	0	-
5	0.18	0.083
10	0.29	0.069
20	0.41	0.043
40	0.47	0.025
70	0.50	0.015
130	0.53	0.008
250	0.56	0.005

Table 5.5.1.3: Data for Exposure to Polarised 325nm Laser.

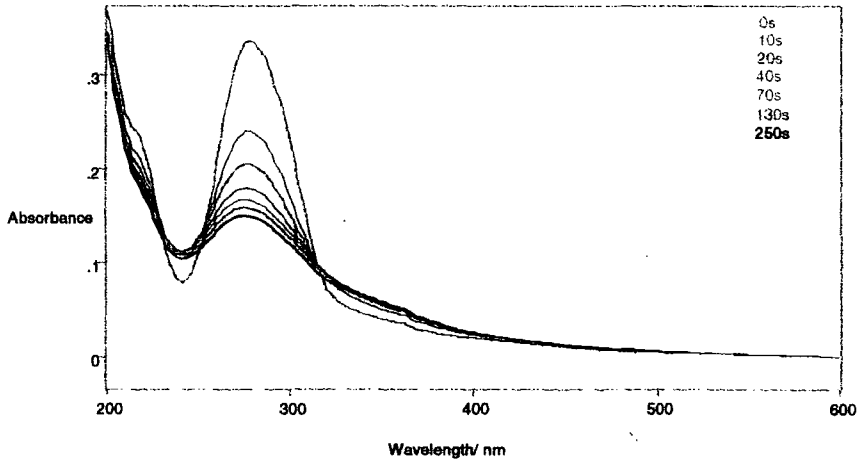

Figure 5.5.1.13: UV Spectra of Polyazide Exposed to Polarised 325nm Laser.

The change in concentration of the chromophore can be monitored, Figure 5.5.1.14 and from this data, the quantum yield for the reaction can be calculated, Figure 5.5.1.15.

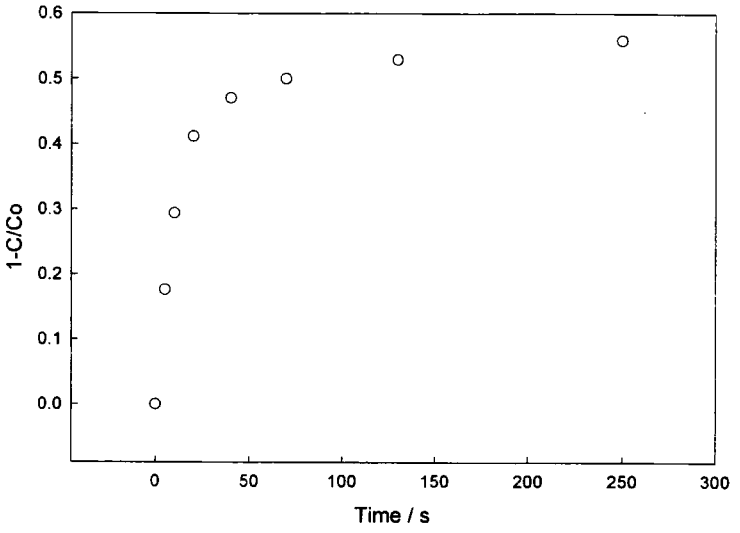

Figure 5.5.1.14: Fraction of Chromophores Converted Upon Exposure to Polarised 325nm Laser.

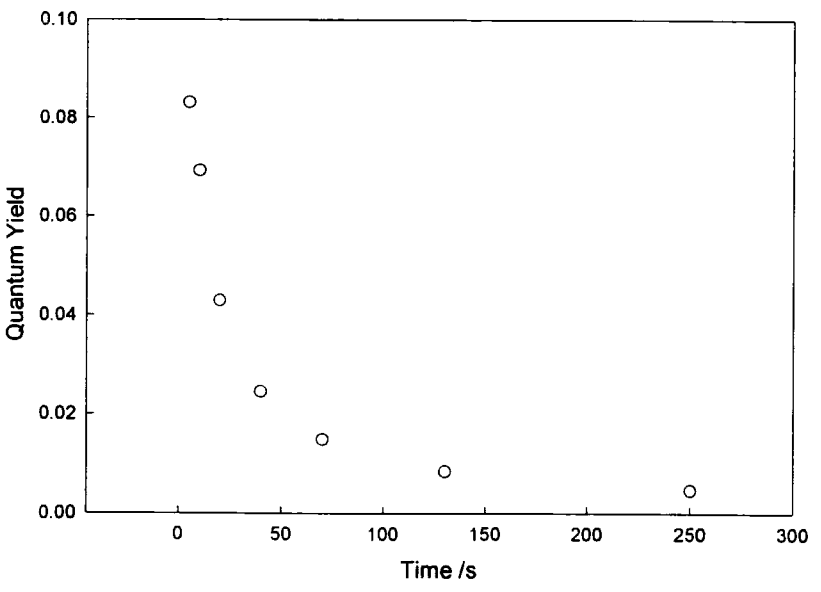

Figure 5.5.1.15: Quantum Yield for the Photoreaction using the 325nm Laser.

As the laser radiation is monochromatic and its intensity was measured, the errors introduced into the deuterium lamp calculation were greatly reduced and therefore the quantum yield is a more realistic value. The quantum yield values are small, much less than one, indicating that although photon absorption is occurring, not every photon is giving rise to a reaction. Significant numbers of photons will be absorbed into the aromatic system and will not induce reaction.

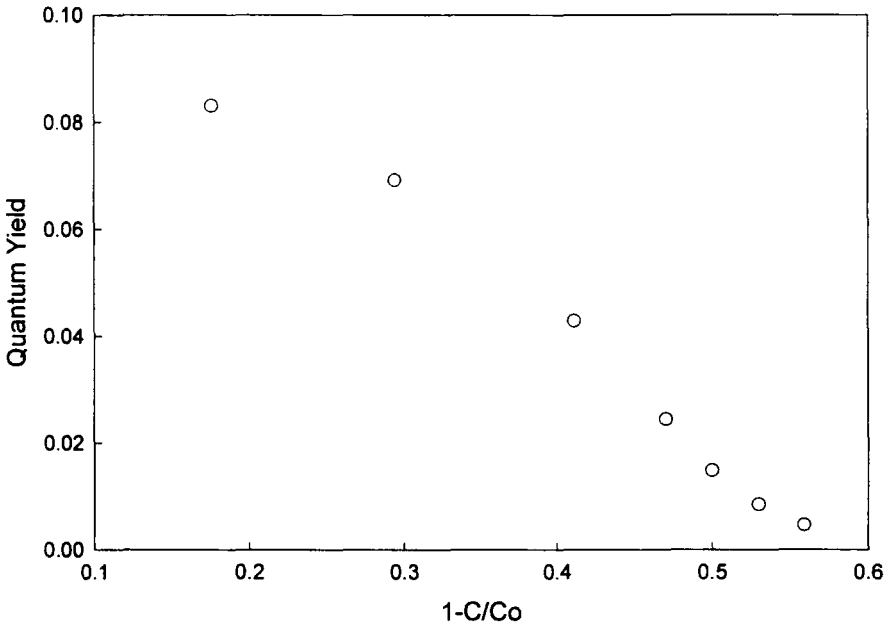

Figure 5.5.1.16: Quantum Yield as a Function of Concentration of Reacted Chromphores.

Ideally, a solution of Polyazide should have been irradiated with the laser as this is the most likely situation to give azobenzene formation. However, the Polyazide became insoluble before this reaction could be carried out.

As there is no evidence for azobenzene formation upon reaction of the azide groups, it is likely that insertion into C-H bonds or hydrogen abstraction is occurring. These reactions products will absorb in the UV region of the spectrum. The

broadening of the main peak is most likely due to the overlapping absorbances of the reaction products with the residual azide species.

In 1968, Reiser *et al* [9] undertook a study of photolysis reactions in aromatic azides. Their findings substantiate the evidence gathered for the photolysis of polyazide. The studies were carried out using 1-azidonapthalene which was irradiated with UV light either in solution or whilst being held in a polymer matrix.

For continuous irradiation using a low intensity UV source, such as a deuterium lamp, irradiation of a 10^{-4} M solution of 1-azidonapthalene in hexane produces a mixture of amines, but no azo-species nor polymer formed by proton abstraction. In a hydrocarbon matrix irradiated at 77K, the major product formed was 1,1′-azonapthalene, with a trace amount of polymer. Flash photolysis of 1-azidonapthalene solution resulted in the formation of azonapthalene, and in a polystyrene matrix, amines were the sole reaction product.

In summary, at high nitrene concentrations (flash photolysis), recombination is favoured and at low nitrene concentration (deuterium irradiation), proton abstraction is the preferred mechanism. When the azide concentration is high, proton abstraction and azo-compound formation is preferred. Azo-compounds are also favoured at low temperatures. Immobility of the nitrene species in the polymer matrix inhibits recombination and reaction with an azide.

Therefore, for polyazide, irradiation with the deuterium lamp gives low nitrene concentrations and proton abstraction will be favoured, hence no azobenzene species observed. The extent of the reaction is much greater in solution than in the matrix due to increased mobility of the nitrene moiety. For laser irradiation, high nitrene concentrations are achieved which should favour the formation of azo-species.

However, this reaction is inhibited due to the immobility of the nitrene. Amines are the most likely reaction product.

The rate of reaction in the solid form is much slower than the reaction rate in solution due to the steric restraints imposed by the rigid medium. The rate of nitrene depletion is dependant upon two factors: rate of diffusion of nitrogen from the reactive site and the rate at which favourable reaction configurations (transition state) is reached by the electron deficient nitrogen and an abstractable proton. Reiser[9] *et al* showed that transition state formation was the rate determining step. Nitrenes near their critical configuration react first. The distribution of configurations determine the shape of the observable decay curve; the reaction timescale is set by the rate of configurational diffusion in the system.

5.5.2. Infrared Studies

Polyazide was spin-cast onto a ZnSe substrate, giving a film 40nm thick. Infrared spectra of the unexposed sample were recorded and the initial dichroic ratio was calculated to be 0.99 for the band centred at 2127 cm^{-1} and 0.98 for the band centred at 1275 cm^{-1}. Both dichroic ratios are close to one, indicating that there is no preferential orientation inherent within the sample before exposure begins. Figures 5.5.2.1 & 5.5.2.2 show both the parallel and perpendicular IR spectrum of unexposed Polyazide, the stars indicate the azide peaks.

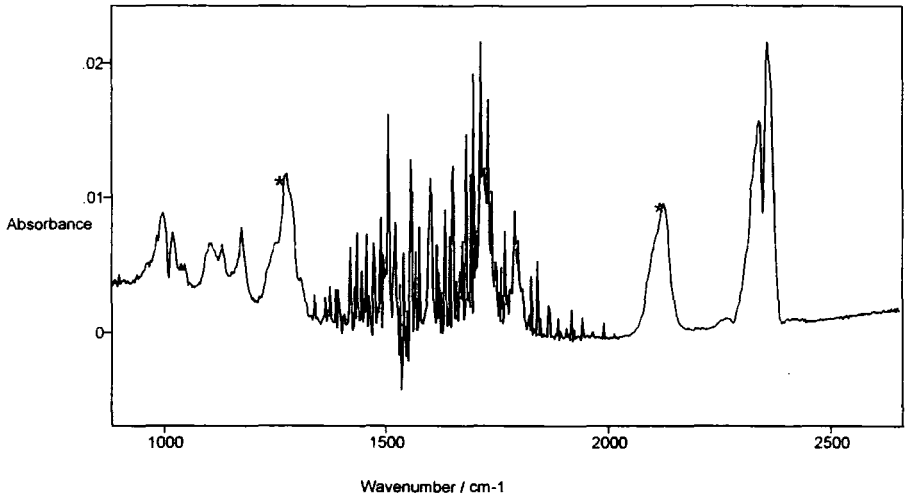

Figure 5.5.2.1: IR Spectrum of Polyazide (Perp).

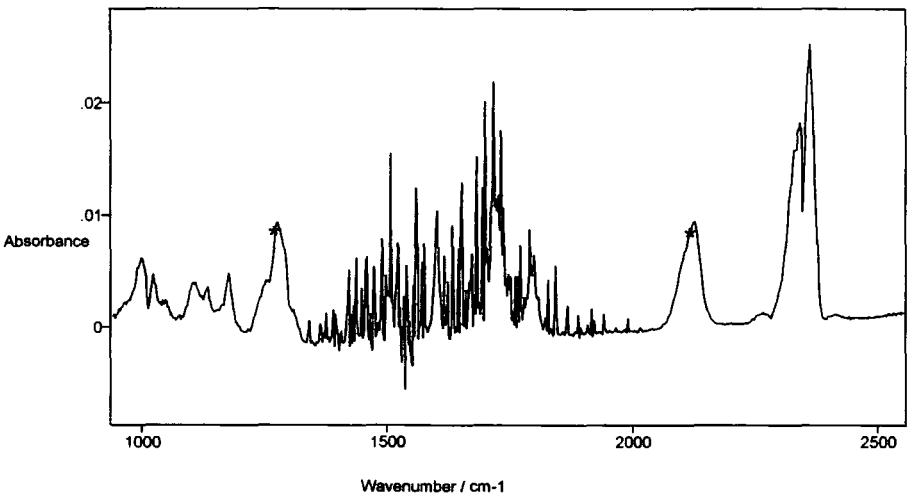

Figure 5.5.2.2: IR Spectrum of Polyazide (Para).

The film was then exposed for one hour to radiation from the deuterium lamp with a parallel polarisation vector. After this time, the IR spectra were once again recorded. It was noticed that after one hours irradiation, there was no observable change in the azide peaks. The dichroic ratios for the 2127 cm^{-1} and the 1275 cm^{-1} bands were calculated to be 1.0 and 0.98 respectively. Irradiation continued for a further hour, but still no change was observed. This continued until the sample had

received 89 hours polarised exposure. Despite receiving prolonged deuterium irradiation, the IR spectra remained unchanged.

This is unsurprising if the results obtained from the UV studies are considered. These show that approximately 9% of the chromophores react. This is within experimental error and as such, it is unlikely that such a small change will be detected and hence the dichroic ratio appears to remain constant.

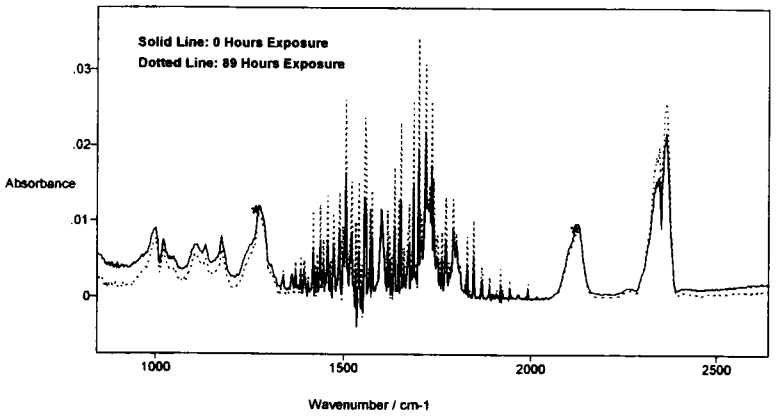

Figure 5.5.2.3: IR Spectrum of Polyazide (Perp) After 89hrs Polarised Exposure.

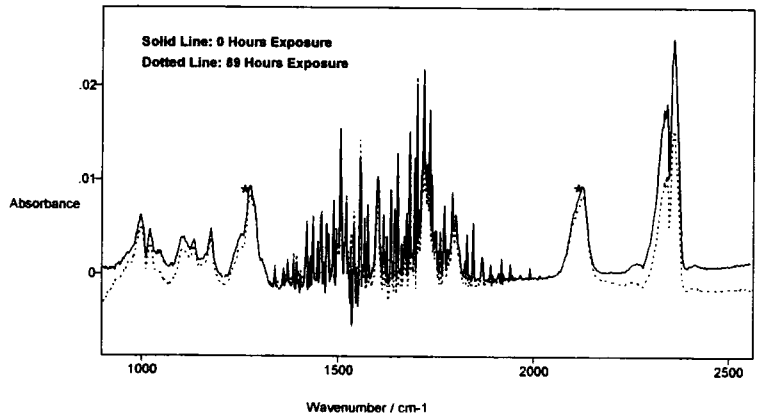

Figure 5.5.2.4: IR Spectrum of Polyazide (Para) After 89hrs Polarised Exposure.

It has been shown that exposure using polarised deuterium radiation did not promote sufficient reaction such that infrared spectral changes were evident. This evidence supports the results from UV spectroscopy; irradiation of the Polyazide film with the deuterium lamp promotes little azide reaction.

5.5.3. NMR Studies

Both UV and IR spectroscopy show that little reaction is occurring in the polyazide film upon irradiation with the deuterium lamp. In solution, UV spectroscopy shows that reaction does occur. Therefore, NMR experiments were carried out in an attempt to elucidate what was happening in solution and why the same process was not observed in the solid film. A solution of Polyazide in deuterated chloroform was irradiated with unpolarised radiation from the deuterium lamp and the subsequent reactions followed by NMR. Figures 5.5.3.1 & 5.5.3.2 show the NMR spectra of Polyazide before exposure, and after 3 hours exposure, Figures 5.5.3.3-5.5.3.6.

Assignment of the NMR peaks is shown in section 5.3. Figures 5.5.3.3-5.5.3.6 show that after three hours exposure, there is no observable change in the NMR spectra; no peaks decrease and no new peaks arise. This result is unsurprising when the possible reaction mechanisms are considered. It has been shown that azobenzene formation is not occurring which leaves insertion into C-H bonds and proton abstraction as the possible reaction mechanisms. Control over how and where reaction is occurring is not achievable. Insertion can occur into the C-H bonds of the backbone, of the side chain and also of the methyl group. Proton abstraction can also occur in these places. The NMR spectra of the Polyazide shows very broad peaks and any change in peaks size would have to be quite significant to be observed. The lack

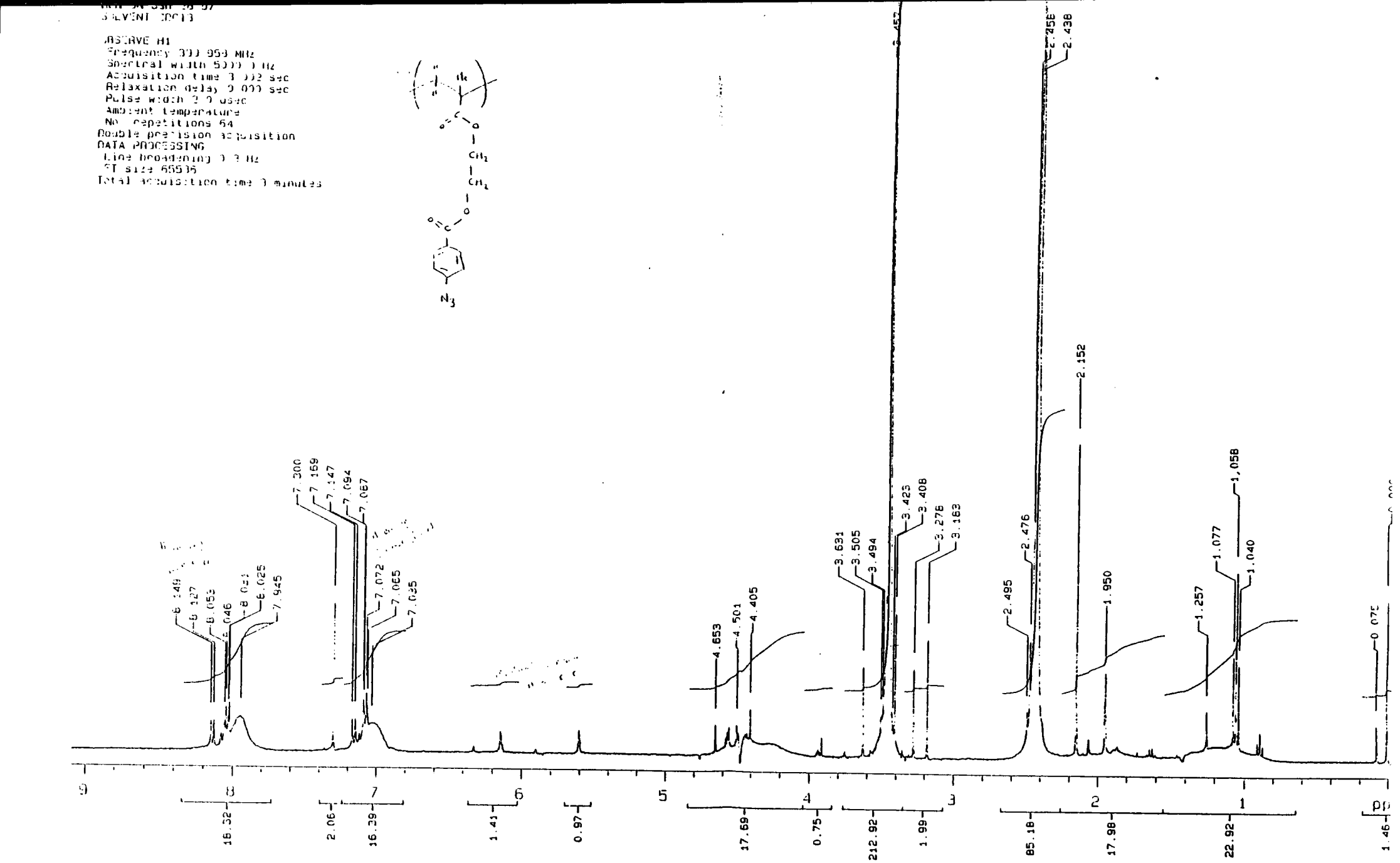

Figure 5.5.3.1: ^{1}H NMR Spectrum of Polyazide in $CDCl_3$ Before Exposure

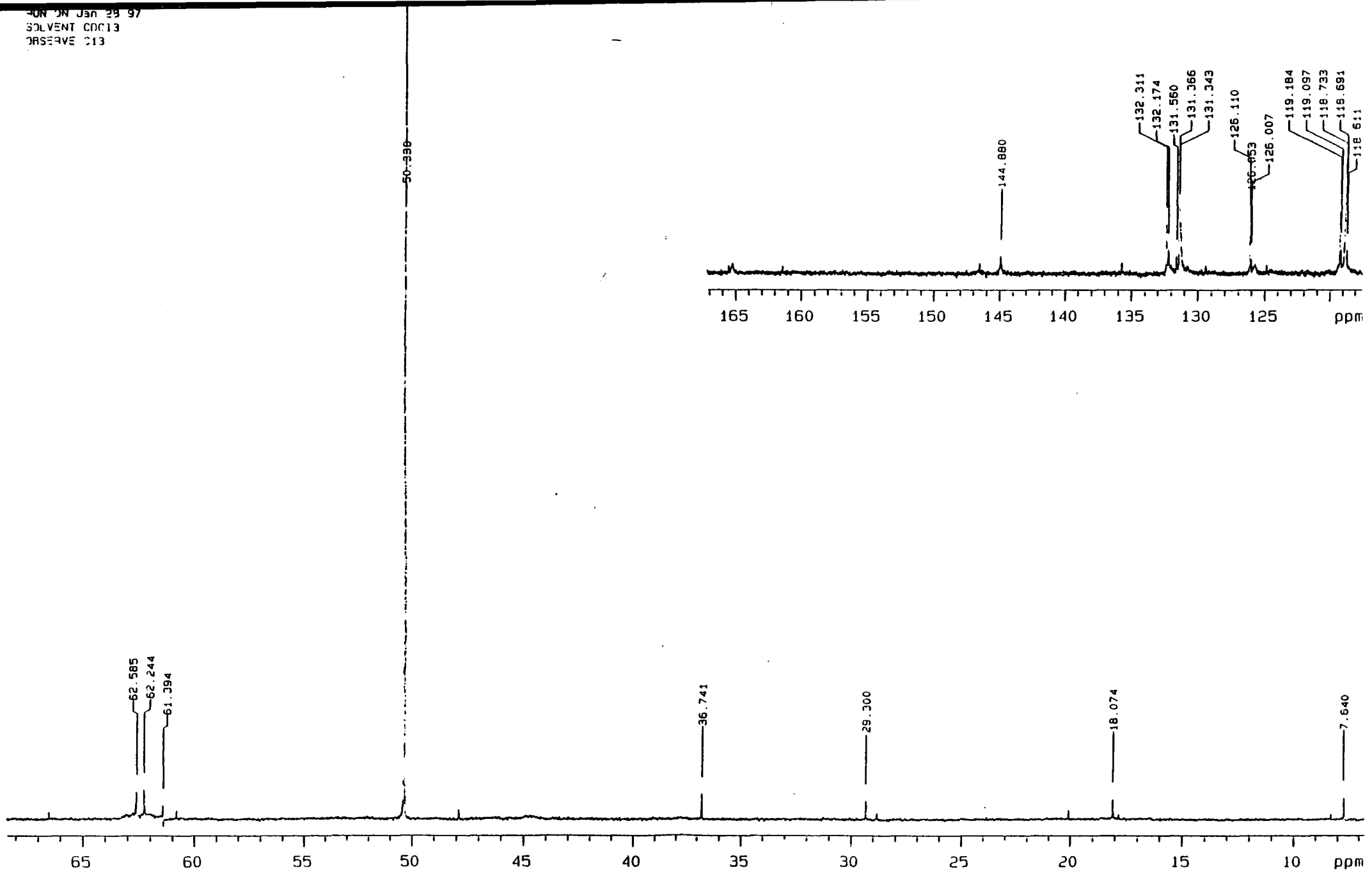

Figure 5.5.3.2: ^{13}C NMR Spectrum of Polyazide in $CDCl_3$ Before Exposure.

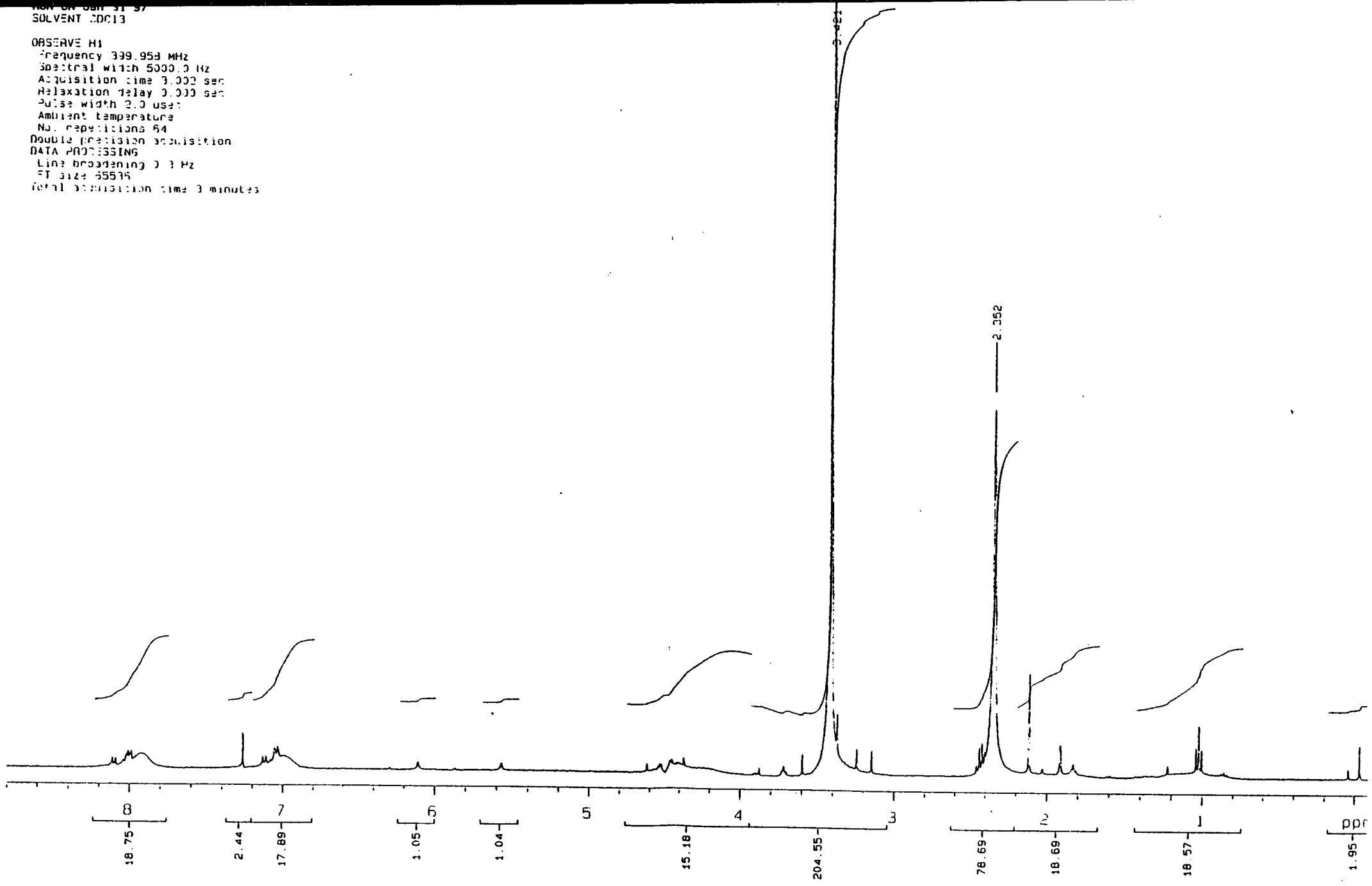

Figure 5.5.3.3: ^{1}H NMR Spectrum of Polyazide in $CDCl_3$ After 3 Hours Exposur

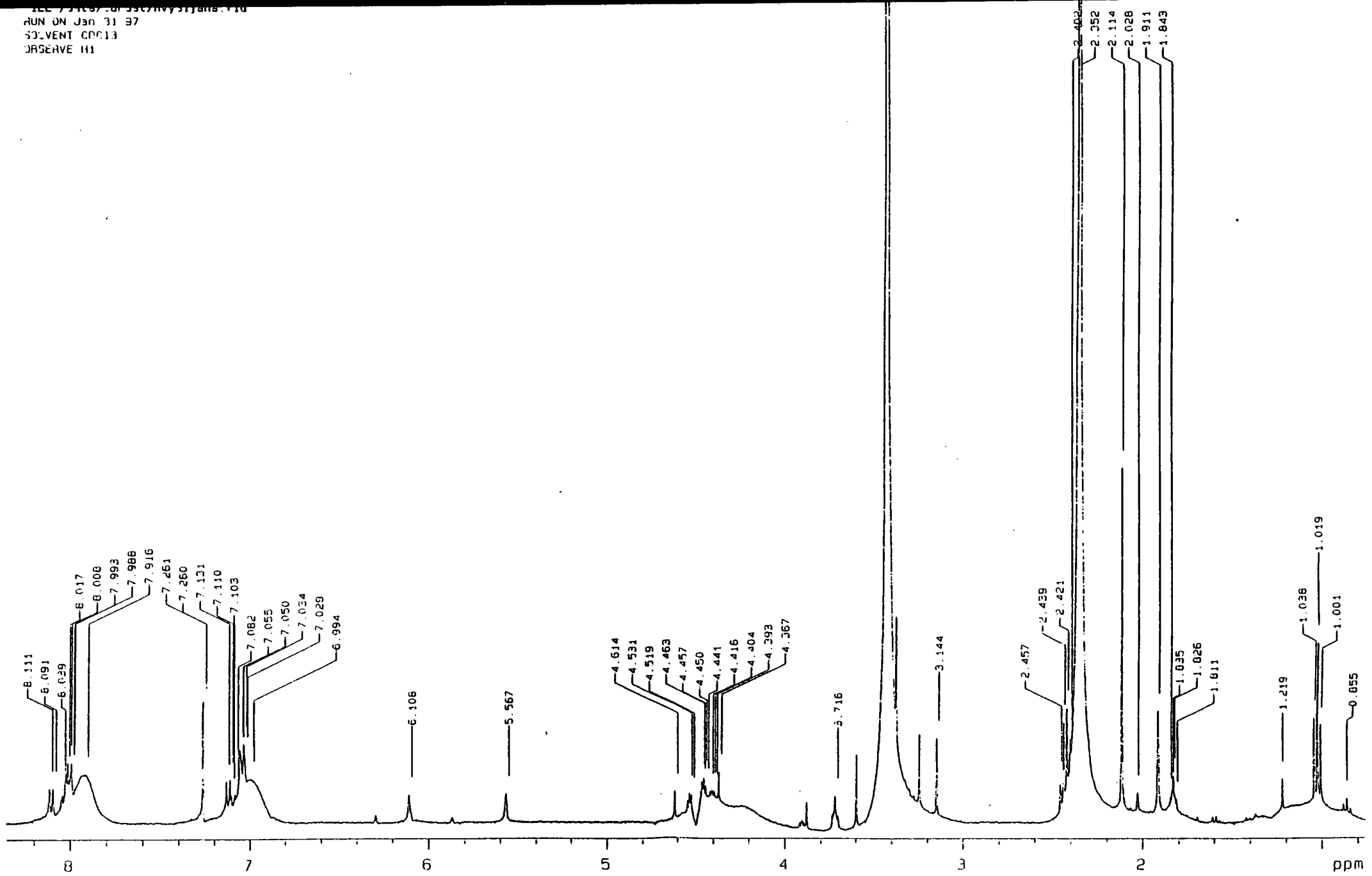

Figure 5.5.3.4: ^{1}H NMR Spectrum of Polyazide in $CDCl_3$ After 3 Hours Exposure.

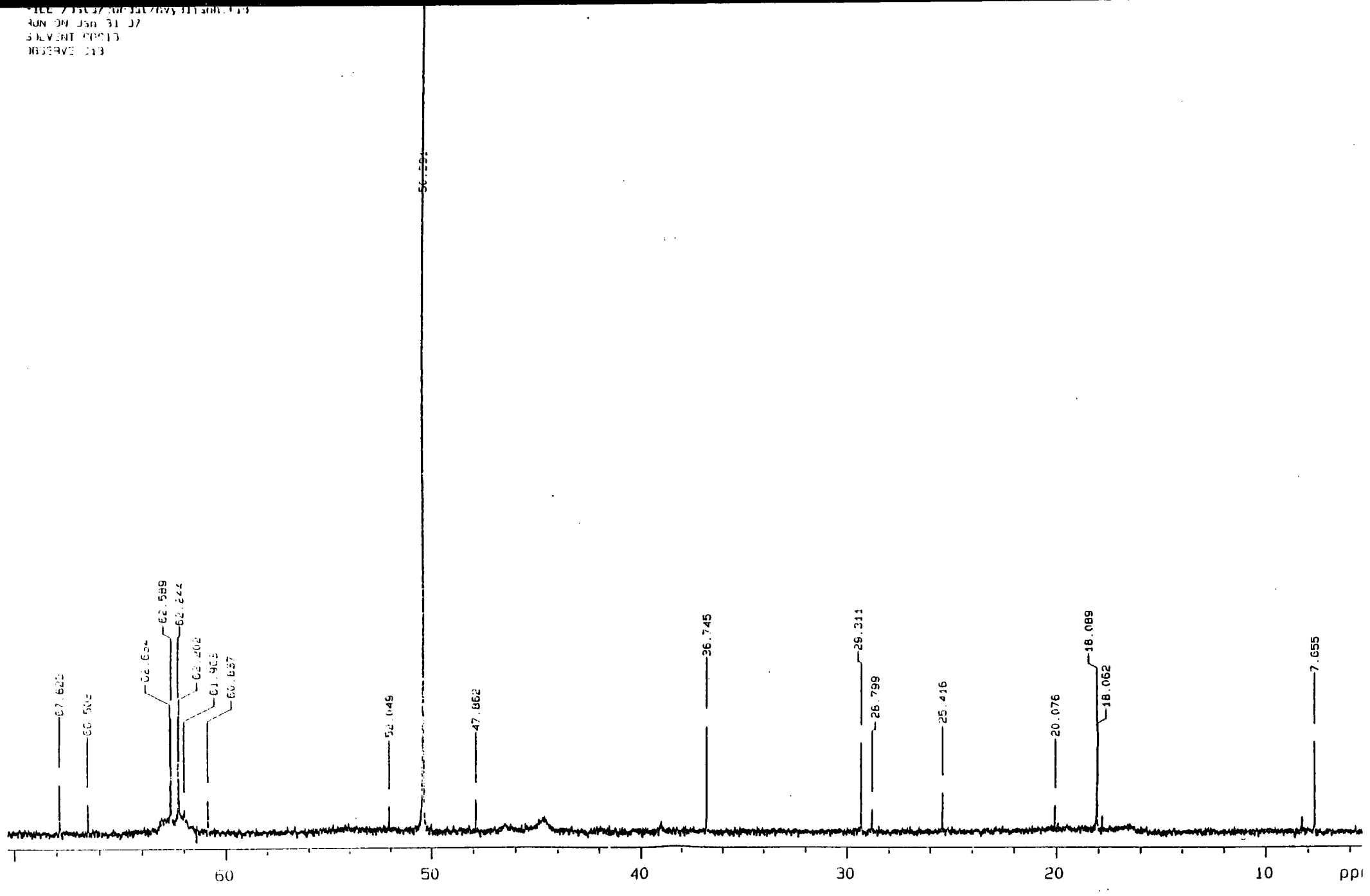

Figure 5.5.3.5: ^{13}C NMR Spectrum of Polyazide in $CDCl_3$ After 3 Hours Exposure

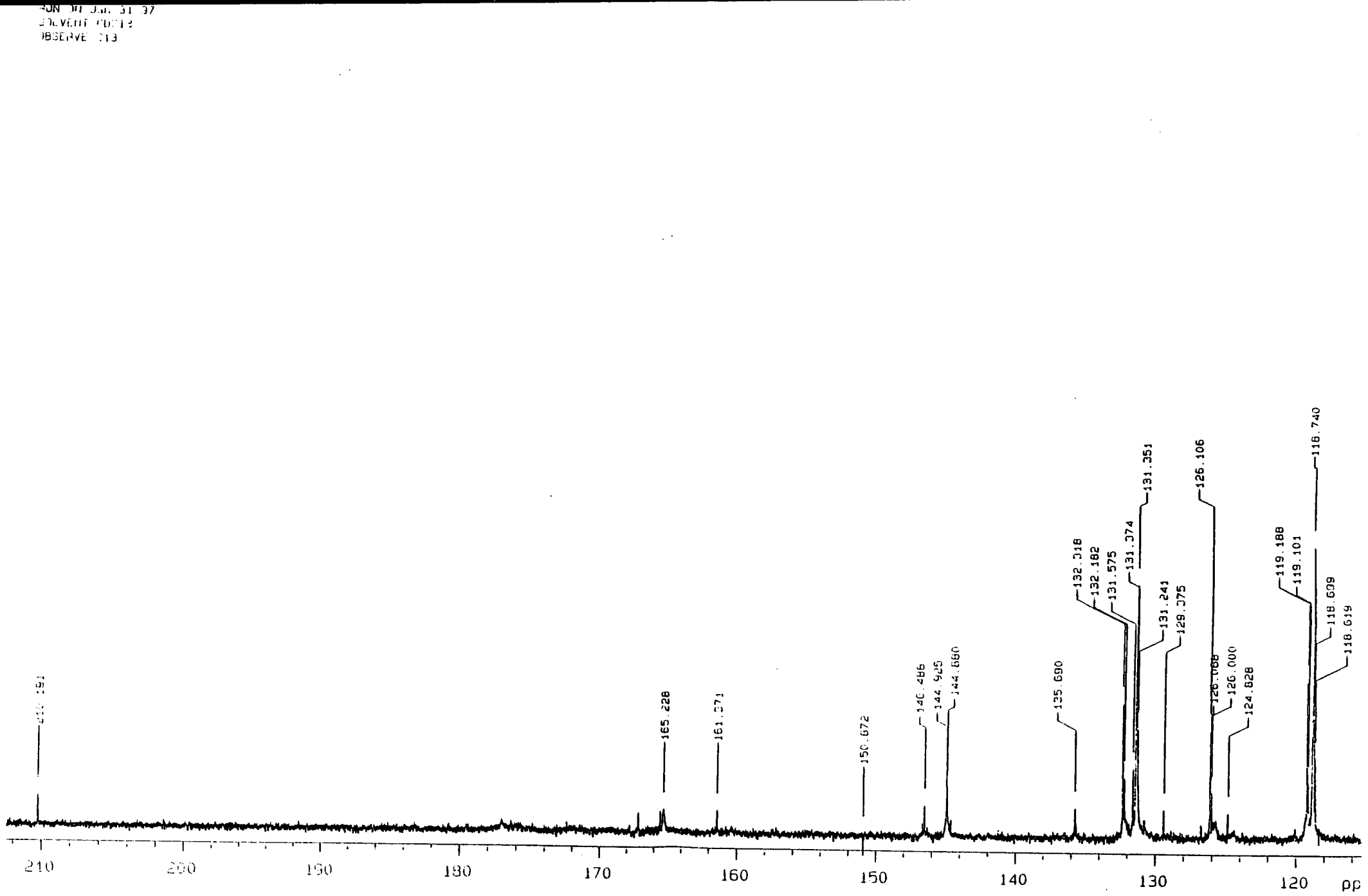

Figure 5.5.3.6: ^{13}C NMR Spectrum of Polyazide in $CDCl_3$ After 3 Hours Exposur

of control over the reaction could mean every possible insertion and proton abstraction can occur, giving rise to small changes in the corresponding peaks. A change in a particular carbon peak of ~10% would be barely detectable, and could not be distinguished from experimental error. Although reaction is occurring in this system, it is impossible to identify the reacting species or be certain where in the system the reaction takes place.

After being stored for two months at 253K, it was found that the Polyazide was no longer soluble in any of the solvents previously used to make its solutions, indicating some sort of reaction has occurred. In an attempt to elucidate what had occurred, solid state ^{13}C and ^{15}N NMR was carried out on the sample. ^{13}C NMR spectra are shown in Figures 5.5.3.7 & 5.5.3.8.

Two signals are expected from the carbons situated in the carbonyl groups in the polymer as they are located in two different chemical environments. Peaks should occur in the region of 160-180ppm[7]. Figure 5.5.3.7 shows that two peaks are observed in this region, however, both peaks have small shoulders on the right hand side. These shoulders may indicate the presence of carbonyl groups in differing environments to those in the unreacted sample. Insertion or abstraction occurring at the carbons located near the carbonyl groups would slightly alter the groups chemical environment and thus alter its chemical shift. From this data, it is not possible to say what or where reaction is occurring, only that more than two types of carbonyl group are present in the insoluble sample.

In the case of ^{15}N NMR, three signals are expected from an unreacted sample. This is due to the three nitrogens present in the sample occupying slightly different chemical environments. If the azide group has reacted, then two of these signals

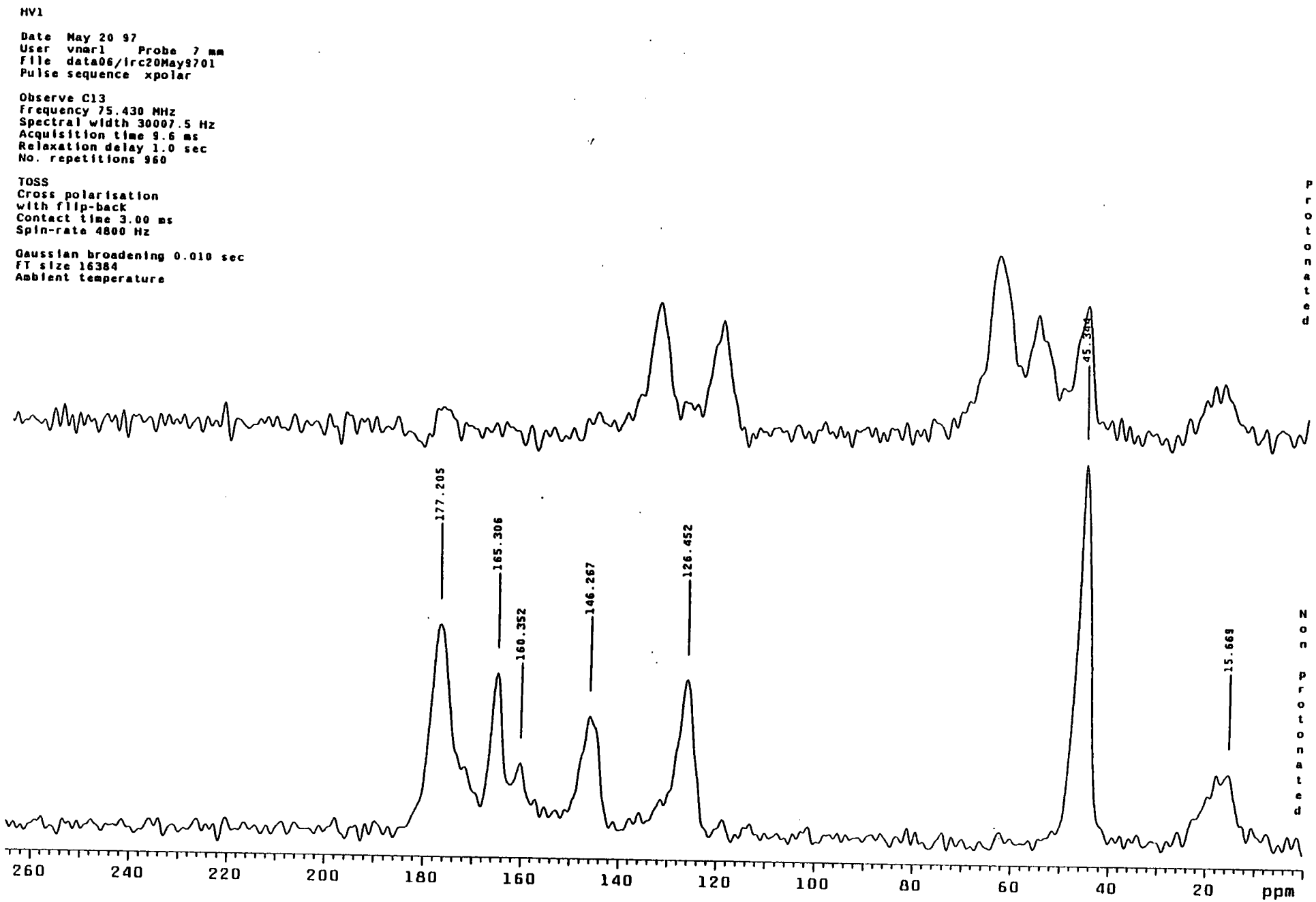

Figure 5.5.3.7: Solid State ^{13}C NMR Spectrum of Polyazide After Storage for 2 Months at 253K.

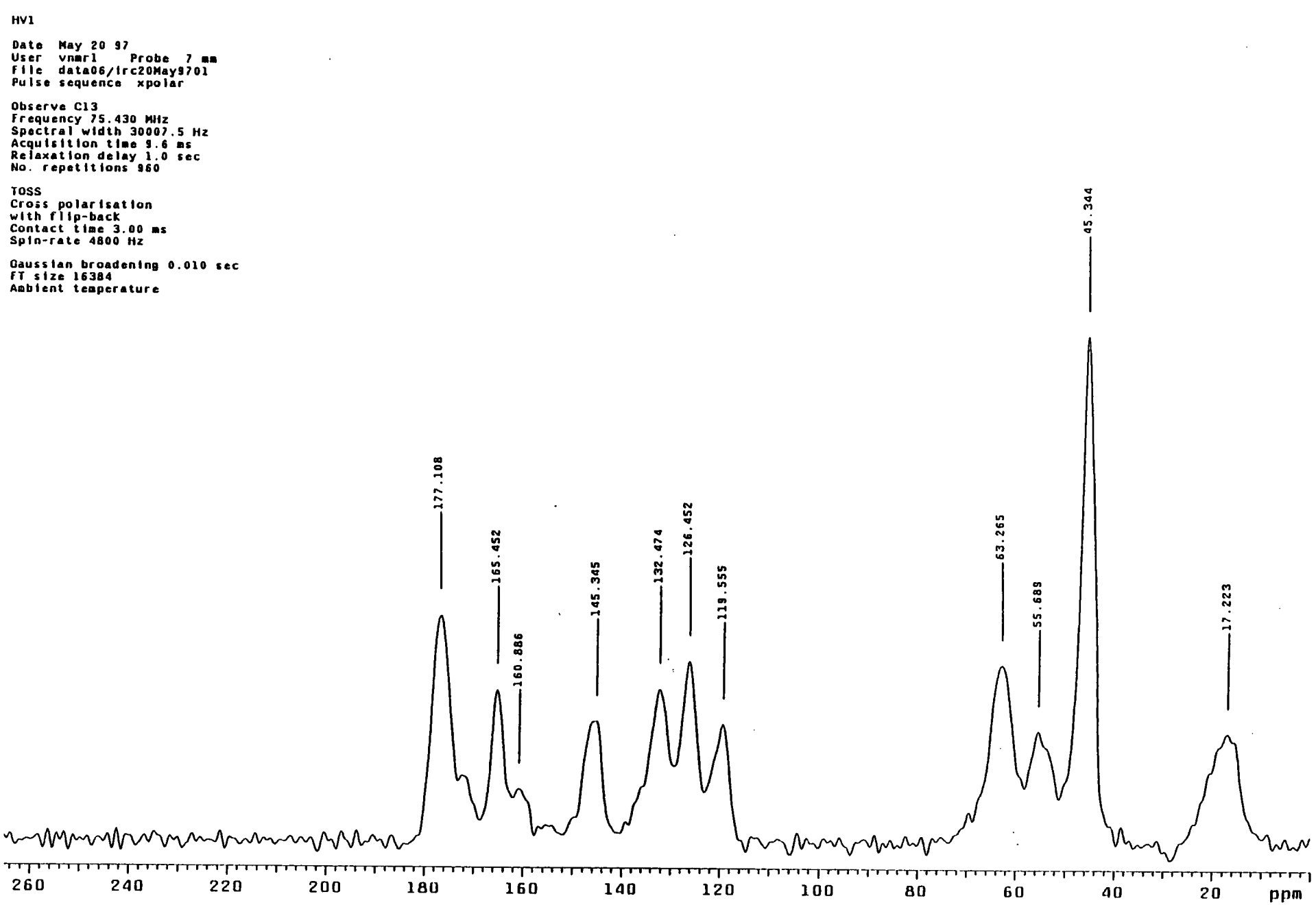

Figure 5.5.3.8: Solid State ^{13}C NMR Spectrum of Polyazide After Storage for 2 Months at 253K.

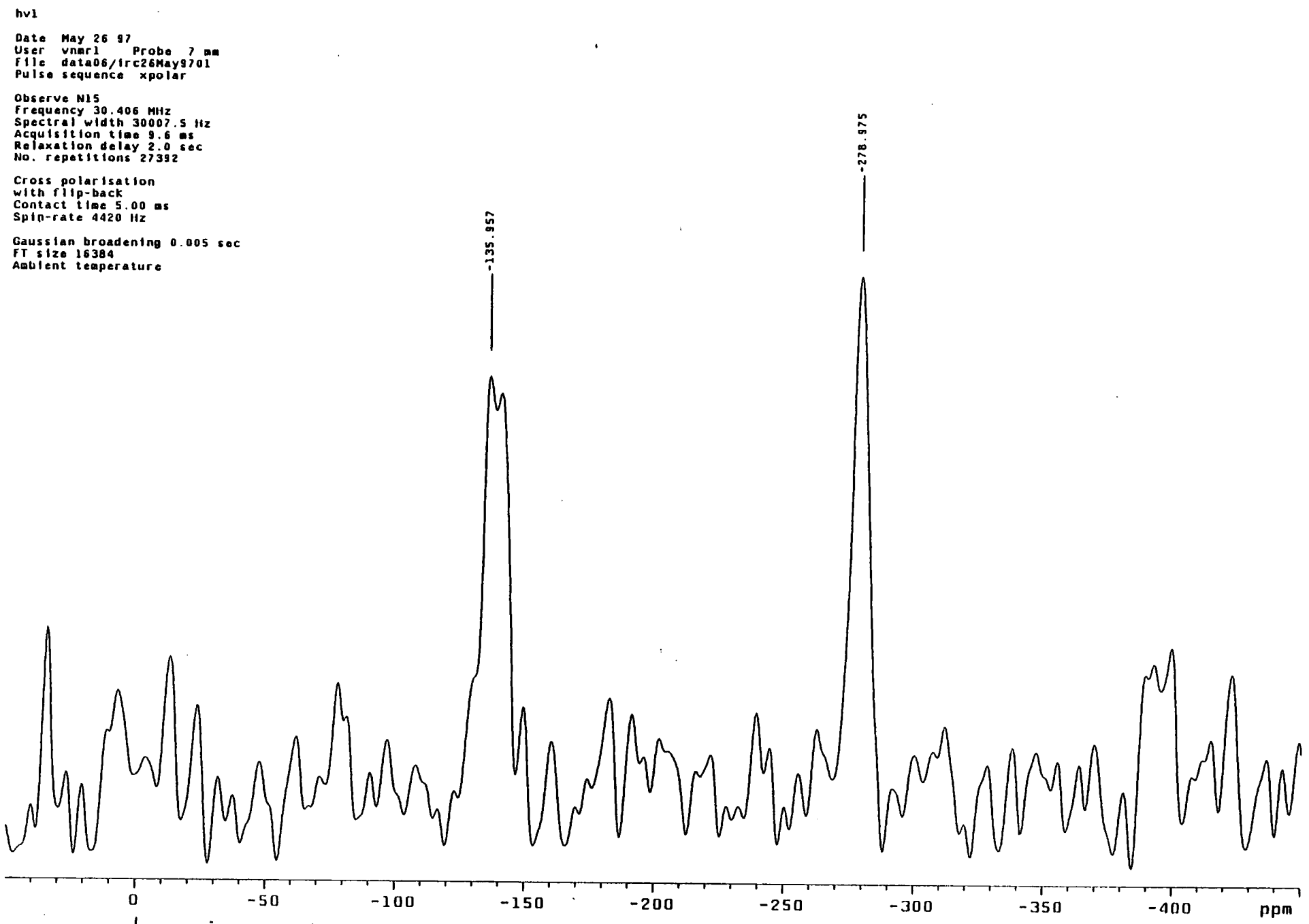

Figure 5.5.3.9: Solid State ^{15}N NMR Spectrum of Polyazide After Storage for 2 Months at 253K.

should decrease due to the loss of molecular nitrogen and new peaks form due to the formation of new, differing reaction products. Figure 5.5.3.9 shows the ^{15}N NMR spectrum for Polyazide.

The signal to noise ratio is poor, despite an acquisition time of 15 hours, due to the low natural abundance of ^{15}N.

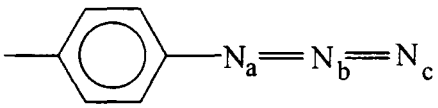

The observed spectrum, Figure 5.5.3.9, is essentially that of the starting material, containing three nitrogen signals: N_a gives rise to the signal at 278ppm whilst the doublet at 136ppm corresponds to N_b and N_c[10].

Due to the poor signal:noise ratio, greater than 20% of the azide groups present in the pure material would need to react via the same mechanism, giving rise to the same reaction product before the occurrence of a new peak could be detected. As it needs only a few molecules to react before an insoluble product is obtained, a change of ~20% is highly unlikely. Once reaction begins, the polymer is held in a more rigid structure, making motion and hence further reaction more difficult.

From the solid state NMR data, it is shown that there are more carbonyl peaks present than expected in the pure Polyazide, indicating reaction occurring in the region of these species. No new peaks are evident in the spectrum due to the small number of azide moieties actually reacting. ^{15}N NMR shows only peaks due to the starting azide material due to the poor signal:noise ratio as well as the low extent of reaction.

5.5.4. Birefringence Studies

Birefringence measurements are carried out using the methodology described in Chapter 2.8. The sample birefringence was measured in varying positions on the slide, as described in section 2.8.3. For the Polyazide there were no comparison experiments performed between annealed and unannealed samples due to the thermal instability of the polymer.

For measurements taken at the centre of the sample, the plots shown in Figure 5.5.4.1 are observed.

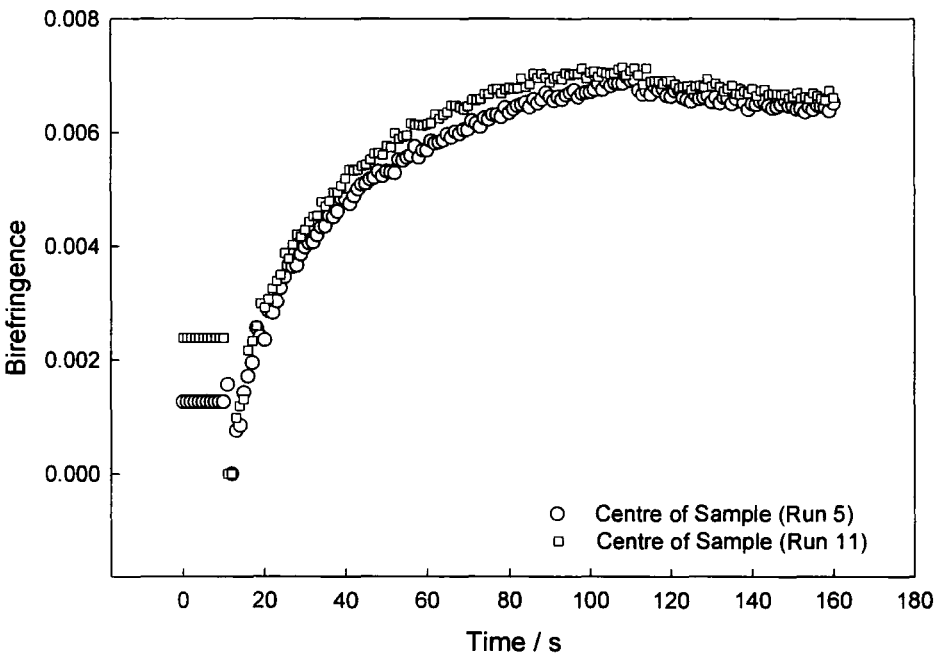

Figure 5.5.4.1: Birefringence Curve for Polyazide: Measurements Made in the Centre of the Sample.

It can be seen for Figure 5.5.4.1, that at the point in time where the He-Cd laser is switched on, the birefringence falls. This indicates an initial orientation in the film which is destroyed by the He-Cd radiation. At the lowest point on the curve, the sample has little or no birefringence. The absolute birefringence value of a particular

sample cannot be measured and therefore the lowest point on each curve is set to zero. The value of the birefringence then begins to climb and gradually levels out. After 100s exposure the He-Cd laser is switched off, although the monitoring He-Ne laser remains on. A small drop in birefringence is observed before the values level off once more.

The overall change in birefringence is 0.007. This value is a factor of ten smaller than the photoinduced birefringence of a high T_g poly (ether ketone) doped with an azobenzene containing polymer (0.08)[11]. Only a very small anisotropy is introduced into the polyazide film.

The curves obtained when monitoring the birefringence on the upright edge of the sample vary greatly in overall induced birefringence as well as the rate at which saturation occurs, Figure 5.5.4.2.

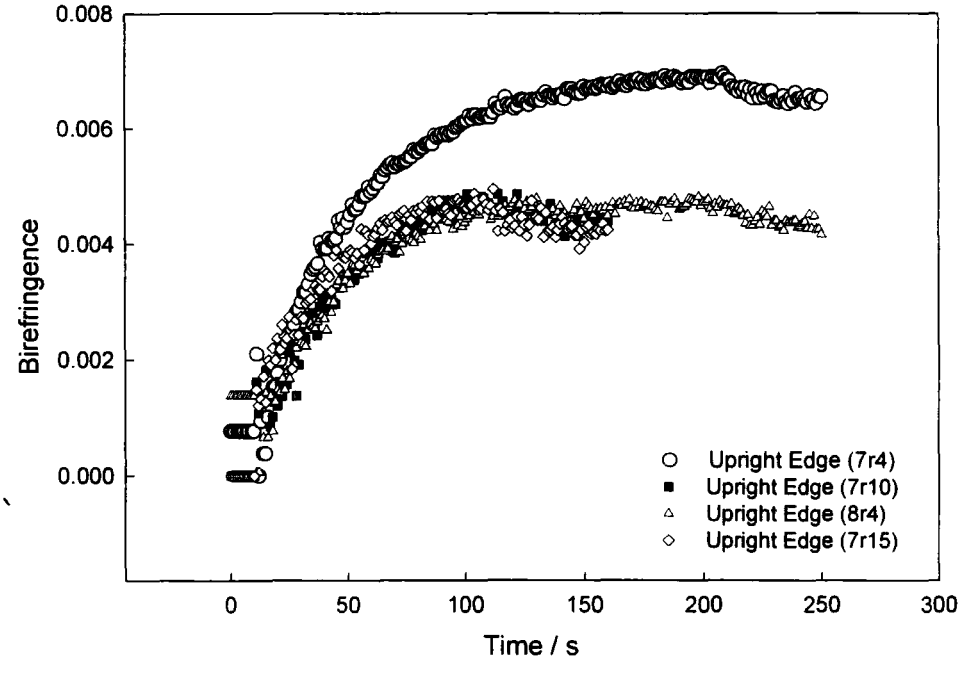

Figure 5.5.4.2: Birefringence Curve for Polyazide: Measurements Made on the Upright Edge of the sample.

When the laser is switched on, the birefringence shows either an initial fall or rise. This change is followed by an gradual increase to a plateau, where a drop is noticed when the He-Cd laser is switched off. The magnitude of the birefringence is generally much smaller than that achieved in the centre of the sample. The curves obtained at the top edges of the samples, Figure 5.5.4.3, follow the trends of those observed for the upright edges, although the changes in induced birefringence vary greatly.

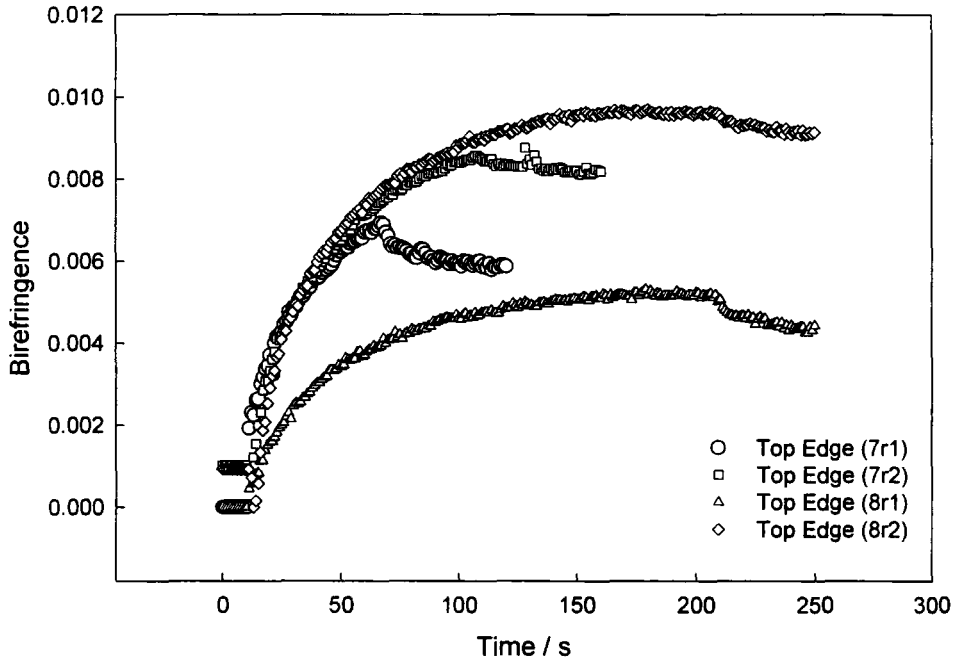

Figure 5.5.4.3: Birefringence Curve for Polyazide: Measurements Made on the Top Edge of the sample.

Decay of birefringence when the laser is switched off is governed by relaxation of the sample to its equilibrium state as well as by a temperature gradient. As the laser radiation is absorbed, it heats the polymer film. When the laser is turned off, heat dissipates through the film, changing the temperature of the analysed spot. The depth of the drop is related to the mobility of the sample; the more mobile, the

larger the drop. In polymers where there is a large difference between the operating temperature and the T_g of the sample, this decay is small[12].

These results show that what were thought to be initially isotropic films clearly are not. There is much variation in photoinduced birefringence for one sample, depending upon the region of the sample analysed, although the anisotropy induced in all samples is small. Fluctuations in sample thickness, roughness and local orientations greatly influence the results obtained in this experiment.

5.5.5. Fabrication of a simple Liquid Crystal Cell

A film of Polyazide on quartz was exposed for varying time scales to the vertically polarised UV laser. A schematic diagram of the film and exposure times is shown in Figure 5.5.5.1.

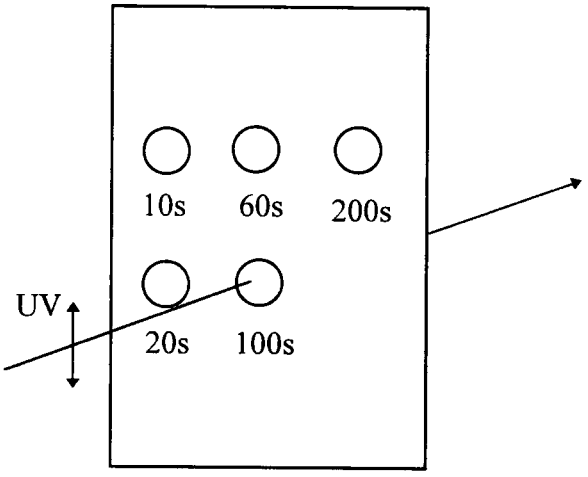

Figure 5.5.5.1: Exposure Times for Polyazide.

The exposed film as then used in the construction of a liquid crystal cell. Rubbed polyimide was oriented such that its alignment direction was perpendicular to the polarisation vector of the incoming UV radiation. When viewed using an optical

microscope with crossed-polarisers, the irradiated areas appear as dark spots on a dark background.

Figure 5.5.5.2: Non-Twisted Alignment.

The rubbed polyimide film is aligning the liquid crystal along the rubbing direction. As we continue up through the thickness of the cell, the influence of the polyimide layer on the liquid crystal decreases and they assume a more random orientation, giving rise to a grey colouration when viewed through crossed polarisers. In the region when the polyazide has been irradiated, a much darker spot is observed. This is due to the polyazide film aligning the liquid crystal in the same direction as the polyimide, thus less light passes through the sample relative to the random orientation and the irradiated area appears darker. This result is contrary to expectations and further supports the evidence that azobenzene moieties are not being formed.

A second sample was irradiated as shown in Figure 5.5.5.1. When the liquid crystal cell was constructed, the polyimide rubbing direction was parallel to that of the incoming UV polarisation direction. The images presented in Figure 5.5.5.3 - Figure 5.5.5.7 are observed when the cell is viewed through crossed-polarisers.

Figure 5.5.5.3: 10s Exposure.

Figure 5.5.5.4: 20s Exposure

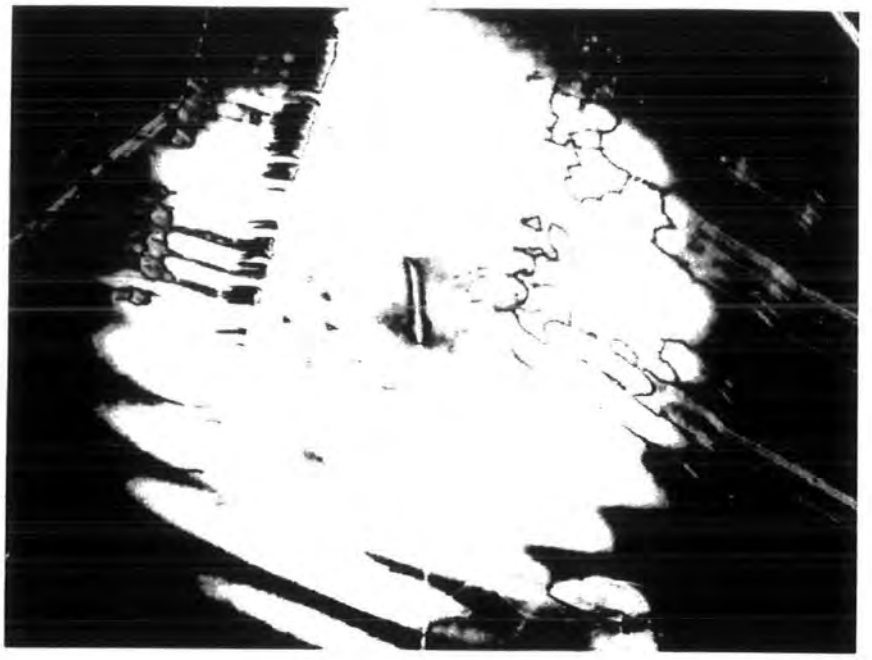

Figure 5.5.5.5: 60s Exposure

Figure 5.5.5.6: 100s Exposure.

Figure 5.5.5.7: 200s Exposure.

The cell images shown in Figure 5.5.5.3 - Figure 5.5.5.7 show bright white spots at low exposure times. As the cell is viewed through crossed polarisers, this indicates that the light passing through the first polariser is being twisted by an angle in the region of 90°, allowing it to pass through the second polariser. This is attributed to the twisted alignment of the liquid crystals. The brightness of the white spot gives some indication of the degree of twist, the brighter the spot, the closer the angle is to 90°.

The formation of a cell in which the liquid crystal twists indicates that the alignment directions of the two films are perpendicular. A schematic diagram of desired and measured liquid crystal alignment in polyazide is shown in Figure 5.5.5.8.

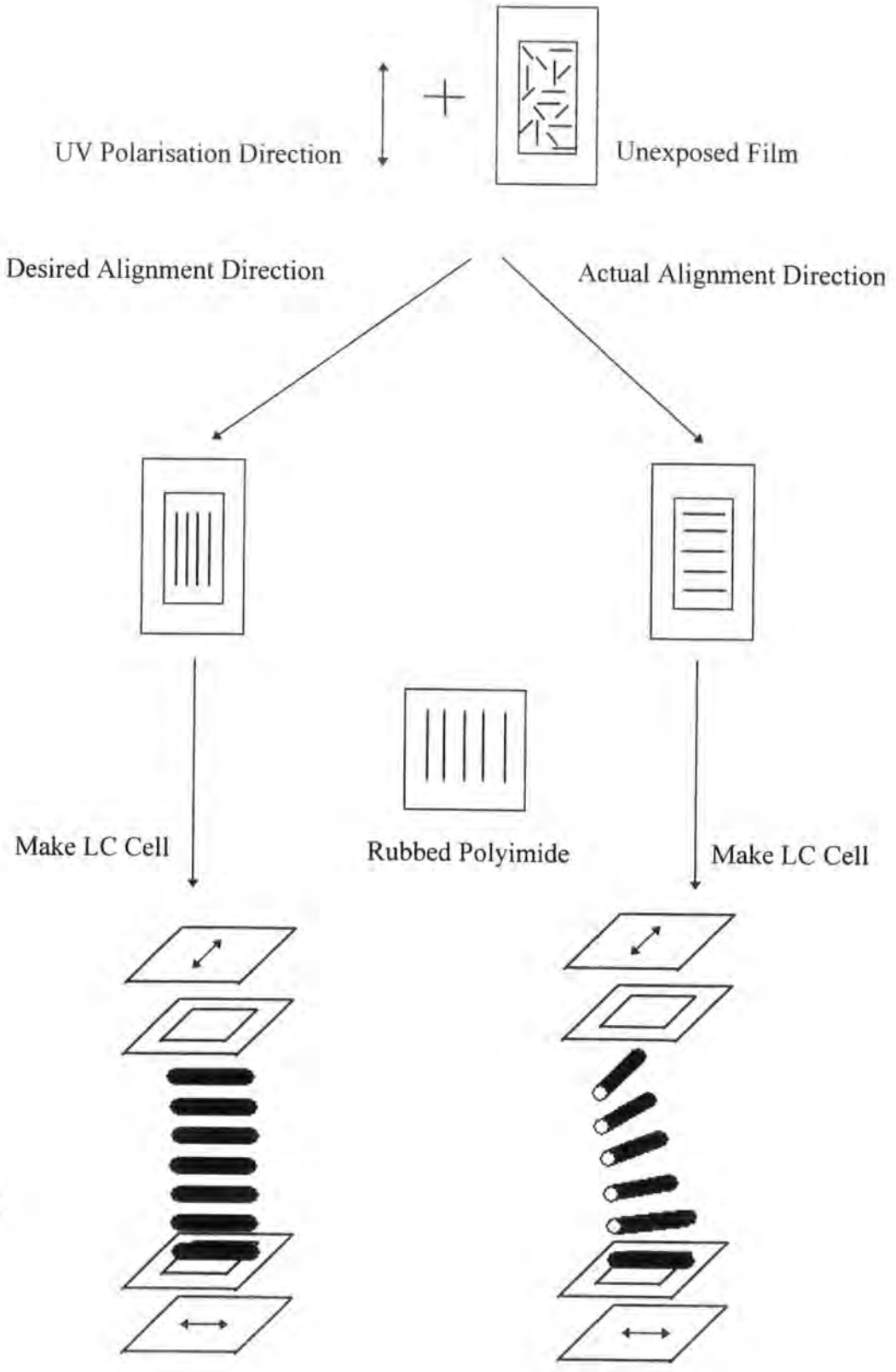

Figure 5.5.5.8: Alignment in Polyazide cell.

It was hoped that the polyazide would align the liquid crystals in a direction parallel to the polarisation vector of the incoming radiation. As can be seen from Figure 5.5.5.8, if this were true, then constructing a cell with the rubbed polyimide alignment direction perpendicular to the polarisation direction of the UV would result in twisted alignment of the liquid crystals, this is not observed Figure 5.5.5.2. From Figure 5.5.5.3 - Figure 5.5.5.7, it is clear that a twisted display has been formed by the fabrication of a cell in which the rubbing direction and the UV polarisation direction are parallel. The polyazide film is aligning the liquid crystals in a direction perpendicular to the UV polarisation direction.

As the exposure time increases, the centre of the white spot darkens. This 'burn out' is due to prolonged exposure of the sample. The increased irradiation time naturally leads to an increase in the intensity of UV radiation the sample is exposed to. Once the azide groups parallel to the polarisation vector are depleted, those slightly off normal to this direction begin to react. At long exposure times, the magnitude of this off-axis depletion increases. At this stage, the anisotropy in the sample which leads to liquid crystal alignment is removed, and hence the appearance of dark spots in the cell.

A film of the polyazide was masked and exposed to the polarised radiation from the deuterium lamp. The constructed cell, with desired and rubbed polyimide alignment directions perpendicular, shows no liquid crystal alignment. This is unsurprising as the previously constructed cell indicates that the desired parallel alignment direction is not achieved. Therefore, irradiation of polyazide was repeated and a cell constructed in an identical manner to that described for the sample

irradiated by the laser which shows twisted alignment. Liquid crystal alignment was not observed.

5.6. Conclusions

Poly(p-azidobenzoate ethyl methacrylate) has been shown to be a very unpredictable and unreliable material. A lifetime of only two months whilst being stored at 253K greatly limits it usefulness. The reactivity of this polymer varies greatly with irradiation source as well as with the physical state of the film. Using the deuterium lamp as the radiation source, reaction is observed in both solution and in the film, however, the extent of the reaction varies greatly. In solution, a large proportion of the azide species react. In the film, considerably fewer chromophores are depleted, despite prolonged exposure times. This indicates that mobility of the reacting species is important when attempting photo-cross-linking reactions. When the He-Cd (325nm) laser is the radiation source, the film reacts much more readily, almost 50% of the azide species are consumed. Laser radiation is monochromatic and of high intensity, this is shown to be much more effective at bringing about reaction than the deuterium lamp.

Azobenzenes, the desired reaction product, are not observed in any reactions using either the laser or the deuterium lamp, in either solid or solution form. This may be attributed to the low concentrations of nitrenes formed upon irradiation with the deuterium lamp. Although the laser will yield a higher nitrene concentration, the mobility of the chains is hindered due to the relatively rigid orientation in which the chains are held in the film.

It was shown that twenty five hours polarised irradiation of the film with the lamp effects little change in azide concentration. This goes some way to explaining the lack of infrared dichroism shown by the polymer. Any change in the IR spectrum will be so small that it is outweighed by errors associated with the calculation of the absorbance area.

Although the polyazide was shown to be birefringent, the anisotropy introduced into the film by photo-reaction is very small. The area irradiated by the laser has a diameter of 3-4mm^2. Therefore, measurements were made at numerous locations on the sample. The results obtained show both the magnitude of the birefringence and the rate at which maximum birefringence is achieved differ greatly, with no obvious trend regarding the area analysed.

Polyazide aligns liquid crystals in a simple cell in the direction perpendicular to that of the polarisation direction of the exposing laser radiation. Over-exposure of the sample occurs at prolonged irradiation times and liquid crystal alignment is lost. Alignment is not achieved when the deuterium lamp is the radiation source.

Initially, the polyazide system appeared to have potential as a liquid crystal alignment layer. However, photo-induced orientation of the polymer does not occur via the desired azobenzene formation mechanism. The reactions giving rise to the anisotropy in the films can only be postulated. No proof can be offered as to the identity of the photo-reaction products. Indeed, such is the instability of the material that random, thermal reactions cannot be ruled out.

Cell formation indicates orientation in the film which brings about liquid crystal alignment. However, bulk measurements do not give rise to the same

conclusions. Effects of exposure at the surface of the film appear more pronounced than in the bulk. Surface orientation is achieved although bulk alignment is not.

In conclusion, this polymer is unsuitable for use in liquid crystal display devices due to its instability and lack of understanding as to how and where reaction is occurring.

References

1) Nitrenes, Ed: W.Lwowski, Wiley & Sons 1970.

2) The Chemistry of the Azido Group, Ed: S.Patai, Interscience Publishers 1971.

3) Azo and Diazo Chemistry, H.Zollinger, Interscience Publishers 1961.

4) E.Wasserman, G.Smolinsky & W.A.Yager, J.Am.Chem.Soc, 86, 3166, 1964.

5) J.S.Swenton, *Tetrahedron Lett*, 3421, 1969.

6) K.E.Foster, PhD Thesis 1997.

7) Organic Spectroscopy, D.W.Brown, A.J.Floyd & M.Sainsbury, Wiley & Sons 1988.

8) Theory & Applications of Ultraviolet Spectroscopy, H.H.Jaffe & M.Orchin, Wiley & Sons 1962.

9) A.Reiser, F.W.Willets, G.C.Terry, V.Williams & R.Marley, *Trans Faraday Soc*, **64**, 3265, 1968.

10) NMR-Basic Principles & Progress, Volume 18, G.J.Martin, M.L.Martin & J-P. Gousenard, Springer Verlag, Berlin 1981.

11) A.Natansohn, P.Rochon & C.Barrett, *Chem Mater,* 1995, **7**, 1612.

12) M.S.Ho, A.Natansohn & P.Rochon, *Macromolecules*, 1995, **28**, 6124.

13) A.Resier, G.Bowes & R.J.Horne, *Trans Faraday Soc,* **62**, 3162, 1966.

14) S.Xie, A.Natansohn & P.Rochon, *Chem Mater*, 1993, **5**, 403.

15) X.Meng, A.Natansohn & P.Rochon, *Polymer*, **38** (11), 1997, 2677.

16) D.Brown, A.Natansohn & P.Rochon, *Macromolecules*, 1995, **28**, 6116.

Chapter Six

Conclusions and Future Work

6. Conclusions and Future Work

6.1. Conclusions

The objective of this project was to assess the suitability of two novel polymers regarding their potential as liquid crystal alignment layers. A known polymer system, poly (vinyl cinnamate) was used as a model compound in this work. The well characterised [2+2] cycloaddition reactions allowed appraisal of the four chosen techniques; UV spectroscopy, polarised FTIR, birefringence and cell fabrication to be carried out. PVCi was also employed in determining the effect of radiation source upon observed reactivity.

The two radiation sources used were a broad wavelength range deuterium lamp (λ=185-370nm) and a vertically polarised He-Cd UV laser (λ=325nm). The initial aim, in terms of the deuterium lamp, was to use a band pass filter to select the desired wavelength radiation (λ~325nm) and to polarise the radiation using an external polariser. However, when the band pass filter was in place, the intensity of light falling onto the sample was reduced to such an extent, when compared to the lamp with no filter present, that no reaction was observed over a reasonable timescale (many hours). It was therefore decided that the whole spectral range of the deuterium lamp would be employed. This then led to problems in assessing the photon density falling onto the sample.

The chemical actinometer Aberchrome 540 had been chosen to be used in conjunction with the band pass filter as its sensitivity range was in the region λ=310-370nm. Without the filter in place, the lamp radiation falling onto the sample covers the spectral range λ=185-370nm. A chemical actinometer covering this range could

not be found and hence the Aberchrome 540 was used. This brought uncertainty into the measured intensity which was passed on in subsequent quantum yield calculations. This uncertainty was duly noted and irradiation using the deuterium lamp was carried out.

When unpolarised radiation was used, UV studies showed that ~50% of the cinnamate side chains react. However, when this radiation was polarised, this value was reduced to 20%. In comparison, when the vertically polarised UV laser was used as the irradiating source, ~80% of the chromophores present in the sample were shown to undergo reaction. From this work on PVCi, it was concluded that although the deuterium lamp promotes the cycloaddition reaction, the rate of reaction is very slow, especially when compared to exposure to the UV laser.

The differences in polymer reactivity with radiation source were further evident in the other techniques studied. The deuterium lamp did not induce sufficient reaction for birefringence studies or cell fabrication to give rise to any noticeable change in the sample due to this exposure, despite the fact that UV studies show that ~20% of the chromophores react. Reaction was evident in the IR spectrum however, as explained in chapter 3.3.2, due to the complexity of the experimental design, this change could not be separated from experimental error.

Due to geographical restrictions, IR studies could not be carried out on samples exposed to the UV laser. However, UV studies, birefringence studies and cell fabrication studies were possible. The birefringence results showed some very interesting features: inherent orientation in the majority of PVCi samples studied. This initial orientation was not removed by annealing and is thought to arise from chain entanglements. PVCi does show anisotropy when irradiated with the UV laser

although the magnitude of this anisotropy is small, indicating only a small degree of order. However, this small degree of order is sufficient to align liquid crystals in a simple liquid crystal cell.

The studies on the model cinnamate compound highlight difficulties with certain aspects of the techniques chosen as well as providing the opportunity to perfect experimental techniques and analysis methods. Other techniques such as force microscopy and grazing incidence X-ray diffraction were considered, however, the contrast between exposed and unexposed regions in the film was shown to be slight. X-ray diffraction requires a significant extent of order before a profile can be obtained and order of this magnitude is not achieved by exposure of the polymer film to polarised radiation.

The studies then moved on and the photochemical reactions of two new systems were studied. The first polymer system was based on anthracene and was expected to form a dimer across the 9,10-position of the anthracene moiety upon irradiation with UV light. UV spectroscopy showed that chromophore depletion did occur upon irradiation however, horizontally polarised radiation induces almost three times as much reaction as vertically polarised radiation. This indicated that there is inherent orientation within the sample and that the anthracene species are lying preferentially with their long axes parallel to the polarisation direction of the horizontally polarised radiation.

Both unpolarised radiation from the deuterium lamp and vertically polarised laser radiation show very distinctive quantum yield decay curves. It is postulated that energy migration is occurring and although there is no direct evidence for this, energy migration is known to occur in anthracene systems.

Results of IR and birefringence studies confirm the existence of initial orientation in the polyanth system. The cause of this initial order is unknown, however, the constant factor in the preparation of all samples is the spinning process and this may be a good starting point for further investigations into the inherent order within this system. Polyanth was shown to align liquid crystals in a simple cell. This alignment proceeds up to a finite exposure time, after which, alignment is lost. This is thought to be due to loss of anisotropy in the sample due to energy migration.

From the results on the studies of polyanth, it is concluded that this system does have the potential to become a polymer alignment layer for use in a liquid crystal display device.

The final polymer system studied was based on an azide species. Upon exposure to UV radiation, azides lose molecular nitrogen and form nitrenes. Nitrenes can undergo may types of reaction and it was hoped that recombination of two nitrenes to form an azo compound would be favoured.

The polyazide species is thermally unstable and undergoes little reaction upon exposure to the deuterium lamp. Almost four days exposure promoted no reaction as observed by IR spectroscopy. UV spectroscopy shows reaction does occur although only 9% of the chromophores present react after 25 hours exposure to vertically polarised radiation. Neither UV nor IR spectroscopy show any evidence for the desired azobenzene formation.

Exposure to the UV laser does promote reaction in ~60% of the chromophores, although absorption due to the formation of an azobenzene moiety is not evident. NMR studies were carried out in an attempt to elucidated the reactions occurring in this system. Solution state NMR showed no change in the spectrum upon exposure.

After 2 months of storage at 253K, the polymer became insoluble and therefore solid state NMR studies were performed on the insoluble system. The results for ^{13}C NMR studies showed the presence of more carbonyl peaks than expected and no evidence of new peaks and ^{15}N NMR showed only the peaks expected for the starting material. NMR studies did not provide any further insight into the reactions occurring in polyazide.

Polyazide was found to exhibit birefringence upon exposure to UV light. However, the magnitude of the birefringence was small and varied greatly within and between samples as did the rate at which maximum birefringence was achieved. Some regions of a sample could be isotropic whilst others showed definite order before exposure.

Although the polyazide did align liquid crystals in a simple cell, further studies concerning this polymer as a potential alignment layer would not be recommended as the system is too unstable to be stored in the solid state for any period of time and its reactivity upon exposure to UV light is unpredictable.

In conclusion, of the two novel polymer systems studied, poly (9-anthraceneoate ethyl methacrylate) is the only system upon which further research as to its applicability as an alignment layer is worthwhile, both in terms of time and money.

6.2. Future Work

As has been shown by this project, poly (9-anthracenoate ethyl methacrylate) has the potential to become an alignment layer for use in liquid crystal displays.

The possibility of energy migration occurring in this system needs to be substantiated. In order to do this, photophysical measurements must be carried out on the system. Not only will this provide evidence as to the extent of energy migration but will also give information regarding the state of the migrating energy, singlet or triplet?

The orientation of the anthracene species is important for dimer formation, the sandwich topology being the ideal situation. Are there ways of making this topology more probable? It would be interesting to investigate the changes in reactivity of the polyanth system upon changing the length of the spacer group between the two carbonyl moieties. Will lengthening the spacer group provide increased side chain flexibility or simply cause greater entanglement of the side chains, possibly forcing two anthracene species together? A typical value for the molecular weight above which entanglements occurs (M_e) could not be found for an anthracene-containing system. However, for a sample of poly (methyl methacrylate) (PMMA) which is ~75% syndiotactic, values of M_e in the region of 10^5 have been determined[1].

The results of this work suggest that the anthracene moieties are in the polyanth system are initially ordered, however, the cause of this ordering is unknown. The production of a series of films spin cast at varying speeds using differing solution concentrations would be an ideal starting point for investigations into the cause of this inherent order.

The most significant underlying problem when devising a potential liquid crystal alignment layer is that the actual alignment mechanism is not fully understood. Topological, steric, polar and van der Waals forces may all play a part in aligning liquid crystals. Until the actual alignment mechanism is understood, the design of the 'perfect' alignment layer will be a trial and error process.

References

1) L.J.Fetters, D.J.Lohse & R.H.Colby, Physical Properties of Polymers Handbook, Ed: J.E.Mark. AIP Press, New York, 1996.

Appendices

Appendix for Chapter Three

UCAL 4.06 UNICAL SUMMARY REPORT

PVC1 ENDED: 05/19/95 10:36: Poly(vinyl cinnamate)

PARAMETERS		MOLECULAR WEIGHT VALUES		
CONCENTRATION (mg/mL)	.704	Mn (avg) =	2.505E	5
INJECTION VOLUME (mL)	.100	Mw (avg) =	4.572E	5
OPT SENSITIVITY (mv/Pa)	1.000	Mz (avg) =	6.952E	5
INLET PRESSURE (kPa)	1.993	Mp =	4.025E	5
FLOW RATE (mL/min)	1.000	Mv (avg) =	4.179E	5
VISCOMETER OFFSET (mL)	-.014	Mn(no RI) =	1.859E	5
ACQ. START TIME (min)	10.000			
ACQ. STOP TIME (min)	20.000	POLYDISPERSITY RATIOS		
DATA INTERVAL (sec)	1.200	Mw/Mn =	1.825	
SIGMA (mL)	.177	Mz/Mn =	2.776	
TAU (C)	.094	SKEWNESS OF DISTRIBUTION		
TAU (V)	.074	SKEW(n) =	2.123	
THRESHOLD	.020	SKEW(w) =	1.686	

METHOD: UCAL-NARROW	INTEGRATED DETECTOR SIGNALS		BASELINE	X	Y
CAL FILE C210495	CONC (mv-mL) =	6.46	L. VISC	100	58.42
	VISC (mv-mL) =	4.57	R. VISC	291	87.22
MARK-HOUWINK CONSTANTS					
ALPHA .605	IV (dL/g)	1.304	L. CONC	105	2125.23
LOG K -3.275	VISCOTEK MODELE	200	R. CONC	311	2150.90

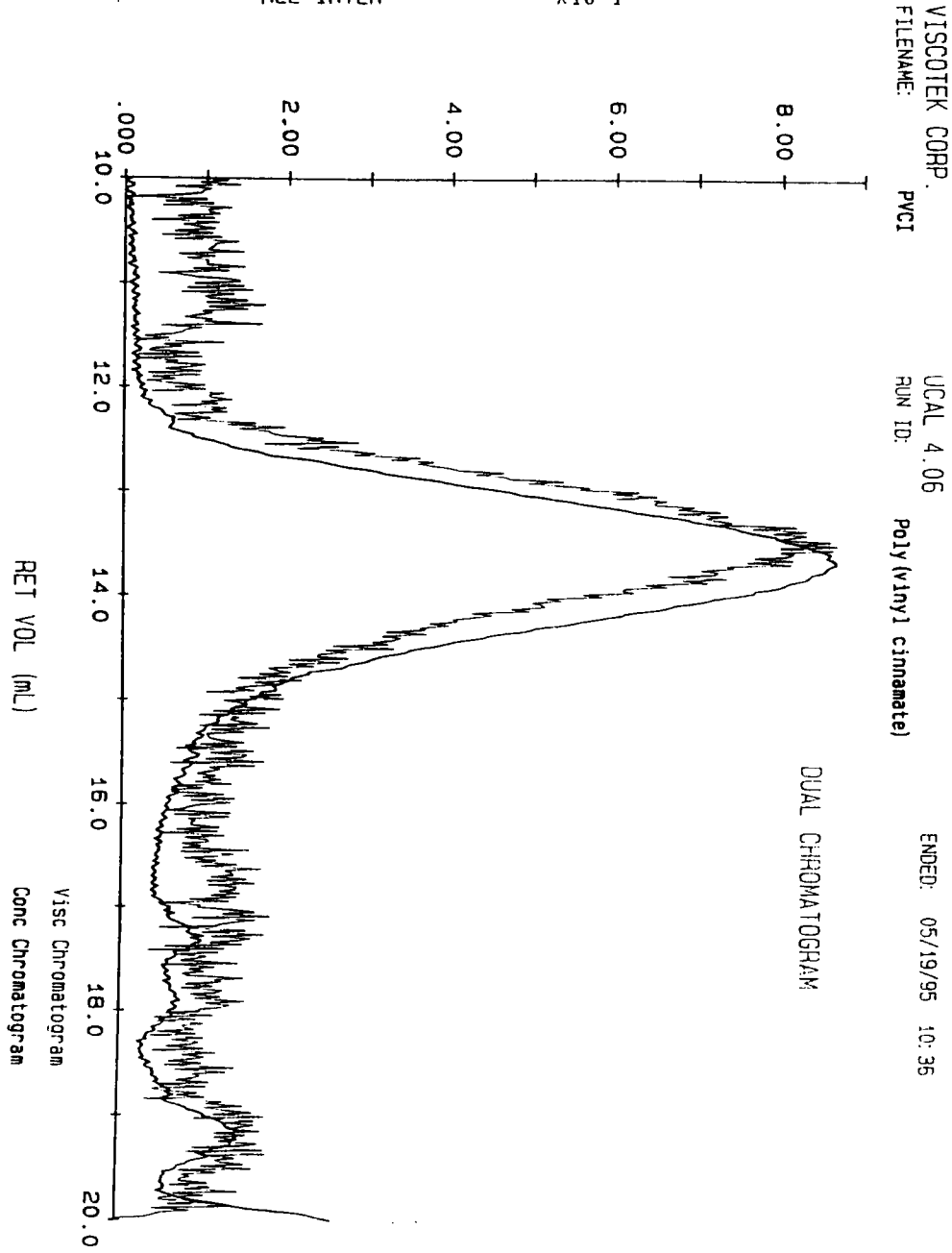

GPC Trace for Poly (Vinyl Cinnamate)

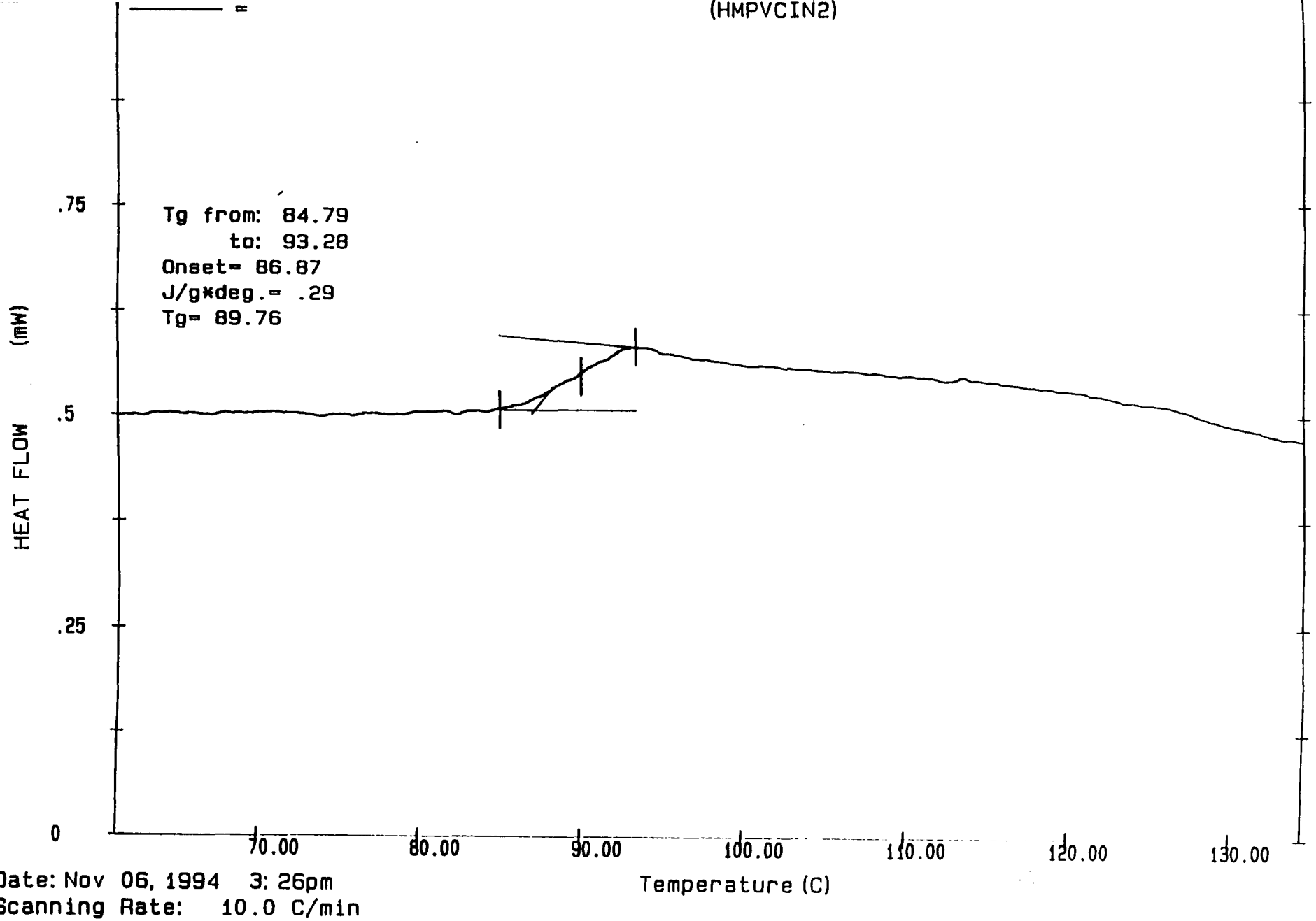

Date: Nov 06, 1994 3:26pm
Scanning Rate: 10.0 C/min
Sample Wt: 1.586 mg Path: \NC\
File 1: HMPVCIN2

PERKIN-ELMER DSC7

DSC Trace for Poly (Vinyl Cinnamate)

Appendix for Chapter Three

Exposure (s)	1-C/Co	Quantum Yield
0	0	-
300	0.11	1.28
600	0.18	0.77
900	0.21	0.60
1200	0.25	0.49
1500	0.25	0.44
1800	0.28	0.40
2100	0.28	0.32
2400	0.29	0.28
2700	0.29	0.26
3000	0.31	0.21
3300	0.34	0.24
3600	0.36	0.20
3900	0.36	0.18
4200	0.36	0.18
4500	0.36	0.15
4800	0.37	0.17
5100	0.38	0.14
5400	0.38	0.15
5700	0.41	0.14
6000	0.43	0.15
6300	0.43	0.12
6600	0.43	0.12
6900	0.43	0.13
7200	0.43	0.13

Table 1: Data for Unpolarised Radiation.

Exposure (s)	1-C/Co	Quantum Yield
0	0	-
3600	0.13	0.19
7200	0.15	0.10
10800	0.16	0.075
14400	0.18	0.063
18000	0.19	0.056
22080	0.21	0.050
25200	0.21	0.044

Table 2: Data for Vertically Polarised Radiation.

Exposure (s)	1-C/Co	Quantum Yield
0	0	-
3600	0.097	0.16
7200	0.11	0.092
10800	0.13	0.071
14400	0.13	0.053
18000	0.15	0.048
21600	0.16	0.045
25200	0.16	0.039
28800	0.18	0.038
32400	0.18	0.033
36000	0.18	0.030
39600	0.19	0.030

Table 3: Data for Horizontally Polarised Radiation.

Exposure (s)	1-C/Co	Quantum Yield
0	0	-
5	0.05	0.26
15	0.09	0.17
25	0.12	0.14
35	0.16	0.13
50	0.21	0.12
65	0.24	0.10
80	0.27	0.095
100	0.31	0.089
120	0.34	0.081
150	0.39	0.073
190	0.43	0.064
240	0.46	0.054
300	0.51	0.048
370	0.55	0.042
460	0.58	0.036
570	0.63	0.031
710	0.66	0.026
890	0.69	0.022
1130	0.72	0.018
1730	0.76	0.012

Table 4: Data for Laser Irradiation.

Exposure Time (Hours)	Absorbance Parallel	Absorbance Perpendicular	Dichroic Ratio
0	0.24	0.21	1.10
3	0.13	0.36	0.38
6	0.19	0.42	0.46
9	0.53	0.21	2.49
12	0.30	0.45	0.67
15	0.28	0.48	0.59
18	0.25	0.19	1.27
22	0.34	0.25	1.38
25	0.44	0.20	2.24
30	0.31	0.20	1.60

Table 5: Dichroic Ratio for PVCi Irradiated with Vertically Polarised Light.

Exposure (mins)	1	2	3	4	D_{+120}	D_{-120}
0	0.54	0.53	0.63	0.72	0.75	0.84
2	0.53	0.55	0.72	0.77	0.69	0.76
4	0.53	0.81	0.63	0.74	0.71	1.29
6	0.71	0.64	0.63	0.81	0.88	1.02
8	0.72	0.62	0.71	0.81	0.89	0.87
10	0.54	0.60	0.78	0.79	0.68	0.77
12	0.53	0.59	0.70	0.74	0.72	0.84
14	0.53	0.57	0.71	0.74	0.72	0.80

Table 6: Data for PVCi Dichroism.

Exposure (mins)	1	2	3	4	D_{+120}	D_{-120}
0	0.26	0.30	0.34	0.27	0.96	0.88
2	0.26	0.31	0.32	0.28	0.92	0.97
4	0.26	0.30	0.32	0.28	0.92	0.94
6	0.26	0.29	0.32	0.29	0.90	0.90
8	0.25	0.28	0.28	0.28	0.89	1.0

Table 7: Data for Repeated PVCi Dichroism Experiment

Appendix for Chapter Four

Polymer Laboratories
PL Caliber GPC Software

13:52 Thu Feb 29 1996

Unknown CC185.005

Acquired :
Operator

Concentration :
Injection Volume :
Solvent :
Column Set :

Anth 1

Detector :
Temperature :
Flow Rate : 1.000
Standards :

Method 1
Comments :

Calibration Using : Narrow Standards
Calibration Limits : 14.62 to 25.93 Mins
Flow Rate Marker : found at : 27.67

Curve Used : 2nd Order Polynomial
Last Calibrated : Thu Feb 29 11:54:36 1996
in Standards at : 27.92 Mins

Broad Peak Start : 16.00 End : 22.35 Mins

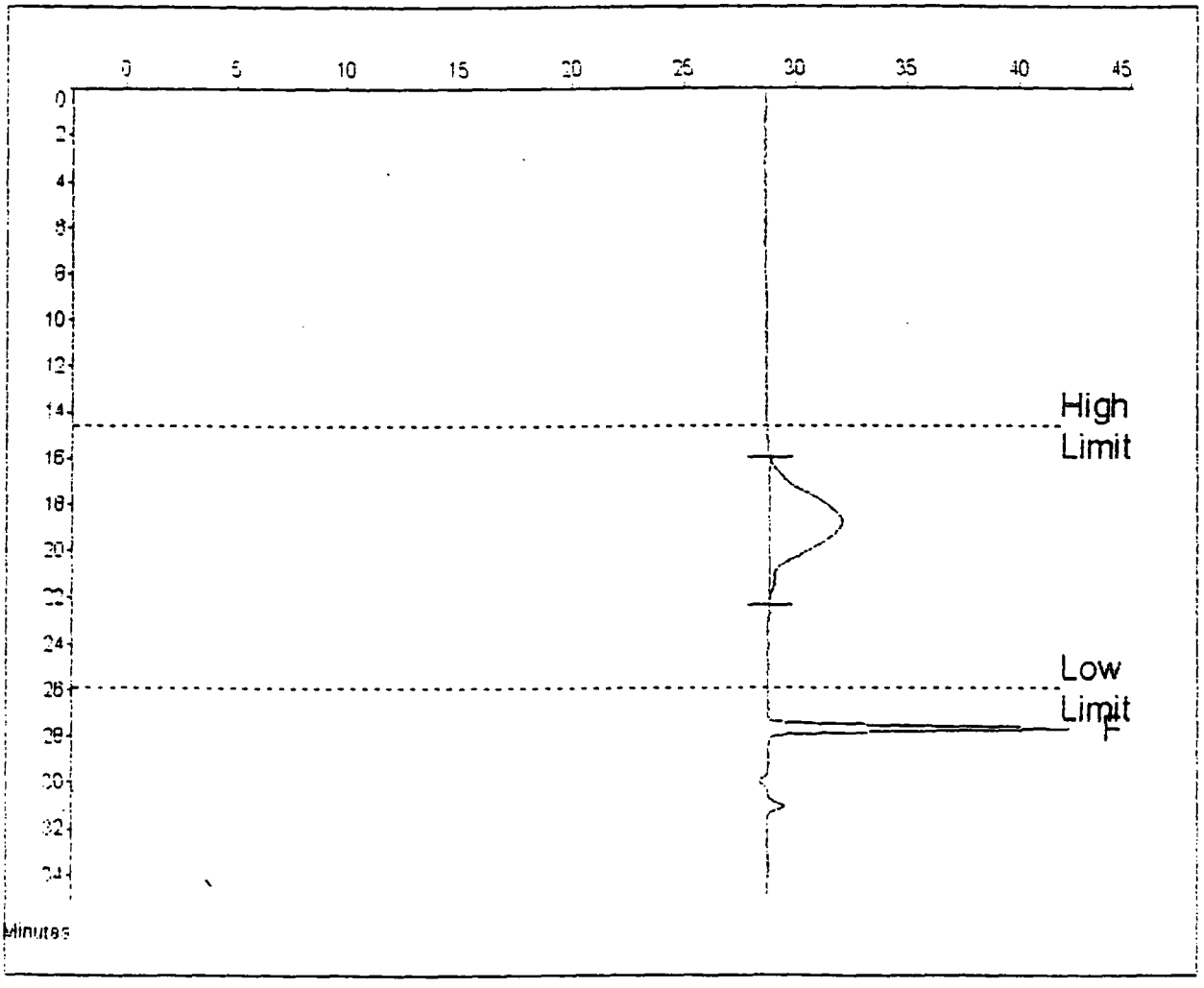

Molecular Weight Averages

Mp =	19211	Mz =	55283
Mn =	14029	Mz+1 =	69495
Mw =	29817	Mv =	25915
Polydispersity =	2.054	Peak Area =	104727

GPC Trace for Poly (9-Anthracenoate Ethyl Methacrylate)

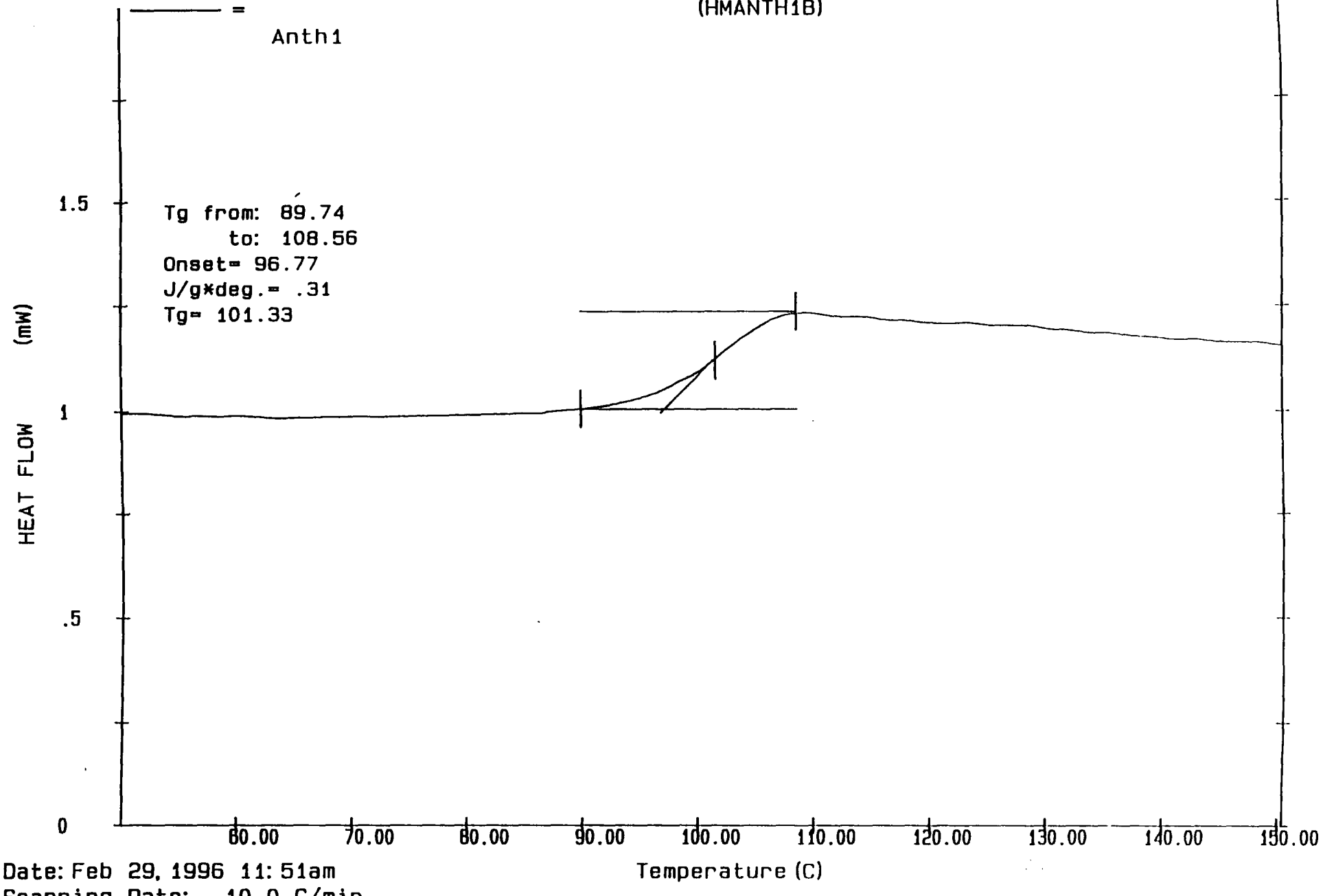

Date: Feb 29, 1996 11:51am
Scanning Rate: 10.0 C/min
Sample Wt: 4.251 mg Path: \GF\
File 1: HMANTH1B

PERKIN-ELMER DSC7

DSC Trace for Poly (9-Anthracenoate Ethyl Methacrylate)

Appendix For Chapter Four

Exposure / hours	Orientation	1142cm^{-1}	1196cm^{-1}	D (1142)	D (1196)
0	para	0.22	0.24	0.63	0.36
	perp	0.75	0.67		
1	para	0.21	0.23	0.90	0.45
	perp	0.50	0.50		
2	para	0.22	0.23	1.08	0.54
	perp	0.44	0.42		
3	para	0.22	0.48	1.27	0.54
	perp	0.37	0.26		
4	para	0.28	0.35	2.40	0.97
	perp	0.25	0.35		
5	para	0.27	0.34	2.20	0.94
	perp	0.28	0.35		
6	para	0.28	0.38	1.92	0.96
	perp	0.32	0.4		
8	para	0.25	0.26	2.84	0.91
	perp	0.19	0.29		
10	para	0.23	0.28	2.51	1.02
	perp	0.20	0.28		

Table 1: Absorbances and Dichroic Ratios for Polyanth.

Exposure / hours	Orientation	1142cm^{-1}	1196cm^{-1}	D (1142)	D (1196)
0	para	0.27	0.30	0.63	0.60
	perp	0.43	0.50		
1	para	0.19	0.25	0.86	0.71
	perp	0.22	0.35		
2	para	0.19	0.25	0.97	0.79
	perp	0.19	0.20		
3	para	0.24	0.19	0.97	0.87
	perp	0.24	0.21		
4	para	0.27	0.26	1.08	0.93
	perp	0.25	0.28		
5	para	0.28	0.27	1.24	0.98
	perp	0.23	0.27		
6	para	0.25	0.26	1.05	1.11
	perp	0.24	0.23		

Table 2: Absorbances and Dichroic Ratios for Polyanth.

Exposure / hours	Orientation	1142cm^{-1}	1196cm^{-1}	D (1142)	D (1196)
0	para	0.27	0.30	0.62	0.54
	perp	0.43	0.56		
1	para	0.26	0.28	0.67	0.55
	perp	0.39	0.51		
2	para	0.26	0.31	0.96	0.92
	perp	0.24	0.33		
3	para	0.26	0.34	0.99	1.07
	perp	0.27	0.32		
4	para	0.31	0.37	1.14	1.21
	perp	0.27	0.31		
5	para	0.32	0.38	1.18	1.28
	perp	0.27	0.30		
6	para	0.32	0.36	1.25	1.30
	perp	0.26	0.28		
8	para	0.30	0.36	1.16	1.22
	perp	0.26	0.29		

Table 3: Absorbances and Dichroic Ratios for Polyanth.

Appendix for Chapter Five

Polymer Laboratories
PL Caliber GPC Software

10:17 Wed Mar 05 1997

Unknown 10228 022

Acquired
Operator

Concentration
Injection Volume
Solvent
Column Set

Detector
Temperature
Flow Rate 1.000
Standards

Method
Comments

Calibration Using Narrow Standards Use Linear Polynomial
Calibration Limits 14.85 to 25.02 Mins Last Calibrated Thu Feb 20 12:14:25 1997
Flow Rate Marker found at 17.95 vs Standard at 17.98 Mins

Broad Peak Start 14.93 End 21.95 Mins

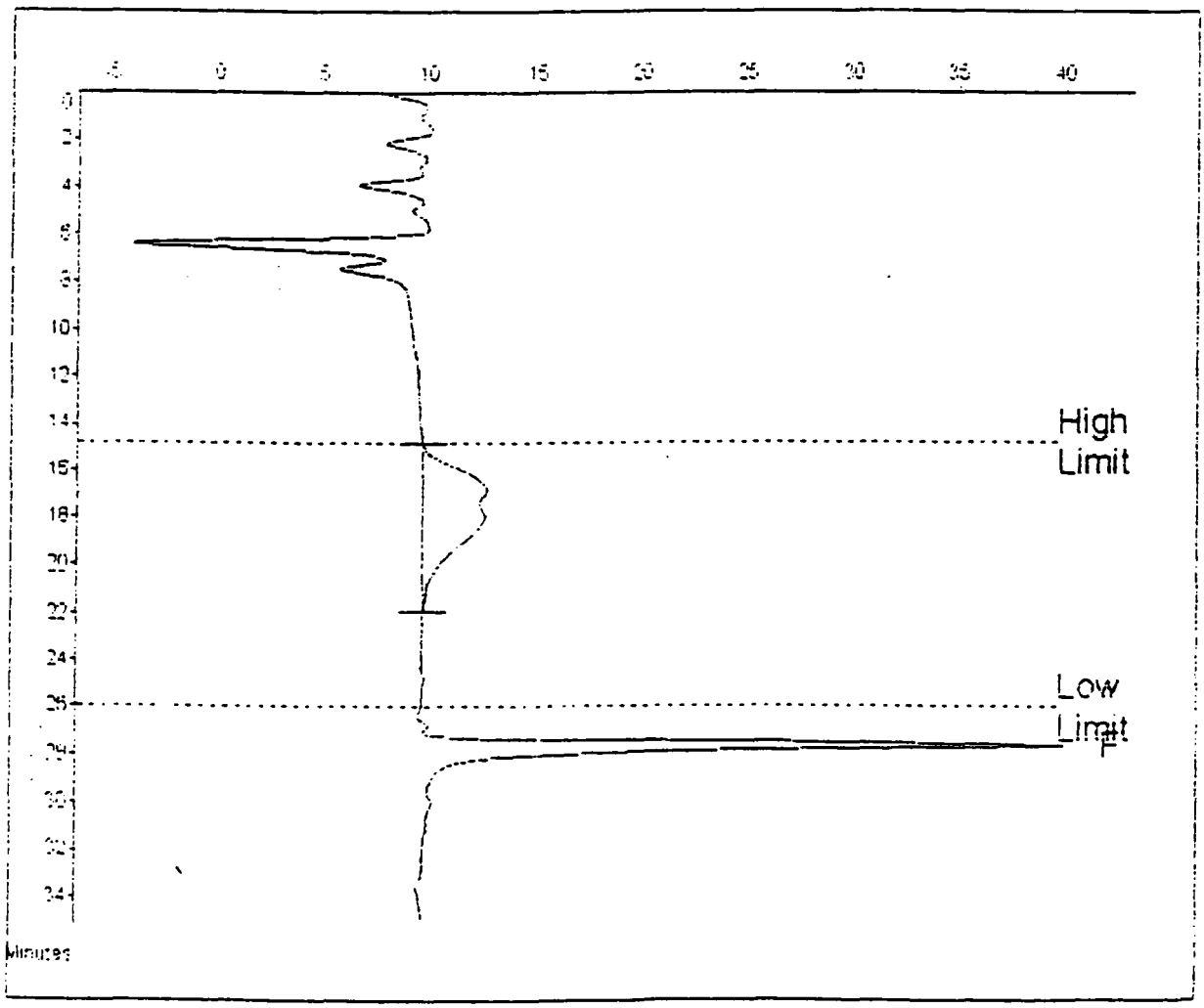

Molecular Weight Averages

Mp =	110607	Mz =	173099
Mn =	25623	Mz+1 =	251054
Mw =	81714	Mv =	70862
Polydispersity =	3.069	Peak Area =	128540

GPC Trace for Poly (p-Azidobenzoate Ethyl Methacrylate)

COLLOQUIA, LECTURES AND SEMINARS FROM INVITED SPEAKERS

1994

October 5 Prof. N. L. Owen, Brigham Young University, Utah, USA
Determining Molecular Structure - the INADEQUATE NMR way

October 19 Prof. N. Bartlett, University of California
Some Aspects of Ag(II) and Ag(III) Chemistry

November 2 Dr P. G. Edwards, University of Wales, Cardiff
The Manipulation of Electronic and Structural Diversity in Metal Complexes - New Ligands

December 7 Prof. D. Briggs, ICI and University of Durham
Surface Mass Spectrometry

1995

January 18 Dr G. Rumbles, Imperial College, London
Real or Imaginary Third Order Non-linear Optical Materials

February 1 Dr T. Cosgrove, Bristol University
Polymers do it at Interfaces

March 1 Prof. E.J. Meier, Eindhoven University of Technology, Netherlands
Dendrimers and Supramolecular Polymer Chemistry

April 26 Dr M. Schroder, University of Edinburgh
Redox-active Macrocyclic Complexes : Rings, Stacks and Liquid Crystals

May 4 Prof. A. J. Kresge, University of Toronto

The Ingold Lecture Reactive Intermediates : Carboxylic-acid Enols and Other Unstable Species

May 9 Prof. R. Townsend, Unilever Exploratory Research Council

Polymer for the Year 2000 - The Challenge Ahead.

May 30 Prof. P. Calvert, University of Arizona, USA

Freeforming: Chemical Methods for the Processing of Polymers, Ceramics and Composites

October 11 Prof. P. Lugar, Frei Univ Berlin, FRG

Low Temperature Crystallography

November 17 Prof. David Bergbreiter, Texas A&M, USA

Design of Smart Catalysts, Substrates and Surfaces from Simple Polymers

November 22 Prof. I Soutar, Lancaster University

A Water of Glass? Luminescence Studies of Water-Soluble Polymers.

December 8 Professor M.T. Reetz, Max Planck Institut, Mulheim

Perkin Regional Meeting

1996

January 10 Dr Bill Henderson, Waikato University, NZ

Electrospray Mass Spectrometry - a new sporting technique

January 17 Prof. J. W. Emsley , Southampton University

Liquid Crystals: More than Meets the Eye

January 31 Dr J. Penfold, Rutherford Appleton Laboratory,

Soft Soap and Surfaces

February 28 Prof. E. W. Randall, Queen Mary & Westfield College

New Perspectives in NMR Imaging

March 12 RSC Endowed Lecture - Prof. V. Balzani, Univ of Bologna

Supramolecular Photochemistry

March 13 Prof. Dave Garner, Manchester University

Mushrooming in Chemistry

August 15 Prof. K.B. Wagener, University of Florida, USA

Catalyst Selection and Kinetics in ADMET Polymerisation

November 6 Dr Melinda Duer, Chemistry Department, Cambridge

Solid-state NMR Studies of Organic Solid to Liquid-crystalline Phase Transitions

November 12 Professor R. J. Young, Manchester Materials Centre, UMIST

New Materials - Fact or Fantasy?

Joint Lecture with Zeneca & RSC

November 20 Professor J. Earnshaw, Deptartment of Physics, Belfast

Surface Light Scattering: Ripples and Relaxation

November 27 Dr Richard Templer, Imperial College, London

Molecular Tubes and Sponges

December 3 Professor D. Phillips, Imperial College, London

"A Little Light Relief"

December 4 Professor K. Muller-Dethlefs, York University

Chemical Applications of Very High Resolution ZEKE Photoelectron Spectroscopy

1997

January 22 Dr Neil Cooley, BP Chemicals, Sunbury

Synthesis and Properties of Alternating Polyketones

February 26 Dr Tony Ryan, UMIST

Making Hairpins from Rings and Chains

March 11 Dr A. D. Taylor, ISIS Facility, Rutherford Appleton Laboratory

Expanding the Frontiers of Neutron Scattering

March 19 Dr Katharine Reid, University of Nottingham

Probing Dynamical Processes with Photoelectrons

May 7 Prof. M. Harrington, Caltech, Pasadena, USA

Polymers both Enable and Limit the Discovery of Protein Alterations in Studies Ranging from Gene Regulation to Mad Cow Disease

May 20 Prof. J. Jin, President, Korean Chemical Society

Poly PPV and its Derivatives - Synthesis, Structure and Properties

June 13 Prof. Dr. S. Kobayashi, Kyoto University, Japan

Synthesis of Polyesters via Enzymatic Polymerisation

CONFERENCES AND COURSES ATTENDED

January 1995 IRC Polymer Physics and Engineering Courses

Leeds and Bradford Universities

July 1995 ISOM11

Durham University

May 1996 Structural Hierarchy in Polymers

36th Moretonhampstead Conference

April 1996 Macro Group UK Family Meeting

Manchester University

April 1997 Macro Group UK Family Meeting

Leeds University

July 1997 Polymers at Surfaces and Interfaces III

Durham University